

Prepared in cooperation with the Ministry of Petroleum, Energy and Mines,
Islamic Republic of Mauritania

Second Projet de Renforcement Institutionnel du Secteur Minier de la République Islamique de Mauritanie (PRISM-II)

Synthesis of Geological, Structural, and Geochronologic Data:

Phase V, Deliverable 53

By Dwight C. Bradley, Paul O'Sullivan, Michael A. Cosca, Holly A. Motts, John D. Horton, Cliff D. Taylor, Georges Beaudoin, Gregory K. Lee, Jahan Ramezani, Dan B. Bradley, Jamey V. Jones, and Samuel Bowring

Open-File Report 2013–1280 Chapter A

U.S. Department of the Interior
U.S. Geological Survey

U.S. Department of the Interior
SALLY JEWELL, Secretary

U.S. Geological Survey
Suzette M. Kimball, Acting Director

U.S. Geological Survey, Reston, Virginia: 2015

For more information on the USGS—the Federal source for science about the Earth, its natural and living resources, natural hazards, and the environment, visit http://www.usgs.gov or call 1–888–ASK–USGS.

For an overview of USGS information products, including maps, imagery, and publications, visit http://www.usgs.gov/pubprod

To order this and other USGS information products, visit http://store.usgs.gov

Suggested citation:
Bradley, D.C., O'Sullivan, Paul, Cosca, M.A., Motts, H.A., Horton, J.D., Taylor, C.D., Beaudoin, Georges, Lee, G.K., Ramezani, Jahan, Bradley, D.B., Jones, J.V., and Bowring, Samuel, 2015, Synthesis of geological, structural, and geochronologic data (phase V, deliverable 53), chap. A *of* Taylor, C.D., ed., Second projet de renforcement institutionnel du secteur minier de la République Islamique de Mauritanie (PRISM-II): U.S. Geological Survey Open-File Report 2013–1280-A, 328 p., http://dx.doi.org/10.3133/ofr20131280. [In English and French.]

ISSN 2331-1258 (online)

Any use of trade, firm, or product names is for descriptive purposes only and does not imply endorsement by the U.S. Government.

Although this information product, for the most part, is in the public domain, it also may contain copyrighted materials as noted in the text. Permission to reproduce copyrighted items must be secured from the copyright owner.

Multiple spellings are used in various literatures, and may be reflected in the text.

This report is preliminary and has not been reviewed for conformity with U.S. Geological Survey editorial standards or for stratigraphic nomenclature.

The report is being released in both English and French. In both versions, we use the French-language names for formal stratigraphic units.

Contents

1.0. Geologic Map and Structural Geologic Map 2
1.1. Sources of Information 2
1.2. Mapping Conflicts 4
1.3 Map Units 4
1.4 Color Scheme 4
1.5 Map-units and Abbreviations 4
1.6 Structure Map (Deliverable 52) 4
1.7 Acknowledgments 5
2.0. Geochronology 5
2.1. Analytical Methods 13
2.2. Sample Information 14
3.0. Geochronological Results from the Taoudeni Basin 14
3.1. Groupe de Char 14
3.2. Groupe d'Atar 16
3.3. Groupe d'Assabet El Hassiane 19
3.4. Groupe d'Aioun 19
3.5. Groupe de Khang Naam 26
3.6. Groupe de Jbéliat 26
3.7. Groupe de Téniagouri 26
3.8. Groupe de Nouatil, Formation de Serize 36
3.9. Groupe d'Oujeft 39
3.10. Groupe de Tichit (Ordovician) 45
3.11. Groupe de Néma, Formation de Saïlé (Cretaceous) 45
4.0. Geochronological Results from the Central Mauritanide Orogen 45
4.1. Groupe de Djonaba 48
4.2. Groupe de Gadel 49
4.3. Groupe de Gueneiba 51
4.4. Groupe d'El Mseigguem 53
4.5. Groupe d'El Ghabra 57
4.6. Groupe d'El Fadra 57
4.7. Cortège de Kelbé 59
4.8. Quartz Veins in the Central Mauritanides 59
5.0. Northern Mauritanide Orogen 61
5.1. Groupe de Oumachoueima, Formation de Sainte Barbe 62
5.2. Groupe de Oumachoueima Undivided 65
5.3. Groupe de Oumachoueima, Atilis Quartzite Member 65
5.4. Groupe d'Eizzene, Formation de Raoui 68
5.5. Complexe d'Inchiri, Groupe de Hajar Dekhen – Kleouat 68
6.0. Rgueïbat Shield 68
6.1. Group de Lebzenia, Formation d'Aouéoua 68
6.2. Complexe d'Amsaga near Mennerat Iguilid Tungsten Occurrence 73
6.3. Anorthosite in Complexe d'Amsaga Amsaga 78
6.4. Complexe de Tiris 78

6.5. Complexe d'Idjil, Formation de Tazadit....80
6.6. Formation de Seyala....80
6.7. Groupe de Blekhzaymat....84
6.8. Quartz veins cutting the Groupe de Blekhzaymat....90
6.9. Complexe de Ghallamane....90
6.10. Complexe de Tsalabia el Khadra....94
6.11. Cortège de Gleibat Tenebdar....96
7. Discussion....96
7.1. Detrital Zircon Barcodes....96
7.2. Char Barcode and the Mesoproterozoic Detrital Zircon Signature of the West African Craton....98
7.3. The Assabet Barcode and Implications for Rodinia Supercontinent Reconstructions....98
7.4. The Oujeft Barcode and Relationship to Pan-African Orogeny....99
7.5. The Téniagouri Barcode and Relationship to Pan-African Orogeny....104
7.6. Late Paleozoic Orogenesis in the Mauritanides....104
7.7. Discussion of Problematic Detrital Zircon Results....104
7.8. Implications for Correlation and Mapping....106
8. Geologic and Tectonic Framework of Mauritania....107
8.1. Archean Geology and Tectonics....107
8.2. Paleoproterozoic Geology and Tectonics....108
8.3. Mesoproterozoic to Paleozoic Tectonic Record in the Taoudeni Basin....109
8.4. Mesoproterozoic to Paleozoic Tectonic Record in the Mauritanide Orogen....110
8.5. Tindouf Basin....111
8.6. Mesozoic to Cenozoic Geology and Tectonics....112
8.7. Mauritanian Tectonic Evolution in the Context of the Supercontinents Nuna, Rodinia, Gondwana, and Pangea....112
9. References Cited....114
Tables and Table Links....121
Appendix A1. Analytical Methods for $^{40}Ar/^{39}Ar$ Geochronology....137
Appendix A2. Analytical Methods for U-Pb CA-TIMS Geochronology at Massachusetts Institute of Technology....137
Appendix A3. U-Pb Zircon SHRIMP-RG Techniques (U.S. Geological Survey-Stanford University)....138
Appendix A4. Analytical Methods for U-Pb LAICPMS Geochronology by Apatite to Zircon, Inc. at Washington State University....138
Appendix A5. Analytical Methods for Apatite Fission Track Geochronology by Apatite to Zircon, Inc....140

Figures

1. Map of Mauritania (outlined in gray) showing sources of map information. The 1:200,000-scale geologic quadrangles are numbered using the coordinates of the southeastern corner of each sheet; for the Atar sheet, number 2014, this point is at 20°N, 14°W 3
2. Generalized geologic map of Mauritania showing sample locations for new U-Pb igneous ages.....6
3. Generalized geologic map of Mauritania showing sample locations for new U-Pb detrital zircon ages.....7
4. Generalized geologic map of Mauritania showing sample locations for new $^{40}Ar/^{39}Ar$ and apatite fission track ages 8
5. Generalized geologic map of Mauritania showing U-Pb geochronology sample locations from published literature. Ages are summarized in Table 9 9
6. (*A*) Generalized geologic map of Mauritania showing $^{40}Ar/^{39}Ar$, K/Ar, and Re/Os geochronology sample locations from published literature. (*B*) Detail for the Central Mauritanides 10
7. Generalized tectonic map of Mauritania, adapted, in part, from maps by Pitfield and others (2004) and Lahondère and others (2003, 2005). Key to numbered localities: 1—Unconformity below Cambrian-Ordovician, western Tindouf Basin; 2—Unconformity below Ordovician, eastern Tindouf Basin; 3—Astroblem; 4—Approximate boundary between Zednes and Tiris Archean domains; 5—Unconformity below Mesoproterozoic Groupe de Char; 6—Taziast klippe; 7—Mafic sills of Central Atlantic Magmatic Province, CAMP; 8—Assabet foreland-basin deposits; 9—Unconformity below Groupe de Jbéliat glacial deposits; 10—Frontal thrust in Northern Mauritanides; 11—Tacarat-Inemmaudene Shear Zone; 12—Guelb er Richat, subsurface laccolith; 13—Stratigraphic section in Figure 8; 14—Akjoujt sector of Mauritanide thrust belt; 15—Archean tectonic windows beneath Mauritanide thrust belt; 16—Oujeft foreland-basin deposits; 17—Frontal thrust in Central Mauritanides; 18—Early Neoproterozoic basement in Central Mauritanides; 19—Parautochthon in Central Mauritanides; 20—Allochthon in in Central Mauritanides; 21—Unconformity below Mesozoic-Cenozoic coastal basin deposits; 22—Kandou Formation, Hercynian foreland basin; 23—Gorgol Noir suture zone in Central Mauritanides; 24—Inchiri district.....12
8. Stratigraphic column for the Adrar region of the Taoudeni Basin; the lithologic column is adapted from Deynoux and others (2006), the nomenclature is from Pitfield and others (2004), and the age control is from the present study and Rooney and others (2010).....15
9. Detrital zircon data and photographs for sample CT22 from the Groupe de Char. (*A*) Basal sandstones of the Groupe de Char (red) unconformably overlying a pale greenish paleosol developed on a granitoid of the Complexe d'Amsaga. (*B*) Sandstone of the Groupe de Char where sampled for detrital zircons. (*C*) Concordia diagram. (*D*) Age distribution shown in two forms: a probability density function (red curve) and a histogram with 50-m.y. bins (blue boxes). This is one of the two samples that we collected on a brief reconnaissance trip early in 2007; hence the different sample numbering scheme.....16
10. Detrital zircon data and photographs for sample DB07RIM23a from the Groupe d'Atar. (*A* and *B*) Outcrop photographs of sandstone at the sample location. (*C* and *D*) Photomicrographs under plane light and crossed polars, respectively. Note the lack of penetrative deformation. In these and subsequent photomicrographs, the field of view is 2.5 mm across. (*E*, *F*, and *G*) Concordia diagrams and the corresponding zircon age distribution based on the first analysis of sample DB07RIM23a (lab number 952-12). (*H*, *I*, and *J*) Comparable data based on the reanalysis (lab number 1284-04). In this and subsequent plots, age distributions show filtered data only, and paired concordia diagrams with blue and red ellipses represent unfiltered and filtered data, respectively.....17

11. Detrital zircon data and photographs for sample DB07RIM31a from the Groupe d'Assabet El Hassiane. (*A*) Outcrop photograph of conglomerate at the sample location; sample is from the sand matrix. (*B* and *C*) Photomicrographs under plane light and crossed polars, respectively. (*D* and *E*) Concordia diagrams. (*F*) Age distribution 20
12. Detrital zircon data and photographs for sample DB07RIM59a from the Groupe d'Assabet El Hassiane. (*A*) Outcrop photograph from sandstone near the sample location; rocks at exact sample location were not photogenic. (*B* and *C)* Photomicrographs under plane light and crossed polars, respectively. (*D* and *E*) Concordia diagrams. (*F*) Age distribution.....22
13. Detrital zircon data and photographs for sample CT07RIM70-1 from the Groupe d'Aioun, Formation de Freidi. (*A*) Outcrop photograph of sandstone at the sample location; photograph by Cliff Taylor. (*B* and *C*) Concordia digrams. (*D*) Age distribution.....24
14. Detrital zircon data and photographs for sample CT07RIM71-1 from the Groupe d'Aioun, Formation de Seyal. (*A* and *B*) Distant and close-up outcrop photographs of sandstone at the sample location. Photographs by Cliff Taylor. (*E*) Age distribution 25
15. Detrital zircon data and photographs for sample CT07RIM72-1 from the Groupe de Khang Naam, Formation de Lehbilé. (*A*) Outcrop photograph of sandstone at the sample location; photograph by Cliff Taylor. (*B* and *C*) Concordia diagrams. (*D*) Age distribution 27
16. Detrital zircon data and photographs for sample DB07RIM29c from the Groupe de Jbéliat near Atar. (*A* and *B*) Outcrop photographs of the sample location. (*C* and *D*) Photomicrographs under plane light and crossed polars, respectively. (*E* and *F*) Concordia diagrams. (*G*) Age distribution.....28
17. Detrital zircon data and photographs for sample CT07RIM73-1 from the Groupe de Jbéliat in the Kiffa area. (*A* and *B*) Outcrop photographs of sandstone at the sample location. Photographs by Cliff Taylor. (*C* and *D*) Concordia diagrams. (*E*) Age distribution.....30
18. Detrital zircon data and photographs for sample DB07RIM80a from diamictite that was previously mapped as the Groupe de Jbéliat near the Senegal River. (*A*) Outcrop photograph of the cap dolostone, showing contorted laminae, and chert. (*B*) Outcrop photograph of the sample horizon, a few meters below the cap carbonate. (*C* and *D*) Photomicrographs under plane light and crossed polars, respectively. (*E* and *F*) Concordia diagrams. (*G*) Age distribution.....32
19. Zircon age data and photographs for the Formation de Bouly, Groupe de Téniagouri, near Atar. (*A*) Outcrop photograph of the sample location, a ~10-meter-high cutbank along a oued. (*B*) Close-up of the sampled ash horizon, just above the base of the cutbank and the thickest of about 10 ash layers. (*C* and *D*) Photomicrographs under plane light and crossed polars, respectively. (*E*) Concordia diagram based on SIMS analyses. (*F*) Age distribution based on SIMS data showing that this tuff layer includes detrital zircons. (*G*) Reflected-light photomicrograph of zircons dated by CA-TIMS, showing a variety of grain types. (*H*) Concordia diagram based on CA-TIMS analyses. (*I*) Weighted average age (green line) based on $^{206}Pb/^{238}U$ zircon ages (red bars) that comprise the cluster of CA-TIMS ages at 623.3±5.5 Ma, as shown in (*I*) 33
20. Detrital zircon data and photographs for sample DB07RIM77a from the Sub-groupe de Tichilit el Beïda of the Groupe de Téniagouri. (*A*) Outcrop photograph of the sample location, specifically the thick bed of light-colored, tuffaceous, turbiditic sandstone in the upper right. (*B* and *C*) Photomicrographs under plane light and crossed polars, respectively. (*D* and *E*) Concordia diagrams. (*F*) Age distribution.....35
21. Detrital zircon data and photographs for sample DB07RIM28a from the Groupe de Nouatil. (*A*) Outcrop photograph of sandstone at the sample location. (*B* and *C*) Concordia diagrams (*D*) Age distribution.....37

22. Detrital zircon data and photographs for sample DB07RIM26a from the Groupe d'Oujeft, Formation de Chinguetti near Atar. (*A*) Outcrop photograph of the roadcut along the Atar-Ouadane highway, showing the graffiti-covered sample horizon of sandstone. (*B*) Close-up of the sample horizon. (*C* and *D*) Photomicrographs under plane light and crossed polars, respectively. Red circle encloses an originally detrital quartz grain with rounded core and diagenetic quartz overgrowth. (*E* and *F*) Concordia diagrams. (*G*) Age distribution 38
23. Detrital zircon data and photographs for sample DB07RIM61a from the Groupe d'Oujeft, Formation de Chinguetti near Ouadane. (A) Outcrop photograph of sandstone at the sample location. (*D*) Age distribution 40
24. Detrital zircon data and photographs for sample DB07RIM75a from the Groupe d'Oujeft, Sous-groupe d'Aghaoujeft. (*A* and *B*) Outcrop photographs of sandstone at the sample location. (*C* and *D*) Photomicrographs under plane light and crossed polars, respectively. (*E* and *F*) Concordia diagrams. (*G*) Age distribution 41
25. Detrital zircon data and photographs for sample CT07RIM60-1 from the Formation de Moudjeria of the Groupe d'Oujeft. (*A, B,* and *C*) Outcrop photographs of sandstone at the sample location. Photographs by Cliff Taylor. (*D* and *E*) Concordia diagrams. (*F*) Age distribution 43
26. Detrital zircon data and photographs for sample DB07RIM74a, from rocks mismapped as Groupe d'Oujeft, Moudjeria Formation. (*A*) Outcrop photograph of the sandstone from sample location. (*B* and *C*) Photomicrographs under plane light and crossed polars, respectively. (*D* and *E*) Concordia diagrams. (*F*) Age distribution.....44
27. Detrital zircon data and photographs for sample CT07RIM59-1, from the Groupe de Tichit, Formation de Tabarit El Kbir. (*A* and *B*) Outcrop photographs of sandstone at the sample location. Photographs by Cliff Taylor. (*C* and *D*) Concordia diagrams. (E) Age distribution 46
28. Detrital zircon data and photographs for sample CT07RIM62-1, from the Groupe de Néma, Formation de Saïlé. (*A* and *B*) Outcrop photographs of sandstone at the sample location. Photographs by Cliff Taylor. (*B* and *C*) Concordia diagrams. (*E*) Age distribution.....47
29. Detrital zircon data and photographs for sample DB07RIM76a, from the Groupe de Djonaba. (*A*) Outcrop photograph of sandstone at the sample location. (*B* and *C*) Photomicrographs under plane light and crossed polars, respectively. (*D* and *E*) Concordia diagrams. (*F*) Age distribution.....48
30. Detrital zircon data and photographs for sample DB07RIM65a, from the Groupe de Gadel. (*A*) Outcrop photograph of metasandstone at the sample location. (*B* and *C*) Concordia diagrams. (*D*) Age distribution.....50
31. (*A*) Outcrop photograph of the sample location of sample DB07RIM66a, a deformed, metamorphosed conglomerate from the Groupe de Gadel. (*B* and *C*) Argon age-release spectra for two white mica fractions 51
32. Detrital zircon data and photographs for sample DB07RIM69a, from the Groupe de Gueneiba. (*A*) Outcrop photograph of metasandstone from the sample location. (*B* and *C*) Photomicrographs of quartz-rich metasandstone under plane light and crossed polars, respectively. (*D* and *E*) Concordia diagrams. (*F*) Age distribution 52
33. Detrital zircon data and photographs for sample CT07RIM55-1, from the Formation d'Ouechkech of the Groupe d'El Mseigguem. (A) Outcrop photograph of metasandstone from the sample location. Photography by Cliff Taylor. (*B* and *C*) Concordia diagrams. (*D*) Age distribution.....54
34. Detrital zircon data and photographs for sample GB07RIM63a, from the Formation d'Oued Erdi of the Groupe d'El Ghabra. (*A*) Outcrop photograph of deformed volcanic conglomerate from the sample location. Photography by Georges Beaudoin. (*B* and *C*) Concordia diagrams. (*D*) Age distribution 55

35. Detrital zircon data and photographs for sample DB07RIM73a, from the Formation d'Ould Moïlîd of the Groupe d'El Ghabra. (*A*) Outcrop photograph of metagraywacke from the sample location. (*B* and *C*) Photomicrographs of foliated metagraywacke under plane light and crossed polars, respectively. (*D* and *E*) Concordia diagrams. (*F*) Age distribution.....56

36. Detrital zircon data and photographs for sample DB07RIM62a, from the Groupe d'El Fadra. (*A* and *B*) Outcrop photographs of metagraywackw from the sample location—an area of sparse, low outcrop. (*C* and *D*) Photomicrographs of foliated metasandstone under plane light and crossed polars, respectively. (*E* and *F*) Concordia diagrams. (*G*) Age distribution 58

37. Zircon data and photographs for sample DB07RIM64a, from the Cortège de Kelbé. (A and B) Outcrop photographs of foliated granite from the sample location. (C and D) Concordia diagrams for unfiltered and filtered LAICPMS data. (E) Unfiltered SIMS data; all data were strongly discordant. (F) Age distribution based on LAICPMS results 60

38. Outcrop photographs and corresponding argon age-release spectra for white mica fractions from quartz veins in the central Mauritanides. (*A* and *B*) Sample GB07RIM52a. (*C* and *D*) Sample GB07RIM61a. (*E* and *F*) Sample GB07RIM62c. (*G* and *H*) Sample GB07RIM69a 61

39. Zircon data and photographs for sample CT07RIM10-1 from the Formation de Sainte Barbe. (A) Concordia diagram showing unfiltered SIMS data. Coloring of error ellipses according to Th/U shows that the spread of ages is not due to a mix of igneous and metamorphic zircons. (B and C) Concordia diagrams for unfiltered and filtered LAICPMS data. (D) Age distribution showing filtered LAICPMS results. (E) Histogram showing detail in the Archean part of the time scale, based on combined results from LAICPMS and SIMS analyses. (F) Weighted mean of 207Pb/206Pb ages that form the youngest maximum, which we interpret as the age of the igneous rock 63

40. Detrital zircon data and photographs for sample DB07RIM01a from the Formation de Sainte Barbe. (*A*) Outcrop photograph of metasandstone from the sample location. (*B* and *C*) Photomicrographs of protomylonitic metasandstone under plane light and crossed polars, respectively. (*D* and *E*) Concordia diagrams. (*F*) Age distribution 64

41. Detrital zircon data and photographs for sample CT07RIM02-1, from the Formation de St. Barbe. (*A* and *B*) Outcrop photographs of the sample location. The iron carbonate pod in (*B*) is a few meters structurally below the sampled horizon of chloritic metasandstone in (A). (*C* and *D*) Concordia diagrams. (*E*) Age distribution 66

42. Detrital zircon data and photographs for sample CT21, from an undivided part of the Groupe d'Oumachoueima. (*A*) Outcrop photograph of metasandstone at the sample location. Photograph by Cliff Taylor. (*B*) CL (cathodoluminescent) SEM images of selected zircons showing that late Neoproterozoic ages were obtained from a range of zircon types, and not from rims. Individual images are 200 microns on a side. (*C*) Concordia diagram showing unfiltered data. (*D*) Age distribution. This is one of the two samples that we collected on a brief reconnaissance trip early in 2007; hence the different sample numbering scheme 67

43. Detrital zircon data and photographs for sample DB07RIM02a, from the Atilis quartzite member of the Formation d'Irarchene El Hamra, Groupe d'Oumachoueima. (*A*) Outcrop photograph of the sample location. (*B* and *C*) Photomicrographs of quartzite under plane light and crossed polars, respectively. (*D* and *E*) Concordia diagrams showing unfiltered and filtered data. (*F*) Age distribution 69

44. Detrital zircon data and photographs for sample DB07RIM03a, from the Formation de Raoui of the Groupe de Eizzene. (*A* and *B*) Photomicrographs of quartzite under plane light and crossed polars, respectively. (*C* and *D*) Concordia diagrams showing unfiltered and filtered data. (*E*) Age distribution.....71

45. Detrital zircon data and photographs for sample DB07RIM17a, from the Groupe de Hajar Dekhen – Kleouat of the Complexe d'Inchiri. (*A*) Outcrop photograph of quartzite from the sample location—an area of sparse exposure. (*B* and *C*) Photomicrographs of quartzite under plane light and crossed polars, respectively. (*D* and *E*) Concordia diagrams showing unfiltered and filtered data. (*F*) Age distribution....72
46. Detrital zircon data and photographs for sample GB07RIM80a, from the Formation d'Aouéoua of the Groupe de Lebzenia. (*A*) Outcrop photograph of quartzite from the sample location. Photography by Georges Beaudoin. (*B* and *C*) Concordia diagrams showing unfiltered and filtered data. (*D*) Age distribution....74
47. (*A*) Outcrop photograph of the sample location of sample GB07RIM82D, a quartz vein that cuts the Formation d'Aouéoua in the Tasiast region. Photograph by Georges Beaudoin. (*B*) Argon age-release spectrum for white mica....75
48. Geochronological data and photographs of granitoid sample DB07RIM25a from the Complexe d'Amsaga. (*A* and *B*) Outcrop photographs of granitoid from the sample location. (*C* and *D*) Photomicrographs of altered granitoid under plane light and crossed polars, respectively. (*E*) Concordia diagram showing complex, intractable zircon systematics. (*F*) Argon age-release spectrum for white mica....76
49. Detrital zircon data and photographs for sample DB07RIM25C, from quartzite in the Complexe d'Amsaga. (*A*) Outcrop photograph of the sample location. (*B* and *C*) Concordia diagrams showing unfiltered and filtered data. (*D*) Age distribution....77
50. Concordia diagram for sample CT07RIM25-1, anorthosite from the Complexe d'Amsaga....78
51. Zircon data and photographs for samples DB07RIM32-1a and CT07RIM22-1, different phases of an anorthosite body in the Complexe d'Amsaga. (*A*) Outcrop photograph of anorthosite sample DB07RIM32-1. (*B* and *C*) Concordia diagrams for coarse-grained anorthosite, sample DB07RIM32-1. (*B*) SIMS data, unfiltered. (*C*) LAICPMS data, filtered. (*D*) Concordia diagram for fine-grained anorthosite, sample CT07RIM22-1....79
52. (*A*) Outcrop photograph of the sample location of sample DB07RIM45b, Complexe de Tiris. (*B*) Argon age-release spectrum for white mica....80
53. (*A*) Outcrop photograph of calcrete breccia, sample CT07RIM27, from the carapace of the Mhaoudât #4 iron mine. (*B*) Histogram of apatite fission-track ages. We interpret the apatite population as detrital, and eroded from rocks that mostly cooled through 100°C during the Jurassic....81
54. Geochronological data and photographs for sample DB07RIM46a and b, from quartzite in the Formation de Tazadit in the Complexe d'Idjil. (*A* and *B*) Outcrop photographs of the horizon sampled for DB07RIM46a and DB07RIM46b, respectively. (*C* and *D*) Corresponding concordia diagrams showing unfiltered and filtered data. (*E*) Detrital zircon age distribution for sample DB07RIM46a. (*F*) Argon age-release spectrum for white mica from sample DB07RIM46b....82
55. Detrital zircon data and photographs for sample DB07RIM36a, from the Formation de Seyala. (*A, B,* and *C*) Outcrop photographs of the sample location. (*D* and *E*) Photomicrographs of a clast of previously metamorphosed and deformed ferruginous quartzite under plane light and crossed polars, respectively. (*F* and *G*) Concordia diagrams of LAICPMS results showing unfiltered and filtered data. (*H*) Age distribution....83
56. Detrital zircon data and photographs for sample DB07RIM55a, from the southern Groupe de Blekhzaymat. (*A*) Outcrop photograph of conglomeratic sandstone from the sample location. (*B* and *C*) Photomicrographs of sandstone under plane light and crossed polars, respectively. (*D* and *E*) Concordia diagrams showing unfiltered and filtered data. (*F*) Age distribution....85

57. Detrital zircon data and photographs for sample DB07RIM54a from the northern Groupe de Blekhzaymat. (*A*) Outcrop photograph of sandstone from the sample location. (*B* and *C*) Photomicrographs of sandstone under plane light and crossed polars, respectively. (*D, E,* and *F*) Concordia diagrams and age distribution from the first analysis (lab number 952-12). (*G, H,* and *I*) Concordia diagrams and age distribution from the reanalysis (lab number 1284-04).....87

58. Zircon geochronological data and photographs for sample CT07RIM37-1 from the northern Groupe de Blekhzaymat. (*A* and *B*) Outcrop photographs of the sample location. (*C*) Concordia diagram showing SIMS results. (*D, E,* and *F*) LAICPMS results: concordia diagrams for unfiltered and filtered data, and corresponding age distribution. (*G*) Weighted average age based on combined SIMS and LAICPMS data 89

59. Outcrop photographs (by Georges Beaudoin) and corresponding argon age-release spectra for white mica fractions from quartz veins cutting the Groupe de Blekhzaymat. (A and B) Sample GB07RIM40b. (*C* and *D*) Sample GB07RIM42b.....91

60. Geochronological data and photographs for sample DB07RIM53a from the Complexe de Ghallamane. (*A*) Outcrop photograph of metasandstone from the horizon sampled for DB07RIM53a. (*B* and *C*) Photomicrographs of DB07RIM53a under plane light and crossed polars, respectively. (*D, E,* and *F*) Concordia diagrams and corresponding age distribution plot from the first analysis of sample DB07RIM53a (lab number 952-14). (*G, H,* and *I*) Concordia diagrams and corresponding age distribution plot from the reanalysis (lab number 1284-7). (*J*) Argon age-release spectrum for metamorphic white mica from sample DB07RIM53c 92

61. Geochronological data and photographs for sample DB07RIM52a from the Complexe de Tsalabia el Khadra. (*A*) Outcrop photograph of the sample location. (*B, C,* and *D*) show the age distribution and concordia diagrams for the first analysis of sample DB07RIM52a (lab number 952-13). (*E, F,* and *G*) are for the reanalysis (lab number 1284-6).....94

62. (*A*) Outcrop photograph of granite from the sample location for sample DB07RIM51a, Cortège de Gleibat Tenebdar. (*B*) Concordia diagram showing SIMS data.....96

63. Composite age-distribution plots of the four detrital zircon barcodes arranged from young to old down the page. (*A*) The Oujeft barcode, which combines data from samples DB07RIM26a, DB07RIM28a, DB07RIM61a, DB07RIM75a, CT07RIM60-1. (*B*) The Téniagouri barcode, which is based on sample DB07RIM77a. (*C*) The Assabet barcode, which combines data from samples DB07RIM31a, DB07RIM59a, CT07RIM70-1, CT07RIM71-1, and CT07RIM72-1. (*D*) The Char barcode, which is based on combined data from samples DB07RIM23a (reanalysis) and CT22.....97

64. Map of the West African Craton and flanking orogens showing generalized paleocurrent directions (green arrows) and locations of detrital zircon samples that carry the Assabet barcode (blue stars). Paleocurrent directions are from fluvial facies of the Groupe d'Assabet El Hassiane at Guelb El Richat (Moussine-Puchkine and Bertrand-Sarfati, 1997), the Groupe de Cheikhia in the Hank region (Moussine-Puchkine and Bertrand-Sarfati, 1997), the Groupe d'Aioun in the extreme south of Mauritania (Lahondère and others, 2005, their figs. 13 and 14), and the Bombouaka Group in Ghana (Junner, 1940). Detrital zircon locations are from the present study except the Volta Basin and Dahomeyide samples, which are from Kalsbeek and others (2008).....100

65. Four alternative reconstructions of the hypothetical supercontinent Rodinia, as modified from Evans (2009) from the original sources indicated. The continents are shown in the same colors on each Neoproterozoic world map. West Africa is colored brown; its Mauritanide margin is highlighted in red and its Dahomeyide margin in blue. The white arrows in each reconstruction are positioned over the Taoudeni Basin and represent the generalized paleocurrent direction for strata carrying the Assabet barcode, in restored coordinates. The gray belts show Mesoproterozoic ("Grenville-age") orogenic belts that broadly correspond to the age of detrital zircons. None of these reconstructions provides an obvious explanation for Mesoproterozoic detritus on the West African craton 101

66. Proposed reconstruction of a portion of the hypothetical supercontinent Rodinia, modified from Johannson (2009). West Africa's Mauritanide margin is highlighted in red and its Dahomeyide margin in blue. The green arrow is positioned over the Taoudeni Basin; it represents the generalized paleocurrent direction, in restored coordinates, for strata carrying the Assabet detrital zircon barcode. Orogenic belts between 1,300 and 900 Ma are shown in pink. West Africa in this reconstruction is far from any potential zircon sources of this age 102

67. Provisional correlation chart based on detrital zircon results relating unfossiliferous, tectonized strata within the Mauritanide orogen to the essentially flat-lying Taoudeni Basin succession. Boxes correspond to individual samples; colors indicate the detrital zircon barcode assignment. Boxes with black, upward-pointing arrows are positioned at the "maximum depositional age"; actual depositional ages could be younger. Two options are shown for the age of sample DB07RIM29a of the Groupe de Téniagouri, depending on the interpretation of a complex zircon population. Numbers at the bottoms of the vertical columns are keyed to figure 7 102

68. (*A*) Histogram of U-Pb ages from Mauritania, from data in tables 1 and 9. (*B*) Histogram of $^{40}Ar/^{39}Ar$ ages from Mauritania, from data in tables 3 and 9 113

Tables

1. Summary of USGS igneous zircon geochronology results 120
2. Summary of USGS detrital zircon geochronology results 122
3. Summary of USGS $^{40}Ar/^{39}Ar$ geochronology results 131
4. Apatite fission track (AFT analytical data, sample CT07RIM27-1, lab number 952-02 133
5. $^{40}Ar/^{39}Ar$ analytical data ..... link
4. Apatite fission track (AFT analytical data, sample CT07RIM27-1, lab number 952-0 134
6. U-Pb CA-TIMS analytical data 135
7. LAICPMS analytical data ..... link
8. SIMS analytical data ..... link
9. Compilation of published isotopic ages from Mauritania ..... link

Conversion Factors

SI to Inch/Pound

Multiply	By	To obtain
	Length	
centimeter (cm)	0.3937	inch (in.)
millimeter (mm)	0.03937	inch (in.)
decimeter (dm)	0.32808	foot (ft)
meter (m)	3.281	foot (ft)
kilometer (km)	0.6214	mile (mi)
	Area	
hectare (ha)	2.471	acre
square meter (m^2)	0.0002471	acre
square kilometer (km^2)	0.3861	square mile (mi^2)
	Volume	
cubic kilometer (km^3)	0.2399	cubic mile (mi^3)
	Mass	
gram (g)	0.03527	ounce, avoirdupois (oz)
kilogram (kg)	2.205	pound avoirdupois (lb)
megagram (Mg)	1.102	ton, short (2,000 lb)
megagram (Mg)	0.9842	ton, long (2,240 lb)
metric ton per day	1.102	ton per day (ton/d)
megagram per day (Mg/d)	1.102	ton per day (ton/d)
metric ton per year	1.102	ton per year (ton/yr)
	Pressure	
kilopascal (kPa)	0.009869	atmosphere, standard (atm)
kilopascal (kPa)	0.01	bar
	Energy	
joule (J)	0.0000002	kilowatt hour (kWh)

ppm, parts per million; ppb, parts per billion; Ma, millions of years before present; m.y., millions of years; Ga, billions of years before present; 1 micron or micrometer (µor µm) = 1×10^{-6} meters; Tesla (T) = the field intensity generating 1 Newton of force per ampere (A) of current per meter of conductor

Temperature in degrees Celsius (°C) may be converted to degrees Fahrenheit (°F) as follows:

°F=(1.8×°C)+32

Temperature in degrees Fahrenheit (°F) may be converted to degrees Celsius (°C) as follows:

°C=(°F-32)/1.8

Coordinate information is referenced to the World Geodetic System (WGS 84)

Acronyms

AMT	Audio-magnetotelluric
ASTER	Advanced Spaceborne Thermal Emission and Reflection Radiometer
AVIRIS	Airborne Visible/Infrared Imaging Spectrometer
BIF	Banded iron formation
BLEG	Bulk leach extractable gold
BGS	British Geological Survey
BRGM	Bureau de Recherches Géologiques et Minières (Mauritania)
BUMIFOM	The Bureau Minier de la France d'Outre-Mer
CAMP	Central Atlantic Magmatic Province
CGIAR-CSI	Consultative Group on International Agricultural Research-Consortium for Spatial Information
DEM	Digital Elevation Model
DMG	Direction des Mines et de la Géologie
EC	Electrical conductivity
EMPA	Electron Microprobe Analysis
EM	Electromagnetic (geophysical survey)
EOS	Earth Observing System
eU	Equivalent uranium
GGISA	General Gold International
GIF	Granular iron formation
GIFOV	Ground instantaneous field of view
GIS	Geographic Information System
HIF	High grade hematitic iron ores
IHS	Intensity/Hue/Saturation
IAEA	International Atomic Energy Agency
IOCG	Iron oxide copper-gold deposit
IP	Induced polarization (geophysical survey)
IRM	Islamic Republic of Mauritania
JICA	Japan International Cooperation Agency
JORC	Joint Ore Reserves Committee (Australasian)
LIP	Large Igneous Province
LOR	Lower limit of reporting
LREE	Light rare-earth element
METI	Ministry of Economy, Trade and Industry (Japan)
MICUMA	Société des Mines de Cuivre de Mauritanie
MORB	Mid-ocean ridge basalt
E-MORB	Enriched mid-ocean ridge basalt
N-MORB	Slightly enriched mid-ocean ridge basalt
T-MORB	Transitional mid-ocean ridge basalt
Moz	Million ounces
MVT	Mississippi Valley-type deposits

NASA	United States National Aeronautics and Space Administration
NLAPS	National Landsat Archive Processing System
OMRG	Mauritanian Office for Geological Research
ONUDI	(UNIDO) United Nations Industrial Development Organization
PRISM	Projet de Renforcement Institutionnel du Secteur Minier
PGE	Platinum-group elements
RC	Reverse circulation drilling
REE	Rare earth element
RGB	Red-green-blue color schema
RTP	Reduced-to-pole
SARL	Société à responsabilité limitée
SEDEX	Sedimentary exhalative deposits
SIMS	Secondary Ionization Mass Spectrometry
SNIM	Société National Industrielle et Minière (Mauritania)
SP	Self potential (geophysical survey)
SRTM	Shuttle Radar Topography Mission
SWIR	Shortwave infrared
TDS	Total dissolved solids
TIMS	Thermal Ionization Mass Spectrometry
TISZ	Tacarat-Inemmaudene Shear Zone
TM	Landsat Thematic Mapper
UN	United Nations
UNDP	United Nations Development Program
US	United States
USA	United States of America
USGS	United States Geological Survey
UTM	Universal Transverse Mercator projection
VHMS	Volcanic-hosted massive sulfide
VisNIR	Visible near-infrared spectroscopy
VLF	Very low frequency (geophysical survey)
VMS	Volcanogenic massive sulfide deposit
WDS	Wavelength-dispersive spectroscopy
WGS	World Geodetic System

Second Projet de Renforcement Institutionnel du Secteur Minier de la Republique Islamique de Mauritanie (PRISM-II)

Synthesis of Geological, Structural, and Geochronologic Data:

Phase V, Deliverable 53

By Dwight C. Bradley,[1] Paul O'Sullivan,[2] Michael A. Cosca,[3] Holly A. Motts,[4] John D. Horton,[5] Cliff D. Taylor,[6] Georges Beaudoin,[7] Gregory K. Lee,[8] Jahan Ramezani,[9] Dan B. Bradley,[10] Jamey V. Jones,[11] and Samuel Bowring[12]

This report is a companion to the new Geologic Map of Mauritania (Bradley and others, 2015; referred to herein as "Deliverable 51") and the new Structural Geologic Map of Mauritania (Bradley and others, 2015a; referred to herein as "Deliverable 52"). Section 1 contains explanatory information for these two digital maps. Section 2 covers the analytical methods used in obtaining new U-Pb ages from 9 igneous rock samples, new detrital zircon ages from 40 sedimentary or metasedimentary rock samples, and new $^{40}Ar/^{39}Ar$ ages from 12 samples of metamorphic rocks and veins. Sections 3 through 6 present the new geochronological results, organized by region. In Section 7, we discuss implications of the new ages for the regional geology and discuss problematic results. Finally, in Section 8, we summarize the geology and tectonic evolution of Mauritania in narrative form, drawing on new and published information, in the context of global tectonics.

The report is being released in both English and French. In both versions, we use the French-language names for formal stratigraphic units.

[1] U.S. Geological Survey, 4210 University Drive, Anchorage, Alaska 99508, U.S.A., email dbradley@usgs.gov. Task leader for geologic map compilation; manuscript preparation and graphics; SIMS zircon geochronology.

[2] Apatite to Zircon, Inc., 1075 Matson Rd., Viola, ID 83872 USA. LAICPMS zircon geochronology; apatite fission-track thermochronology.

[3] U.S. Geological Survey, Denver, Colorado 80225, U.S.A. $^{40}Ar/^{39}Ar$ geochronology.

[4] U.S. Geological Survey, 4210 University Drive, Anchorage, Alaska 99508, U.S.A. GIS map compilation.

[5] U.S. Geological Survey, Denver, Colorado 80225, U.S.A. GIS map compilation.

[6] U.S. Geological Survey, Denver, Colorado 80225, U.S.A. Overall project lead; economic geology; geochronology sampling.

[7] Département de Géologie et de Génie Géologique, 1065 avenue de la Médecine, Québec (Québec) Canada G1V 0A6. Economic geology; geochronology sampling.

[8] U.S. Geological Survey, Denver, Colorado 80225, U.S.A. GIS map compilation.

[9] Dept. of Earth and Planetary Sciences, Massachusetts Institute of Technology, 77 Massachusetts Avenue Cambridge, MA 02139-4307. TIMS zircon geochronology.

[10] U.S. Geological Survey volunteer; now at Harvard University. SIMS zircon geochronology.

[11] U.S. Geological Survey, 4210 University Drive, Anchorage, Alaska 99508, U.S.A. SIMS zircon geochronology.

[12] Dept. of Earth and Planetary Sciences, Massachusetts Institute of Technology, 77 Massachusetts Avenue Cambridge, MA 02139-4307. TIMS zircon geochronology.

1.0. Geologic Map and Structural Geologic Map

The Geologic map of Mauritania (deliverable 51) and the structural geologic map of Mauritania (deliverable 52) were prepared in ARC-GIS v. 10.0. Although the GIS layers are scale-independent, the intended scale for the printed versions is 1:1,000,000. The Arc-GIS geodatabase (v.10) and shapefiles are provided as part of deliverable 92.

1.1. Sources of Information

The maps were compiled by stitching together a number of GIS coverages (fig. 1) from the PRISM-I effort. The following were provided to the U.S. Geological Survey by the Ministère des Mines et de l'Industrie.

- Phase 1, north: geologic mapping in southern Mauritania by the British Geological Survey (BGS), with accompanying legends for both 1:200,000 and 1:500,000 scales (Pitfield and others, 2004).
- Phase 1, south: geologic mapping in northern Mauritania by the Bureau de Recherches Géologiques et Minières (BRGM) with accompanying legends for both 1:200,000 and 1:500,000 scales (Lahondère and others, 2003).
- Phase 1a, northwest: remapping of a portion of BRGM's Phase 1 area in northern Mauritania by the BGS, with accompanying legends for both 1:200,000 and 1:500,000 scales (O'Connor and others, 2005).
- Phase 1a, extreme south: remapping of a portion of BGS's Phase 1 area in southernmost Mauritania by the BRGM, with accompanying legends for both 1:200,000 and 1:500,000 scales (Lahondère and others, 2005).
- New, unpublished mapping of eight 1:200,000-scale sheets by BRGM in the Tagant region, with accompanying rock-unit descriptions in the GIS, but no legend.

The USGS Mauritania project was provided with 32 individual shapefiles of the BGS 1:200,000-scale ("200K") geologic mapping and three shapefiles of the BGS 1:500,000-scale ("500K") geologic mapping (North1, North2, and South). The 500K files already had the 200K files burned into them. These merged 500K maps had been subject to an automated GIS smoothing routine; many vertices were deleted during this procedure, altering the geologic contacts. The merged 500K maps also had been simplified, with the deletion of certain geologic polygons that we deemed too important to not show. We therefore opted to revert to all the original 200K shapefiles, and used the 500K maps only where this was the only option. The problem just described resulted in linework discrepancies between 200K and 500K maps. Minor GIS-induced discrepancies were rectified using Google Earth imagery.

Another source that we consulted is a new bedrock geologic map of Mauritania at 1:1,000,000 scale, which was compiled by BRGM (Lahondère and others, 2010) while the present study was underway. The GIS database used to generate that map was not provided to USGS, but a rasterized pdf was.

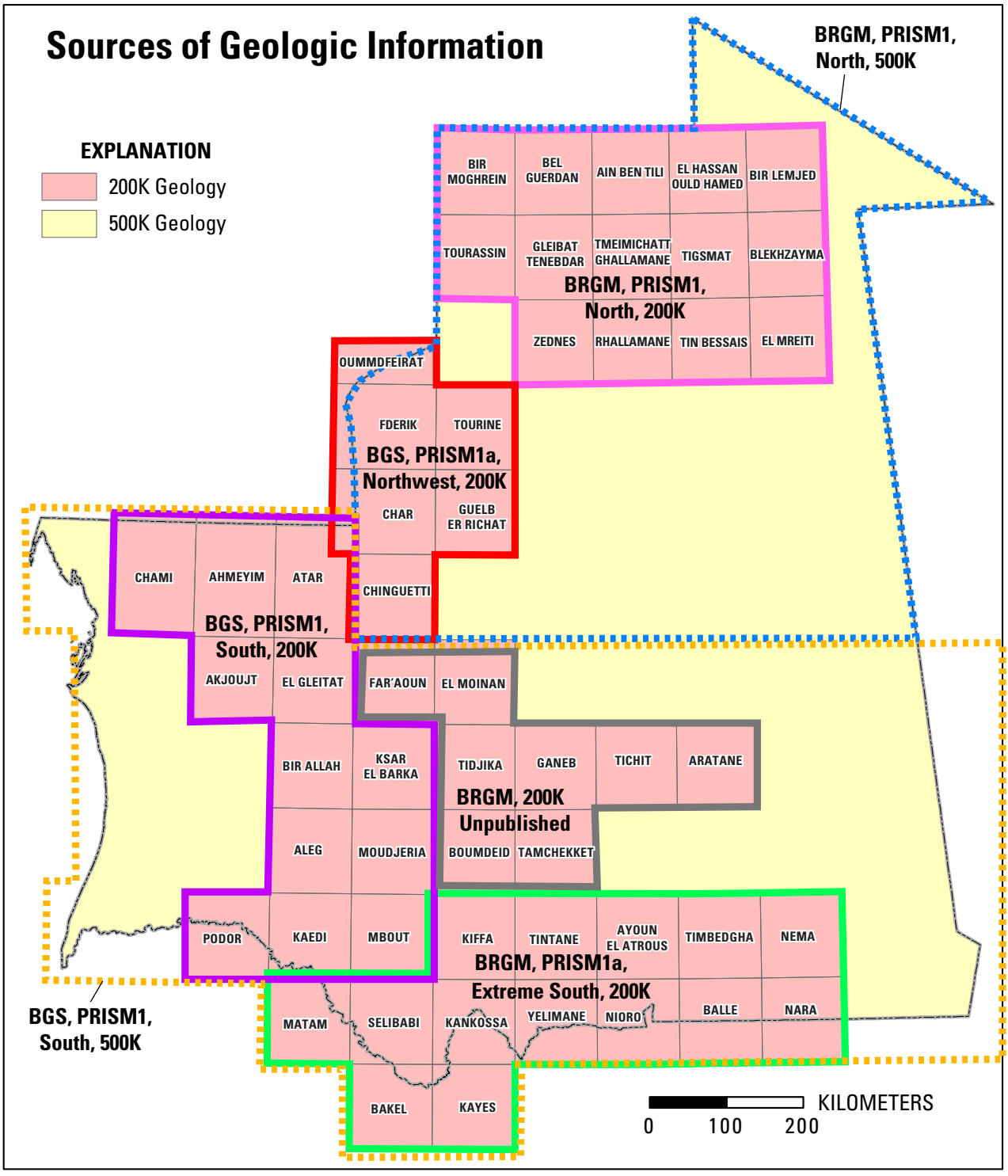


Figure 1. Map of Mauritania (outlined in gray) showing sources of map information. The 1:200,000-scale geologic quadrangles are numbered using the coordinates of the southeastern corner of each sheet; for the Atar sheet, number 2014, this point is at 20°N., 14°W.

1.2. Mapping Conflicts

Another type of mismatch was found along the boundaries between areas that had been mapped by two different teams. Because any geologic map is based on a combination of observation and inference, two mappers are unlikely to produce identical maps of complicated rocks. In such cases, we chose the most recent mapping on the grounds that the newer map had an older one to build on. Thus we adopted the Phase 1a maps: the BGS "Northwest" mapping and the BRGM "Extreme South" mapping. There is no question that a seamless map *looks* better, but moving mapped geologic features for cosmetic reasons alone is an unsound scientific practice. Accordingly, in preparing the 1:1,000,000-scale Geologic Map and Structure Map, we deliberately left any boundary discrepancies where the Phase 1a Northwest, Phase 1a Extreme South, and Tagant map-regions join the older mapping.

1.3 Map Units

Some of the geologic detail that was shown on the original map sheets is impossible to resolve at 1:1,000,000 scale. In addition, certain details are unimportant at the national scale and only clutter the big picture. We consolidated rock units, focusing on the level of Groupes, Cortèges, and Complexes, which correspond to the terms Group, Suite, and Complex, respectively (North American Commission on Stratigraphic Nomenclature, 1983). Thus, the Groupe d'Atar went from 10 mapped formations on the 1:200,000-scale Chinguetti sheet to two divisions on the national-scale map. For straightforward plutonic suites (cortèges), we combined similar rock types, for example lumping all six granitic map-units in the Cortège des Sfariat into a single unit. For complexes, we consolidated on a case-by-case basis; in the Groupe d'Imourène, for example, we reduced the number of units from six to two by combining the igneous components into one unit and the sedimentary units into another.

Some stratigraphic units are too thin to show on a national-scale map and therefore were combined with adjacent units. Small polygons, for example of Quaternary sediments over a single bedrock unit, are not shown.

1.4 Color Scheme

The color scheme is intended to bring out the geology at the level of groupe, cortège, and complexe. Each of these is assigned a basic background color. Subdivisions are discriminated by overprint patterns in various colors. Certain units such as banded iron formations—too important to omit but small enough to be hard to see—are shown as polygons with a heavier-than-normal outline, making them visible at 1:1,000,000 scale.

1.5 Map-Units and Abbreviations

For the French-language version of the map, abbreviations for geologic units continue the scheme developed during PRISM Phase 1. As noted above, rock units are organized at the level of groupe, cortège, and complexe. These are identified on our map with two uppercase letters or one uppercase and one lowercase letter; they are the same as on the 1:200,000-scale legends for the PRISM Phase 1 and 1a map areas (Lahondère and others, 2003, 2005; Pitfield and others, 2004; O'Connor and others, 2005). Subdivisions below the level of groupe, cortège, and complexe are indicated by one more additional lowercase letters, or in a few cases, numbers. Wherever possible, these are the same as used on the PRISM Phase 1 and 1a legends; but some of our map units are new combinations requiring new abbreviations.

1.6 Structure Map (Deliverable 52)

The 1:1,000,000-scale Structural Geology Map of Mauritania was compiled from the same digital sources as the Geologic Map (deliverable 51). A simplified geologic map with a subdued color scheme serves as the base; the purpose is to show the first-order age constraints for the various structures. The rocks on the base map are divided into 14 units. We distinguish supracrustal rocks (sedimentary, volcanic, and metamorphic equivalents) versus intrusive rocks and mid- to lower-crustal rocks for each major age division (Archean, Paleoproterozoic, Mesoproterozoic, Neoproterozoic, Phanerozoic, and Quaternary).

The Structure GIS database consists mostly of line features plus a few point features. The faults and dikes on the Structural Geology Map are the same as on the Geologic Map. As indicated in the legend to the structure map, faults are subdivided into sinistral and dextral strike-slip faults, normal faults, thrust (includes reverse) faults, faults of unknown sense, and shear zones. Dikes are subdivided by a combination of age and composition into five categories. Anorthosite dikes are undated but most likely Archean in age, judging from the new Archean zircon ages from anorthosites as reported below. Dikes classed as "Neobirimian" are inferred to be Paleoproterozoic and late orogenic with respect to ca. 2-Ga orogenic events. Felsic versus mafic

dikes of this age group are differentiated on the various 1:200,000-scale geologic quadrangles sheets but are lumped together on the national geologic map. Dikes that are classed as "Post-Birimian" are mainly, if not entirely, related to CAMP, the Central Atlantic Magmatic Province, dated at ca. 200 Ma. The BRGM and BGS used somewhat different classifications of the dikes; our scheme adopted those elements of the two classifications that could be uniformly applied across the country as a whole. To reduce clutter at 1:1,000,000 scale, some faults and some dikes in the GIS database were rendered invisible.

1.7 Acknowledgments

USGS geologic studies in Mauritania built on the excellent work of the Bureau de Recherches Géologiques et Minières and British Geological Survey during Phases 1, 1a, Extreme South, and Central Zone of the PRISM project (Lahondère and others, 2003, 2005, 2010; Marot and others, 2003; Salpeteur, 2005; Pitfield and others, 2004; Gunn and others, 2004; O'Connor and others, 2005). The BRGM group included Didier Lahondère, D. Artignan, A. Cocherie, M. Donzeau, J.-C. Goujou, A.C. Guerrot, F. Guillocheau, C. Helm, A. Marot, J. Le Métour, J.-P. Milesi, Alexis Moussine-Pouchkine, G. Recoche, J. Roger, Ignace Salpeteur, G. Stein, and Denis Thiéblemont. The BGS group included Peter E.J. Pitfield, A.G. Gunn, Eugene A. O'Connor, R.P. Barnes, S. Clarke, S. Coats, John Ford, M. Gillespie, M.P.H. Hawkins, M.S.A. Horstwood, Roger M. Key, S. Loughlin, J.A. McKervey, J. Powell, David I. Schofield, and C.N. Waters. Mauritania now ranks as one of the world's best-mapped countries as a result of these geologic studies.

The USGS research program in Mauritania was facilitated by Mr. Samory Ould Soueidatt, Dr. Mohamed Yeslem Ould El Joud, and Mr. Abdarrahmane Ould Daddah of PRISM; by Director Wane Ibrahima Lamine and geologists Dr. Ely El Mahjoub, Mr. Abdallahi Brahim Khlil, and Mr. Alassane Konate of the DMG; and by former Minister Mohamed El Moctar Ould Mohamed El Hacen and Minister Taleb Abdival of the Ministre du Petrole et des Mines. USGS field parties in 2007 were accompanied by Mauritanian geologists Ahmed Taleb Mohamed, Baydi Thiam, Sid-Ahmed Bouderballa, Abdoullah Samoury, and Mohamed Abdellahi Ould Jeddar. Mike Blackwell and Merlin Thomas of 1st Quantum Minerals, Ltd. helped with arrangements and access at Guelb Moghrein. In the Zouerate district, Mr. Mohamed Ould Woyssatt, Mr. Szymon Oksengorn, and Mr. Ghali Amar of SNIM and Dr. Ahmed Salem Ben Mohamedou of PRISM provided access and field trips.

Logistics during five weeks of field work were handled by Mr. Cheikh Mohamed Abdallahi Atigh of SOMACOGIR. Colonel Sidi Ould Ely Sari, Captain Med-Mahd Ould Ethmane, and a platoon of soldiers from the National Army of Mauritania provided security during field work in northeastern Mauritania. Mr. Tihiya was our desert guide.

We especially thank Andrew Killick and Arthur Merschat for careful reviews that substantially improved this report. These same geologists also reviewed the geologic map of Mauritania (deliverable 51) and the structural geologic map of Mauritania (deliverable 52). Keith Labay and Nora Shew helped with GIS.

2.0 Geochronology

The bulk of this report is on new geochronology. Samples were collected in 2007 during two joint USGS-Mauritania Geological Survey field trips to mineral exploration targets. The USGS effort was a follow-up to geologic mapping in 2001–2005 by the BGS and BRGM in cooperation with the Mauritanian Geological Survey under the acronym "PRISM" (Pitfield and others, 2004; Lahondère and others, 2003; Lahondère and others, 2005; O'Connor and others, 2005). The new results are summarized in tables 1, 2, and 3; ARC-GIS compatible versions of these tables are provided as part of Deliverable 92. Analytical data are provided in tables 4 through 8. Locations of USGS geochronology samples are shown in figures 2, 3, and 4.

Also included in this report is a compilation of previous geochronology. The most reliable dated ages from the literature are listed in table 9; an ARC-GIS compatible version of this table is provided as part of Deliverable 92. Corresponding sample locations shown in figures 5 and 6.

Our new results shed light on the geology and evolution of four of Mauritania's main bedrock provinces. The oldest rocks are in the Rgueïbat Shield in northern Mauritania (fig. 7). The western part of the shield is Mesoarchean in age. It is flanked to the northeast by a Paleoproterozoic orogen, which is commonly referred to as "Eburnean" or "Birimian" after broadly comparable rocks in a broadly equivalent position, albeit 1,100–1,200 km distant, in the southern part of the West African Craton. The Mauritanide orogen is a deeply eroded Neoproterozoic to Permian mountain belt along the western margin of the West African Craton. The foreland basin of the Mauritanides merges with a broad intracratonic basin, the Taoudeni Basin, which contains flat-lying strata ranging from Mesoproterozoic to Cretaceous in age. The western part of the Mauritanide orogen is buried by coastal-plain deposits of the present-day passive margin, which developed during the Jurassic and has been subsiding episodically since then.

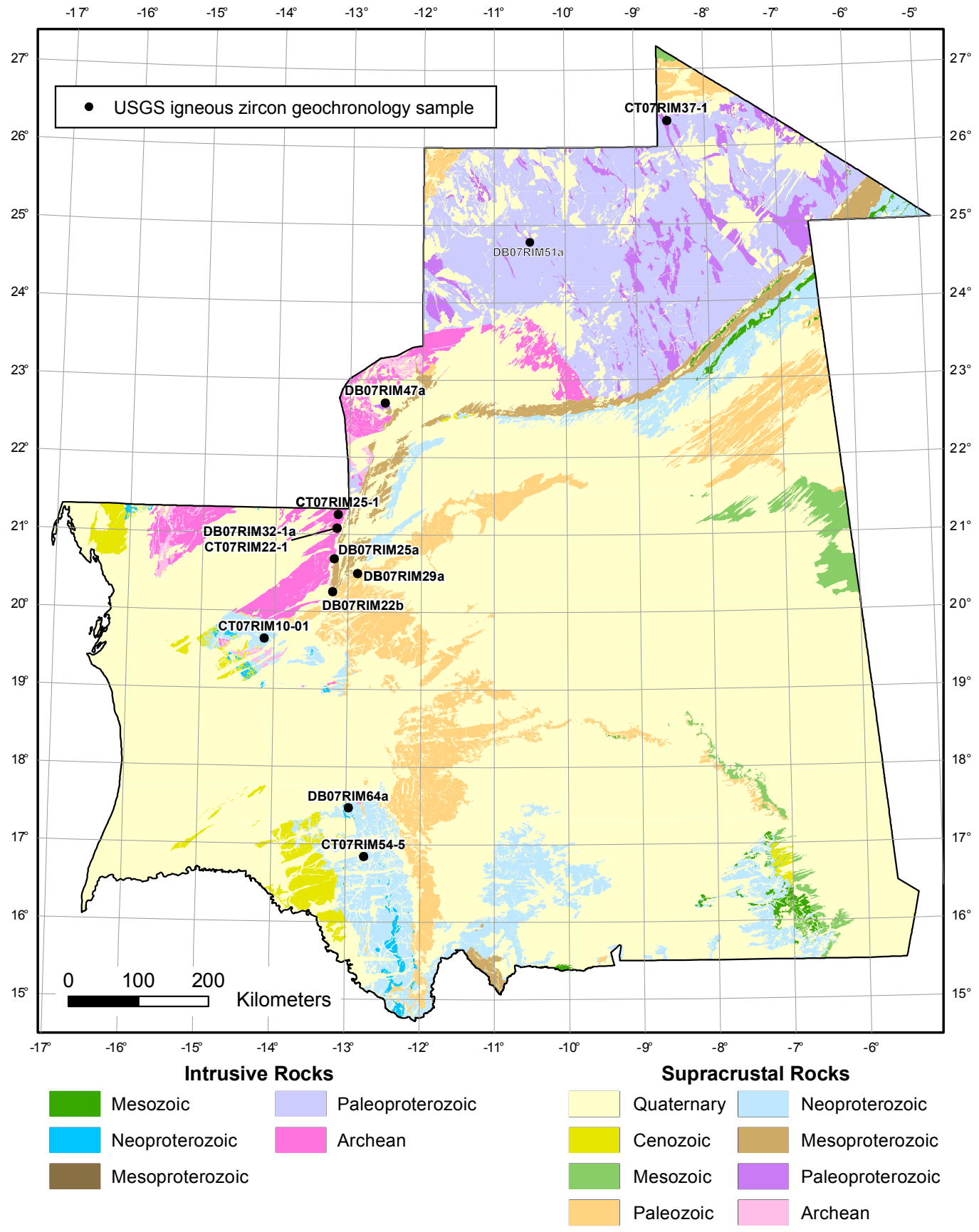


Figure 2. Generalized geologic map of Mauritania showing sample locations for new U-Pb igneous ages.

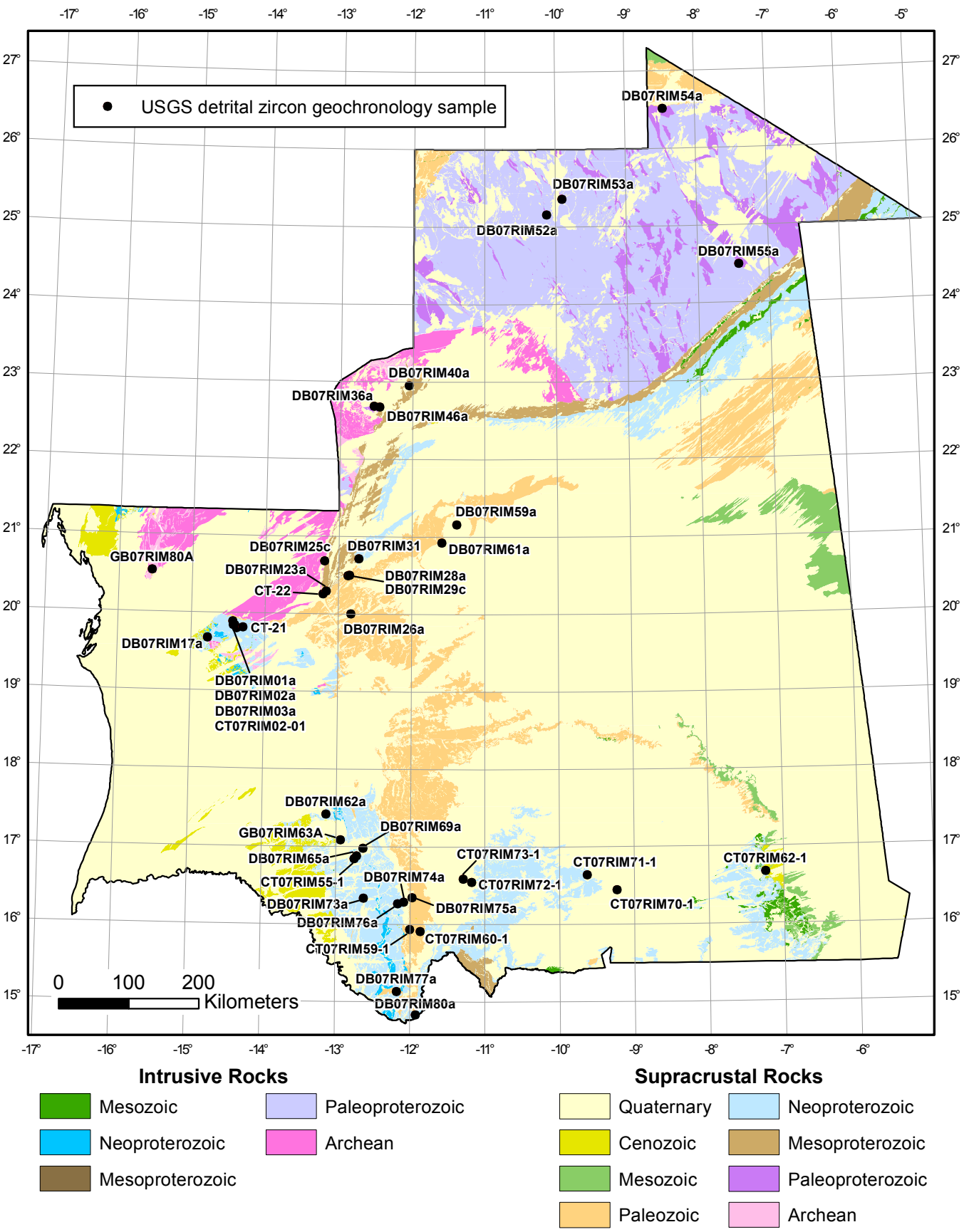


Figure 3. Generalized geologic map of Mauritania showing sample locations for new U-Pb detrital zircon ages.

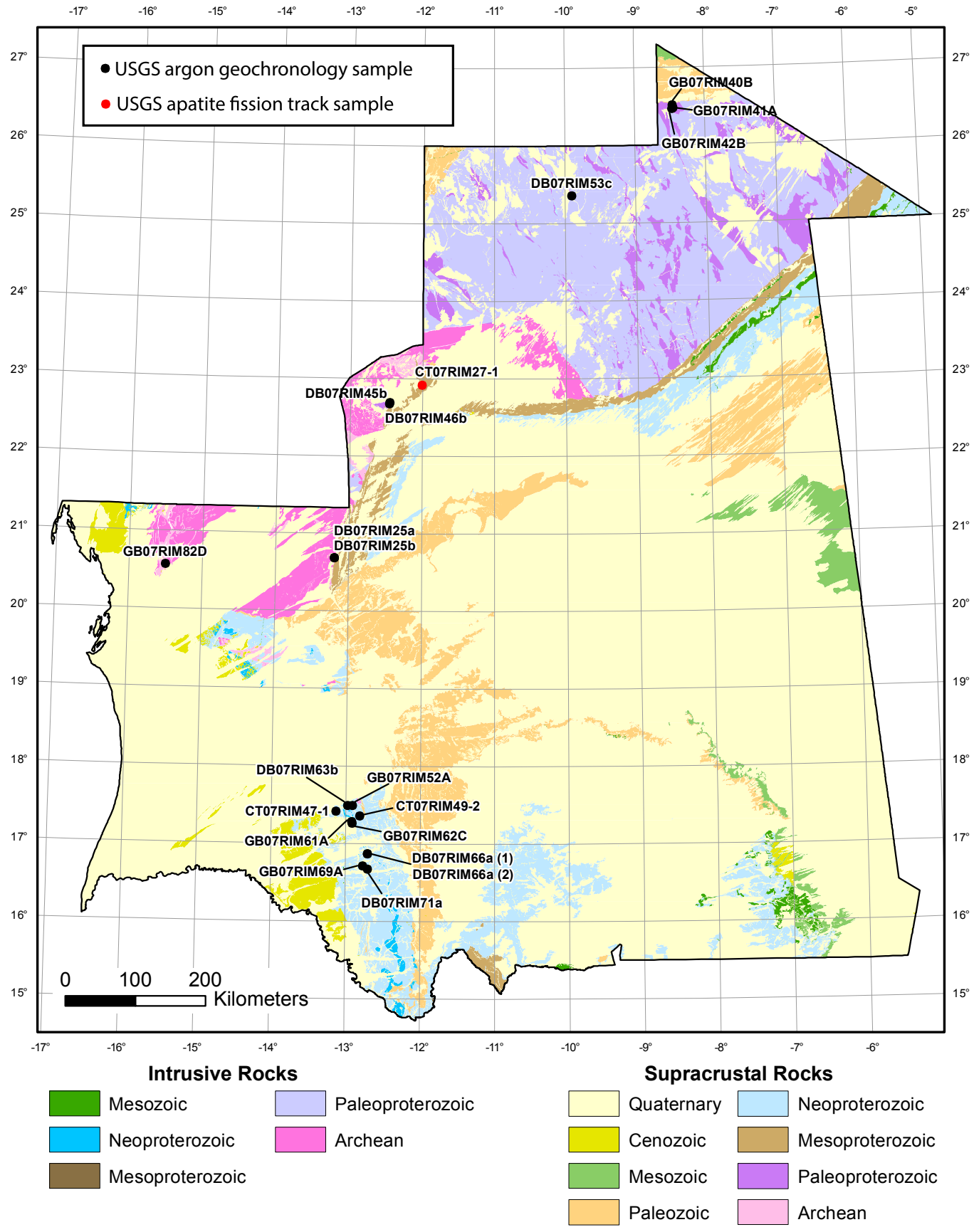


Figure 4. Generalized geologic map of Mauritania showing sample locations for new $^{40}Ar/^{39}Ar$ and apatite fission track ages.

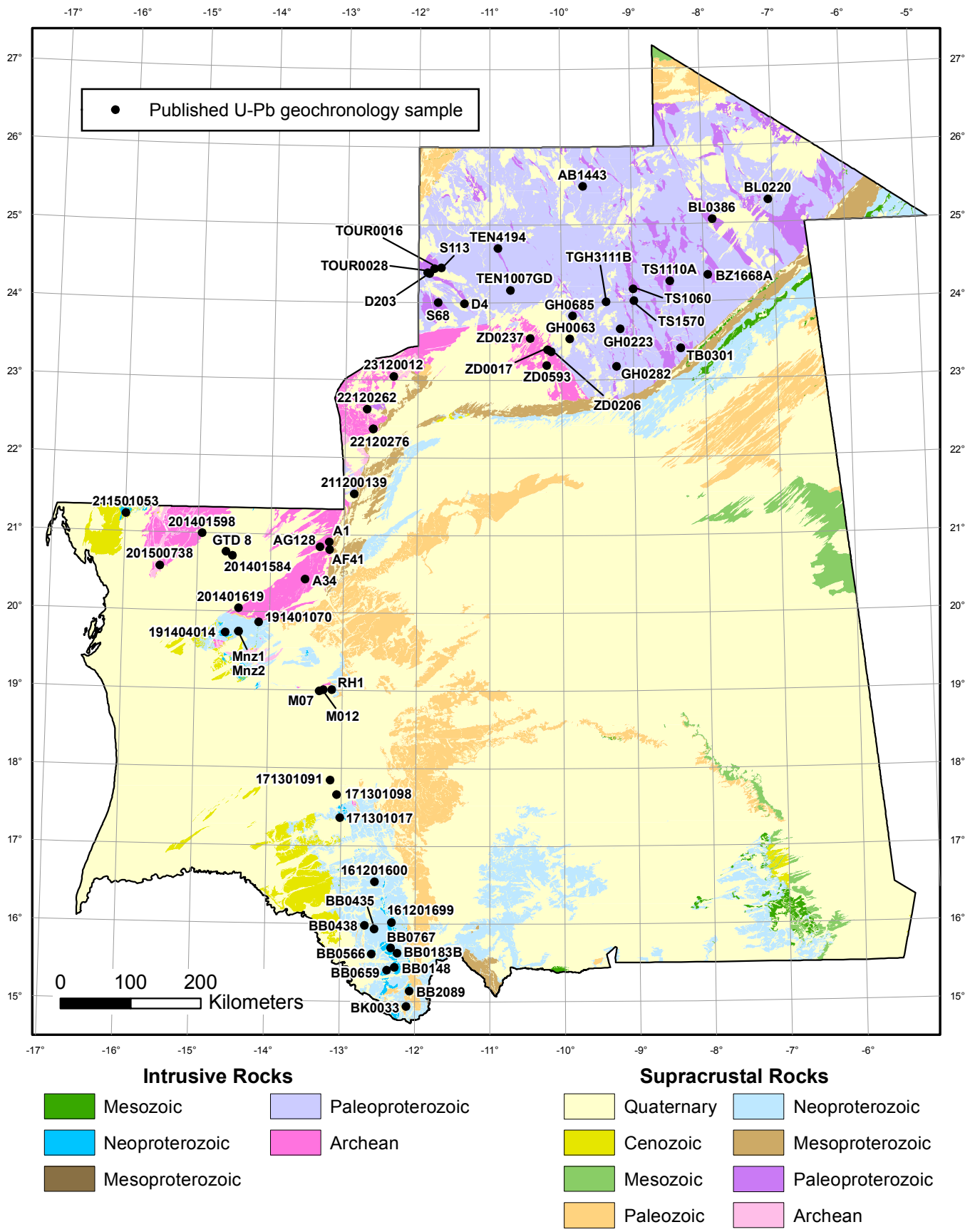


Figure 5. Generalized geologic map of Mauritania showing U-Pb geochronology sample locations from published literature. Ages are summarized in table 9.

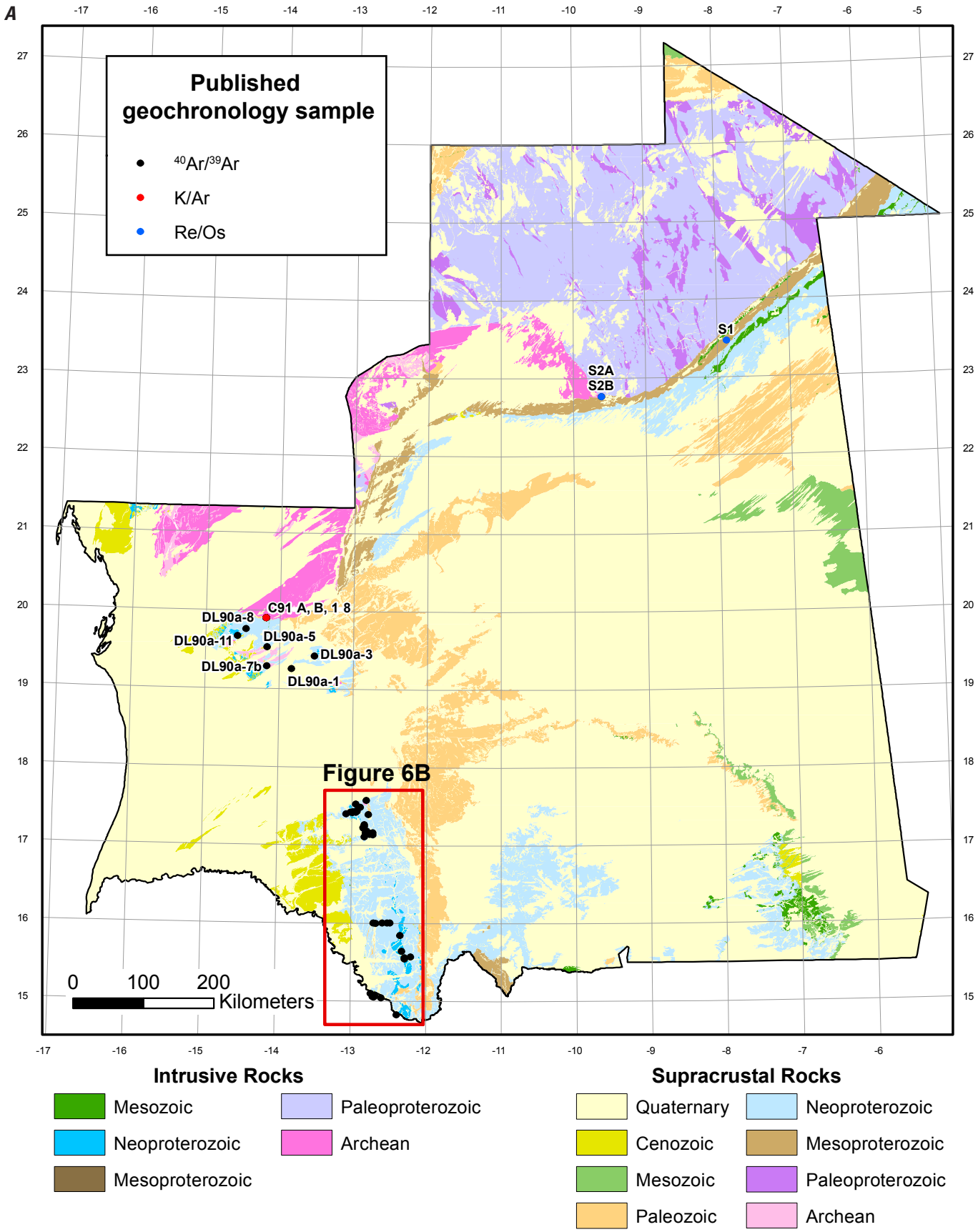


Figure 6. (*A*) Generalized geologic map of Mauritania showing $^{40}Ar/^{39}Ar$, K/Ar, and Re/Os geochronology sample locations from published literature. (*B*) Detail for the Central Mauritanides.—Continued

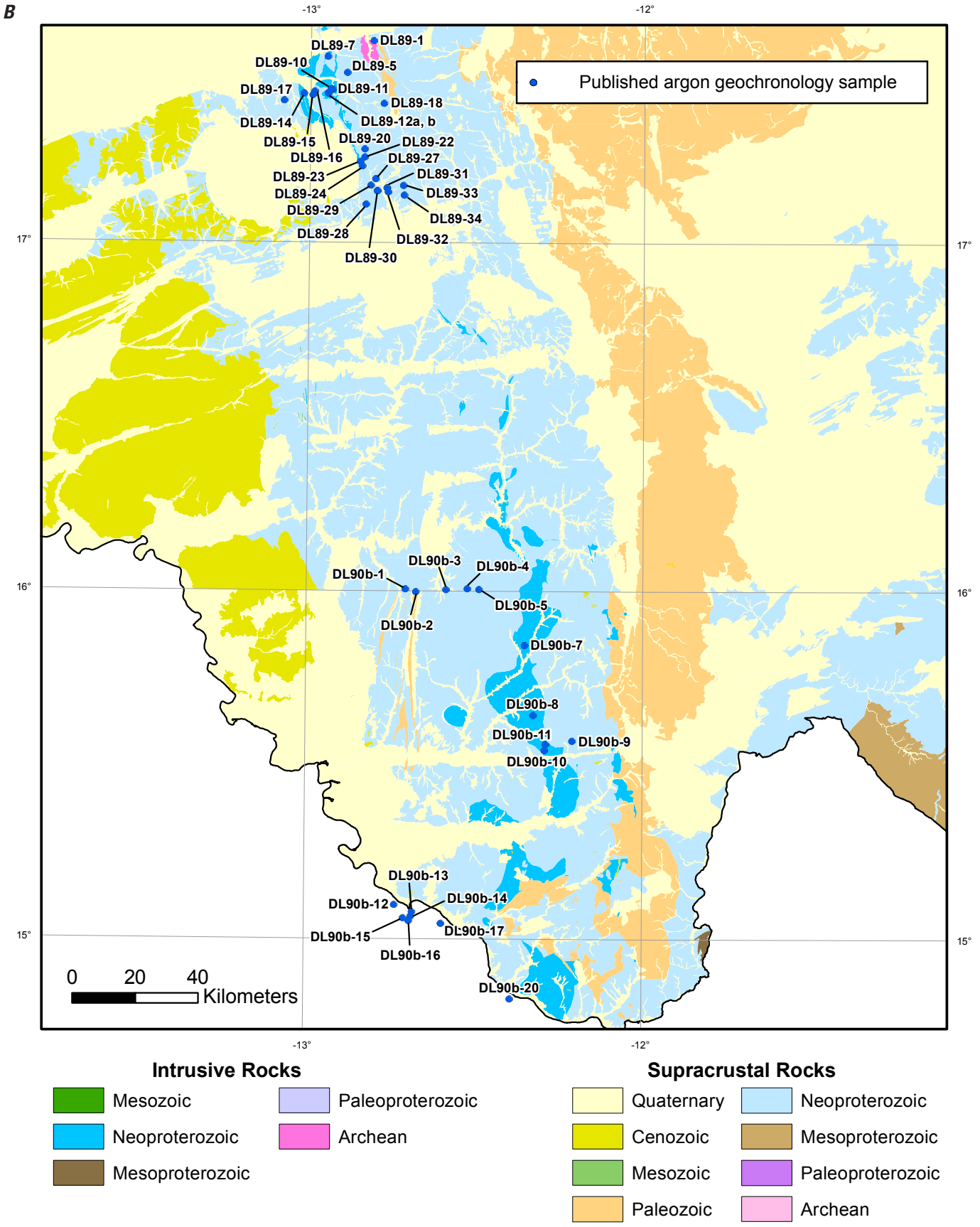


Figure 6. (*A*) Generalized geologic map of Mauritania showing $^{40}Ar/^{39}Ar$, K/Ar, and Re/Os geochronology sample locations from published literature. (*B*) Detail for the Central Mauritanides.

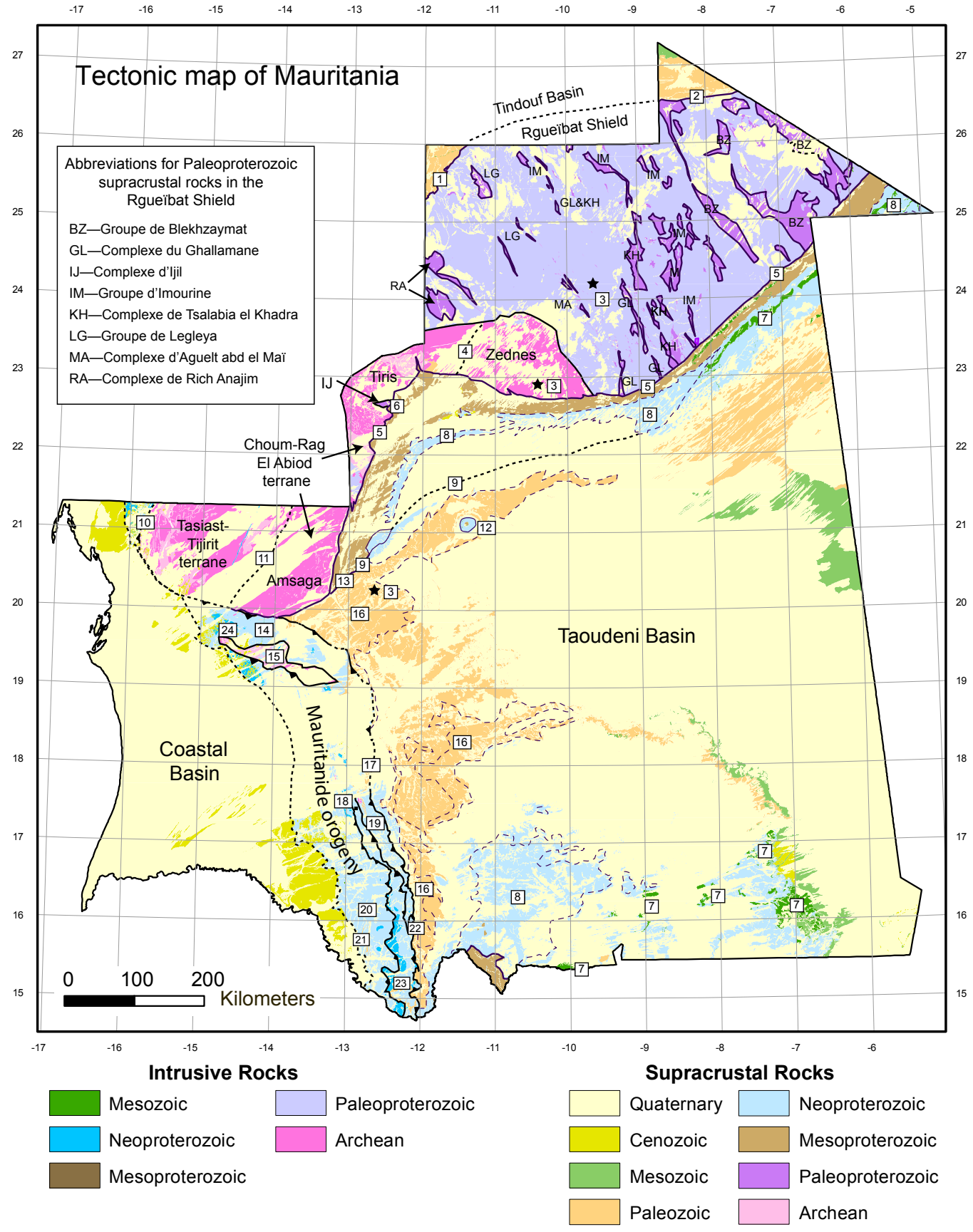


Figure 7. Generalized tectonic map of Mauritania, adapted, in part, from maps by Pitfield and others (2004) and Lahondère and others (2003, 2005). Key to numbered localities: 1—Unconformity below Cambrian-Ordovician, western Tindouf Basin; 2—Unconformity (continued)

below Ordovician, eastern Tindouf Basin; 3—Astroblem; 4—Approximate boundary between Zednes and Tiris Archean domains; 5—Unconformity below Mesoproterozoic Groupe de Char; 6—Taziast klippe; 7—Mafic sills of Central Atlantic Magmatic Province, CAMP; 8—Assabet foreland-basin deposits; 9—Unconformity below Groupe de Jbéliat glacial deposits; 10—Frontal thrust in Northern Mauritanides; 11—Tacarat-Inemmaudene Shear Zone; 12—Guelb er Richat, subsurface laccolith; 13—Stratigraphic section in Figure 8; 14—Akjoujt sector of Mauritanide thrust belt; 15—Archean tectonic windows beneath Mauritanide thrust belt; 16—Oujeft foreland-basin deposits; 17—Frontal thrust in Central Mauritanides; 18—Early Neoproterozoic basement in Central Mauritanides; 19—Parautochthon in Central Mauritanides; 20—Allochthon in in Central Mauritanides; 21—Unconformity below Mesozoic-Cenozoic coastal basin deposits; 22—Kandou Formation, Hercynian foreland basin; 23—Gorgol Noir suture zone in Central Mauritanides; 24—Inchiri district.

During the sampling program, the USGS field party covered more than 5,000 km in about five weeks. Tight scheduling (and at times, precautions demanded by our military escort) left inadequate time at many sample locations to fully document field relations. Under these conditions, we simply drove through a belt of one or another poorly dated unit until we came to outcropping bedrock, relying on a GPS-enabled laptop tied to the GIS geologic coverages of the PRISM-I mapping.

2.1. Analytical Methods

The new dates were obtained for a variety of purposes using five techniques. Technical details are provided in the appendix.

The apatite-fission-track (AFT) method was used on one sample in an attempt to date supergene enrichment. The AFT analysis was done by Paul O'Sullivan of Apatite to Zircon, Inc. Analytical data are given in table 4.

$^{40}Ar/^{39}Ar$ ages were obtained on white mica from metamorphic rocks (five samples) and hydrothermal veins (seven samples). Analyses were done by Michael Cosca at the U.S. Geological Survey Argon Geochronology Lab in Denver. These record cooling below about 350° C and constrain the ages of metamorphism and hydrothermal mineralization, respectively. Argon analytical data are given in table 5.

Zircons were dated by the U-Pb method using three different analytical techniques. The most precise and accurate results were obtained by means of the CA-TIMS method (Chemical Abrasion-Thermal Ionization Mass-Spectrometry) on single crystals. In conventional TIMS analysis, zircon grains or grain fragments are dissolved in acid, Pb and U are chemically purified, and the various isotopes of Pb and U are then analyzed. "Chemical abrasion" refers to an innovative new step that is done before anything else, during which grains are annealed at high temperatures and then *partially* digested in acid to remove those damaged portions of each zircon most likely to cause problems with the age determination (Mattinson, 2010). We used the CA-TIMS method on one sample, an ash layer a few meters above the Jbéliat tillite, to accurately place it in the chain of Neoproterozoic glacial events. The CA-TIMS analysis was done at Massachusetts Institute of Technology by Jahan Ramezani and Samuel Bowring. CA-TIMS analytical data are given in table 6.

Most of our zircon samples were dated using Laser-Ablation Inductively Coupled Mass-Spectrometry (LAICPMS) by Paul O'Sullivan (of Apatite to Zircon, Inc.) at Washington State University. This method uses a laser beam to liberate U and Pb from the target zircon, obliterating most of the grain. Whereas it generally yields less precise ages than CA-TIMS, this technique is far less expensive and allows for the analysis of many individual zircons from a given sample. All but a few of our detrital zircon analyses were done using the LAICPMS method. Unless otherwise specified, we analyzed 120 individual grains per sample. This is enough to justify stringent standards for filtering out discordant results, which are potentially misleading. In plotting the histogram and probability density curve for each sample we discounted (1) results having error/age greater than 4% (that is, large error ellipses); (2) results having a probability of concordance less than 0.15 as per Ludwig (1998); (3) results having fewer than 5 of 47 concordant scans; and (4) failed analyses. The effects of filtering can be seen by comparing the filtered versus unfiltered concordia diagrams for particular samples. We also used the LAICPMS method on a few plutonic and volcanic samples. This is useful in the case of volcanic rocks containing a mix of igneous and detrital zircons, or any igneous rocks having many but not all grains plagued by lead loss or inheritance. Concordia ages, which were calculated using the Isoplot Excel add-in (http://www.bgc.org/isoplot_etc/isoplot.html) are quoted for LAICPMS zircon analyses. LAICPMS analytical data are given in table 7.

A few igneous- and detrital-zircon samples were dated using Secondary Ion Mass Spectrometry (SIMS) at the USGS-Stanford SHRIMP-RG facility at Stanford University. Analyses were done in four sessions between 2007 and 2012 by Dwight Bradley, Cliff Taylor, Jamey Jones, and Dan Bradley in various combinations. The SIMS method uses a narrow ion beam to liberate U and Pb from a shallow spot that is typically much smaller than the target zircon. This makes it particularly useful for obtaining useful ages out of zircons with complex zoning, such as inherited cores or metamorphic rims. For igneous ages, 10 to 20 zircons are typically analyzed; for detrital ages, 60 zircons are typically analyzed. For SIMS analyses, we quote the $^{206}Pb/^{238}U$ age for ages under 1,000 Ma and the $^{207}Pb/^{206}Pb$ age for anything older. Following common protocols for this lab, we discounted results having the ratio error/age greater than 4 percent (that is, large error ellipses); and we discounted results having a calculated

discordance greater than 10 percent or 20 percent as indicated on the diagrams for particular samples. SIMS analytical data are given in table 8.

A few general comments about the rapidly advancing field of detrital zircon geochronology are provided for background. Most zircons crystallize from granitic melts or are of metamorphic origin. Zircon grains are durable and commonly survive the weathering process to become detrital grains in sedimentary rocks. The U-Pb zircon ages obtained from a sandstone or metasandstone typically include some that are concordant (generally interpreted as original igneous ages) and some that are discordant (generally due to partial lead loss, inheritance, or perhaps a combination). The standard practice is to filter for concordance and thus eliminate those grains whose ages are less reliable and potentially misleading. Detrital zircon data can yield several types of information that bear on problems of regional geology and tectonic evolution. At least in active tectonic settings, detrital zircons commonly provide age constraints on the depositional age of the host sandstone or metasandstone, which can be no older than the youngest concordant igneous zircon age. Protocols for assigning a "maximum depositional age" to a rock unit based on detrital zircons have been discussed by Dickinson and Gehrels (2009). In this study, we use their "YPP" criterion, that is, the youngest graphical peak in the probability density plot of filtered zircon ages. Zircon age constraints are especially valuable in strata that are devoid of fossils—a condition that can be linked to the age of the strata, the depositional environment, the state of deformation, the state of metamorphism, a lack of mapping, or some combination of these factors. Detrital zircon age distributions can be used to evaluate possible correlations between sandstone-bearing stratigraphic units. This information has applications in geologic mapping at the local scale, for example, in assigning problematic rocks to one or another map unit, and on a regional scale in matching displaced parts of an originally continuous sedimentary or metasedimentary succession. In addition, detrital zircons can be linked to possible bedrock source regions by their ages; this indeed is what led to the worldwide explosion of detrital zircon research in the first place. Information of the latter type, in turn, can bear on the timing of juxtaposition of packages of rocks—whether at the scale of fault blocks, terranes, or continents—and on basin evolution at an otherwise unattainable level of detail.

2.2. Sample Information

USGS sample numbers from our field work in October and November, 2007, identify the geologist, year, project area, and station number. Thus, sample DB07RIM29a was collected by DB (Dwight Bradley)[13] in 2007 in the République Islamique de Mauritanie (RIM). The station was Bradley's 29th and any trailing letters a, b, c, and so on correspond to different rock types from that location. Two sample numbers that do not follow this scheme—CT21 and CT22— are from a separate field excursion by Cliff Taylor, in Spring 2007. GPS coordinates are based on the WGS 84 datum. All outcrop photographs are by Dwight Bradley except as noted in figure captions.

3.0. Geochronological Results from the Taoudeni Basin

The Taoudeni Basin (fig. 7) is a vast intracratonic basin covering much of the West African Craton. Its sedimentary fill is essentially undeformed except along the orogenic front of the Mauritanides, and where locally faulted along its northern margin. The PRISM-I reports by Pitfield and others (2004) and Lahondère and others (2003, 2005) summarized the stratigraphy. Most of our samples are from the classic section in the Adrar area (fig. 8).

3.1. Groupe de Char

The Groupe de Char, Groupe d'Atar, and Groupe d'Assabet El Hassiane comprise the Supergroupe de Hodh, which is the oldest of three major subdivisions of the Taoudeni Basin stratigraphy (fig. 8). The Groupe de Char rests unconformably on Archean and Paleoproterozoic basement rocks along the northwestern and northern edge of the basin. It mainly consists of sandstone and conglomerate and is about 300 m thick (Benan and Deynoux, 1998). It was long assigned an age near the Mesoproterozoic-Neoproterozoic boundary based on an Rb-Sr age of 998±34 Ma from matrix clays (Clauer and others, 1982). In light of a new age constraint from the younger Groupe d'Atar (see Section 3.2), the Groupe de Char is here reassigned to the Mesoproterozoic. We suggest an age of ca. 1,125 Ma, that is, a little older than the conformably overlying Groupe d'Atar.

Detrital zircons were analyzed from one sample (CT22) from the lowest unit of the Groupe de Char, the Formation d'Agueni. The sample, a buff-colored quartz arenite, is from a few meters above the basal unconformity along the main highway near Atar, in the southeast corner of the Atar 1:200,000-scale sheet (number 2013) (fig. 9). Below the unconformity is a Mesoproterozoic paleosol developed on deformed granitoids of the Complexe d'Amsaga. Benan and Deynoux (1998) interpreted a shoreface depositional facies for this lowest part of the Groupe de Char section.

[13]CT is Cliff Taylor; GB is Georges Beaudoin.

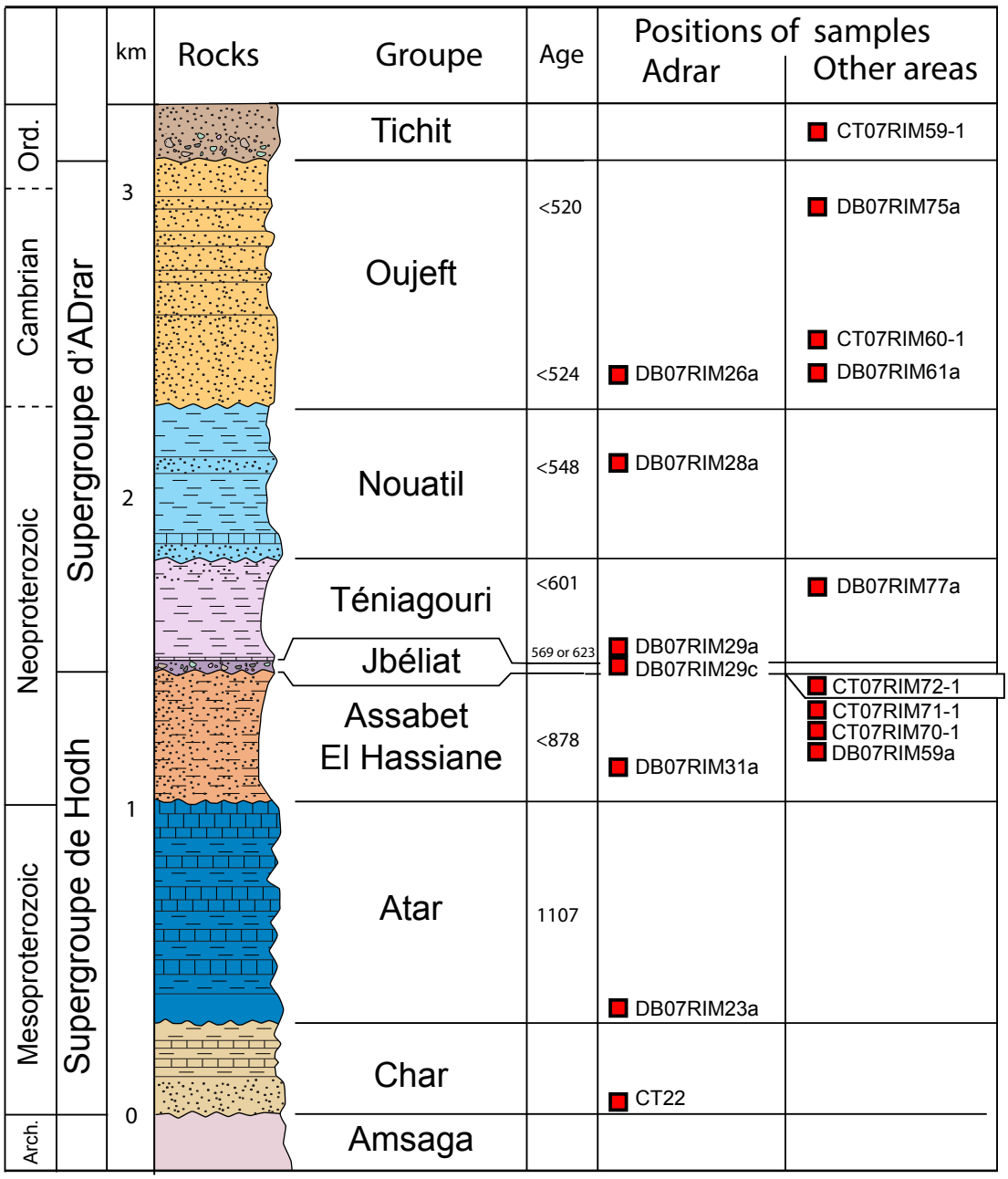


Figure 8. Stratigraphic column for the Adrar region of the Taoudeni Basin; the lithologic column is adapted from Deynoux and others (2006), the nomenclature is from Pitfield and others (2004), and the age control is from the present study and Rooney and others (2010).

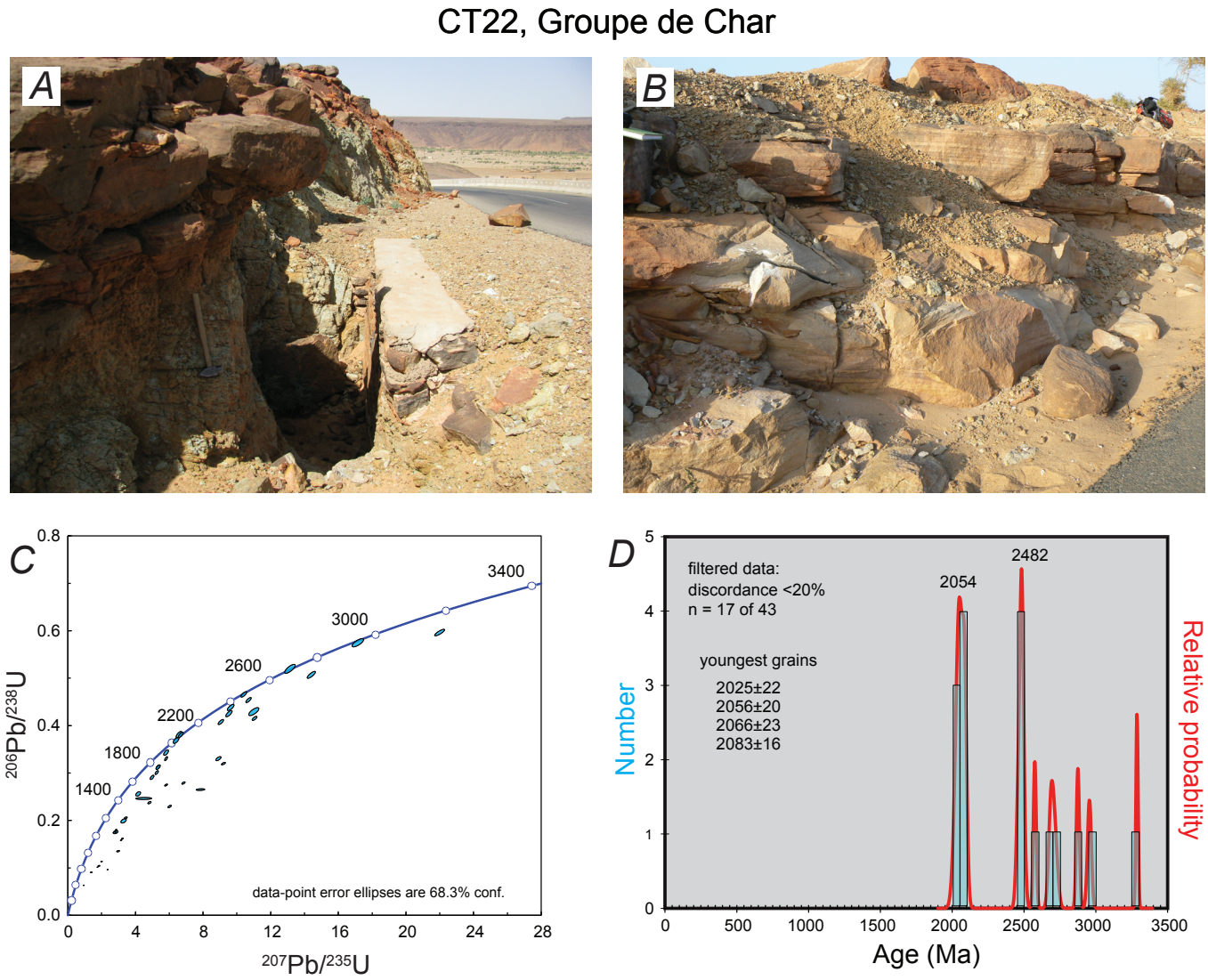


Figure 9. Detrital zircon data and photographs for sample CT22 from the Groupe de Char. (*A*) Basal sandstones of the Groupe de Char (red) unconformably overlying a pale greenish paleosol developed on a granitoid of the Complexe d'Amsaga. (*B*) Sandstone of the Groupe de Char where sampled for detrital zircons. (*C*) Concordia diagram. (*D*) Age distribution shown in two forms: a probability density function (red curve) and a histogram with 50-m.y. bins (blue boxes). This is one of the two samples that we collected on a brief reconnaissance trip early in 2007; hence the different sample numbering scheme.

Of 43 detrital zircons that were analyzed, the majority of results are strongly discordant and rejected on these grounds; only 17 pass a 20 percent discordance filter. This small population shows Paleoproterozoic maxima at 2,482 and 2,054 Ma (fig. 9*D*). There are no Mesoproterozoic zircons that would help constrain the depositional age. The discordant zircons show evidence of lead loss during the Phanerozoic (fig. 9*C*).

3.2. Groupe d'Atar

The 700-m-thick Groupe d'Atar depositionally overlies the Groupe de Char (fig. 8). Except for a basal clastic interval, it is dominantly stromatolitic dolostone. Clays from shaly intervals yielded early Neoproterozoic Rb–Sr and K–Ar ages of 890±35 and 775±52 Ma (Clauer, 1976); these results are the source of the Neoproterozoic depositional age that was assigned to the Groupe d'Atar on previous map compilations (Pitfield and others, 2004; Lahondère and others, 2003). Recently, Rooney and others (2010) reported three nearly identical Re-Os ages (1,106±12 Ma, 1,109±22 Ma and 1,105±37 Ma) from organic-rich strata in the Groupe d'Atar from drillcore from two exploration wells about 200 km apart. These results require a late Mesoproterozoic depositional age. Clauer's (1976, 1982) Rb-Sr ages for the Groupe de Char and Groupe d'Atar thus have turned out to

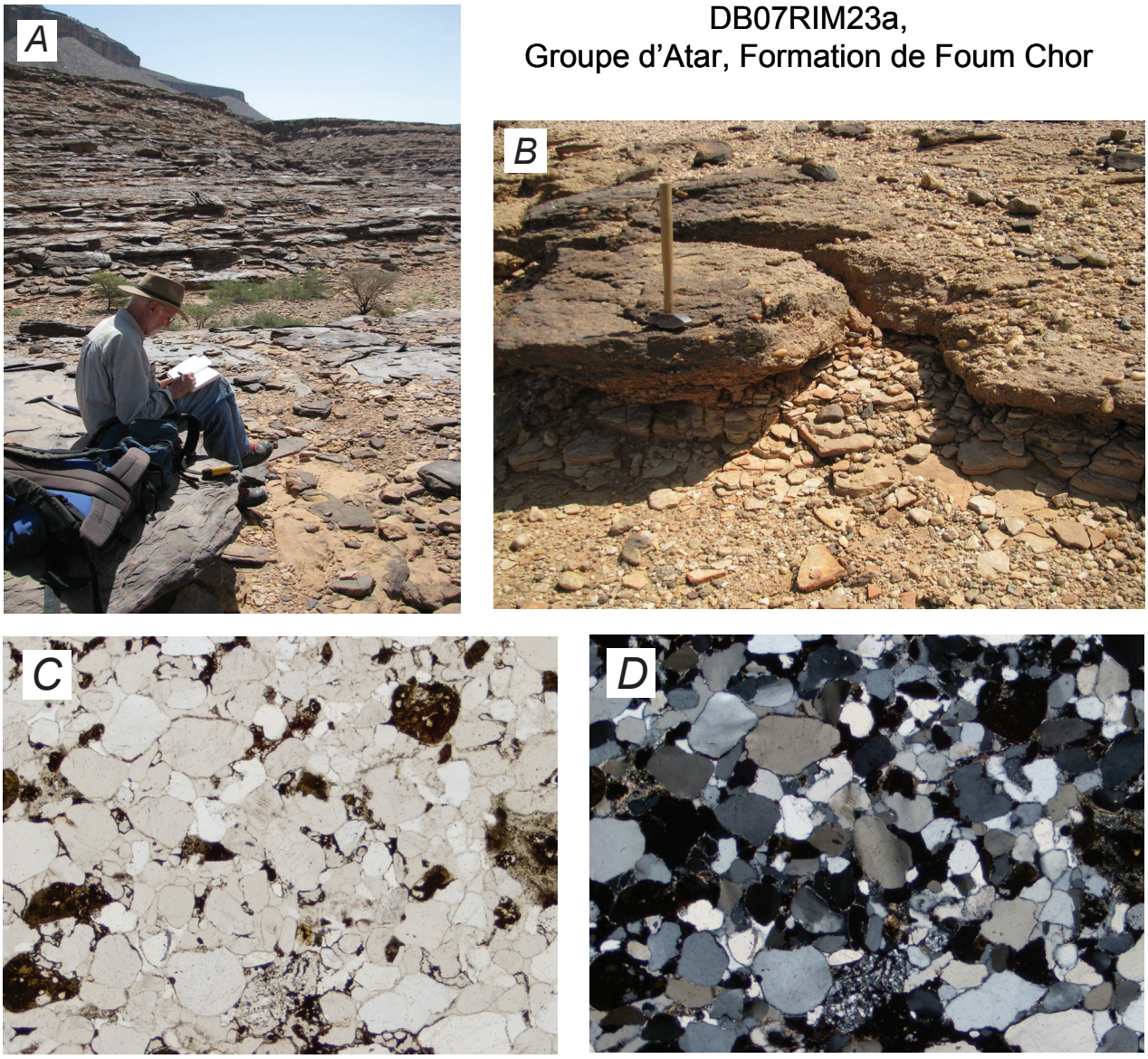


Figure 10. Detrital zircon data and photographs for sample DB07RIM23a from the Groupe d'Atar. (*A* and *B*) Outcrop photographs of sandstone at the sample location. (*C* and *D*) Photomicrographs under plane light and crossed polars, respectively. Note the lack of penetrative deformation. In these and subsequent photomicrographs, the field of view is 2.5 mm across. (*E*, *F*, and *G*) Concordia diagrams and the corresponding zircon age distribution based on the first analysis of sample DB07RIM23a (lab number 952-12). (*H*, *I*, and *J*) Comparable data based on the reanalysis (lab number 1284-04). In this and subsequent plots, age distributions show filtered data only, and paired concordia diagrams with blue and red ellipses represent unfiltered and filtered data, respectively.—Continued

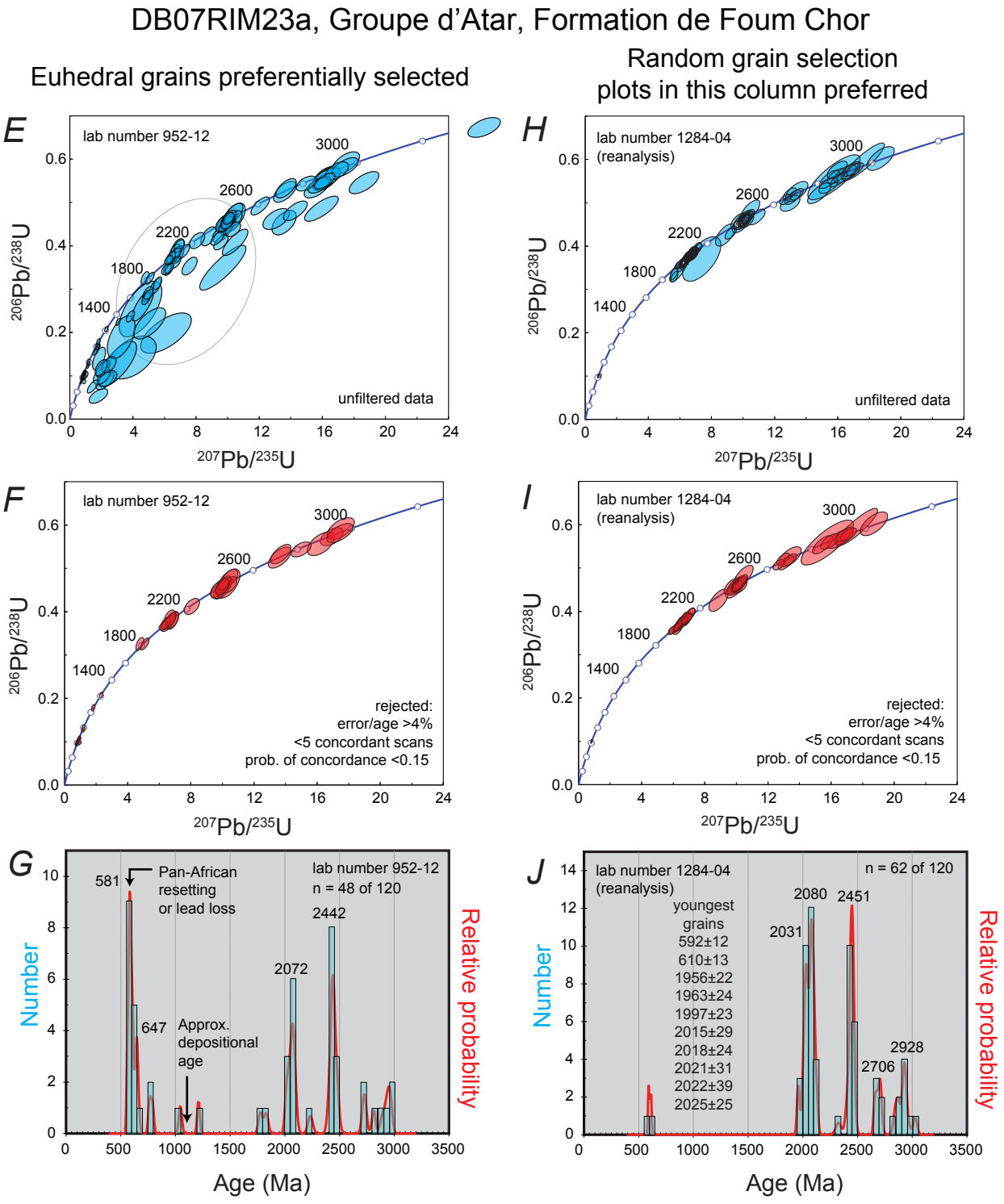


Figure 10. Detrital zircon data and photographs for sample DB07RIM23a from the Groupe d'Atar. (*A* and *B*) Outcrop photographs of sandstone at the sample location. (*C* and *D*) Photomicrographs under plane light and crossed polars, respectively. Note the lack of penetrative deformation. In these and subsequent photomicrographs, the field of view is 2.5 mm across. (*E*, *F*, and *G*) Concordia diagrams and the corresponding zircon age distribution based on the first analysis of sample DB07RIM23a (lab number 952-12). (*H*, *I*, and *J*) Comparable data based on the reanalysis (lab number 1284-04). In this and subsequent plots, age distributions show filtered data only, and paired concordia diagrams with blue and red ellipses represent unfiltered and filtered data, respectively.

be too young by 100 to 300 m.y. We conclude that Rb-Sr ages from clays in Taoudeni Basin strata are unreliable, and that the quoted Rb-Sr ages for the Groupe d'Assabet El Hassiane and Groupe de Jbéliat (see below) are likewise suspect.

Detrital zircons from one Groupe d'Atar sample (RIM07DB23a) were analyzed by LAICPMS. The sample is from along the main highway near Atar, in the southeast corner of the Atar 1:200,000-scale sheet (number 2013). The rock is a pebbly, trough-cross-stratified sandstone from lowest unit of the Groupe d'Atar, the Formation de Foum Chor (figs. 10*A* and *B*). The strata are undeformed, flat-lying, and show no obvious alteration. Two splits of the same sample were run at different times. When the first analysis was done (lab number 952-12), the main goal was to constrain the maximum depositional age; euhedral zircons were therefore selected in preference to rounded ones on the assumption that the former were more likely to have endured only one sedimentary cycle. Out of 120 grains, only 48 passed the LAICPMS filters described in Section 2.0. More than half the zircons suffered lead loss, which appears to be relatively young, Cenozoic to modern (figs. 10*E* and *F*). The probability curve shows major peaks at 2,442, 2,072, and 581 Ma and a minor peak at 647 Ma (fig. 10*G*). This result was a cause for concern because of the geologically constrained Mesoproterozoic depositional age. We therefore ran a blind, second analysis (lab number 1284-04) on an archived split of sample DB07RIM23a. This time, zircons were selected at random. Of 120 zircons analyzed, 62 are concordant. The probability curve shows a major Paleoproterozoic peaks at 2,451, 2,080, and 2,031 and minor Archean peaks at 2,928 and 2,706 Ma (fig. 10*J*). The two probability curves are qualitatively similar, although second run yielded far fewer of the problematically young, Neoproterozoic zircons. The peaks at 2,451, 2,080, and 2,031 Ma are quite similar to the main detrital age peaks in the Groupe de Char. The two zircon ages at ca. 600 Ma are problematic because they are about half a billion years too young. As discussed in Section 7.6, these and numerous other ca. 600-Ma zircons in our Mauritanian sample suite may have been partially reset during a Pan-African event.

3.3. Groupe d'Assabet El Hassiane

The Groupe d'Assabet El Hassiane depositionally overlies the Groupe d'Atar (fig. 8). It consists of sandstone, siltstone, and shale and is generally 300–400 m thick (Deynoux and others, 2006) although it does thicken to 1,300 m in a north-south subbasin running through the Richat area. It was previously assigned a mid-Neoproterozoic age of ca. 695 Ma based on Rb-Sr geochronology of clays (Clauer, 1976; Clauer and others, 1982). We suggest that this is too young by about 200 million years.

Detrital zircons from two samples of the Groupe d'Assabet El Hassiane were analyzed by LAICPMS. Sample RIM07DB31a is from strata assigned to the Sous-groupe de Tin Bessais near Oued Toueiderguilt in the Chinguetti 1:200,000-scale sheet (number 2012). The sample is a reddish brown sandstone that is interbedded with, and forms the matrix of, cobble conglomerate (fig. 11*A*). Of the 120 zircons analyzed, 109 passed the LAICPMS filters. The probability density curve shows a major peak at 1,212 Ma and minor ones at 1,938, 1,510, 1,357, and 975 Ma (fig. 11F). We consider the 975-Ma peak to set the maximum depositional age for this sample; a younger zircon, at 643 Ma, is of uncertain significance, being a single unreplicated age.

Our other sample (DB07RIM59a) is stratigraphically higher in the Groupe d'Assabet El Hassiane from outcrops of the Sous-groupe de Taguilalet, within the ring of Guelb Er Richat in the 1:200,000-scale sheet of the same name (number 2111). The sample is medium-grained, cross-bedded red sandstone (fig. 12*A*). Of the 120 zircons analyzed, 96 pass the LAICPMS filters. The probability density curve shows a major peak at 1,230 Ma, lesser peaks at 1,777, 1,508, 1,348, and 1,036 Ma (fig. 12*F*). The peak at 1,036 Ma sets the zircon-based "maximum depositional age" for this sample; however, it is from a younger part of the Groupe d'Assabet El Hassiane than sample RIM07DB31a, so the depositional age must be 975 Ma or younger.

3.4. Groupe d'Aioun

The Groupe d'Aioun (of Lahondère and others, 2005) is a sandstone-dominated succession that is regarded as a southerly equivalent of the Groupe d'Assabet El Hassiane. Detrital zircons from two samples of the Groupe d'Aioun were analyzed by LAICPMS.

Sample CT07RIM70-1, a coarse-grained sandstone, is from the Formation de Freidi (fig. 13*A*). The GPS coordinates of the sample location put it in an area mapped as the Groupe de Téniagouri, Formation de Bouly (chert and laminated argillite) near Blemh*â*der in the Ayoun el Atrous 1:200,000-scale sheet (number 1609). As there is no mistaking the Formation de Bouly from the Formation de Freidi, the previously mapped contact in this area must be off by a few hundred meters. Of the 120 zircons analyzed, 113 pass the LAICPMS filters. The probability density curve shows a remarkable pattern with major peaks at 2,126, 2,023, 1,745, 1,499, and 1,201 Ma, and lesser peaks at 1,014, 929, and 878 Ma (fig. 13*D*). The youngest peak, at 878 Ma, sets the maximum depositional age of this sample.

Sample CT07RIM71-1, a large-scale cross-stratified quartzose sandstone, is from the Formation de Seyal (fig. 14*A*). The sample location is near Ayoun el Atrous in the 1:200,000-scale sheet of the same name (number 1609). Of the 120 zircons analyzed, 110 passed the LAICPMS filters. The probability density curve is similar to that of sample CT07RIM70-1, with major peaks at 2,042, 1,868, 1,751, 1,557, and 1,175, and lesser peaks at 1,395, 1,259, and 908 Ma (fig. 14*E*). The minor peak at 908 Ma sets the maximum depositional age of this sample.

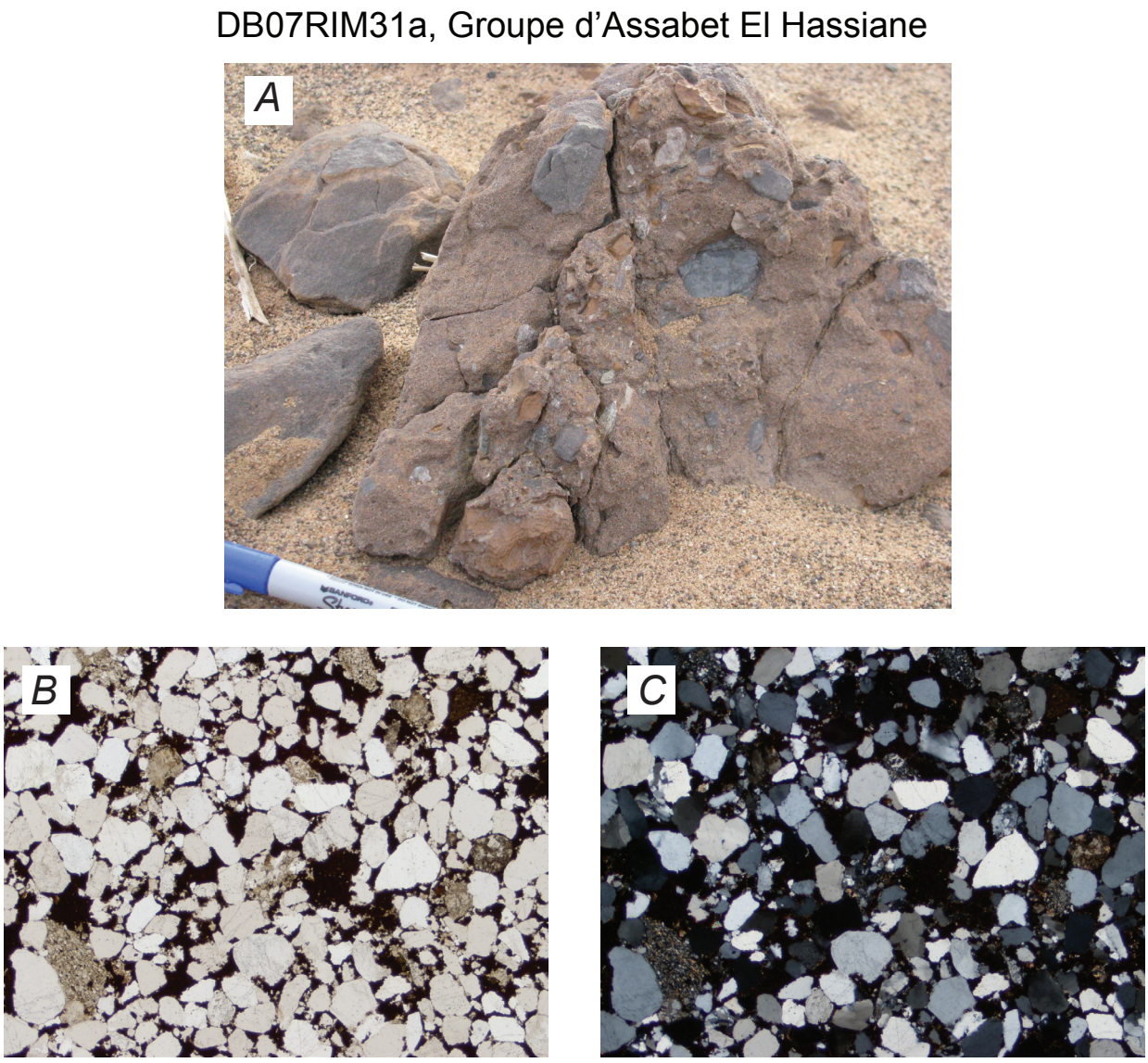


Figure 11. Detrital zircon data and photographs for sample DB07RIM31a from the Groupe d'Assabet El Hassiane. (*A*) Outcrop photograph of conglomerate at the sample location; sample is from the sand matrix. (*B* and *C*) Photomicrographs under plane light and crossed polars, respectively. (*D* and *E*) Concordia diagrams. (*F*) Age distribution.—Continued

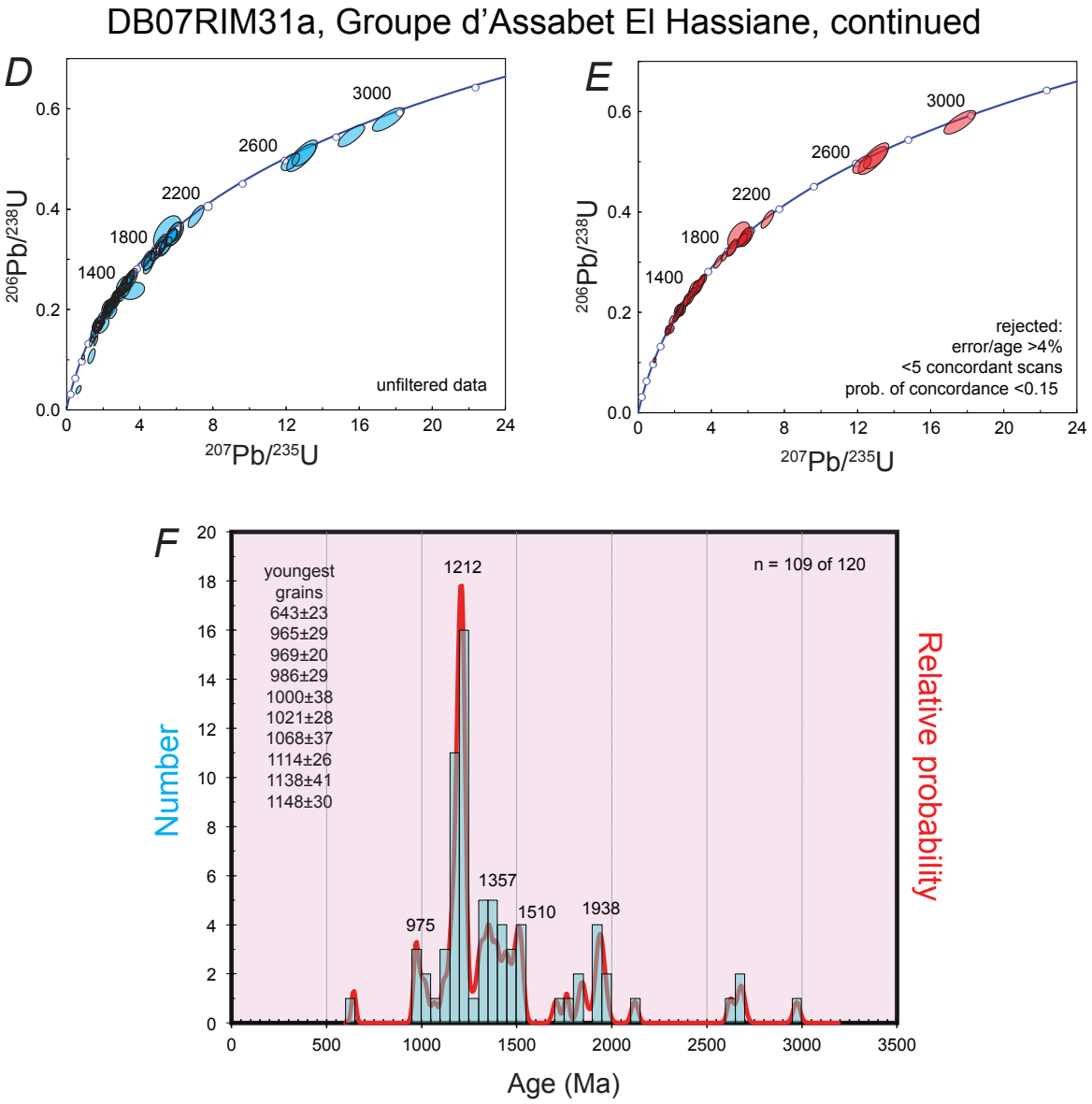


Figure 11. Detrital zircon data and photographs for sample DB07RIM31a from the Groupe d'Assabet El Hassiane. (*A*) Outcrop photograph of the sample location; sample is from the sand matrix. (*B* and *C*) Photomicrographs under plane light and crossed polars, respectively. (*D* and *E*) Concordia diagrams. (*F*) Age distribution.

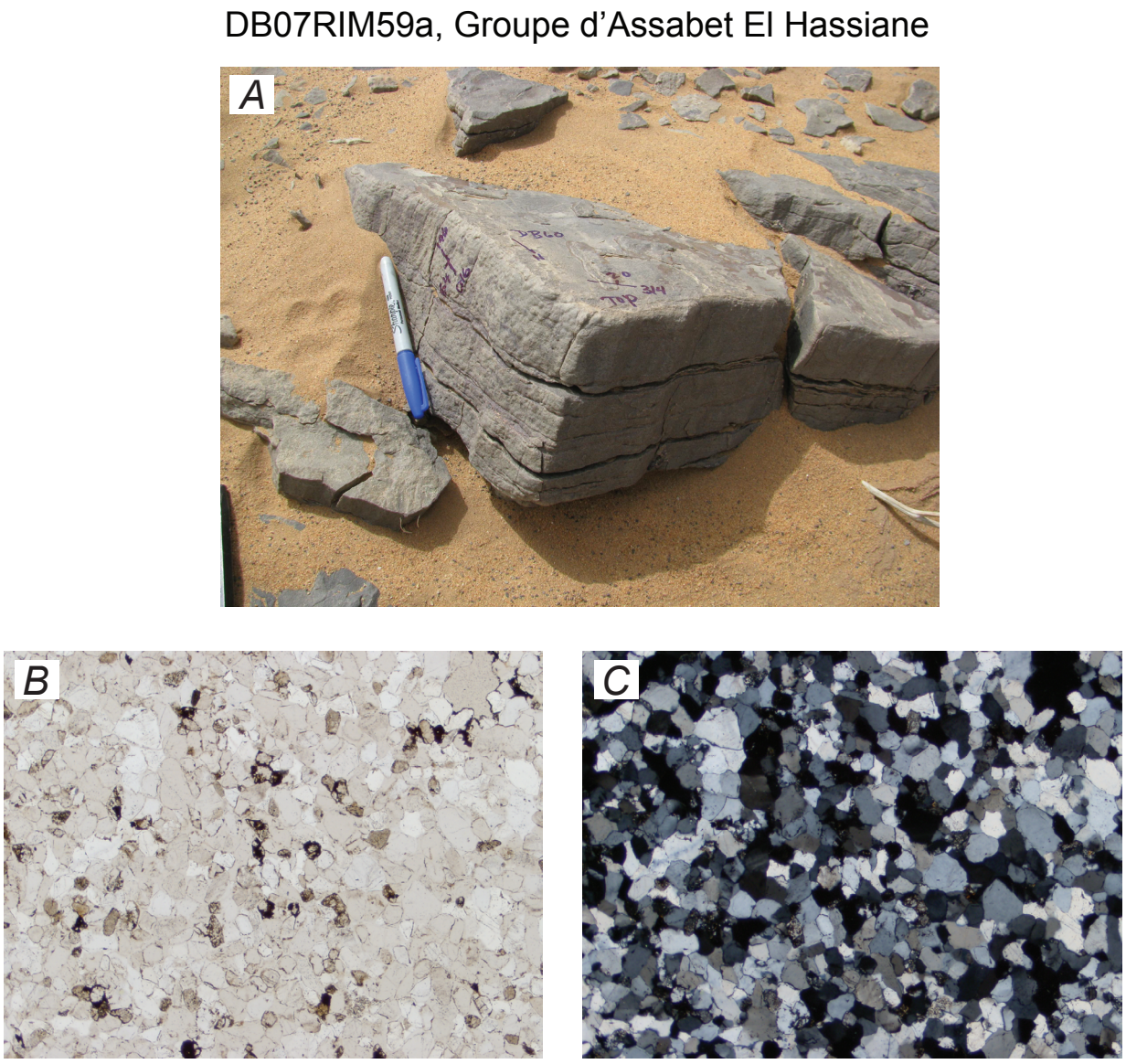


Figure 12. Detrital zircon data and photographs for sample DB07RIM59a from the Groupe d'Assabet El Hassiane. (*A*) Outcrop photograph from sandstone near the sample location; rocks at exact sample location were not photogenic. (*B* and *C)* Photomicrographs under plane light and crossed polars, respectively. (*D* and *E*) Concordia diagrams. (*F*) Age distribution.—Continued

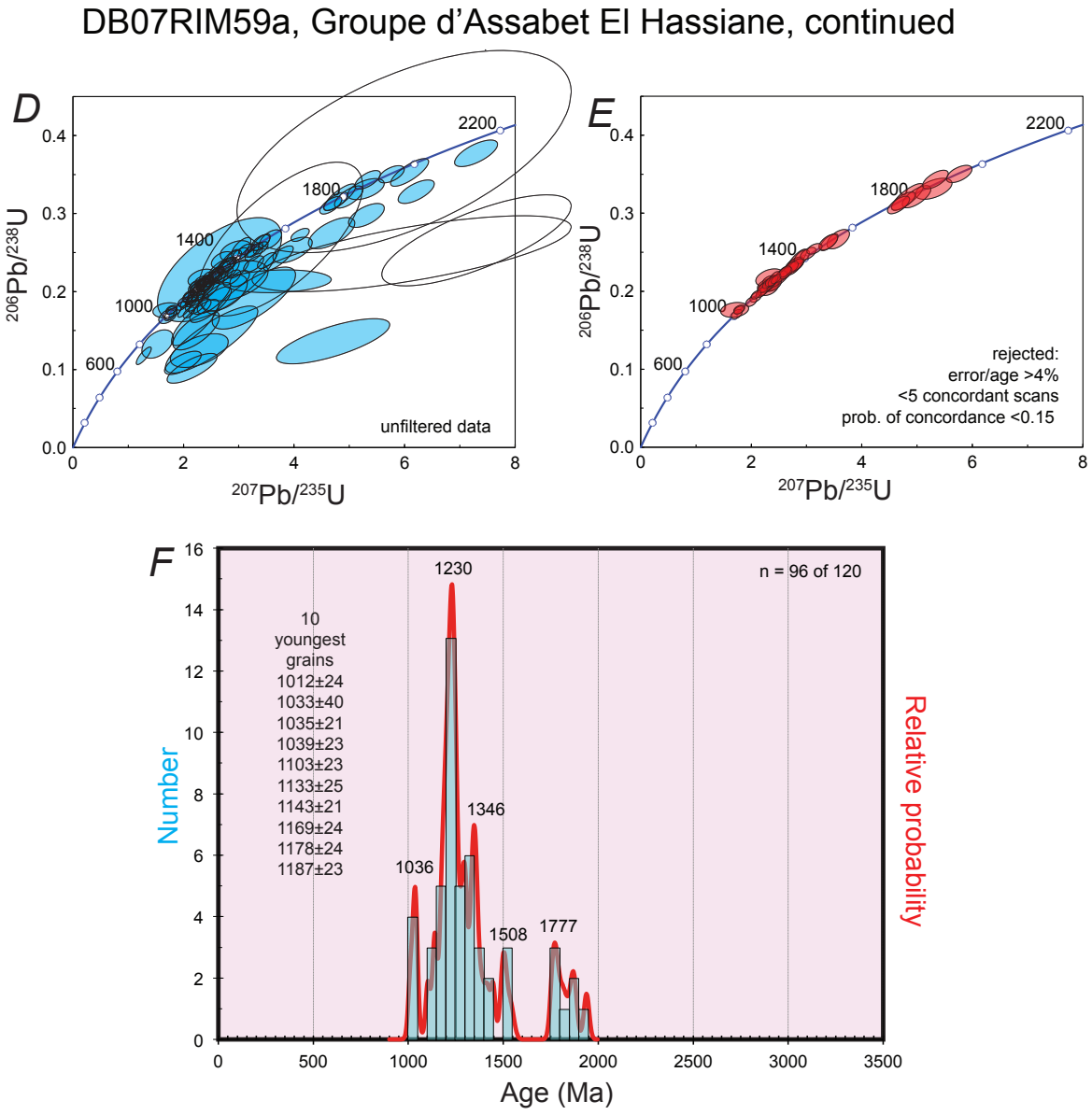


Figure 12. Detrital zircon data and photographs for sample DB07RIM59a from the Groupe d'Assabet El Hassiane. (*A*) Outcrop photograph from sandstone near the sample location; rocks at exact sample location were not photogenic. (*B* and *C)* Photomicrographs under plane light and crossed polars, respectively. (*D* and *E*) Concordia diagrams. (*F*) Age distribution.

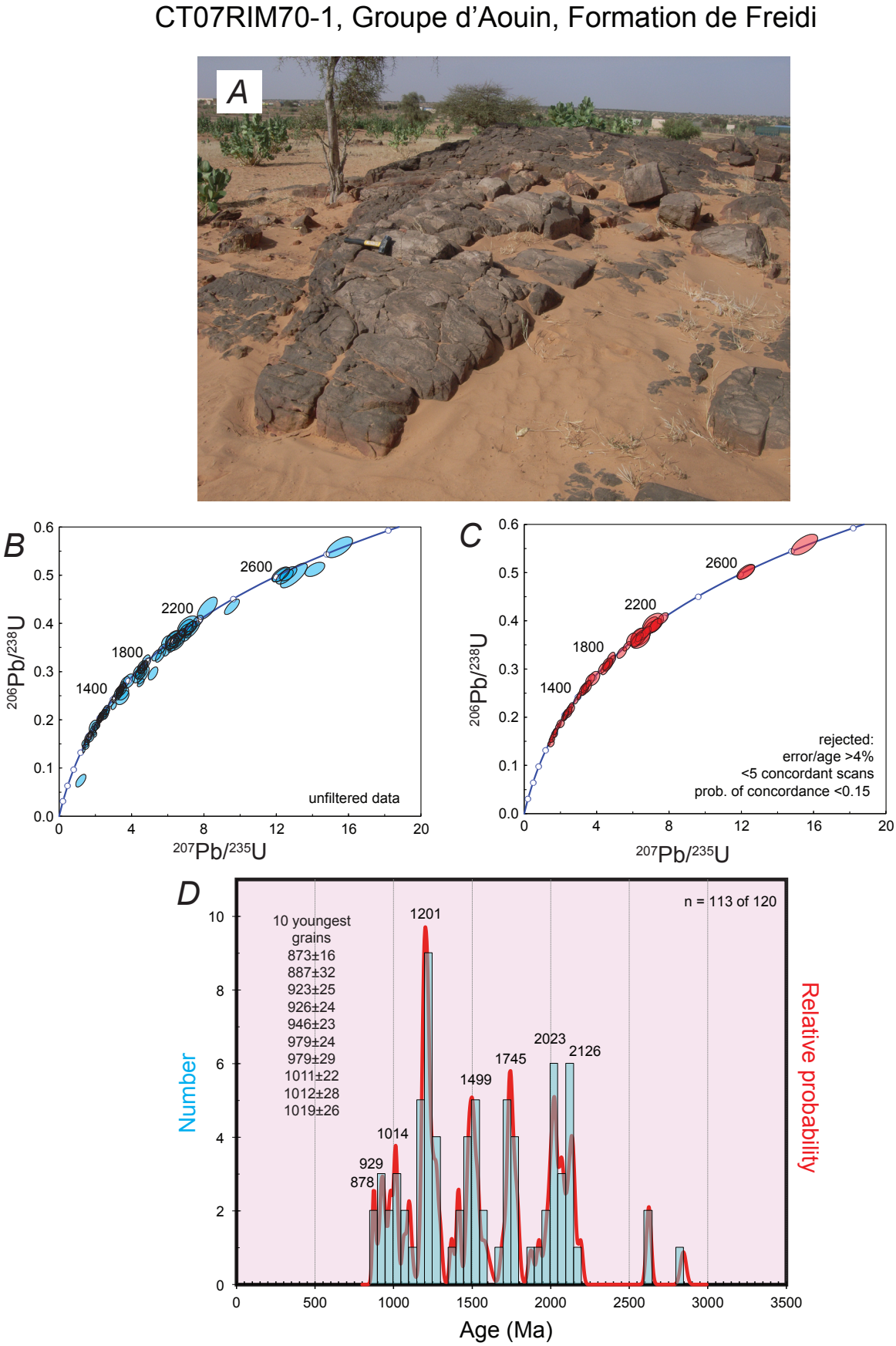


Figure 13. Detrital zircon data and photographs for sample CT07RIM70-1 from the Groupe d'Aioun, Formation de Freidi. (*A*) Outcrop photograph of sandstone at the sample location; photograph by Cliff Taylor. (*B* and *C*) Concordia diagrams. (*D*) Age distribution.

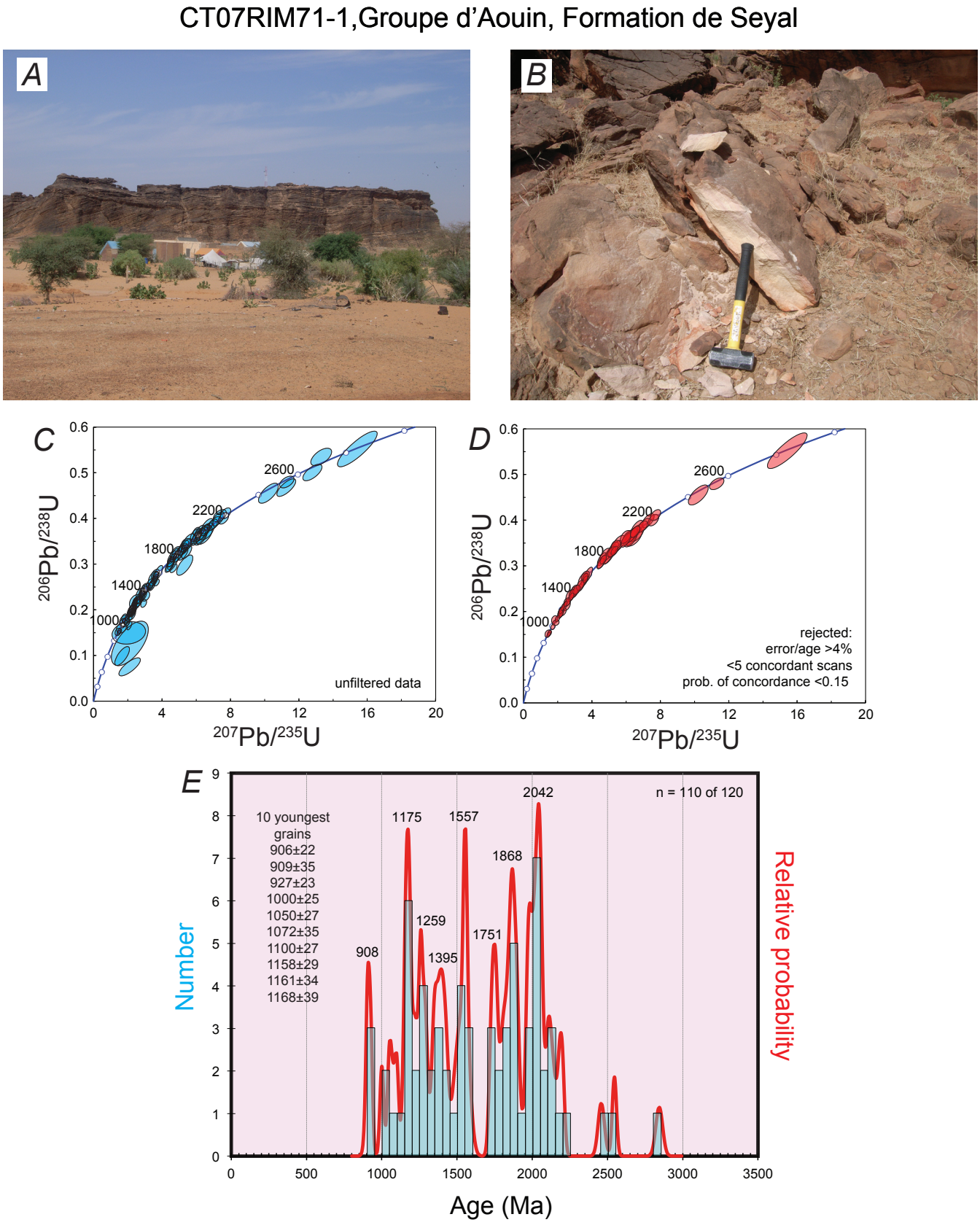


Figure 14. Detrital zircon data and photographs for sample CT07RIM71-1 from the Groupe d'Aioun, Formation de Seyal. (*A* and *B*) Distant and close-up outcrop photographs of sandstone at the sample location. Photographs by Cliff Taylor. (*C* and *D*) Concordia diagrams. (*E*) Age distribution.

3.5. Groupe de Khang Naam

Sample CT07RIM72-1 is a sandstone from the Formation de Lehbilé of the Groupe de Khang Naam of Lahondère and others (2005). In the Adrar area (fig. 8), the stratigraphic level of the Groupe de Khang Naam has been cut out along the unconformity below the Groupe de Jbéliat. The sample locality (fig. 15*A*) is near Oued el Mancour in the eastern part of the Kiffa 1:200,000-scale sheet (number 1611). Of the 120 zircons analyzed, 106 passed the LAICPMS filters. The probability density curve is similar to that of the two samples of the Groupe d'Assabet El Hassiane. A single major peak is at 1,204 Ma; lesser peaks are 2,053, 1,762, 1,487, 1,411, 1,288, 1,128, and 1,029 Ma (fig. 15*D*). The minor peak at 1,029 Ma sets the zircon-based "maximum depositional age" of this sample. The actual depositional age must be younger than 878 Ma because the Formation de Freidi depositionally underlies the Formation de Lehbilé.

3.6. Groupe de Jbéliat

The glaciogenic Groupe de Jbéliat (fig. 8) is one of Mauritania's best-publicized stratigraphic units. It has been correlated with the Neoproterozoic Marinoan glaciation (Deynoux and others, 2006). On the assumption that this was a globally synchronous event, the Groupe de Jbéliat would be 635 Ma (Macdonald and others, 2010). Detrital zircons were analyzed from three Groupe de Jbéliat samples.

Sample DB07RIM29c is from near the main highway between Atar and Chinguetti, in the western part of the Chinguetti 1:200,000-scale sheet (number 2012); note that the relatively new highway is not shown on the topographic base to this map sheet. The sample is a pebbly diamictite with thin silt partings (figs. 16*A* and *B*). The diamictite is overlain by a distinctive horizon of contorted dolostone that is encrusted with sparry barite as described in a nearby location by Shields and others (2007). Of the 120 zircons analyzed, 106 passed the LAICPMS filters. The probability density curve shows major peaks at 1,213 Ma and lesser peaks at 1,752, 1,511, and 1,006 Ma (fig. 16*G*). The youngest, robust probability peak is at 1,006 Ma; this zircon-based "maximum depositional age" is far older than the likely depositional age, near 635 Ma.

Sample CT07RIM73-1 is from a coarse-grained, arkosic, dark red sandstone (figs. 17*A* and *B*) assigned by Lahondère and others (2005) to the Groupe de Jbéliat. The sample location is in the southern Taoudeni Basin in the eastern outskirts of Kiffa **(**Kiffa 1:200,000-scale sheet, number 1611). Of the 120 zircons analyzed, 96 passed the LAICPMS filters. The probability density curve shows major peaks at 1,424 and 1,218 Ma, a lesser peak at 994 Ma, and a smattering of other Paleoproterozoic and Mesoproterozoic ages (fig. 17*E*). The peak at 994 Ma sets the zircon-based "maximum depositional age" of the sample, which is again far older than the likely depositional age near 635 Ma.

Sample DB07RIM80a is from diamictite mapped as the Groupe de Jbéliat near the Mauritanide deformation front just north of Senegal in the Kankossa-Kayes 1:200,000-scale sheet (number 1511–1411). In contrast with sample DB07RIM29c, this diamictite is overlain by a contorted, siliceous cap of dolomite, notably lacking in the barite encrustations that are present at location DB07RIM29c (fig. 18*A*). It also differs in having a chalky, off-white matrix that appears tuffaceous (fig. 18*B*). Of the 120 zircons analyzed, 94 passed the LAICPMS filters. The main probability peak is at 2,072 Ma, with lesser peaks at 2,813, 2,764, 2,138, and 1,479 Ma (fig. 18*G*). Two zircons, at 595±11 and 562±11 Ma, are significantly younger than the supposed depositional age of 635 Ma that would apply if this was a deposit of the global Marinoan glaciation. The overall age distribution is quite different from the two other samples from rocks mapped as Groupe de Jbéliat, which makes us suspect a different age. Taking the two young grains and different zircon age distribution into consideration, we therefore raise the possibility that this deposit is from a younger glaciation than the Jbéliat. It may correlate with one of the Ediacaran tillites of the Appalachians: the Gaskiers (Hoffman and Li, 2009), Squantum (Thompson and Bowring, 2000), or Fauquiers (Hebert and others, 2010). More research on samples from this exposure is warranted.

3.7. Groupe de Téniagouri

The Groupe de Téniagouri depositionally overlies diamictites assigned to the Groupe de Jbéliat (fig. 8), with which it has commonly been combined for regional-scale mapping. Pitfield and others (2004) recognized three divisions: a lower barite and dolomite of the Groupe de Jbéliat's "cap carbonate", a middle mudstone and chert, and an upper turbiditic sandstone. Pitfield and others (2004) referred to the mudstone and chert as the Formation de Bouly.

Sample DB07RIM29a is from near the main highway between Atar and Chinguetti in the western part of the Chinguetti 1:200,000-scale sheet (number 2012). In well-exposed cutbanks of an unnamed oued, (wadi), maroon and green siliceous mudstones that comprise the basal few meters of the Formation de Bouly are interbedded with several layers of tan felsic tuff (figs. 19*A* and *B*). This sample is important for its potential to constrain the age of the Jbéliat glaciation, as it is only 2–3 m stratigraphically above the calc-arenite cap of the tillite, the two being separated by a gap in exposure. The thickest ash bed (1–2 cm thick) was dated by both SIMS and TIMS. The SIMS effort used a mineral separate done by Apatite to Zircon, Inc.

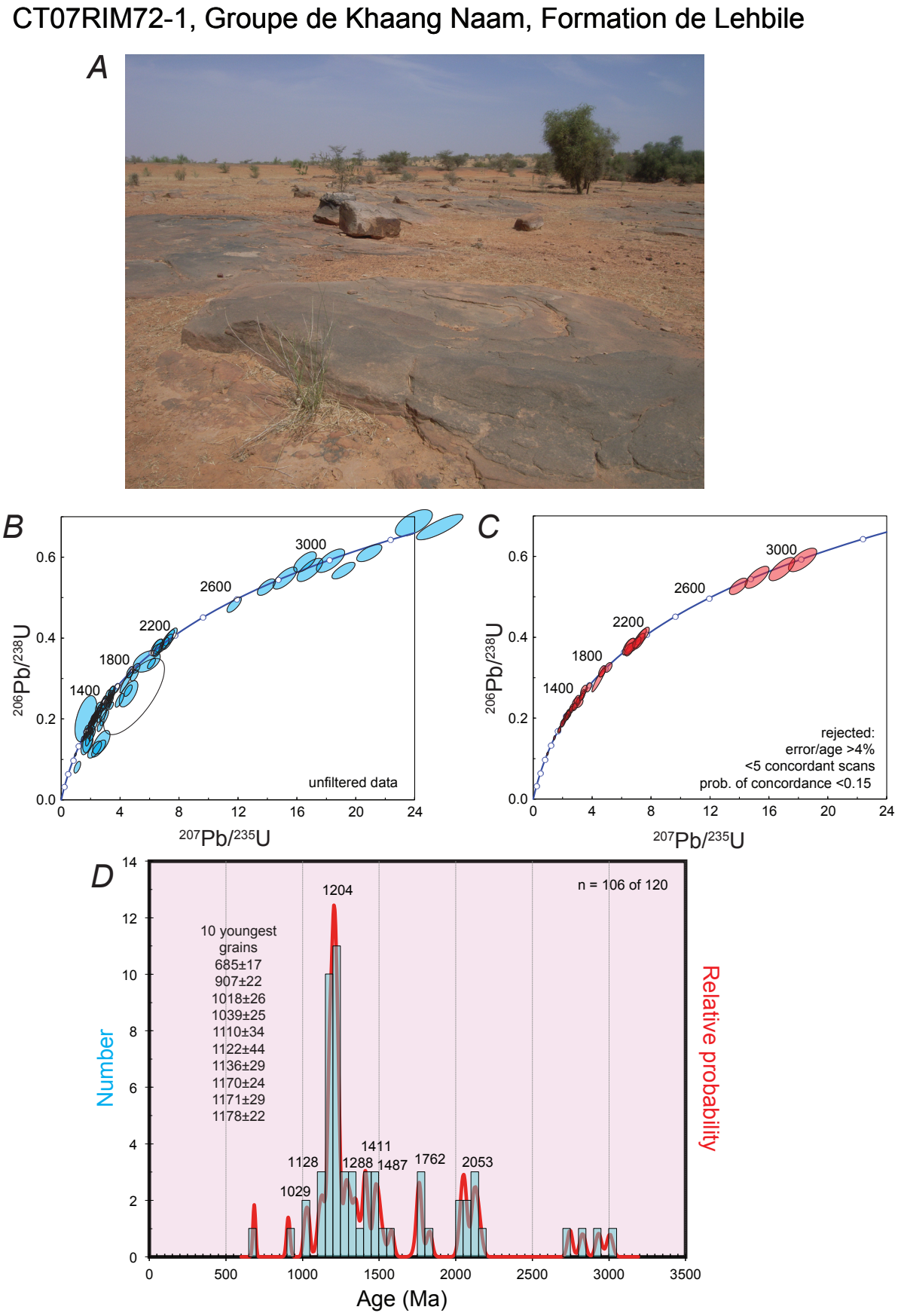


Figure 15. Detrital zircon data and photographs for sample CT07RIM72-1 from the Groupe de Khang Naam, Formation de Lehbilé. (*A*) Outcrop photograph of sandstone at the sample location; photograph by Cliff Taylor. (*B* and *C*) Concordia diagrams. (*D*) Age distribution.



Figure 16. Detrital zircon data and photographs for sample DB07RIM29c from the Groupe de Jbéliat near Atar. (*A* and *B*) Outcrop photographs of the sample location. (*C* and *D*) Photomicrographs under plane light and crossed polars, respectively. (*E* and *F*) Concordia diagrams. (*G*) Age distribution.—Continued

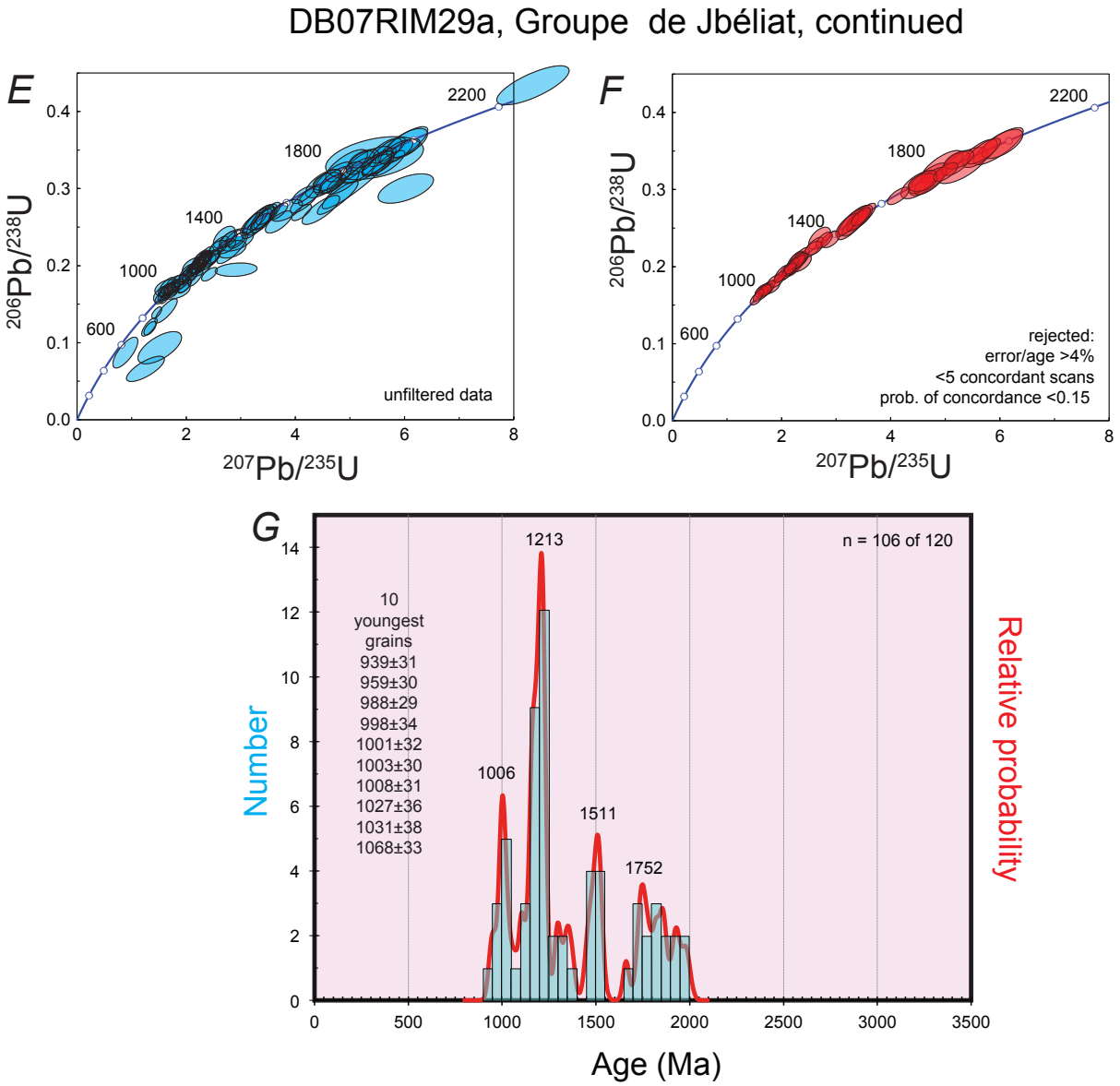


Figure 16. Detrital zircon data and photographs for sample DB07RIM29c from the Groupe de Jbéliat near Atar. (*A* and *B*) Outcrop photographs of the sample location. (*C* and *D*) Photomicrographs under plane light and crossed polars, respectively. (*E* and *F*) Concordia diagrams. (*G*) Age distribution.

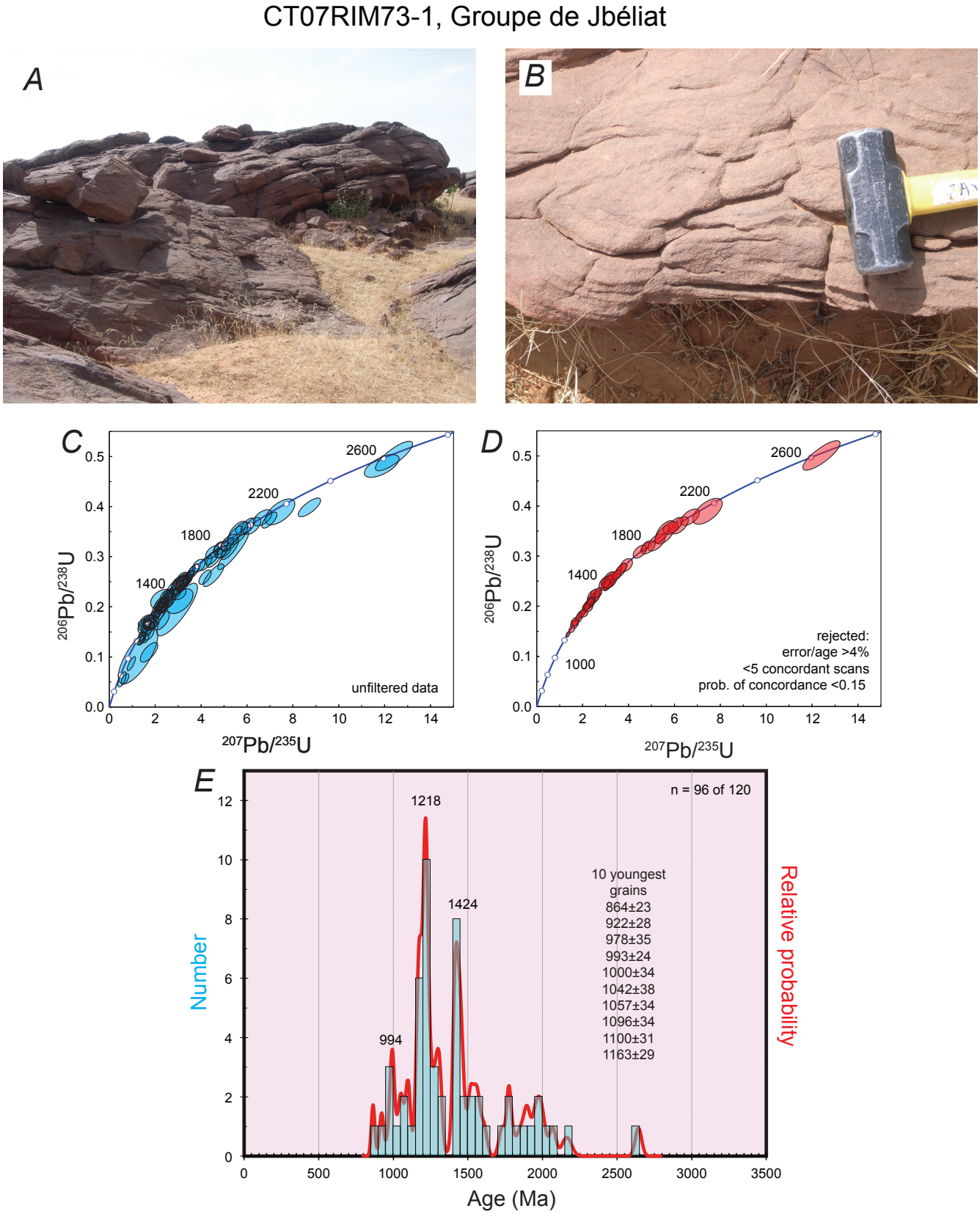


Figure 17. Detrital zircon data and photographs for sample CT07RIM73-1 from the Groupe de Jbéliat in the Kiffa area. (*A* and *B*) Outcrop photographs of sandstone at the sample location. Photographs by Cliff Taylor. (*C* and *D*) Concordia diagrams. (*E*) Age distribution.

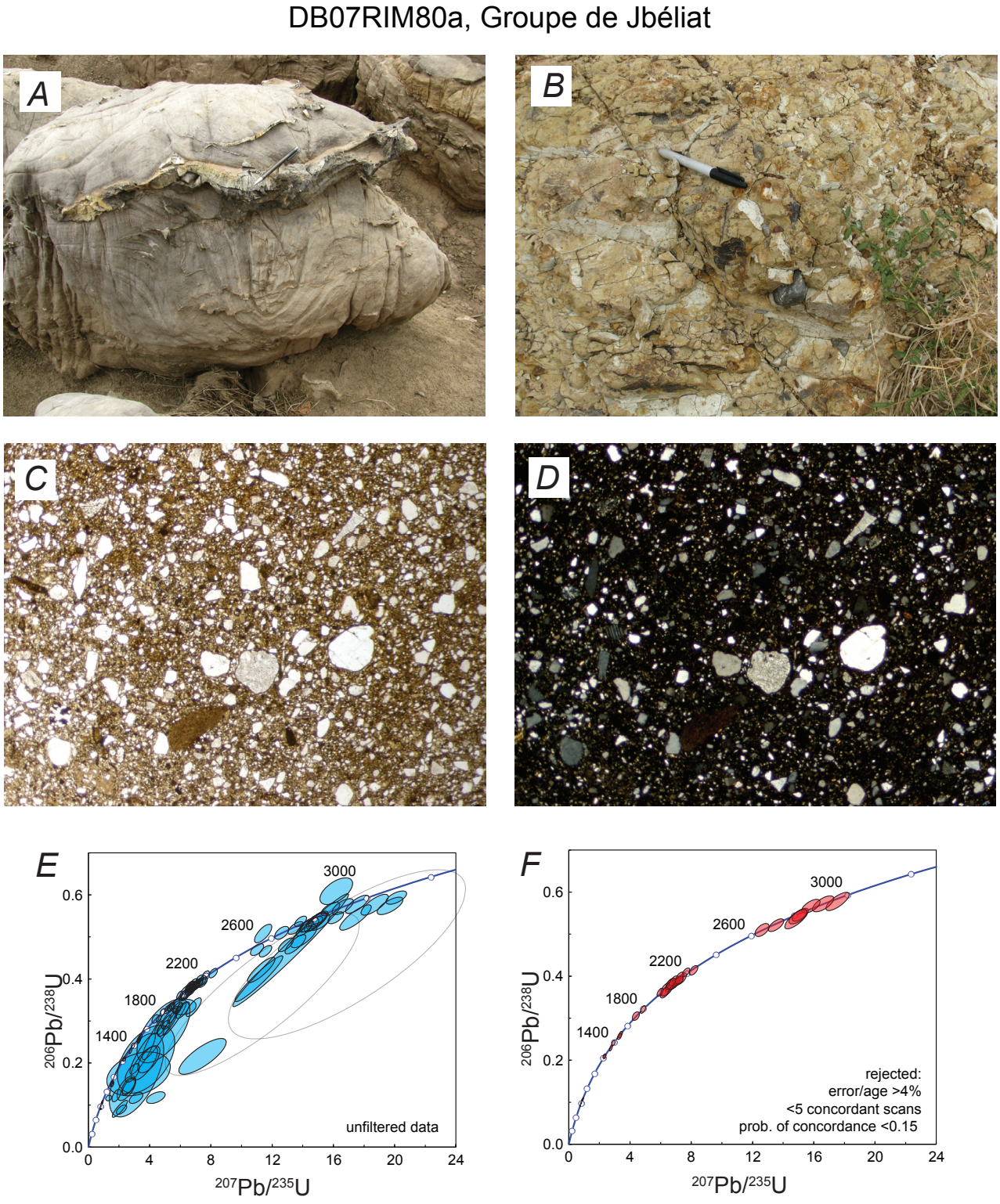


Figure 18. Detrital zircon data and photographs for sample DB07RIM80a from diamictite that was previously mapped as the Groupe de Jbéliat, near the Senegal River. (*A*) Outcrop photograph of the cap dolostone, showing contorted laminae and chert. (*B*) Outcrop photograph of the sample horizon, a few meters below the cap carbonate. (*C* and *D*) Photomicrographs under plane light and crossed polars, respectively. (*E* and *F*) Concordia diagrams. (*G*) Age distribution.—Continued

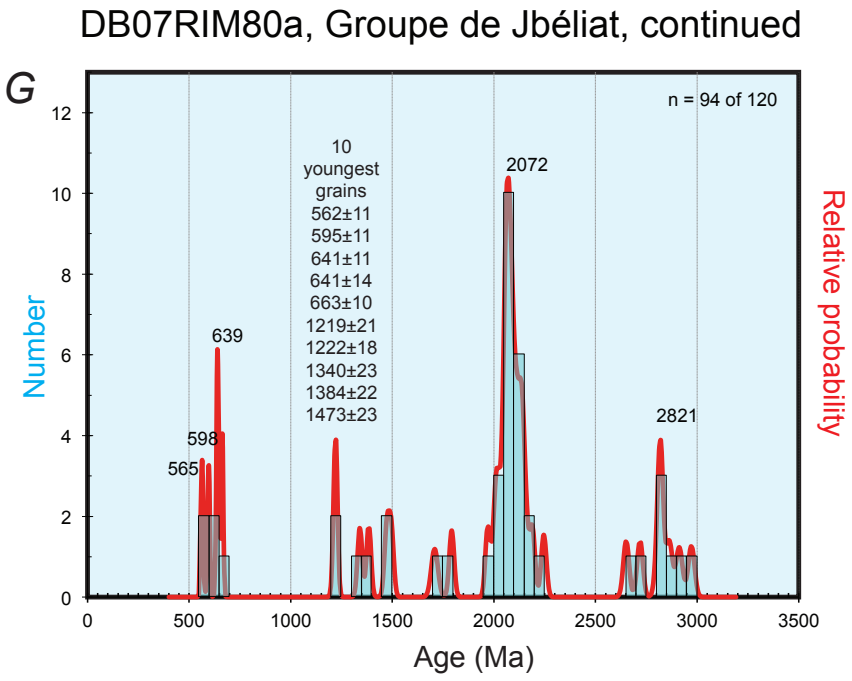


Figure 18. Detrital zircon data and photographs for sample DB07RIM80a from diamictite that was previously mapped as the Groupe de Jbéliat near the Senegal River. (*A*) Outcrop photograph of the cap dolostone, showing contorted laminae and chert. (*B*) Outcrop photograph of the sample horizon, a few meters below the cap carbonate. (*C* and *D*) Photomicrographs under plane light and crossed polars, respectively. (*E* and *F*) Concordia diagrams. (*G*) Age distribution.

The SIMS results showed a dominant age cluster at ca. 653 Ma, a number of older detrital or xenocrystic zircons, and a few younger zircons with concordant ages down to 622 and 605 Ma (figs. 19*E* and *F*). Subsequent high-precision CA-TIMS analyses at MIT revealed still more complexities. Thirteen zircons were dated during three sessions. First, five new zircons from the original mineral separate were dated; these yielded a cluster of ages around 622 Ma and a few older ages. Next we did CA-TIMS analyses on the two youngest zircons from the SIMS mount. A zircon that had yielded a SIMS age of 622.1±5.5 Ma yielded a CA-TIMS age of 590.4±1.7, and a zircon that had yielded a SIMS age of 605.5±3.2 Ma yielded a CA-TIMS age of 569.37±0.36 Ma. Thus, the SIMS ages from this sample turn out to be too old by about 30 m.y. Finally, hoping to rule out the possibility that the 569- and 590-Ma zircons were contaminants, we processed the last remaining uncrushed piece of sample DB07RIM29a and recovered six more zircons. The main population of this subset is around 620 Ma but one zircon is 578±21 Ma. Combining all the CA-TIMS results, sample DB07RIM29a has a dominant zircon population of 623.5±5.5 Ma based on the weighted average $^{206}Pb/^{238}U$ ages of the seven low-error analyses between 617 and 629 Ma (fig. 19*G*). But we suggest that the *dominant* population is xenocrystic and that the eruptive age is approximated by the youngest grain, at 569.4±0.4 Ma.

Sample DB07RIM77a is from the turbiditic upper unit of the Groupe de Téniagouri, which Lahondère and others (2005) assigned to the Sous-groupe de Koumba Ndao. The sample is a medium-grained sandstone from alternating thin-bedded and thick-bedded tuffaceous turbidites (fig. 20*A*); the exposure is in a oued just south of Selibabi in the Selibabi-Bakel 1:200,000-scale sheet (number 1512–1412). Of 120 zircons analyzed, 109 pass the LAICPMS filters. The probability plot has major peaks at 1,522, 1,215, and 601 Ma; lesser peaks are at 1,983, 1,872, 1,302, 1,109, and 988 Ma (fig. 20*F*). The maximum depositional age can be conservatively set at the youngest probability peak, 601 Ma.

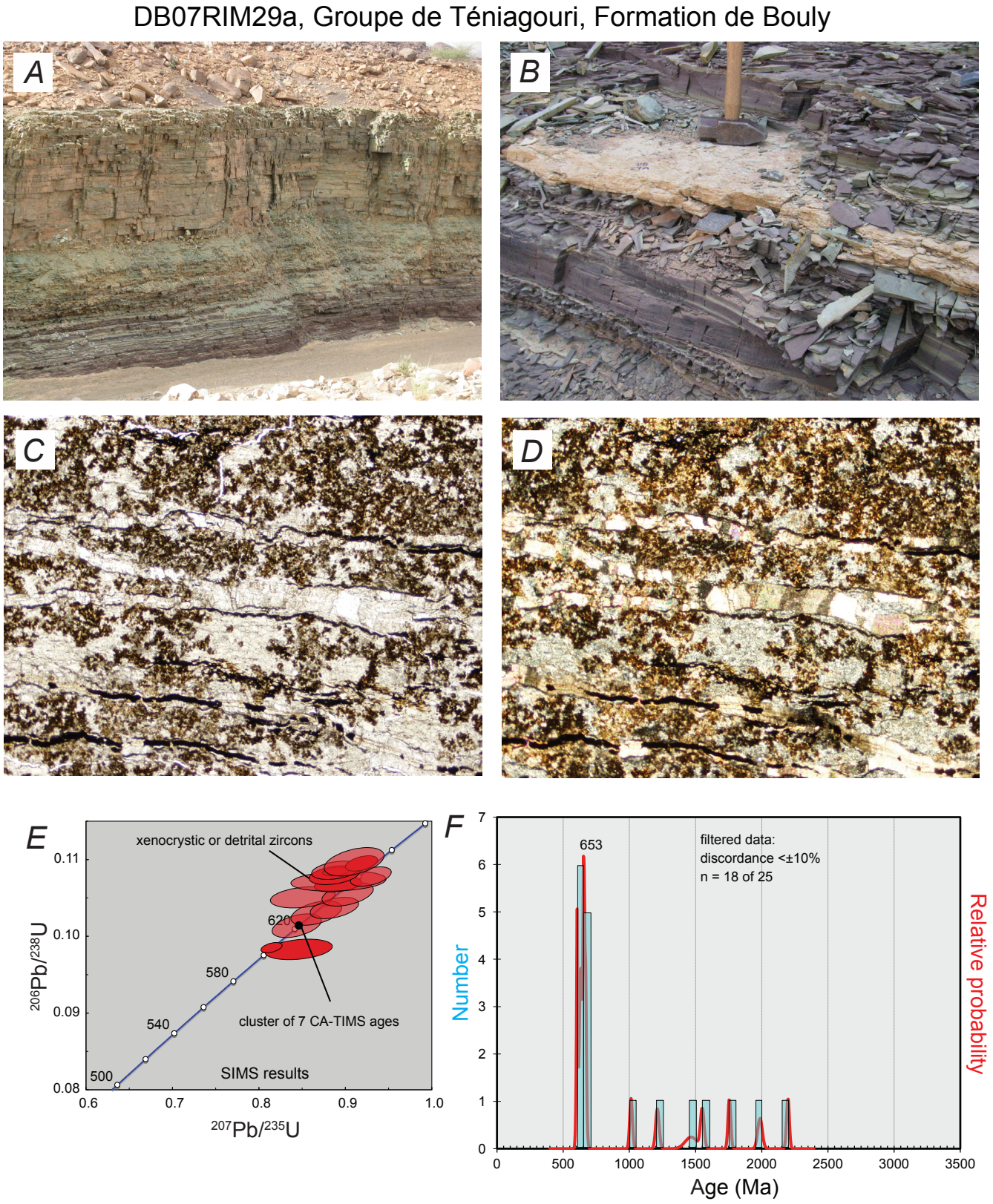


Figure 19. Zircon age data and photographs for the Formation de Bouly, Groupe de Téniagouri, near Atar. (*A*) Outcrop photograph of the sample location, a ~10-meter-high cutbank along a oued. (*B*) Close-up of the sampled ash horizon, just above the base of the cutbank and the thickest of about 10 ash layers. (*C* and *D*) Photomicrographs under plane light and crossed polars, respectively. (*E*) Concordia diagram based on SIMS analyses. (*F*) Age distribution based on SIMS data showing that this tuff layer includes detrital zircons. (*G*) Reflected-light photomicrograph of zircons dated by CA-TIMS, showing a variety of grain types. (*H*) Concordia diagram based on CA-TIMS analyses. (*I*) Weighted average age (green line) based on $^{206}Pb/^{238}U$ zircon ages (red bars) that comprise the cluster of CA-TIMS ages at 623.3±5.5 Ma, as shown in (*I*).—Continued

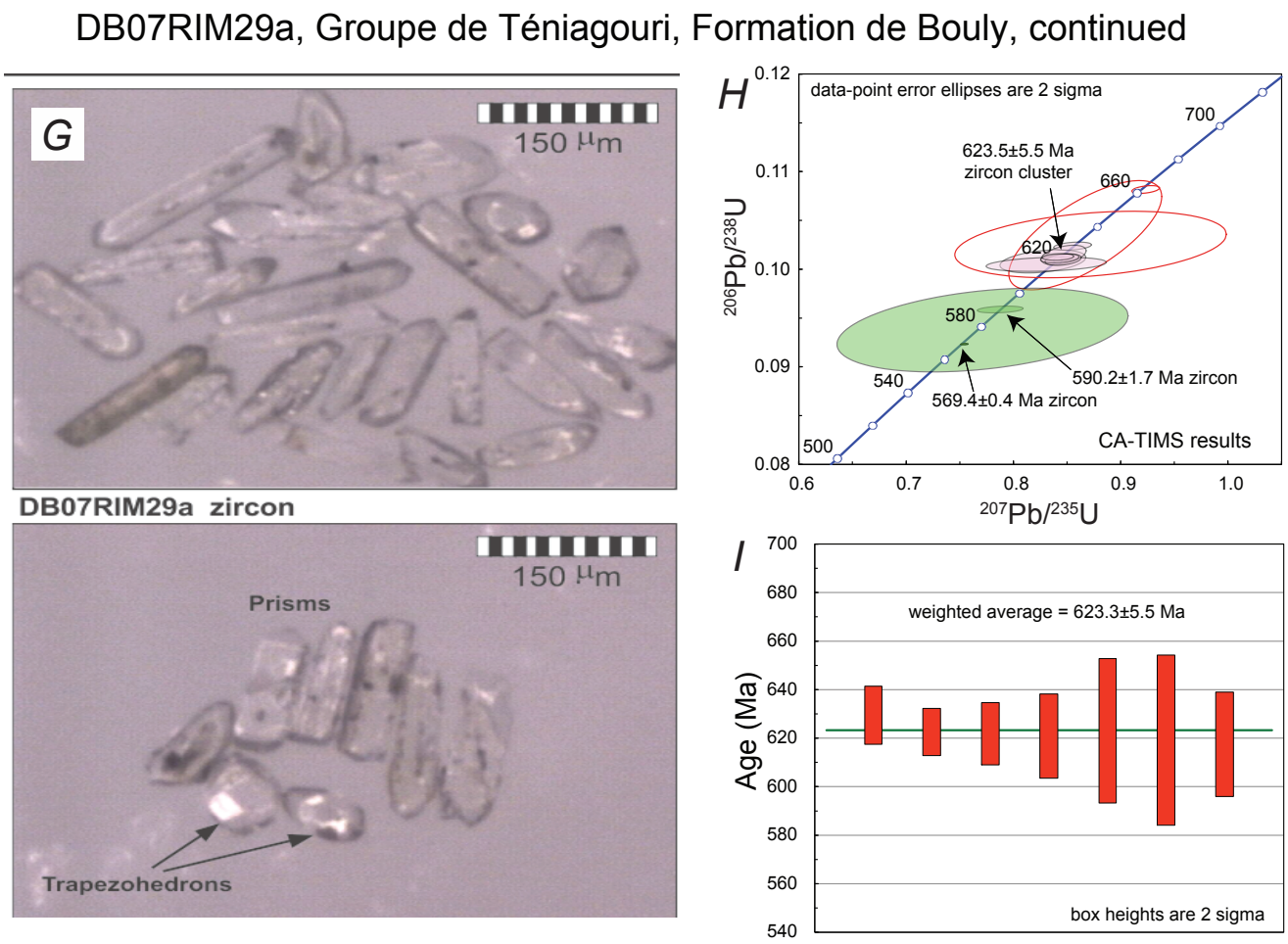


Figure 19. Zircon age data and photographs for the Formation de Bouly, Groupe de Téniagouri, near Atar. (*A*) Outcrop photograph of the sample location, a ~10-meter-high cutbank along a oued. (*B*) Close-up of the sampled ash horizon, just above the base of the cutbank and the thickest of about 10 ash layers. (*C* and *D*) Photomicrographs under plane light and crossed polars, respectively. (*E*) Concordia diagram based on SIMS analyses. (*F*) Age distribution based on SIMS data showing that this tuff layer includes detrital zircons. (*G*) Reflected-light photomicrograph of zircons dated by CA-TIMS, showing a variety of grain types. (*H*) Concordia diagram based on CA-TIMS analyses. (*I*) Weighted average age (green line) based on $^{206}Pb/^{238}U$ zircon ages (red bars) that comprise the cluster of CA-TIMS ages at 623.3±5.5 Ma, as shown in (I).

DB07RIM77a, Group de Téniagouri, Sous-groupe de Koumba Ndao

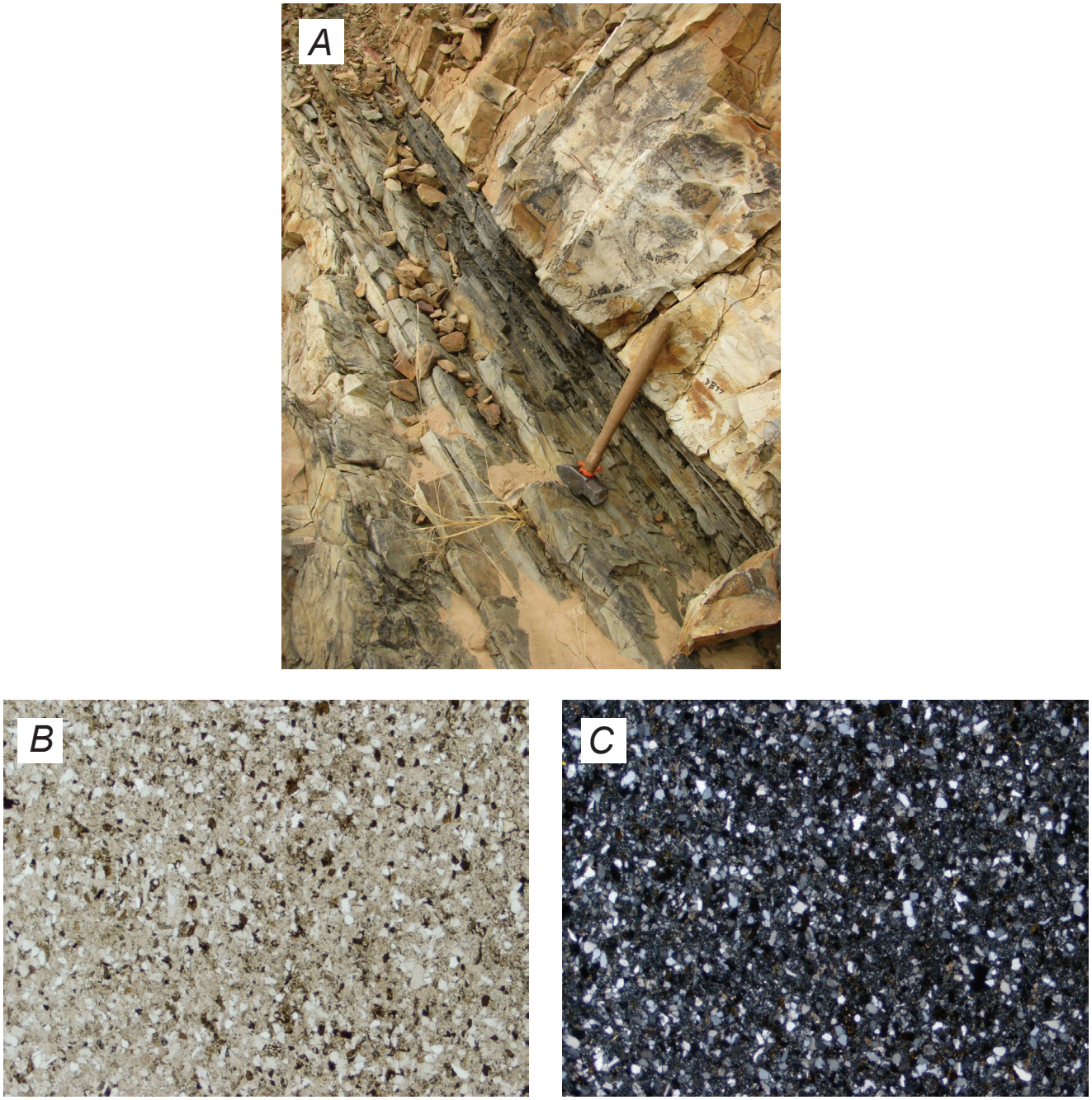


Figure 20. Detrital zircon data and photographs for sample DB07RIM77a from the Sub-groupe de Koumba Ndao of the Groupe de Téniagouri. (*A*) Outcrop photograph of the sample location, specifically the thick bed of light-colored, tuffaceous, turbiditic sandstone in the upper right. (*B* and *C*) Photomicrographs under plane light and crossed polars, respectively. (*D* and *E*) Concordia diagrams. (*F*) Age distribution.—Continued

DB07RIM77a, Group de Téniagouri, Sous-groupe de Koumba Ndao, continued

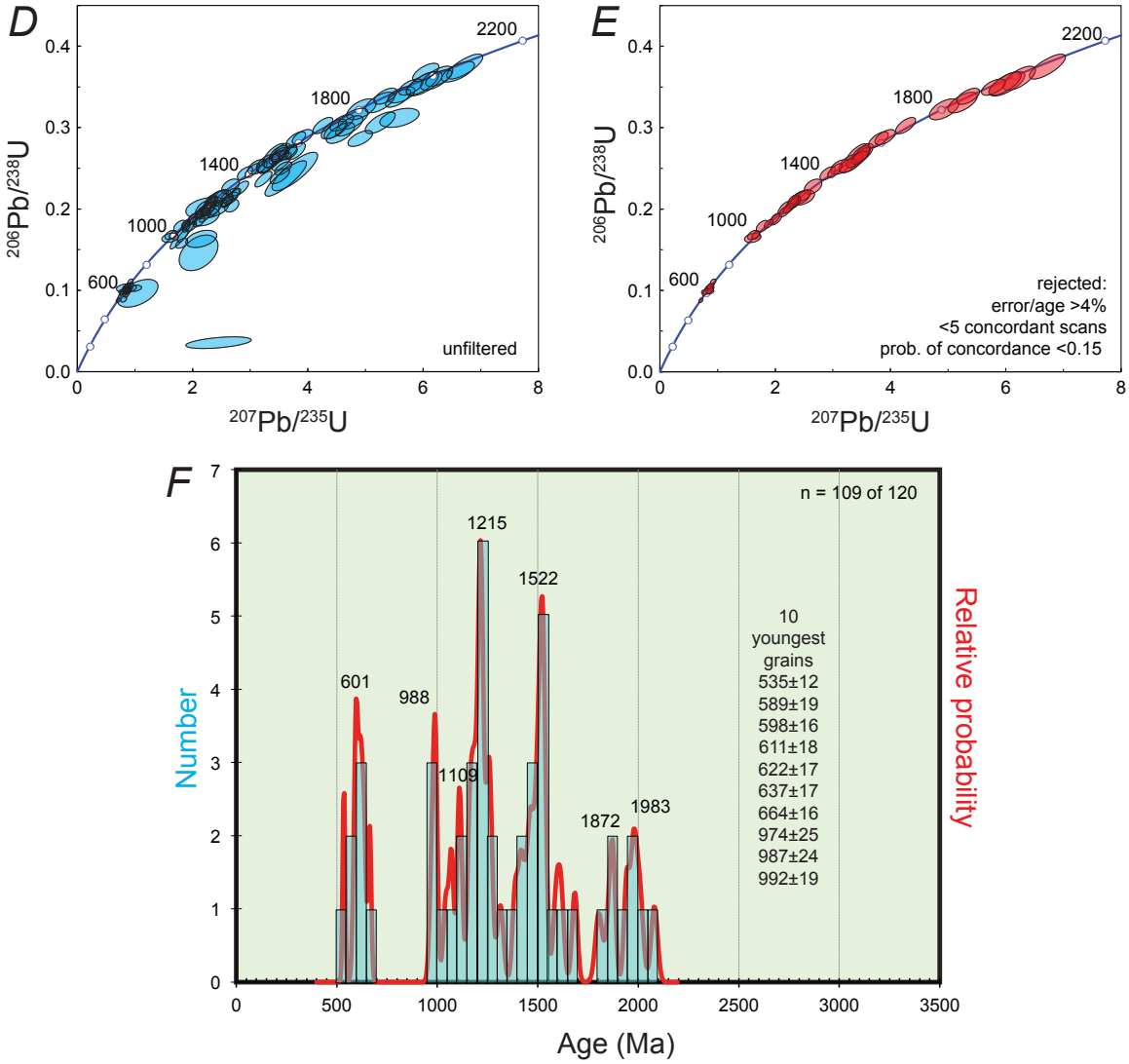


Figure 20. Detrital zircon data and photographs for sample DB07RIM77a from the Sub-groupe de Koumba Ndao of the Groupe de Téniagouri. (*A*) Outcrop photograph of the sample location, specifically the thick bed of light-colored, tuffaceous, turbiditic sandstone in the upper right. (*B* and *C*) Photomicrographs under plane light and crossed polars, respectively. (*D* and *E*) Concordia diagrams. (*F*) Age distribution.

3.8. Groupe de Nouatil, Formation de Serize

As defined by Pitfield and others (2004, Section 4.3.3.1), the Groupe de Nouatil (fig. 8) is mostly sandstone and siltstone, plus minor dolostone, totaling 200–300 m in thickness (Pitfield and others, 2004, Section 4.3.3.3). We sampled the sandstone-dominated Formation de Serize near the middle of the Groupe de Nouatil succession (fig. 21*A*). The sample was collected from roadcuts along the main highway between Atar and Chinguetti, in the western part of the Chinguetti 1:200,000-scale sheet (number 2012). Detrital zircons from sample DB07RIM28a were analyzed by LAICPMS; of 120 zircons analyzed, 75 pass the LAICPMS filters. The probability plot has major peaks at 622 and 581 Ma and lesser peaks at 2,039 and 1,207 Ma (fig. 21*D*). The youngest single zircon, at 466±16 Ma, is of uncertain significance but can be rejected out-of-hand because it is far younger than allowed by the stratigraphic position of the Groupe de Nouatil. The youngest cluster of zircons—which shows as a "shoulder" based on two ages rather than a "peak"—is at 543 Ma and this is taken as the maximum depositional age. This is consistent with its permissible age range of late Neoproterozoic to Cambrian, which is based on stratigraphic position between better-dated units (Pitfield and others, 2004).

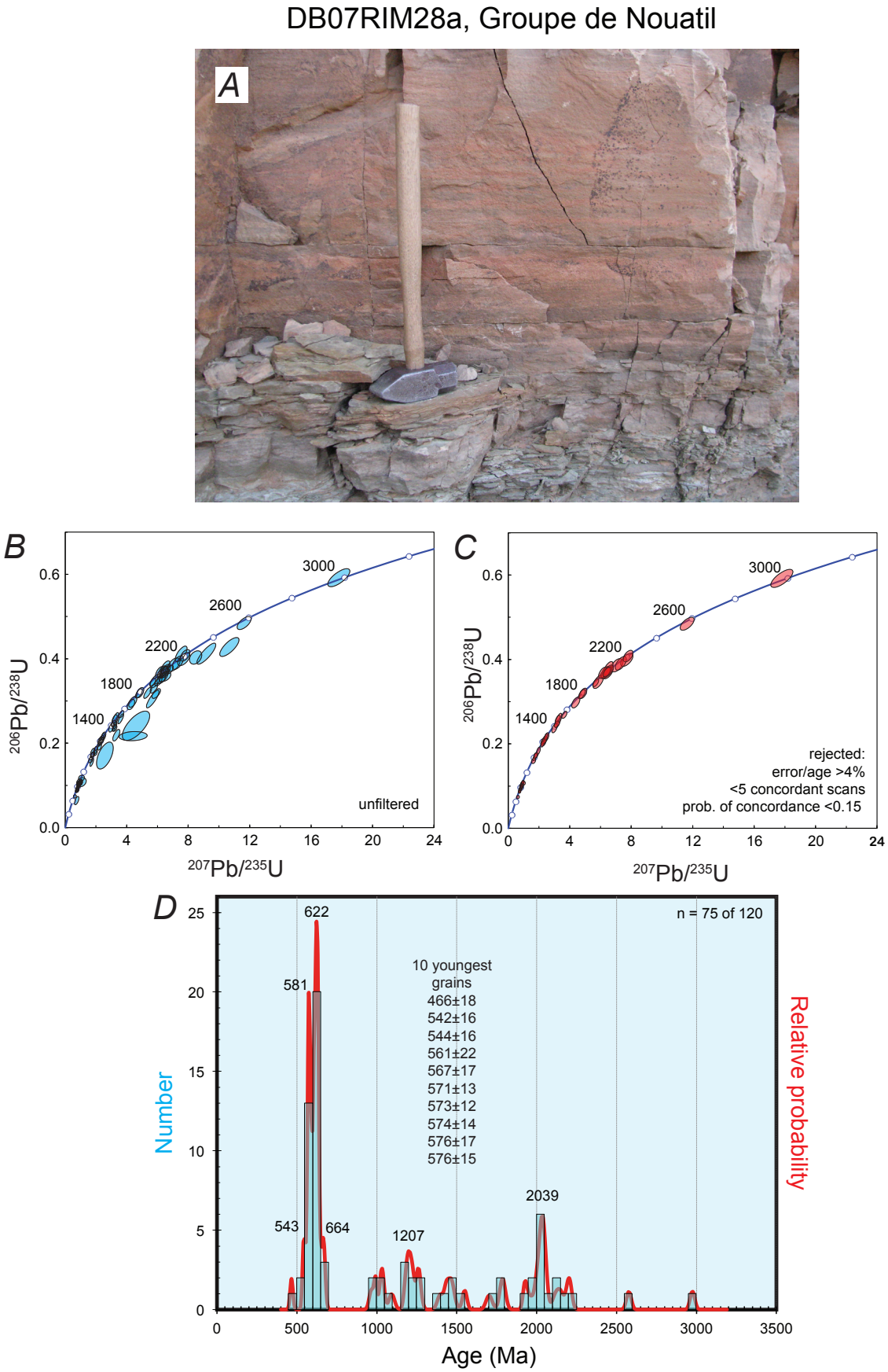


Figure 21. Detrital zircon data and photographs for sample DB07RIM28a from the Groupe de Nouatil. (*A*) Outcrop photograph of sandstone at the sample location. (*B* and *C*) Concordia diagrams. (*D*) Age distribution.

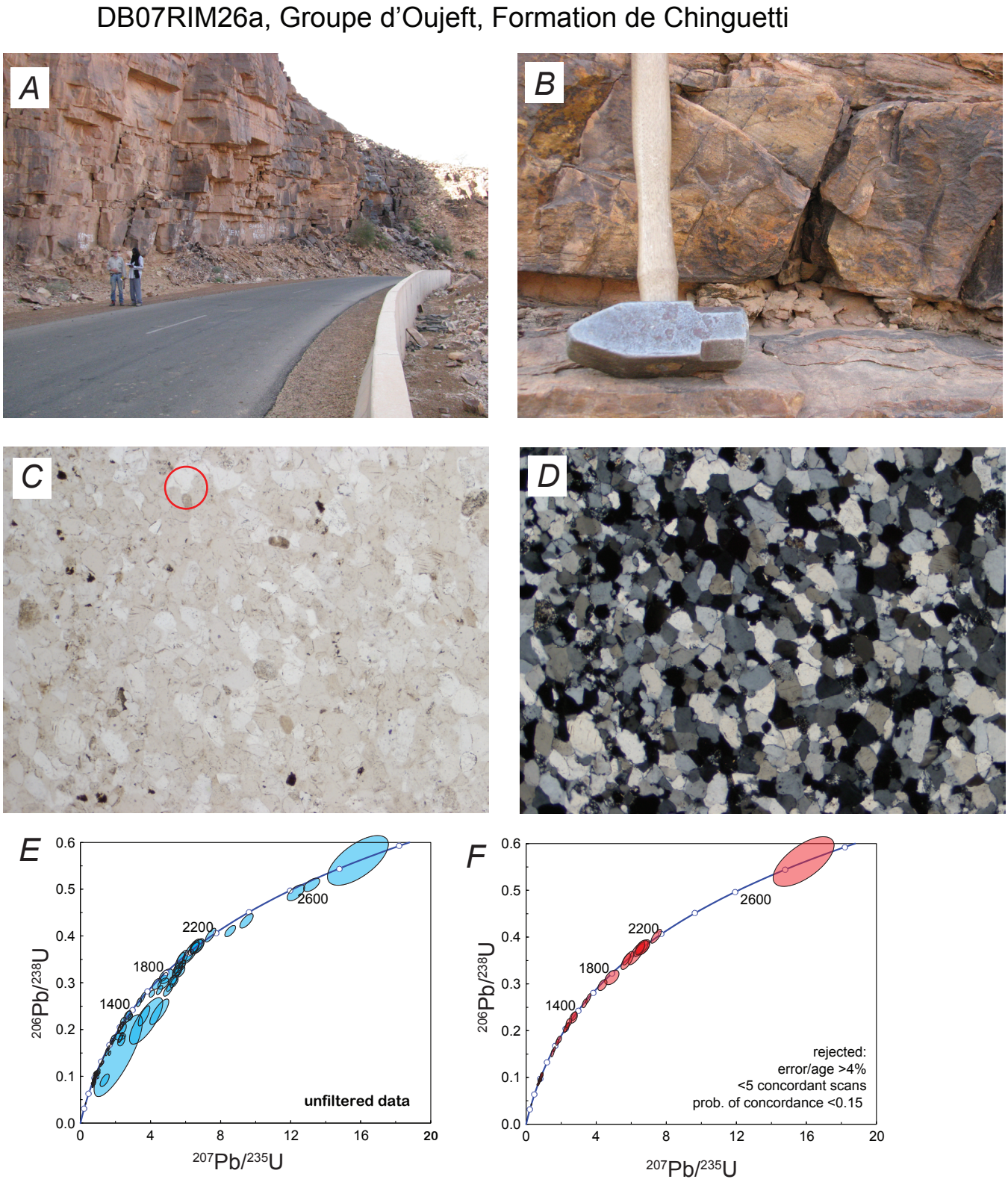


Figure 22. Detrital zircon data and photographs for sample DB07RIM26a from the Groupe d'Oujeft, Formation de Chinguetti near Atar. (*A*) Outcrop photograph of the roadcut along the Atar-Ouadane highway, showing the graffiti-covered sample horizon of sandstone. (*B*) Close-up of the sample horizon. (*C* and *D*) Photomicrographs under plane light and crossed polars, respectively. Red circle encloses an originally detrital quartz grain with rounded core and diagenetic quartz overgrowth. (*E* and *F*) Concordia diagrams. (*G*) Age distribution.—Continued

DB07RIM26a, Groupe d'Oujeft, Formation de Chinguetti, continued

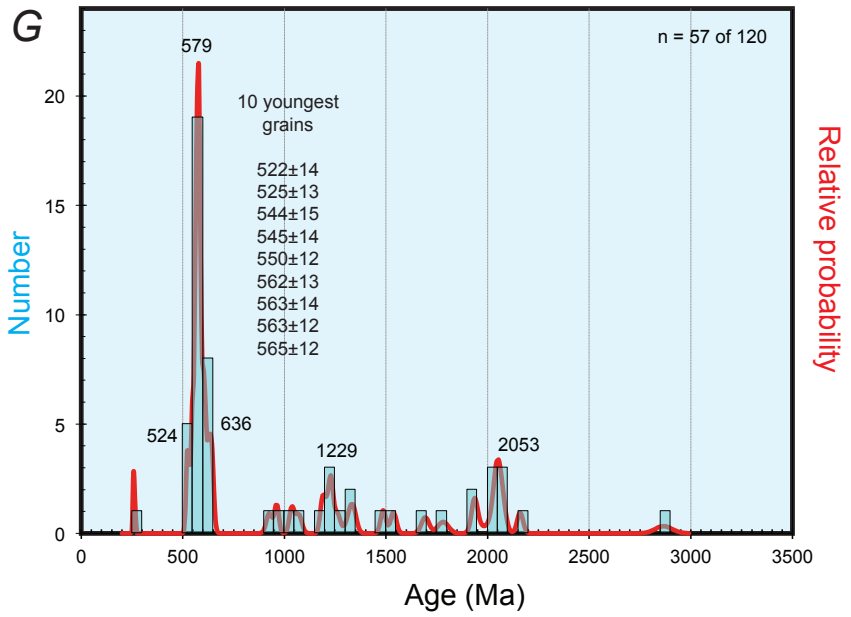


Figure 22. Detrital zircon data and photographs for sample DB07RIM26a from the Groupe d'Oujeft, Formation de Chinguetti near Atar. (*A*) Outcrop photograph of the roadcut along the Atar-Ouadane highway, showing the graffiti-covered sample horizon of sandstone. (*B*) Close-up of the sample horizon. (*C* and *D*) Photomicrographs under plane light and crossed polars, respectively. Red circle encloses an originally detrital quartz grain with rounded core and diagenetic quartz overgrowth. (*E* and *F*) Concordia diagrams. (*G*) Age distribution.

3.9. Groupe d'Oujeft

The Cambrian Groupe d'Oujeft (fig. 8) is a widespread sandstone-dominated unit deposited near the Mauritanide orogenic front. We analyzed five samples from various locations. As will be discussed, the last to be described probably doesn't belong in the Groupe d'Oujeft, and we suggest that it was mismapped.

Detrital zircons were analyzed from two samples of the Formation de Chinguetti. Sample DB07RIM26a is a cross-stratified, medium-grained, reddish-brown sandstone (figs. 22*A* and *B*). from roadcuts along the main highway between Atar and Chinguetti in the western part of the Chinguetti 1:200,000-scale sheet (number 2012). The sampled horizon is covered with graffiti. Of 120 zircons analyzed, 57 pass the LAICPMS filters. The probability plot shows a major peak at 579 Ma and minor peaks at 2,053, 1,229, and 636 Ma (fig. 22*G*). The maximum depositional age is 524 based on the mean of the two youngest overlapping ages, which define a "shoulder" in the probability curve.

Our other sample from the Formation de Chinguetti, DB07RIM61a, is from near Ouadane, just outside the ring of Guelb er Richat in the Ouadane 1:200,000-scale sheet (number 2011). The outcrop is from large-scale cross-stratified, medium-grained, reddish brown sandstone (fig. 23*A*). Of 120 grains analyzed, 89 pass the LAICPMS filters. The probability plot shows a major peak at 573 Ma and minor peaks at 2,047 and 1,199 Ma (fig. 23*D*). Based only on detrital zircons, the maximum depositional age would be set at 573 Ma (mean of the youngest three overlapping ages). On geologic grounds, however, the depositional age of this sample likely around 525 Ma.

Sample DB07RIM75a is from Sous-groupe d'Aghaoujeft (original map unit OjA) near Le Bheyr along the western edge of the Kiffa 1:200,000-scale sheet (number 1611). The outcrops are conspicuous cliffy hills of extremely thick-bedded, reddish-brown, coarse (locally pebbly) sandstone (figs. 24*A* and *B*). Of 120 grains analyzed, 76 pass the LAICPMS filters. The probability plot shows a major peak at 620 Ma and subsidiary peaks, or "shoulders" at 563, 541, and 520 Ma (fig. 24*G*). We set the maximum depositional age at 520 Ma.

Detrital zircons were analyzed from two samples from rocks that had been mapped as Formation de Moudjeria. Sample CT07RIM60-1 is a coarse-grained, red, large-scale cross-stratified sandstone (fig. 25*A*), collected along Oued El Fras near the village of Douboulgui in the Kankossa-Kayes 1:200,000-scale sheet (number 1511 & 1411). Of 120 grains analyzed, 57 pass the LAICPMS filters. The probability plot shows a major peak at 631 Ma and minor ones at 2,129 and 2,072 Ma (fig. 25*F*). The youngest zircons define a "shoulder" at 565 Ma, where we set the maximum depositional age.

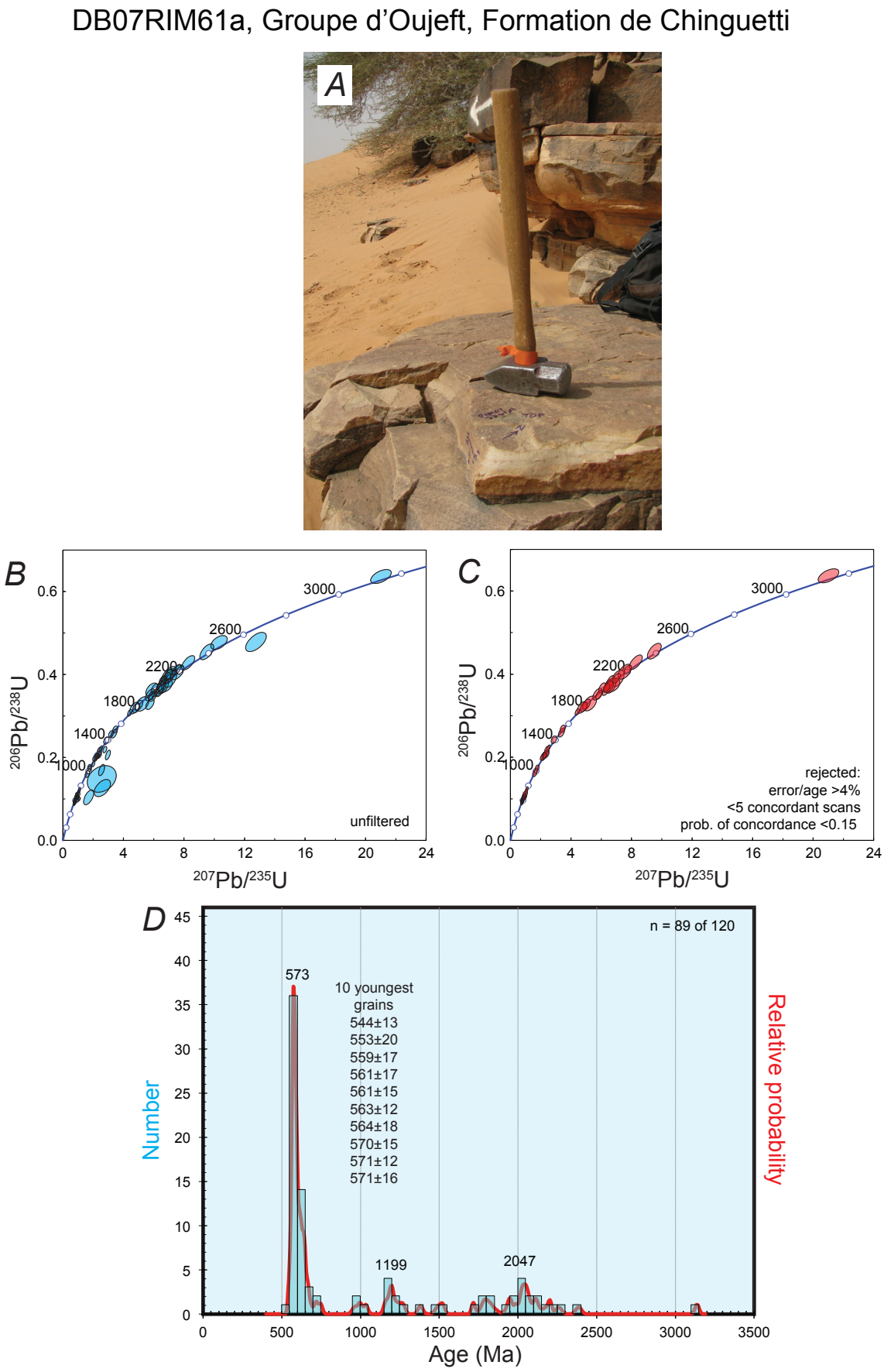


Figure 23. Detrital zircon data and photographs for sample DB07RIM61a from the Groupe d'Oujeft, Formation de Chinguetti near Ouadane. (A) Outcrop photograph of sandstone at the sample location. (*B* and *C*) Concordia diagrams. (*D*) Age distribution.

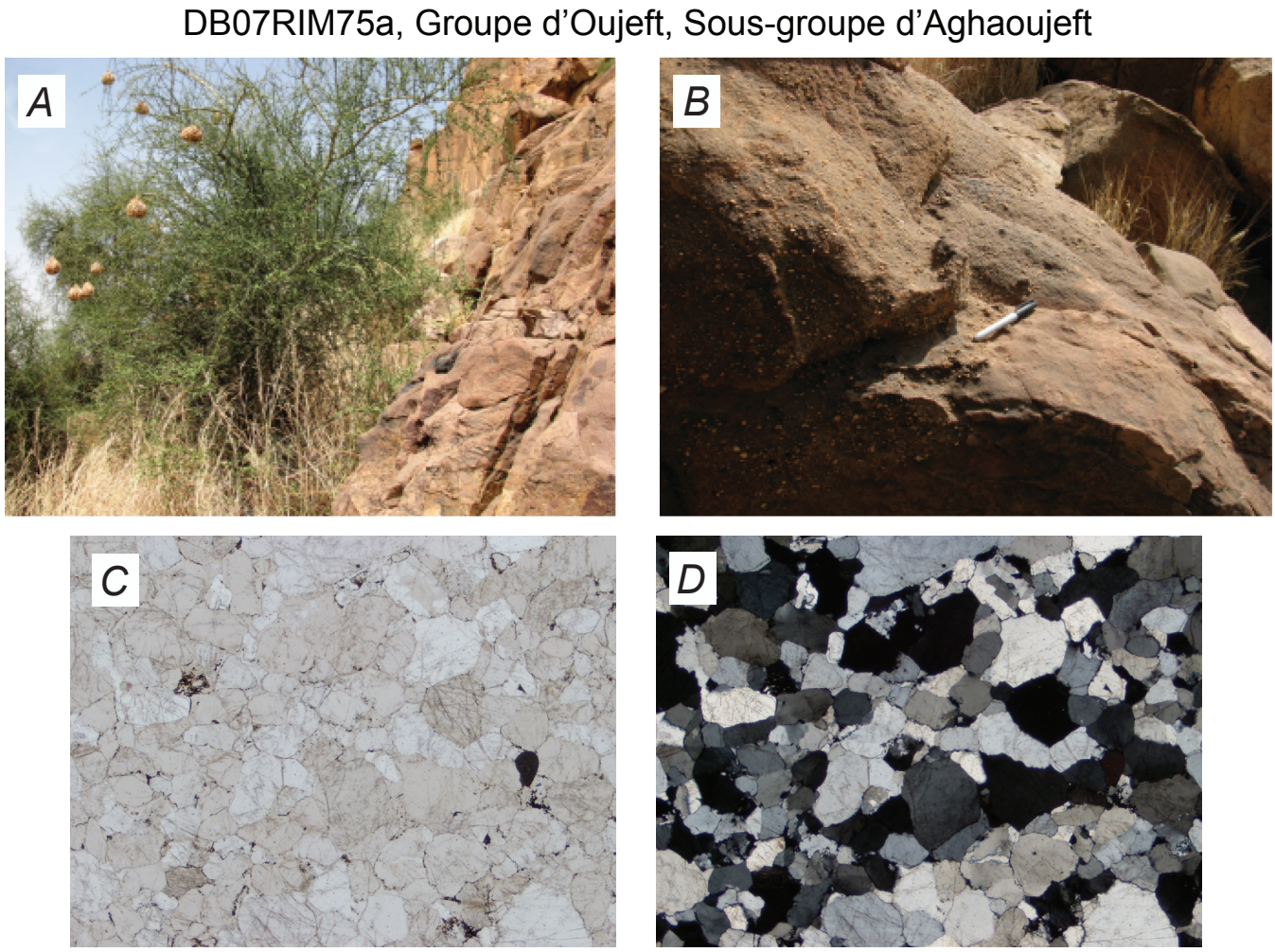


Figure 24. Detrital zircon data and photographs for sample DB07RIM75a from the Groupe d'Oujeft, Sous-groupe d'Aghaoujeft. (*A* and *B*) Outcrop photographs of sandstone at the sample location. (*C* and *D*) Photomicrographs under plane light and crossed polars, respectively. (*E* and *F*) Concordia diagrams. (*G*) Age distribution. —Continued

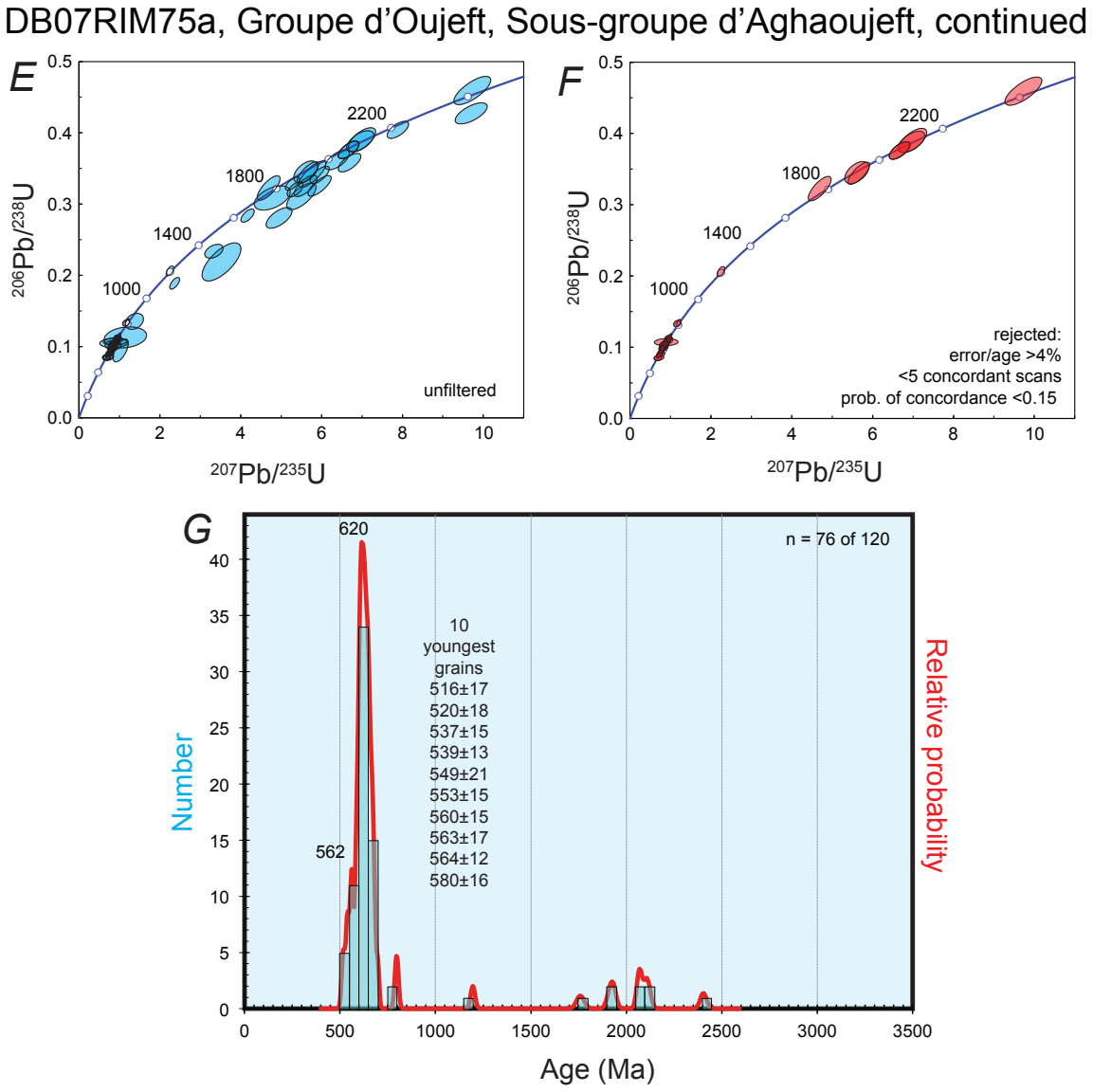


Figure 24. Detrital zircon data and photographs for sample DB07RIM75a from the Groupe d'Oujeft, Sous-groupe d'Aghaoujeft. (*A* and *B*) Outcrop photographs of sandstone at the sample location. (*C* and *D*) Photomicrographs under plane light and crossed polars, respectively. (*E* and *F*) Concordia diagrams. (*G*) Age distribution.

The other Formation de Moudjeria sample (DB07RIM74a) has a totally different detrital zircon age distribution. It is from low outcrops of thick-bedded, reddish brown, medium-grained sandstone (fig. 26*A*) near the Mauritanide deformation front. The sample location is near Oued Moudr, close to the eastern edge of the Mbout 1:200,000-scale sheet (number 1612). Of 120 grains analyzed, 86 pass the LAICPMS filters. The probability plot shows major peaks at 1,529 and 1,212 Ma and minor peaks at 1,929, 1,741, 1,406, 1,141, 1,041, and 906 Ma (fig. 26*F*). The maximum depositional age is 903 Ma based on the mean of the two youngest ages. The detrital zircon signature of this rock is very different from other samples that unquestionably belong in the Groupe de Oujeft. We therefore suggest that the outcrop belt containing sample DB07RIM74a is more complex than shown on the Mbout 1:200,000-scale geologic map (Pitfield and others, 2004). The closest rock unit known to have a similar detrital zircon signature is the Groupe de Djonaba. Accordingly, on the 1:1,000,000-scale geologic map we have moved the eastern boundary of the Groupe de Djonaba outcrop belt about 2 km to the east to include the location of sample DB07RIM74a.

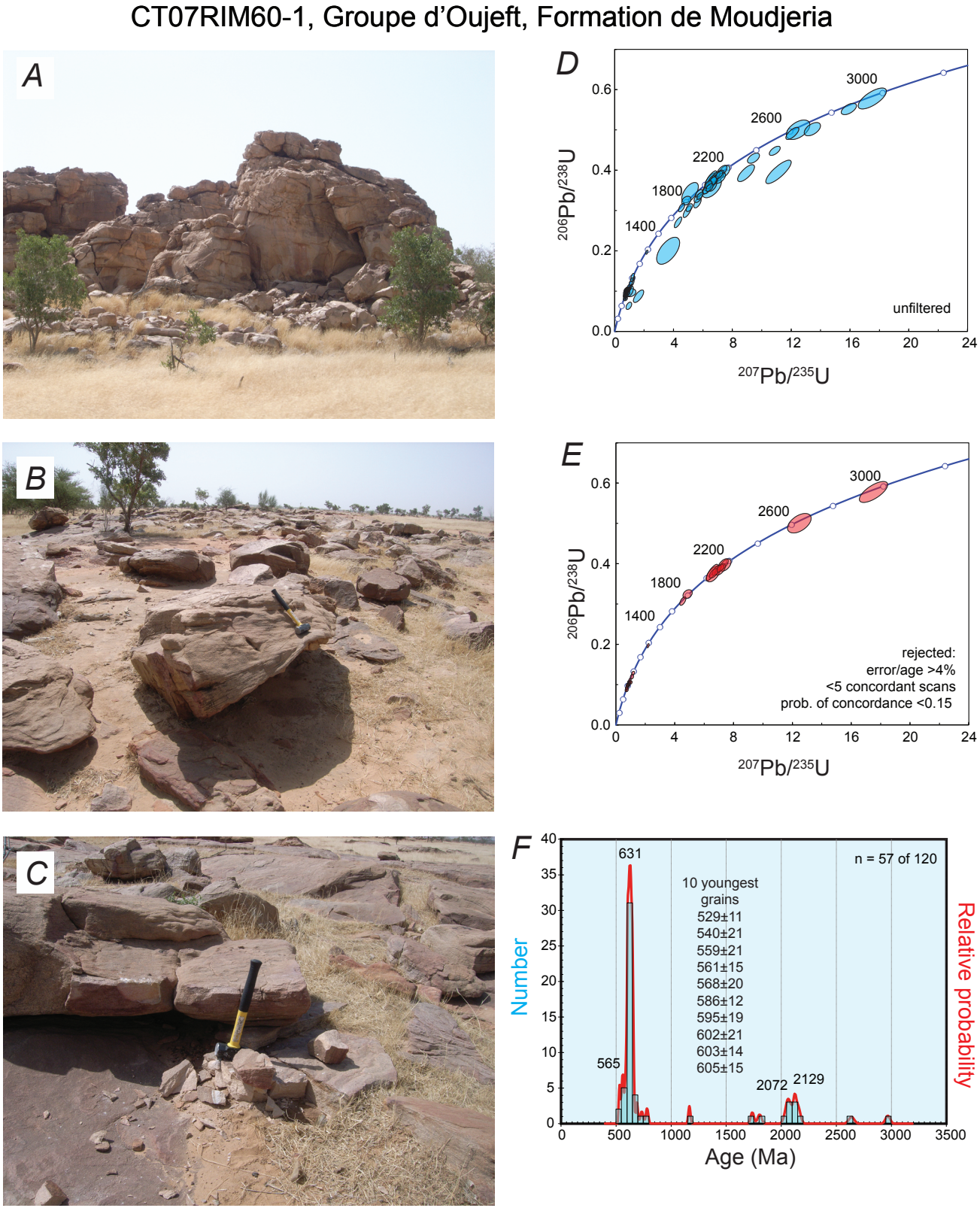


Figure 25. Detrital zircon data and photographs for sample CT07RIM60-1 from the Formation de Moudjeria of the Groupe d'Oujeft. (*A, B,* and *C*) Outcrop photographs of sandstone at the sample location. Photographs by Cliff Taylor. (*D* and *E*) Concordia diagrams. (*F*) Age distribution.

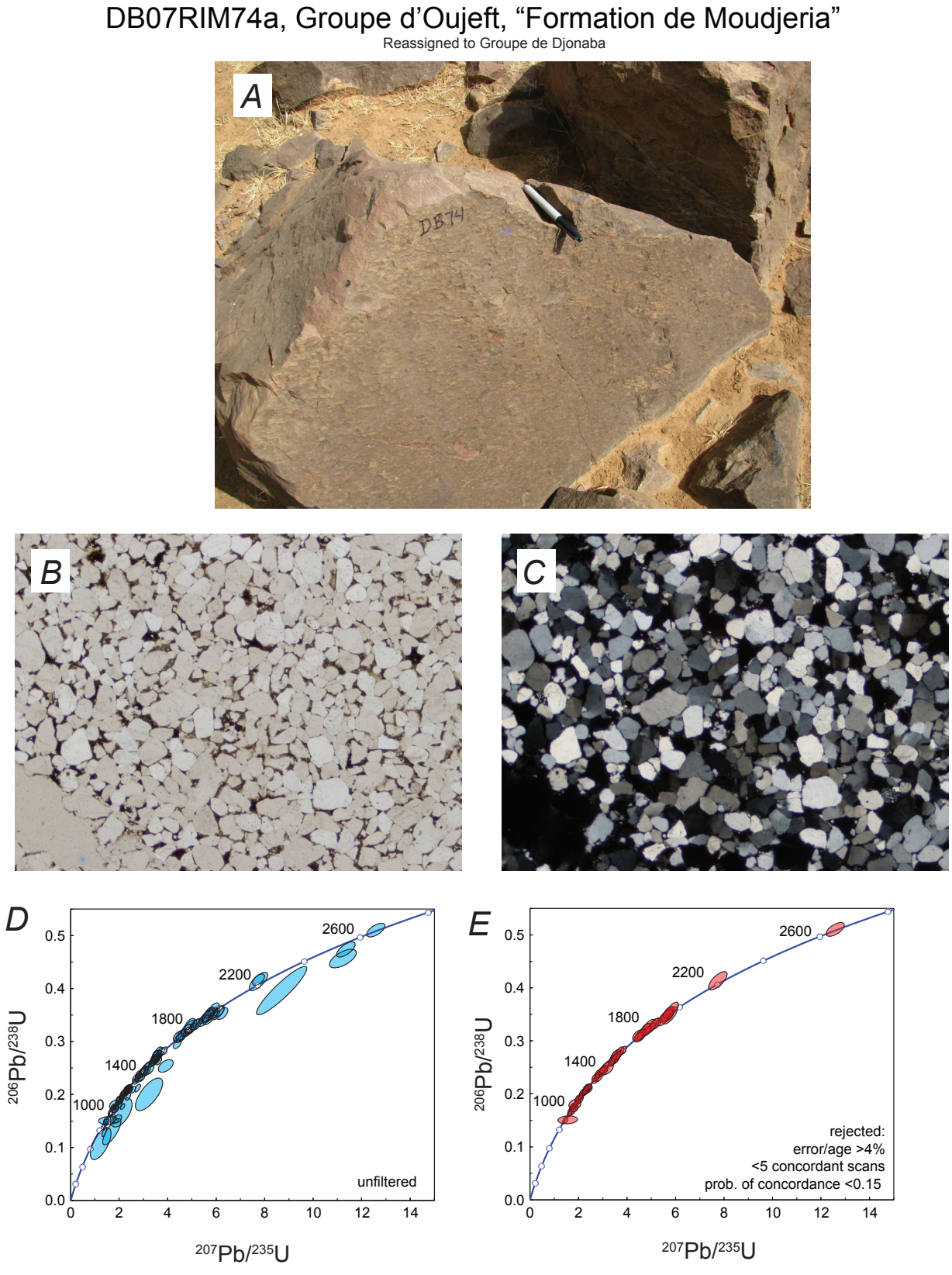


Figure 26. Detrital zircon data and photographs for sample DB07RIM74a, from rocks mismapped as Groupe d'Oujeft, Moudjeria Formation. (*A*) Outcrop photograph of the sandstone from sample location. (*B* and *C*) Photomicrographs under plane light and crossed polars, respectively. (*D* and *E*) Concordia diagrams. (*F*) Age distribution.—Continued

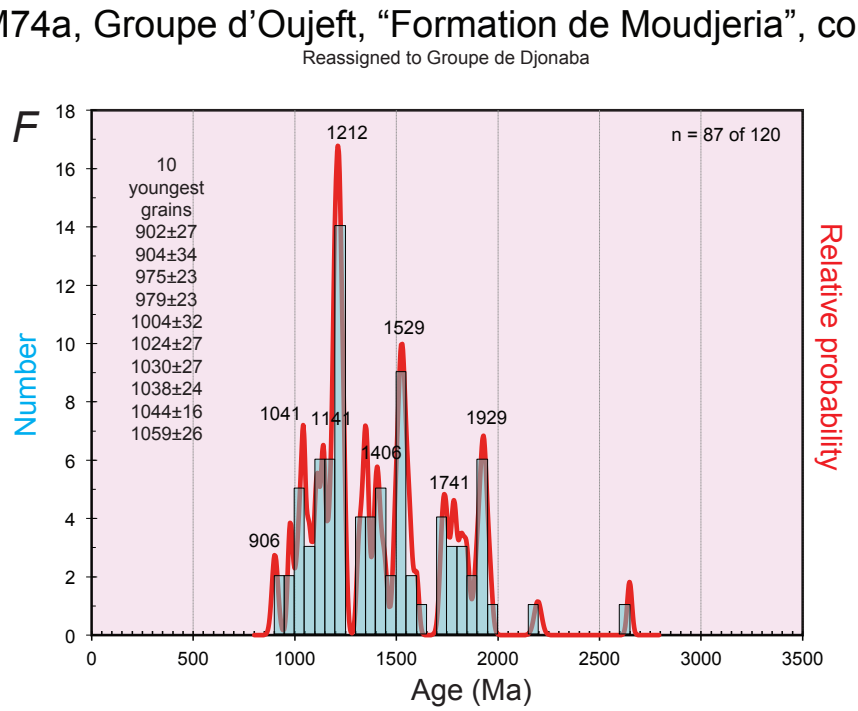


Figure 26. Detrital zircon data and photographs for sample DB07RIM74a, from rocks mismapped as Groupe d'Oujeft, Moudjeria Formation. (*A*) Outcrop photograph of the sandstone from sample location. (*B* and *C*) Photomicrographs under plane light and crossed polars, respectively. (*D* and *E*) Concordia diagrams. (*F*) Age distribution.

3.10. Groupe de Tichit (Ordovician)

The Formation de Tabarit El Kbir is the lowest of five formations in the Groupe de Tichit (fig. 8) and is characterized by quartzose sandstones (Pitfield and others, 2004). Higher in the Groupe de Tichit are glaciogenic strata from the terminal Ordovician glaciation. Sample CT07RIM59-1 is from outcrops of coarse-grained, red, large-scale trough cross-stratified sandstone (fig. 27A). The sample is from near Guénétir in the northeastern corner of the Selibabi-Bakel 1:200,000-scale sheet (number 1512-1412). Of 120 grains analyzed, only 25 pass the LAICPMS filters. The probability plot shows closely spaced major peaks at 601 and 548 Ma and a smattering of other ages (fig. 27*E*). Given the well-established Late Ordovician age for glaciation in Africa (Ghienne, 2003), the detrital zircons from this sample contribute no new information on the depositional age.

3.11. Groupe de Néma, Formation de Saïlé (Cretaceous)

The Groupe de Néma, which consists of continental clastic rocks, crops out in the Hodh region of southeastern Mauritania. It is mostly green mudstone. Its age is poorly constrained but it postdates ca. 199 Ma mafic rocks and is likely mid-Cretaceous (Lahondère and others, 2005). Sample CT07RIM62-1 is a red-weathering massive sandstone (figs. 28*A* and *B*) from the northern outskirts of Néma (Néma 1:200,000-scale sheet, number 1607). Of 120 zircons analyzed, 56 pass the LAICPMS filters. The probability plot shows closely spaced major peaks at 606, 576, and 545 Ma and a minor peak at 2,136 Ma (fig. 28*E*). There are no young zircons that bear on the depositional age.

4.0. Geochronological Results from the Central Mauritanide Orogen

In this section we describe U-Pb detrital zircon, U-Pb igneous zircon, and $^{40}Ar/^{39}Ar$ white mica geochronological results from the Central Mauritanides, which for present purposes is the roughly north-south striking sector of the orogen from latitude 18°30'N south to the Senegal border. During the Hercynian (Carboniferous to Permian) orogeny, multiple, stacked thrust sheets were emplaced into their final position over the West African basement and its cratonic, Toudeni Basin cover (Lécorché and others, 1989). Results from the various supracrustal map units are presented from east (parautochthonous rocks) to west (allochthonous rocks) followed by results from plutonic rocks and cross-cutting veins.

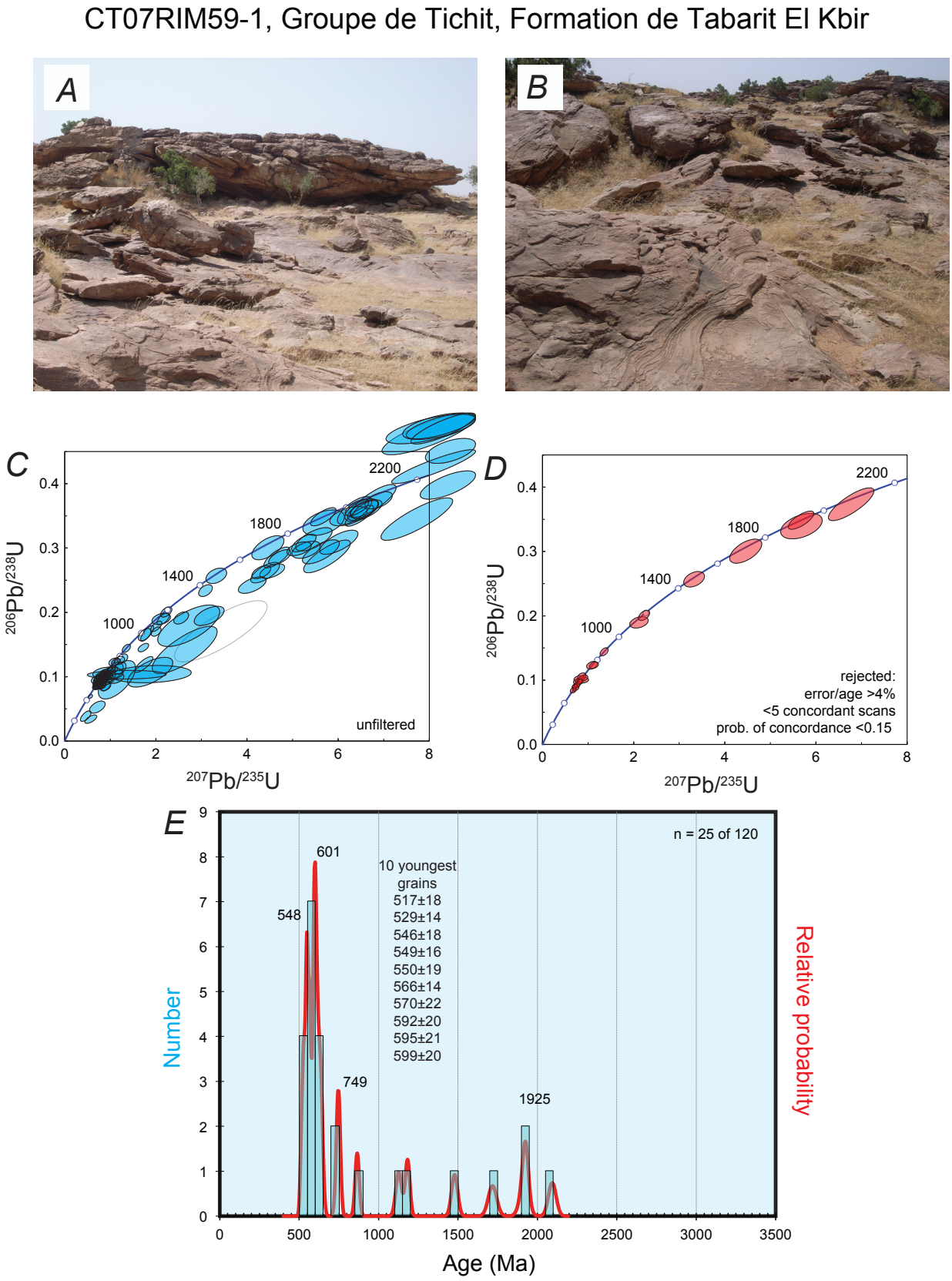


Figure 27. Detrital zircon data and photographs for sample CT07RIM59-1, from the Groupe de Tichit, Formation de Tabarit El Kbir. (*A* and *B*) Outcrop photographs of sandstone at the sample location. Photographs by Cliff Taylor. (*C* and *D*) Concordia diagrams. (*E*) Age distribution.

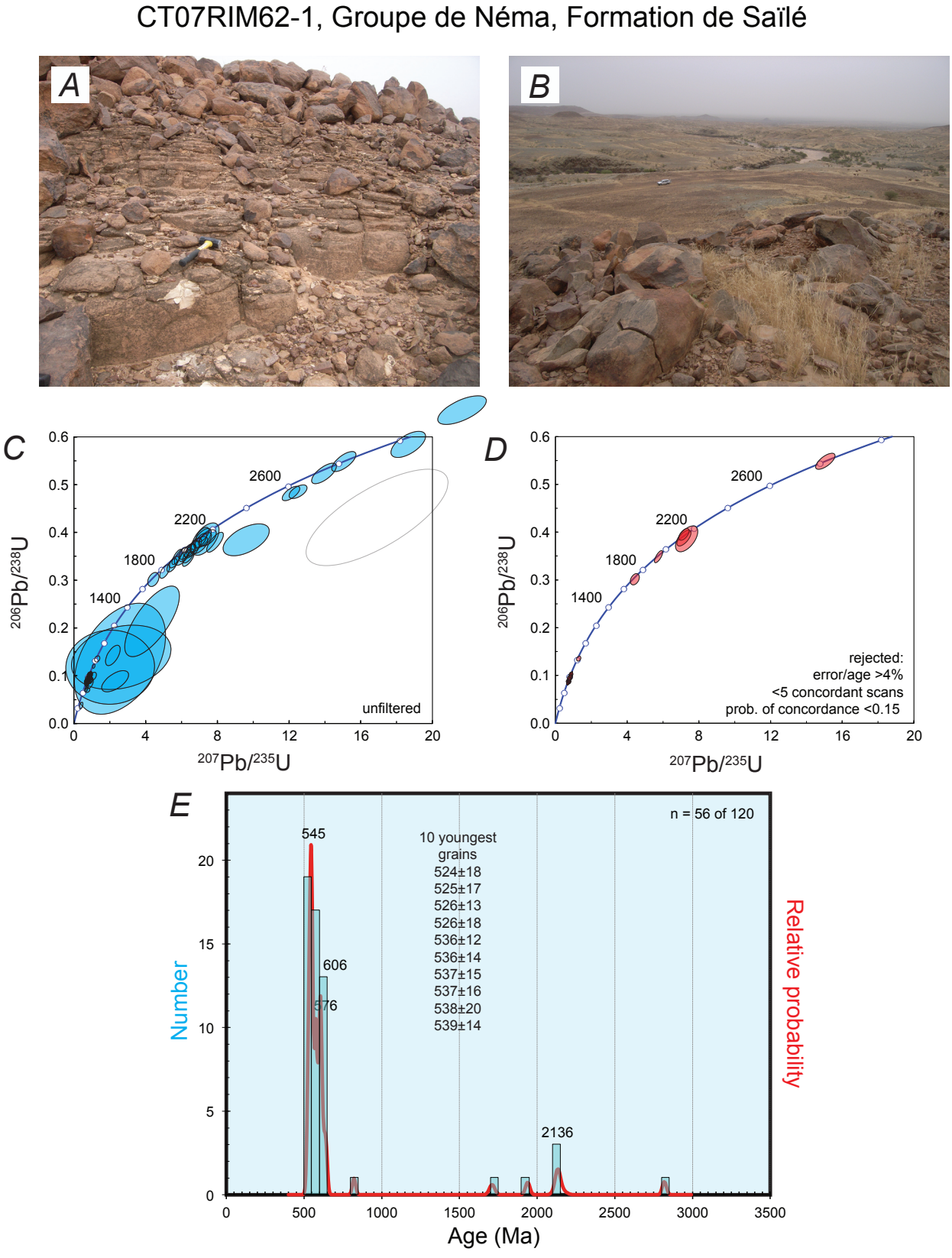


Figure 28. Detrital zircon data and photographs for sample CT07RIM62-1, from the Groupe de Néma, Formation de Saïlé. (*A* and *B*) Outcrop photographs of the sandstone at the sample location. Photographs by Cliff Taylor. (*B* and *C*) Concordia diagrams. (*E*) Age distribution.

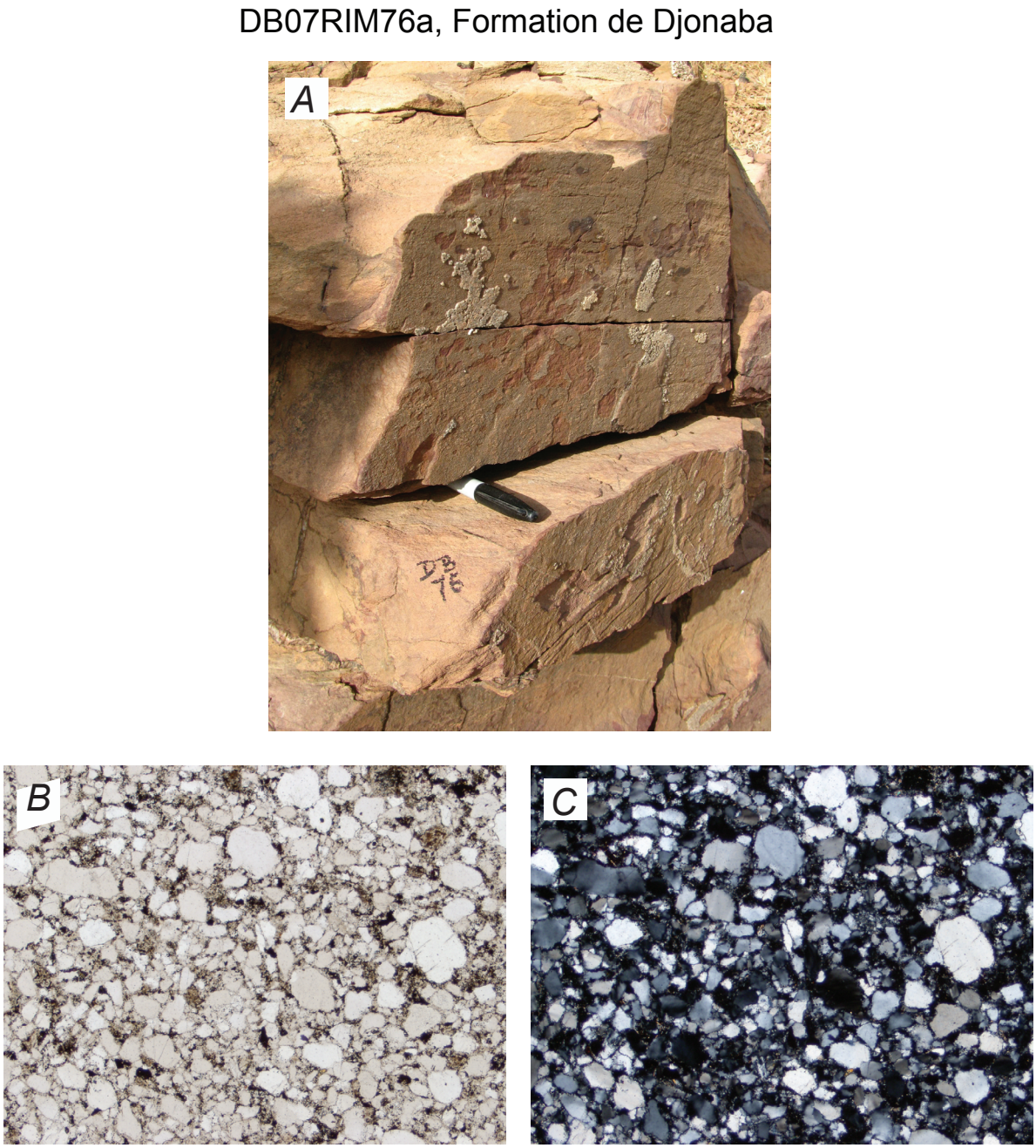


Figure 29. Detrital zircon data and photographs for sample DB07RIM76a, from the Groupe de Djonaba. (*A*) Outcrop photograph of sandstone at the sample location. (*B* and *C*) Photomicrographs under plane light and crossed polars, respectively. (*D* and *E*) Concordia diagrams. (*F*) Age distribution.—Continued

4.1. Groupe de Djonaba

The Groupe de Djonaba is a parautochthonous succession in the easternmost belt of the Central Mauritanides (Pitfield and others, 2004). Sample DB07RIM76a is a reddish, medium-grained sandstone from an outcrop of 50-cm-thick turbiditic sandstone beds alternating with 1-cm-thick siltstone partings (fig. 29*A*), located along Oûdeï el Gharoône near the eastern edge of the Mbout 1:200,000-scale sheet (number 1612). Of 120 grains analyzed, 75 pass the LAICPMS filters. The probability plot shows major peaks at 1,518, 1,282, and 1,224 Ma and minor peaks at 2,053, 1,741, 1,347, 1,094, and 982 Ma (fig. 29*F*). The maximum depositional age is 982 Ma based on the youngest peak. The detrital zircon age distribution is similar to that of the Groupe d'Assabet El Hassiane. Pitfield and others (2004, Section 3.2.2.7) suggested that the Groupe de Djonaba consists of the

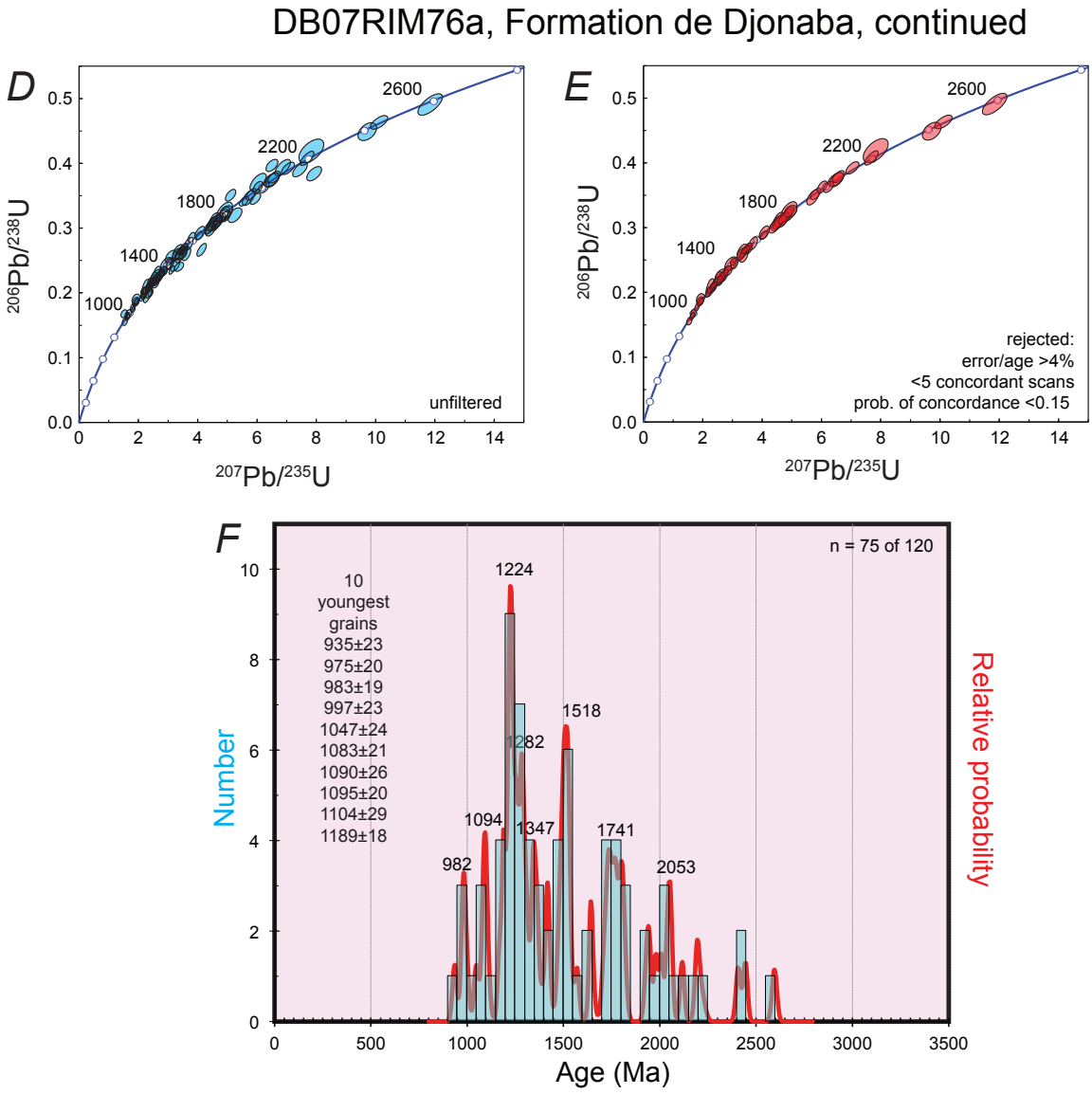


Figure 29. Detrital zircon data and photographs for sample DB07RIM76a, from the Groupe de Djonaba. (*A*) Outcrop photograph of sandstone at the sample location. (*B* and *C*) Photomicrographs under plane light and crossed polars, respectively. (*D* and *E*) Concordia diagrams. (*F*) Age distribution.

deformed equivalents of the Groupes de Jbéliat, de Téniagouri, and de Nouatil. Our results suggest that the Groupe de Djonaba likely also includes deformed strata that correlate with the Groupe d'Assabet El Hassiane.

4.2. Groupe de Gadel

The Groupe de Gadel is a mélange-like tectonic assemblage along the Mauritanide suture zone. It is made up of two contrasting lithologic packages: (1) metamorphosed ultramafic and mafic rocks; and (2) siliciclastic metasedimentary rocks (Pitfield and others, 2004, Section 3.3.3.3). Sample DB07RIM65a, a deformed quartz-rich conglomerate (fig. 30*A*), was analyzed for detrital zircons. The sample location is in an area of patchy outcrop in the northwestern part of the Mbout 1:200,000-scale sheet (number 1612). The GPS location plots about 100 m west of the mapped contact between Groupe de Gadel and Groupe de Mseigguem, but the contact is poorly constrained in this area. Accordingly, on the national-scale geologic map, we moved the contact a short distance west to allow for inclusion of this sample in the Groupe de Gadel. Of 120 grains analyzed, 80 pass the LAICPMS filters. The probability plot shows major peaks at 1,236, 1,182; and 999 Ma and minor peaks at 2,092, 2,046, 1,504, 1,435, 1381, and 1,297 Ma (fig. 30*D*). The maximum depositional age is 999 Ma based on the youngest peak in the age distribution, which represents seven zircons.

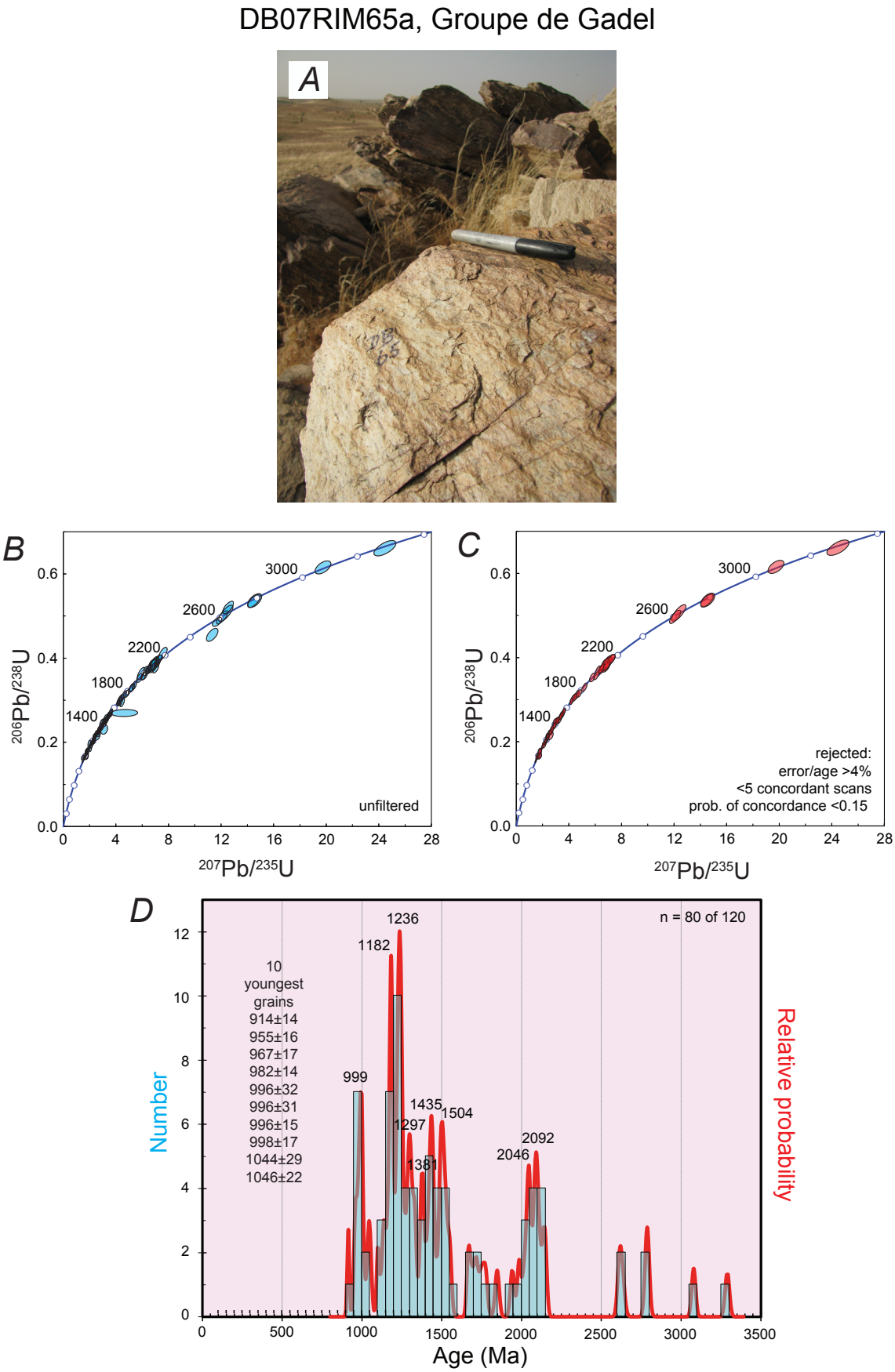


Figure 30. Detrital zircon data and photographs for sample DB07RIM65a, from the Groupe de Gadel. (*A*) Outcrop photograph of metasandstone at the sample location. (*B* and *C*) Concordia diagrams. (*D*) Age distribution.

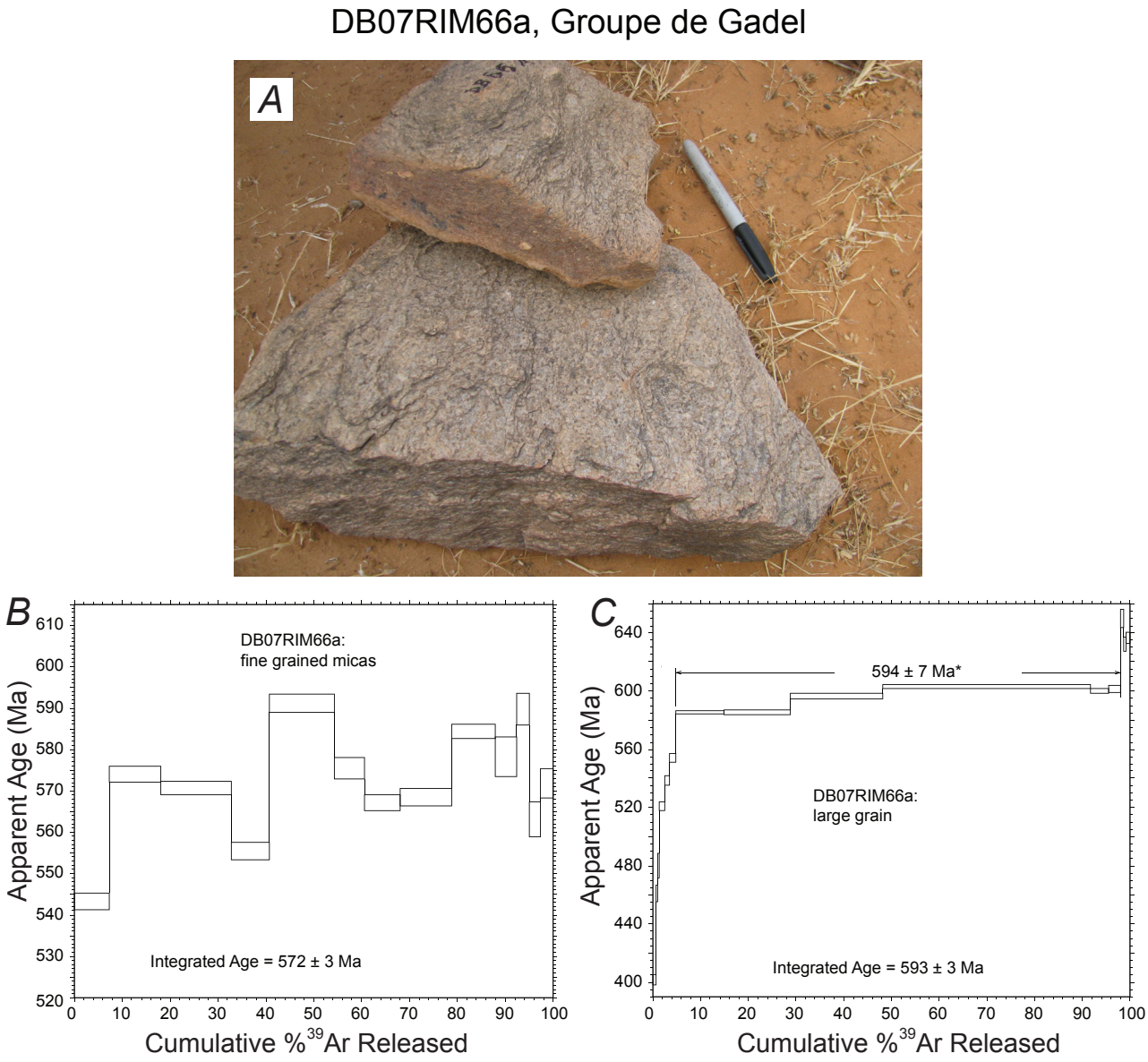


Figure 31. (*A*) Outcrop photograph of the sample location of sample DB07RIM66a, a deformed, metamorphosed conglomerate from the Groupe de Gadel. (*B* and *C*) Argon age-release spectra for two white mica fractions.

Two white mica fractions from sample DB07RIM66A from the Groupe de Gadel were analyzed by the $^{40}Ar/^{39}Ar$ method. The rock is a deformed pebble conglomerate with a micaceous matrix (fig. 31A). The sample is from near sample DB07RIM65a in the northwestern part of the Mbout 1:200,000-scale sheet (number 1612). The $^{40}Ar/^{39}Ar$ data from the first fraction were obtained from heating a single, large mica grain. The age of 594±7 Ma is averaged from 6 heating steps representing about 90% of the gas released and is interpreted as the time this sample cooled below ca. 350°C (fig. 31*B*)**.** A second fraction, consisting of fine-grained micas from the same sample, yielded a more complicated $^{40}Ar/^{39}Ar$ age spectrum (fig. 31*C*), which likely represents contamination or mixtures of grains of differing cooling ages. The integrated $^{40}Ar/^{39}Ar$ age of 572 Ma is similar to the $^{40}Ar/^{39}Ar$ cooling age of the single grain.

4.3. Groupe de Gueneiba

Another component of the Complexe de Gorgol Noir, which marks the Mauritanide suture zone, is the Groupe de Gueneiba. It consists of metabasalts and associated metasedimentary rock. Our detrital zircon sample, DB07RIM69a, is from low outcrops of thinly interbedded green metasandstone and dolostone, near Guelb Ferna at the northern edge of the Mbout

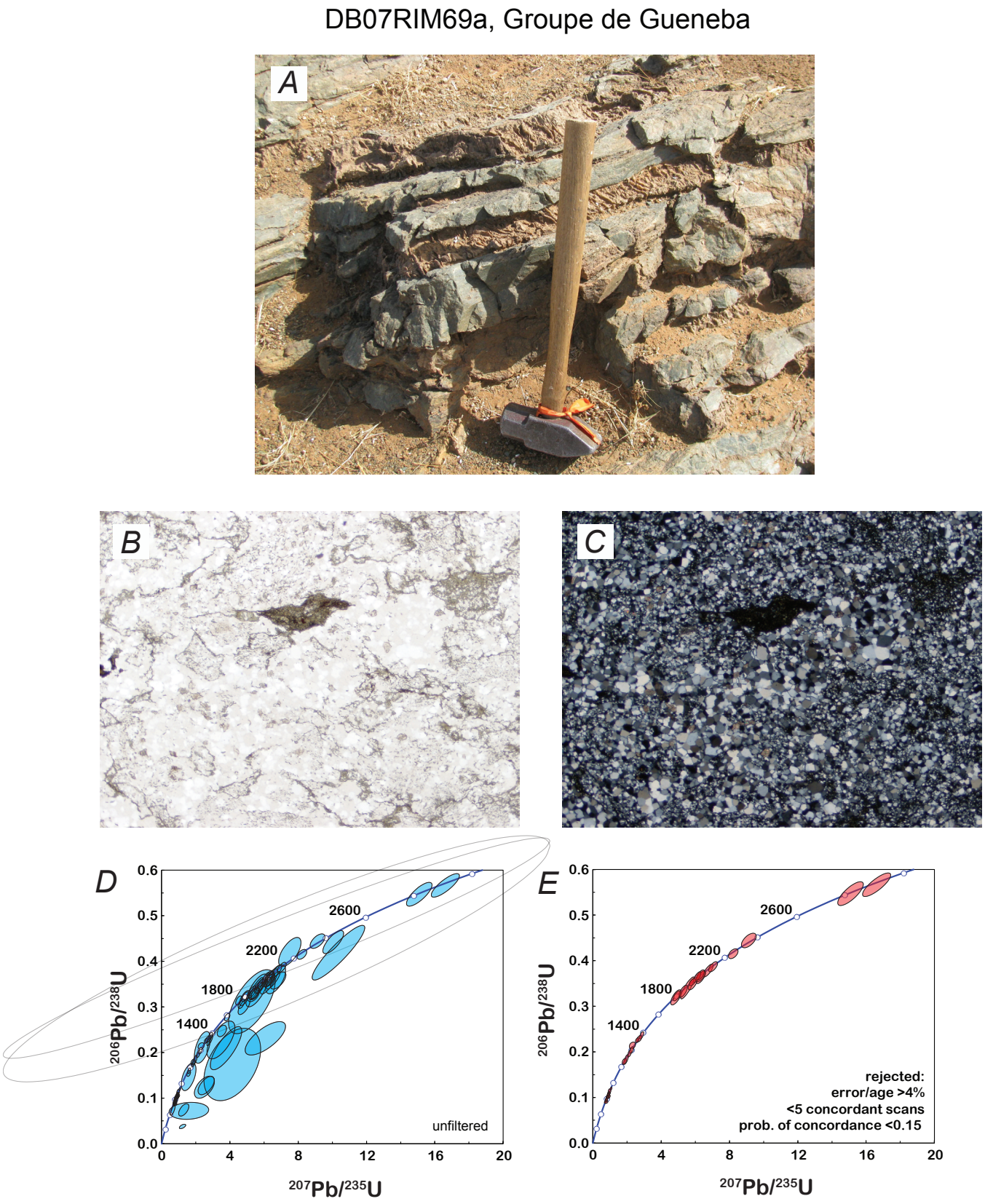


Figure 32. Detrital zircon data and photographs for sample DB07RIM69a, from the Groupe de Gueneiba. (*A*) Outcrop photograph of metasandstone from the sample location. (*B* and *C*) Photomicrographs of quartz-rich metasandstone under plane light and crossed polars, respectively. (*D* and *E*) Concordia diagrams. (*F*) Age distribution.—Continued

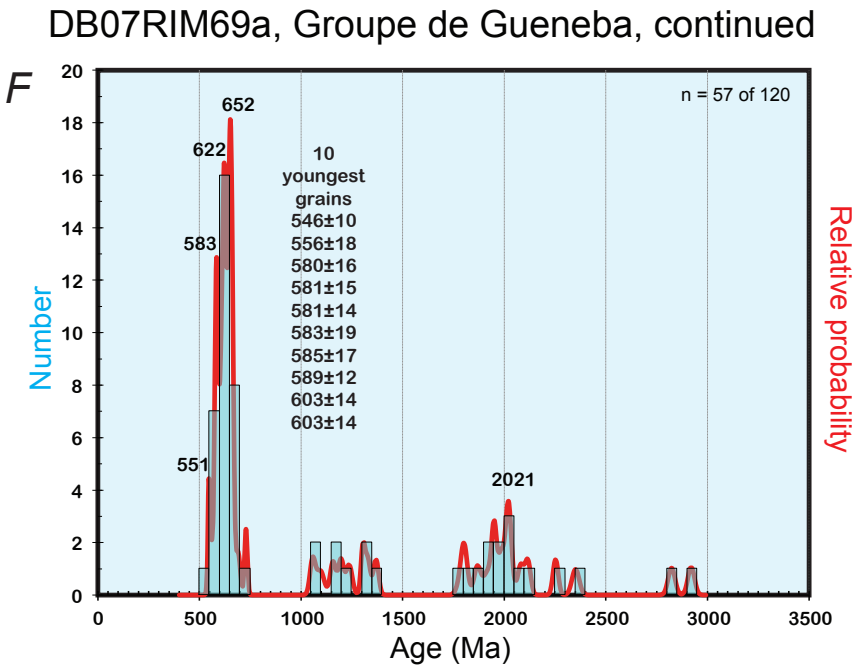


Figure 32. Detrital zircon data and photographs for sample DB07RIM69a, from the Groupe de Gueneiba. (*A*) Outcrop photograph of metasandstone from the sample location. (*B* and *C*) Photomicrographs of quartz-rich metasandstone under plane light and crossed polars, respectively. (*D* and *E*) Concordia diagrams. (*F*) Age distribution.

1:200,000-scale sheet (number 1612). The lithologic assemblage does not match any of those listed in the unit description by Pitfield and others (2004, Section 3.3.4). The sample location itself is shown on the Mbout sheet as Quaternary sand, but it is surrounded on all sides by reg- (desert pavement) blanketed bedrock assigned to the Groupe de Gueneiba. In the absence of additional information, we assign it to the Groupe de Gueneiba.

The metasandstone has been statically recrystallized. Of 120 zircons analyzed, only 57 pass the LAICPMS filters. The probability plot shows closely spaced major peaks at 652, 622, and 583 Ma and a minor peak at 2,021 Ma (fig. 32*F*). The maximum depositional age is set at 551 Ma, a "shoulder" comprising the youngest two overlapping ages.

4.4. Groupe d'El Mseigguem

The Groupe d'El Mseigguem comprises a thrust-bounded package west of the Mauritanide suture zone and east of the Groupe d'El Ghabra (Pitfield and others, 2004, Section 3.4.3). It largely consists of metavolcanic rocks, which range from mafic to felsic in composition.

Sample CT07RIM55-1 is a felsic metasandstone (fig. 33*A*) from the Formation d'Ouechkech of the Groupe d'El Mseigguem near the Bou Grabie mineral occurrence in the northwestern Mbout 1:200,000-scale sheet (number 1612). Of 120 grains analyzed, 52 pass the LAICPMS filters. The probability plot shows a single major peak at 606 Ma and only a smattering of older grains (fig. 32*D*). We set the maximum depositional age at 606 Ma.

Our detrital zircon results are not consistent with other findings from the Groupe d'El Mseigguem. Rocks that have been mapped as the Groupe d'El Mseigguem are intruded by the Oued Djib pluton of the Sous-cortège de Oued Djib, which yielded a U-Pb zircon age of 637±5 Ma (Pitfield and others, 2004, Section 3.4.3.5). A dacitic tuff from the Groupe d'El Mseigguem yielded a U-Pb zircon age of 620±6 Ma (Lahondère and others, 2005, their figure 76). Our sample suggests that the Groupe d'El Mseigguem as presently mapped may be an artificial construct that includes strata that predate and postdate ca. 637-Ma plutonism. Lahondère and others (2005, their figure 78), reported detrital zircon results from a tuffaceous metasedimentary rock from the Groupe d'El Mseigguem; the detrital zircons are reminiscent of the Groupe de Téniagouri as discussed in Section 7.5.

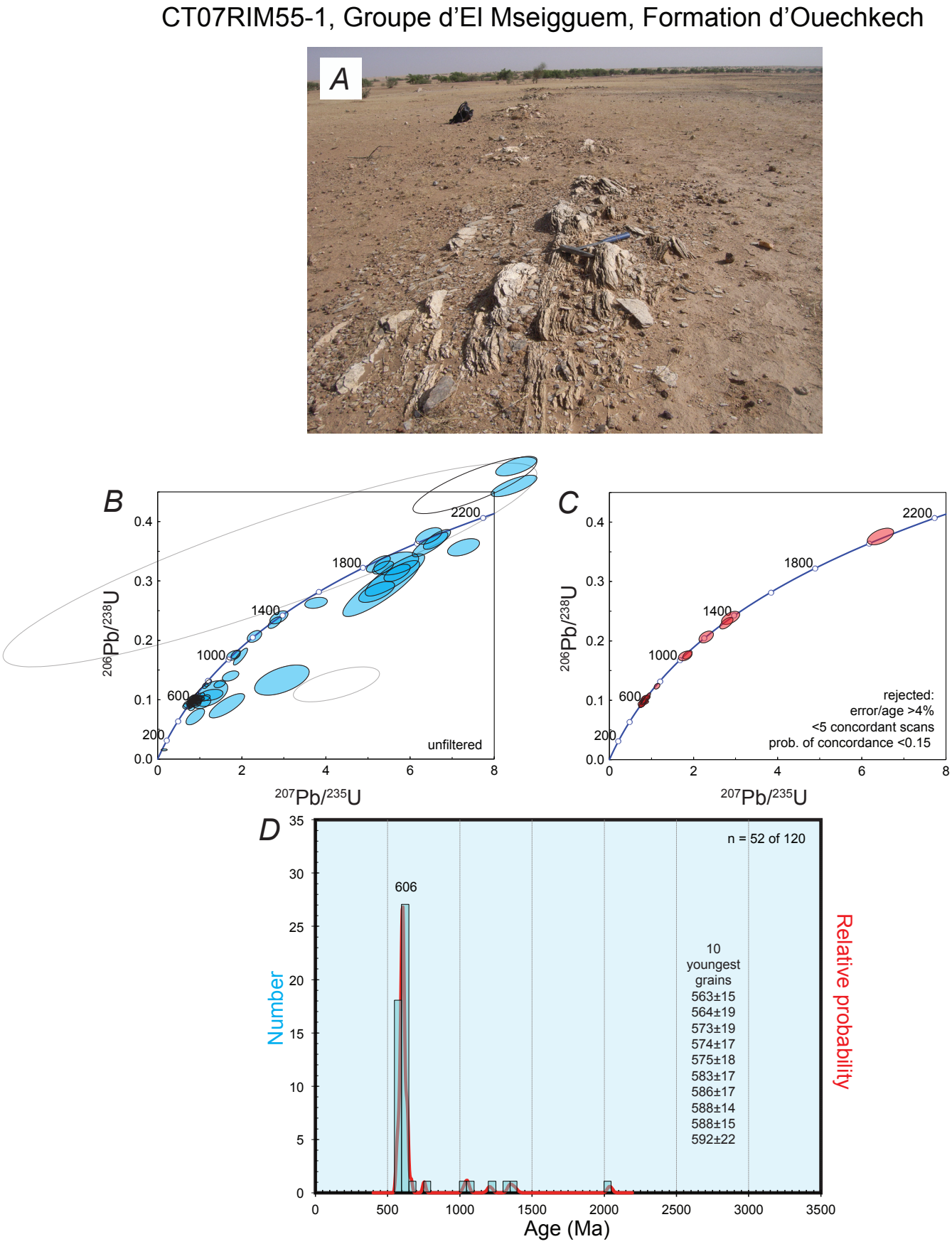


Figure 33. Detrital zircon data and photographs for sample CT07RIM55-1, from the Formation d'Ouechkech of the Groupe d'El Mseigguem. *(*A) Outcrop photograph of metasandstone from the sample location. Photography by Cliff Taylor. (*B* and *C*) Concordia diagrams. (*D*) Age distribution.

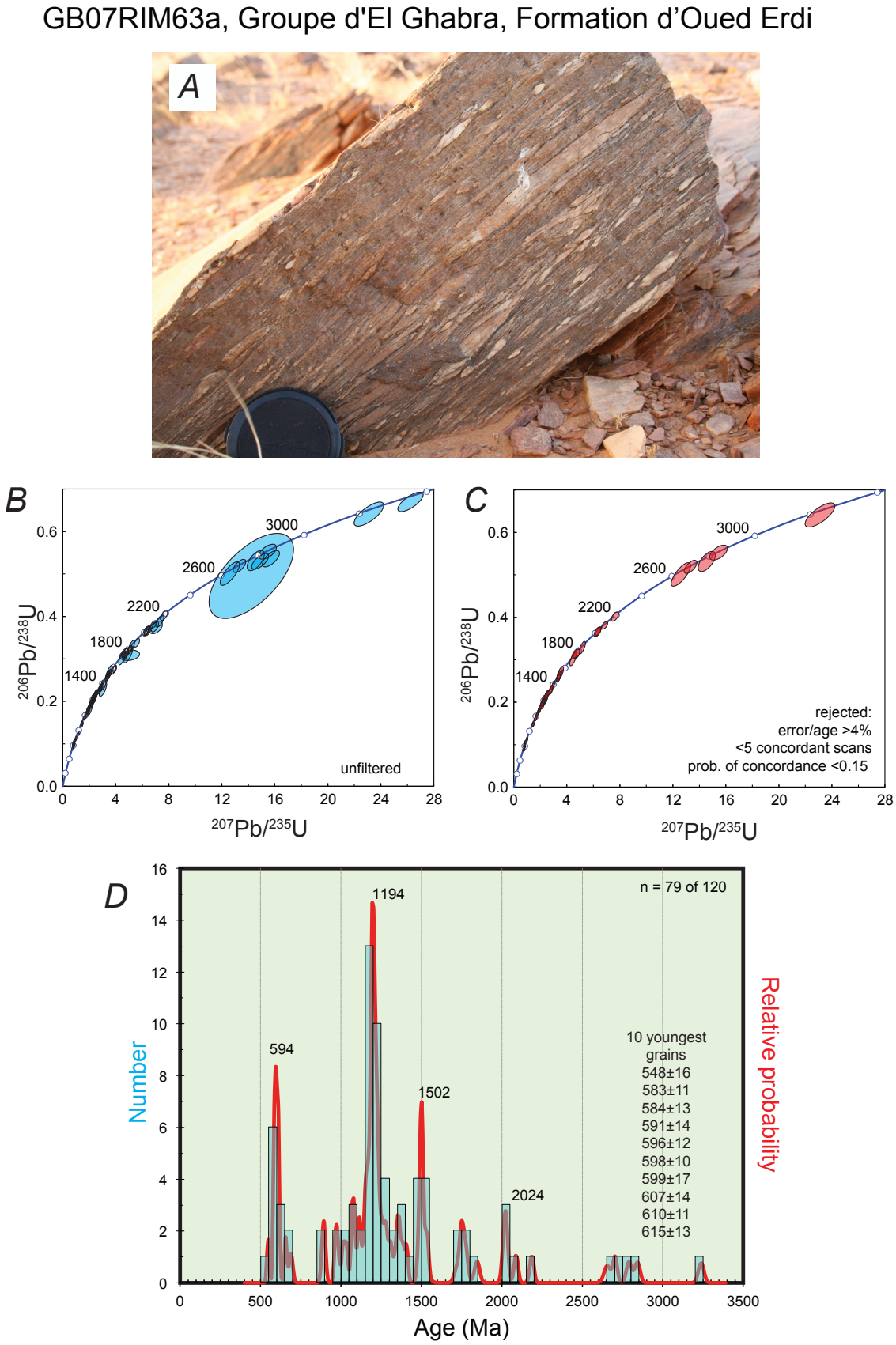


Figure 34. Detrital zircon data and photographs for sample GB07RIM63a, from the Formation d'Oued Erdi of the Groupe d'El Ghabra. (*A*) Outcrop photograph of deformed volcanic conglomerate from the sample location. Photography by Georges Beaudoin. (*B* and *C*) Concordia diagrams. (*D*) Age distribution.

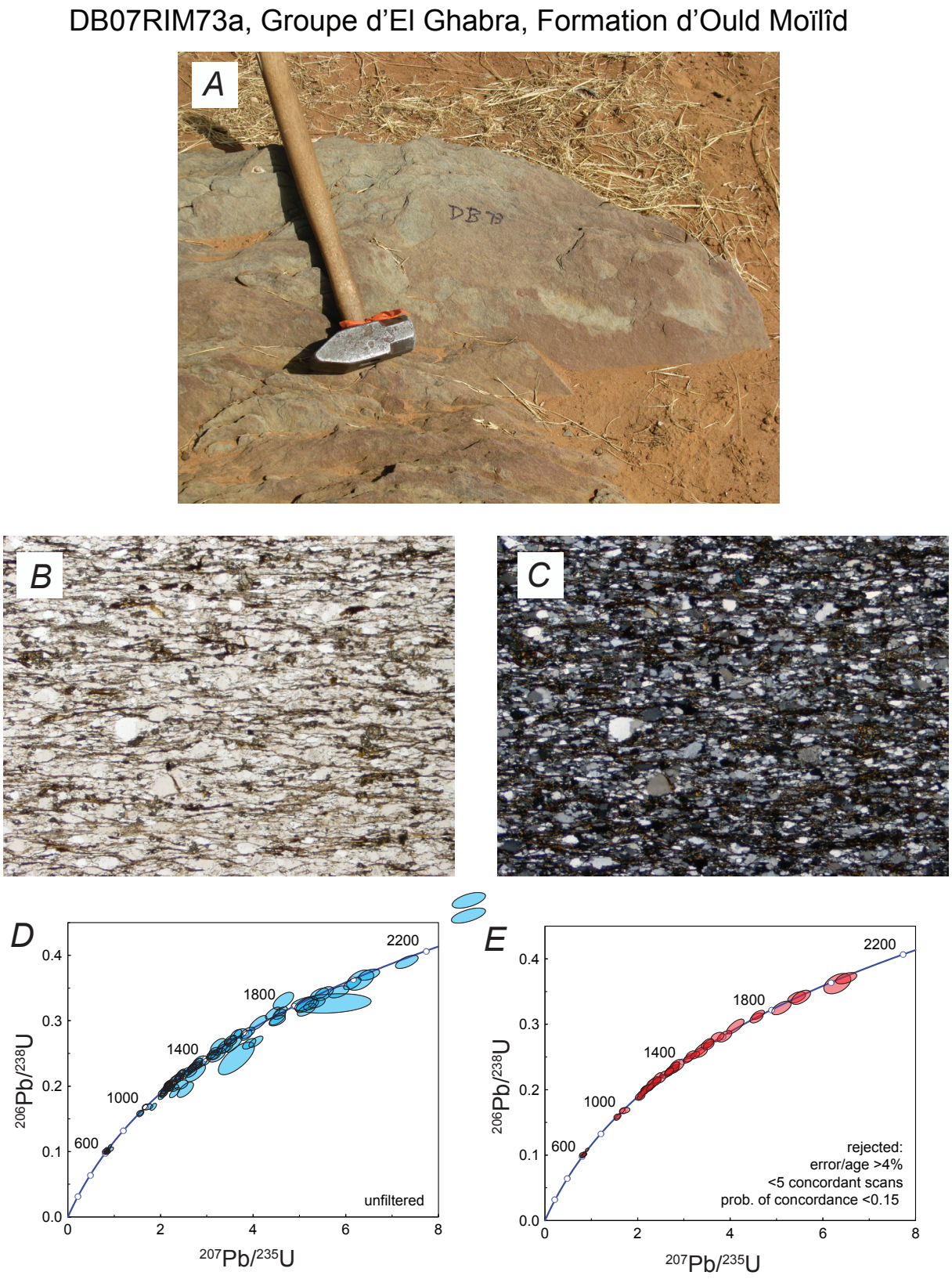


Figure 35. Detrital zircon data and photographs for sample DB07RIM73a, from the Formation d'Ould Moïlîd of the Groupe d'El Ghabra. (*A*) Outcrop photograph of metagraywacke from the sample location. (*B* and *C*) Photomicrographs of foliated metagraywacke under plane light and crossed polars, respectively. (*D* and *E*) Concordia diagrams. (*F*) Age distribution.—Continued

DB07RIM73a, Groupe d'El Ghabra, Formation d'Ould Moïlîd, continued

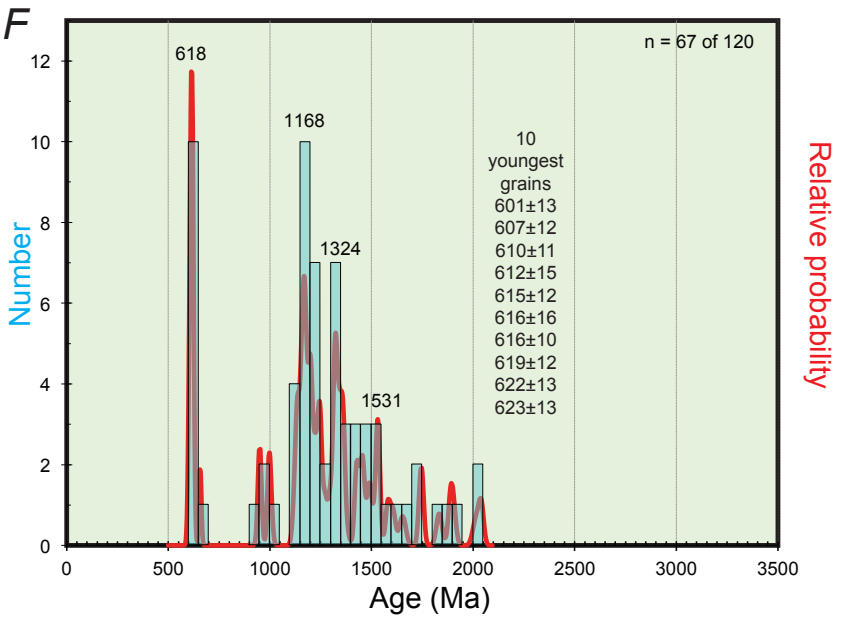


Figure 35. Detrital zircon data and photographs for sample DB07RIM73a, from the Formation d'Ould Moïlîd of the Groupe d'El Ghabra. (*A*) Outcrop photograph of metagraywacke from the sample location. (*B* and *C*) Photomicrographs of foliated metagraywacke under plane light and crossed polars, respectively. (*D* and *E*) Concordia diagrams. (*F*) Age distribution.

4.5. Groupe d'El Ghabra

The Groupe d'El Ghabra is a far-traveled, thrust-bounded package of metavolcanic and metasedimentary rocks, flanked on the west by the Groupe d'El Fadra and on the east by the Groupe d'El Mseigguem (Pitfield and others, 2004, Section 3.4.4). We report detrital zircons from two samples, one from the Formation d'Oued Erdi and one from the Formation d'Ould Moïlîd. In addition, Lahondère and others (2005, their figure 82) reported detrital zircon results from the Formation d'Oua Oua (see Section 7.2).

Sample GB07RIM63a is from the Formation d'Oued Erdi of the Groupe d'El Ghabra in the southwestern corner of the Moudjeria 1:200,000-scale sheet (number 1712). The sample was collected as a felsic metavolcanic conglomerate (fig. 34*A*), with the aim of obtaining an igneous zircon age. The zircon separate, however, turned out to be detrital. Of 120 grains analyzed, 79 pass the LAICPMS filters. The probability plot shows a major peak at 1,194 Ma and minor peaks at 2,024, 1,502, and 594 Ma (fig. 34*D*). The maximum depositional age is 594 Ma based on a nine-zircon peak.

Sample DB07RIM73a is from the Formation d'Ould Moïlîd of the Groupe d'El Ghabra. It was collected from near Oued Boû Dhiâb in the central part of the Mbout 1:200,000-scale sheet (number 1612). The rock is a foliated, medium-grained metagraywacke (fig. 35*A*); no vestige of bedding was visible in low outcrops. Of 120 grains analyzed, 67 pass the LAICPMS filters. The probability plot shows major peaks at 1,324, 1,168, and 618 Ma and a minor peak at 1,531 Ma (fig. 35*F*). The maximum depositional age is 618 Ma based on the youngest peak.

The only published age control for the Groupe d'El Ghabra is provided by ca. 680-Ma intrusive rocks of the Cortège de Kelbé (Section 4.7) that intruded it (Pitfield and others, 2004, Section 3.4.4.5). Neither of our two new detrital zircon samples are consistent with this constraint.

4.6. Groupe d'El Fadra

The Groupe d'El Fadra of Pitfield and others (2004, p. 191) is the most westerly thrust-bounded panel of the allochthonous calc-alkaline volcanic-sedimentary assemblage that comprises the Supergroupe de Mbout. Sample DB07RIM62a is a foliated, chloritic metasandstone (fig. 36*A* and *B*) from the Formation d'Oued Kav, near Magkta Lahjar in the eastern part of the Aleg 1:200,000-scale sheet (number 1713). Of 120 grains analyzed, 65 pass the LAICPMS filters. The probability plot shows major peaks at 614 and 576 Ma and minor peaks at 1203 and 645 Ma (fig. 36*G*). The maximum depositional age is about 576 Ma based on the youngest peak.

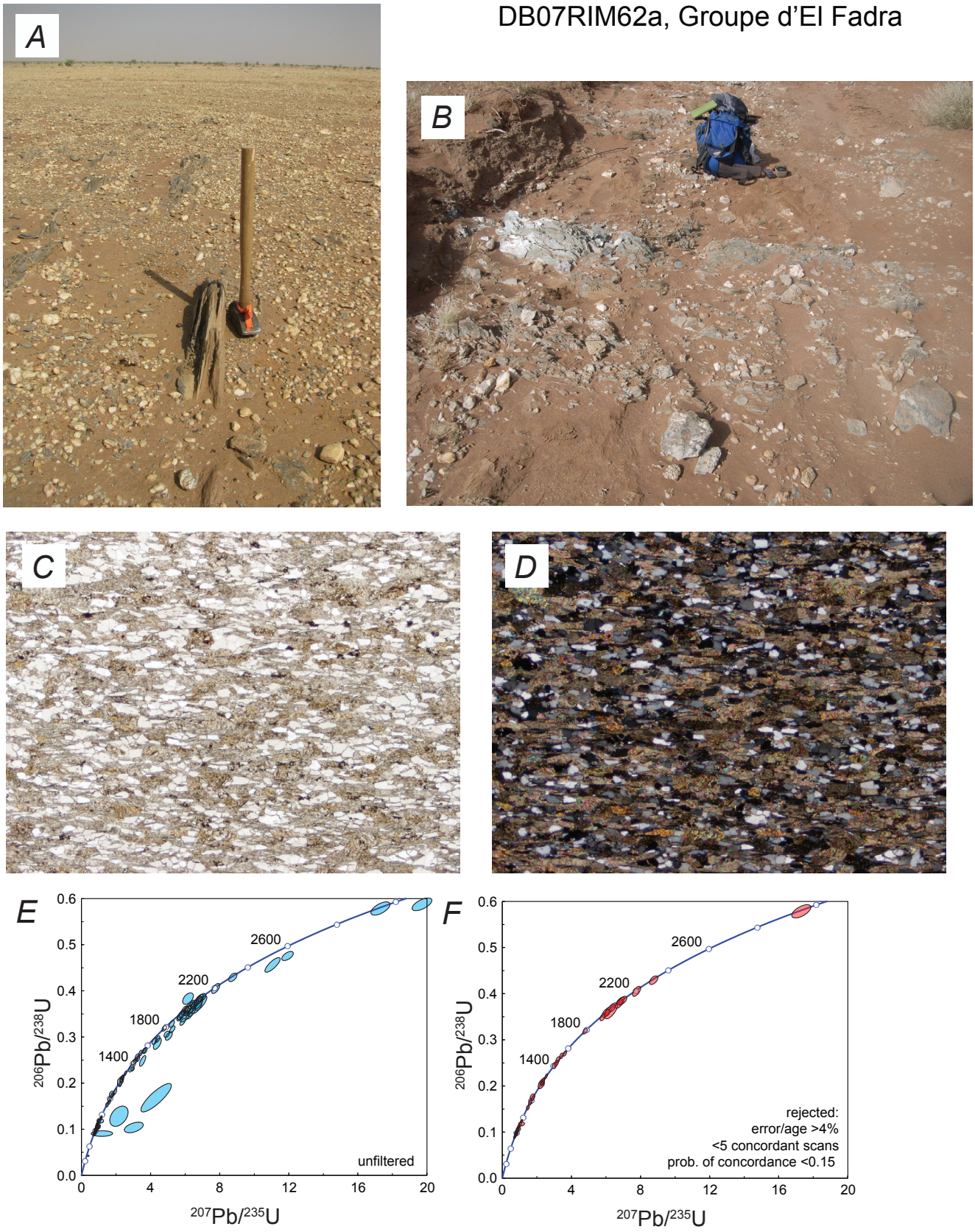


Figure 36. Detrital zircon data and photographs for sample DB07RIM62a, from the Groupe d'El Fadra. (*A* and *B*) Outcrop photographs of metagraywacke from the sample location—an area of sparse, low outcrop. (*C* and *D*) Photomicrographs of foliated metasandstone under plane light and crossed polars, respectively. (*E* and *F*) Concordia diagrams. (*G*) Age distribution.—Continued

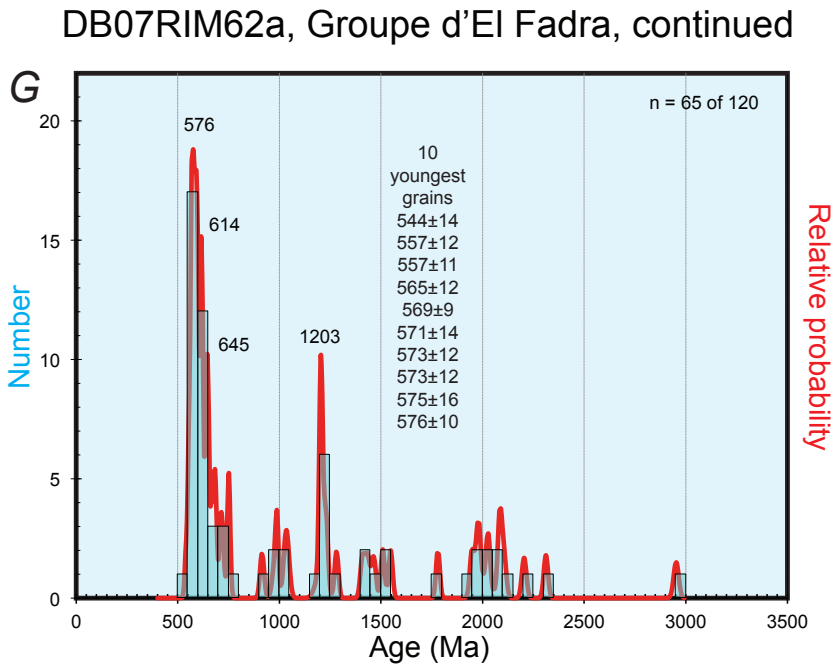


Figure 36. Detrital zircon data and photographs for sample DB07RIM62a, from the Groupe d'El Fadra. (*A* and *B*) Outcrop photographs of metagraywackw from the sample location—an area of sparse, low outcrop. (*C* and *D*) Photomicrographs of foliated metasandstone under plane light and crossed polars, respectively. (*E* and *F*) Concordia diagrams. (*G*) Age distribution.

4.7. Cortège de Kelbé

The Cortège de Kelbé consists of deformed granitic plutons that were intruded into the far-traveled Groupe d'El Mseigguem and the Groupe d'El Ghabra. Published age control is scattered, with Pitfield and others (2004, Section 3.4.7.5) reporting U-Pb zircon ages of 772±49 Ma (unnamed metagranite), 666±83 Ma (Métagranite de Bou Zraibie), 685±18 Ma (Granite du Khîr Fîh), and 636±4 Ma (metaleucogranite of the Sous-cortège d'Oued Djib). At face value, this implies that the Cortège de Kelbé is an artificial grouping of at least three plutonic suites of very different age and thus origin.

Our geochronology sample (DB07RIM64a) is from a foliated granite (figs. 37*A* and *B*) between Magta Lahjar and Cangarafa near the western edge of the Moudjeria 1:200,000-scale sheet (number 1712). The sample was analyzed by SIMS and LAICPMS. Zircons from this deformed granitoid are mostly around 2 Ga in age (fig. 37*F*). We interpret these as inherited (formerly detrital) grains from a metasedimentary protolith; but an alternative possibility is that this is, indeed, a Paleoproterozoic plutonic rock. A very imprecise lower intercept age of 545±140 Ma is calculated from the SIMS data (fig. 37*E*).

4.8. Quartz veins in the Central Mauritanides

Sample GB07RIM52A is from subcrop of a quartz-sericite vein cutting the Groupe de Gadel in the area of the Iguerj mineral occurrence (Moudjeria 1:200,000-scale sheet, 1712) (fig. 38*A*). The $^{40}Ar/^{39}Ar$ age spectrum from this sample (fig. 38*B*) is irregular and difficult to interpret in any precise manner. Most likely there are mixtures of different generations of mica in this sample. The integrated $^{40}Ar/^{39}Ar$ age of 357 Ma is interpreted as the approximate time of cooling of this sample below ca. 350° C.

Samples GB07RIM61A and GB07RIM62C are from subcrop of quartz-sericite veins (figs. 38*C* and *E*) in the vicinity of the Chlakh Lhemir mineral occurrence in the southwestern part of the Moudjeria 1:200,000-scale sheet (number 1712). Both GPS locations plot within an area that was mapped as Quaternary pavement gravel; GB07RIM61A is fairly close to a mapped area of the Groupe de Gàoua, Cambrian quartzite, the area of which should be broadened to include our two sample locations. Sample GB07RIM61a is from a vein that contains visible free gold. The $^{40}Ar/^{39}Ar$ data from sample GB07RIM61A (fig. 38*D*) are consistent with a simple cooling history. The average age of 299±2 Ma calculated from eight laboratory heating steps representing about 60 percent of the argon released is interpreted to reflect cooling below 350° C at this time. The $^{40}Ar/^{39}Ar$ data from sample GB07RIM62C do not form a $^{40}Ar/^{39}Ar$ plateau (fig. 38*F*), but are confidently interpreted to represent cooling of this sample below ca. 350° C at about 295 Ma. There is no evidence to suggest that either sample was affected by any thermal event since original cooling.

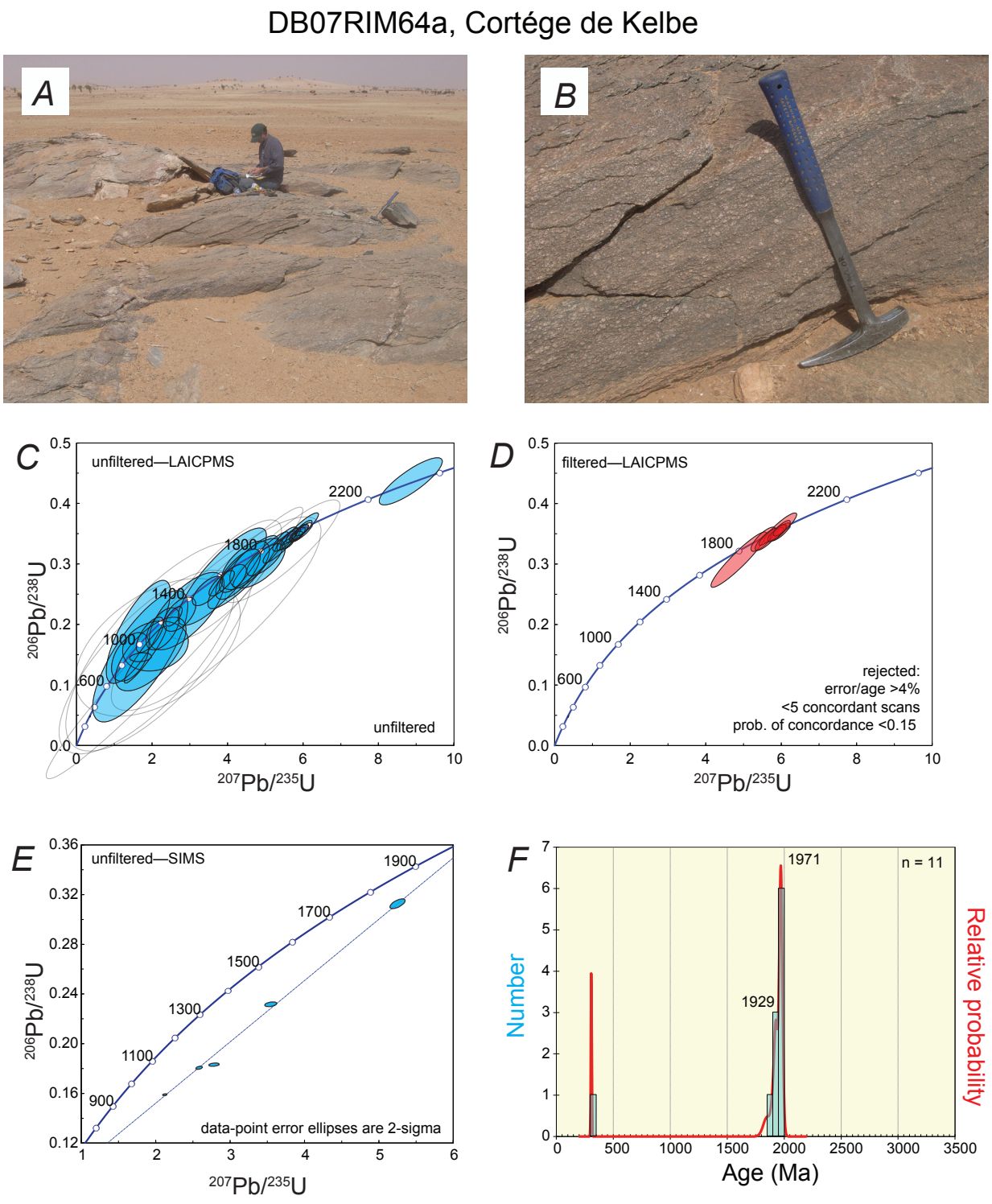


Figure 37. Zircon data and photographs for sample DB07RIM64a, from the Cortège de Kelbé. (*A* and *B*) Outcrop photographs of foliated granite from the sample location. (*C* and *D*) Concordia diagrams for unfiltered and filtered LAICPMS data. (*E*) Unfiltered SIMS data; all data were strongly discordant. (*F*) Age distribution based on LAICPMS results.

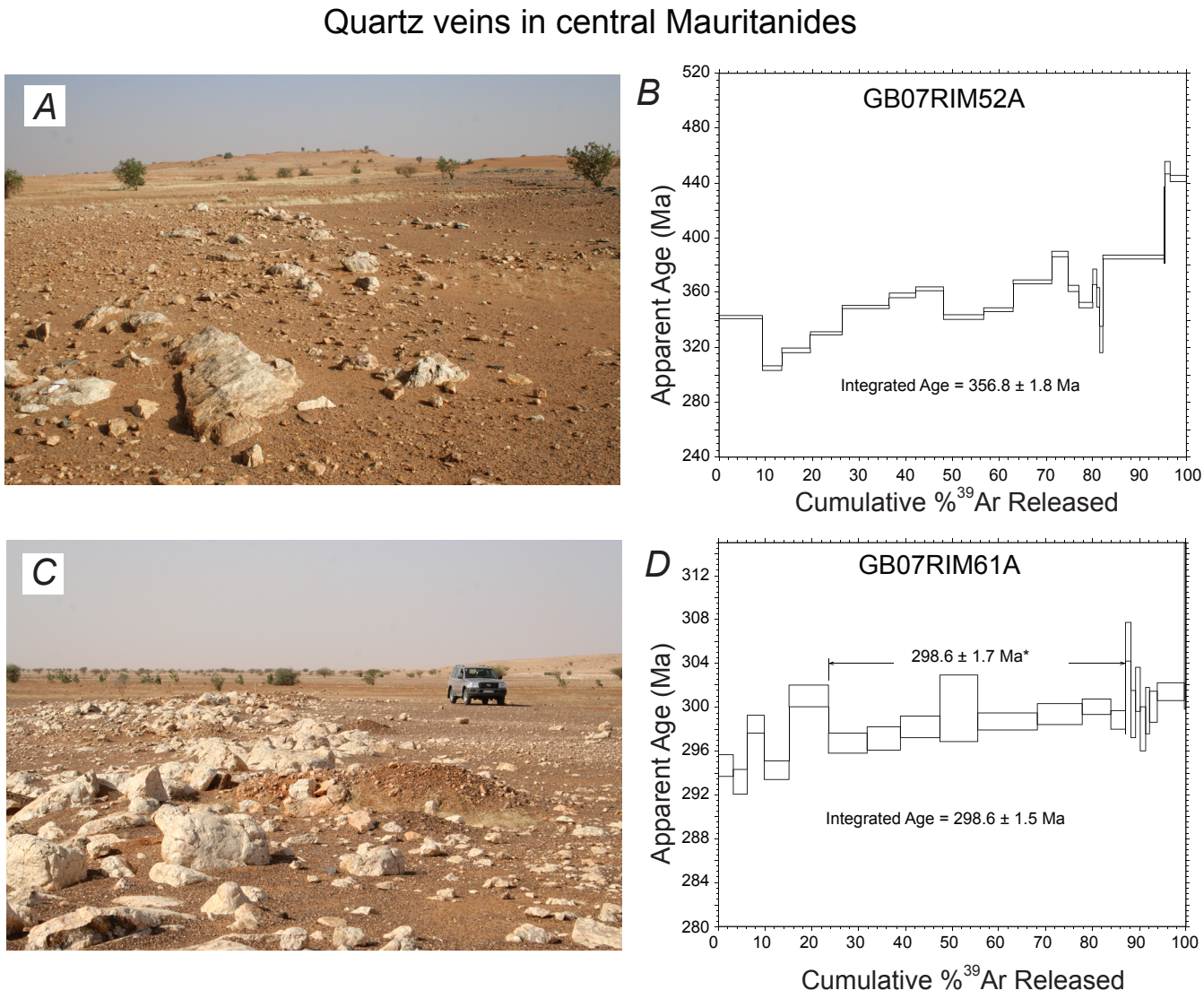


Figure 38. Outcrop photographs and corresponding argon age-release spectra for white mica fractions from quartz veins in the central Mauritanides. (*A* and *B*) Sample GB07RIM52a. (*C* and *D*) Sample GB07RIM61a. (*E* and *F*) Sample GB07RIM62c. (*G* and *H*) Sample GB07RIM69a.—Continued

Sample GB07RIM69A is from subcrop of a quartz-sericite vein cutting phyllite and schist (fig. 38*G*) of the Groupe d'El Fadra, Formation d'Oued Kav at the Vararate Nord mineral occurrence in the northwestern part of the Mbout 1:200,000-scale sheet (number 1612). The $^{40}Ar/^{39}Ar$ data from this sample are poor (fig. 38*H*) and difficult to interpret other than concluding that the overall cooling of this sample below ca. 350° C occurred about 650 Ma. About 60 percent of the argon degassed in one heating step, which precludes any additional interpretation of the $^{40}Ar/^{39}Ar$ data.

5.0. Northern Mauritanide Orogen

In this section we describe U-Pb detrital zircon and U-Pb igneous zircon results from the Northern Mauritanides, which for present purposes is the roughly east-west striking sector of the orogen from latitude 18°30′N to the border with Western Sahara. Most of our samples are from the Akjoujt mining district, where detailed mapping (Martyn and Strickland, 2004; Pitfield and others, 2004) has revealed the structure and geologic history to be exceptionally complex. During the Carboniferous to Permian Hercynian orogeny, multiple, stacked thrust sheets were emplaced into their final position over Archean basement of the Rgueïbat Shield (Dallmeyer and Lécorché, 1990). Key problems involve the protolith ages of strata and the extent, if any, of Neoproterozoic (Pan-African) tectonism.

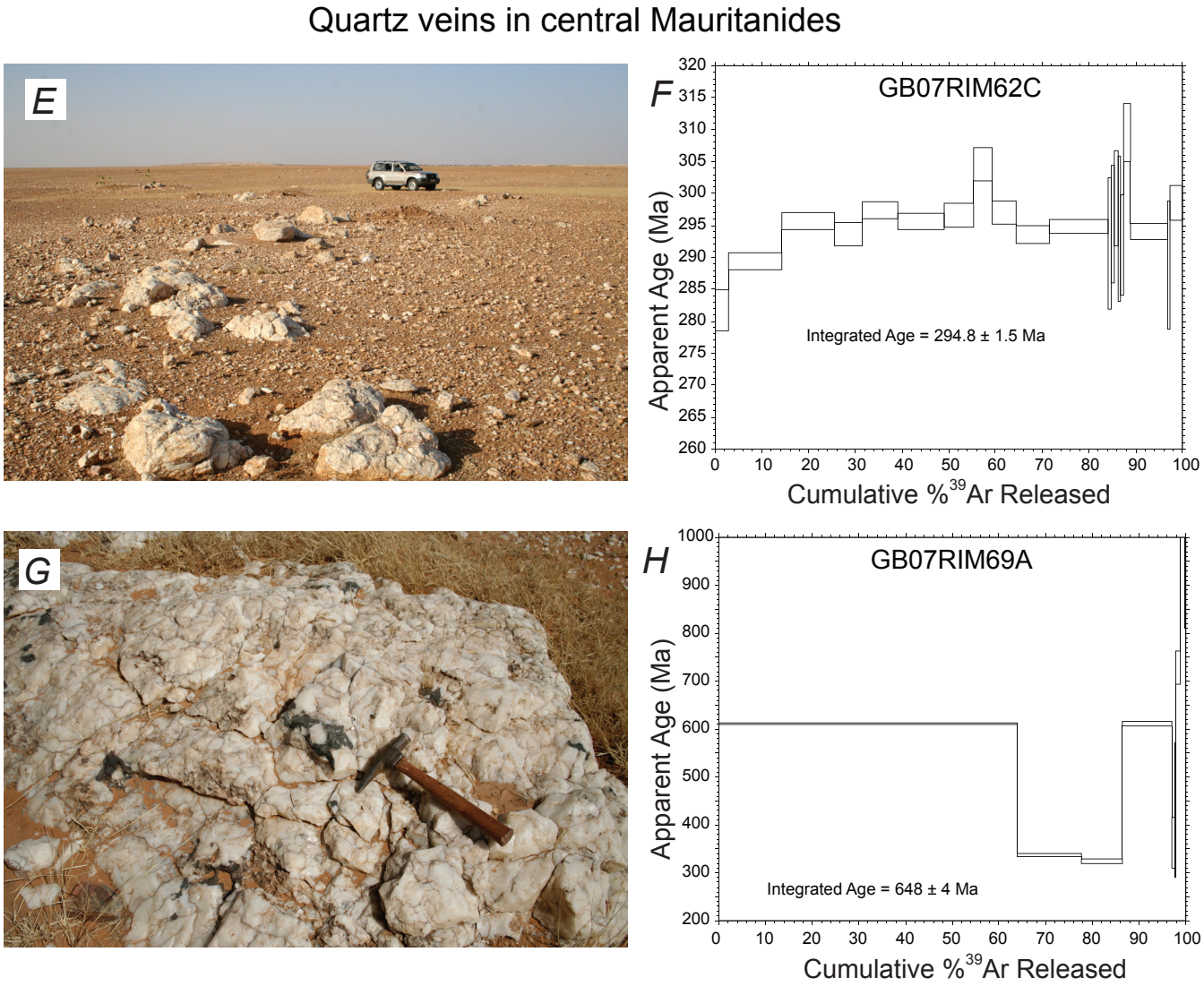


Figure 38. Outcrop photographs and corresponding argon age-release spectra for white mica fractions from quartz veins in the central Mauritanides. (*A* and *B*) Sample GB07RIM52a. (*C* and *D*) Sample GB07RIM61a. (*E* and *F*) Sample GB07RIM62c. (*G* and *H*) Sample GB07RIM69a.

5.1. Groupe de Oumachoueima, Formation de Sainte Barbe

The Formation de St. Barbe hosts copper-gold mineralization in the Akjoujt mining district. U-Pb ages of 2,492±9 on hydrothermal monazite and 1,742±12 on hydrothermal xenotime record Paleoproterozoic mineralization (Meyer and others, 2006).

Formation de Sainte Barbe consists mostly of volcanic rocks. Sample CT07RIM10-1 is a felsic metavolcanic from the Formation d'Akjoujt near the Legleitat El Bird tungsten occurrence (Akjoujt 1:200,000-scale sheet, number 1914). The formation consists largely of proximal volcanics to distal volcaniclastics of dominantly intermediate composition (Pitfield and others, 2004, Section 3.5.4). The sample was expected to yield a straightforward U-Pb igneous age but during our initial attempt to date the rock by the SIMS method, the zircon separate was found to include many detrital grains (fig. 39*A*). We next turned to the LAICPMS method and dated 120 zircons; 50 analyses passed the LAICPMS filters (fig. 39*B* and *C*). The probability curve based on combined TIMS and LAICPMS data shows peaks at 3,068, 2,953, and 2,839 Ma (fig. 39*E*). The most straightforward interpretation is that the youngest zircon peak corresponds to the age of volcanism (2,839±14 Ma) (fig. 39*F*), and the older peaks are detrital. We suggest that the sample is from a fault slice of basement that was incorrectly mapped as part of the Formation de Sainte. Barbe.

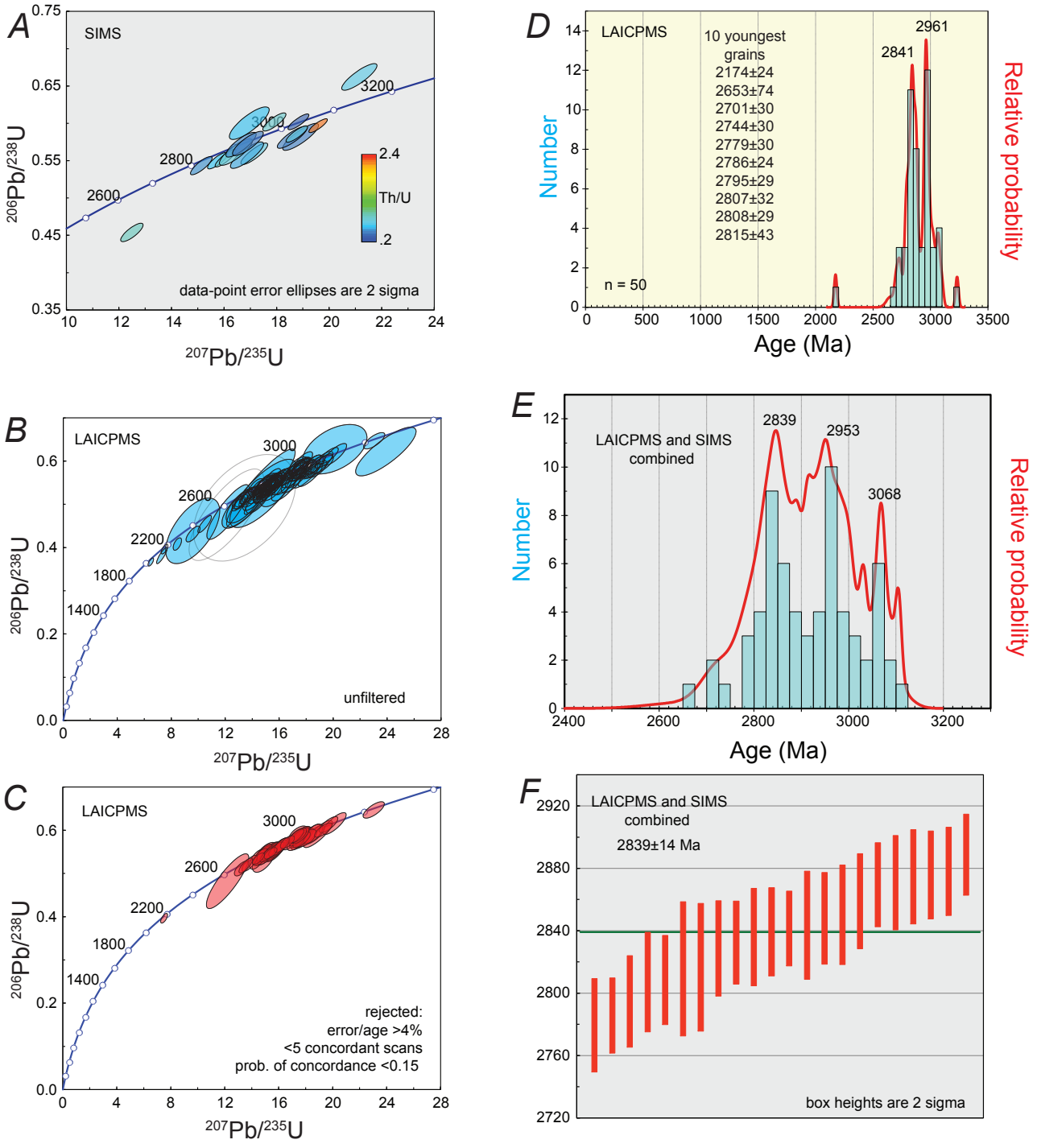


Figure 39. Zircon data and photographs for sample CT07RIM10-1 from the Formation de Sainte Barbe. (*A*) Concordia diagram showing unfiltered SIMS data. Coloring of error ellipses according to Th/U shows that the spread of ages is not due to a mix of igneous and metamorphic zircons. (*B* and *C*) Concordia diagrams for unfiltered and filtered LAICPMS data. (*D*) Age distribution showing filtered LAICPMS results. (*E*) Histogram showing detail in the Archean part of the time scale, based on combined results from LAICPMS and SIMS analyses. (*F*) Weighted mean of 207Pb/206Pb ages that form the youngest maximum, which we interpret as the age of the igneous rock.

DB07RIM01a, Groupe de Oumachoueima, Formation de St. Barbe

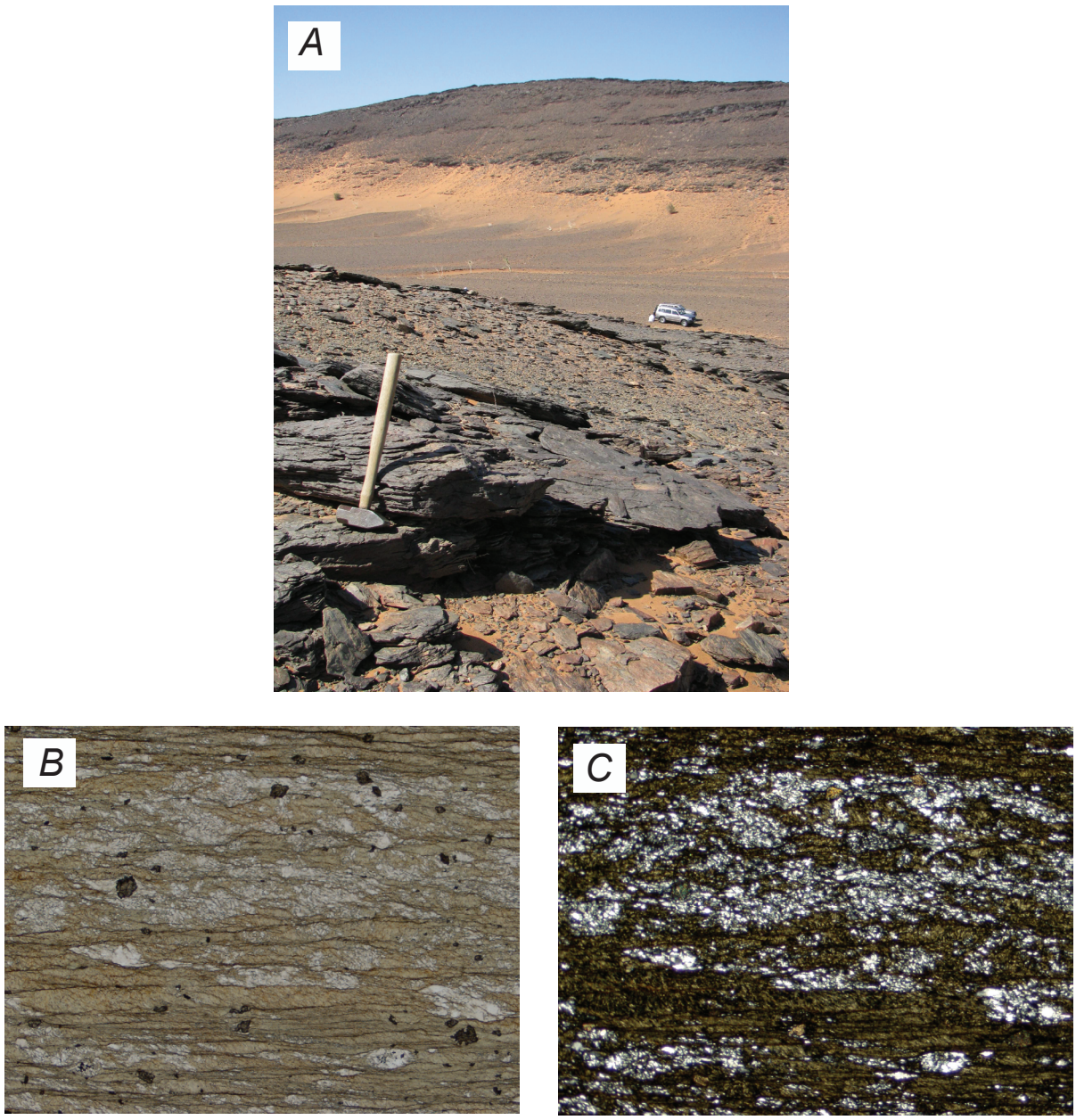


Figure 40. Detrital zircon data and photographs for sample DB07RIM01a from the Formation de Sainte Barbe. (*A*) Outcrop photograph of metasandstone from the sample location. (*B* and *C*) Photomicrographs of protomylonitic metasandstone under plane light and crossed polars, respectively. (*D* and *E*) Concordia diagrams. (*F*) Age distribution.—Continued

Sample DB07RIM01a is a chloritic metasandstone (fig. 40*A*) from a siliciclastic part of the Formation de Sainte Barbe, about 7 km N of Akjoujt (Akjoujt 1:200,000-scale sheet, number 1914). Of 121 zircons dated, 63 pass the LAICPMS filters. The probability curve has major peaks at 622 and 573 Ma and minor ones at 2,047 and 836 Ma (fig. 40*F*). We put the maximum depositional age at 573 Ma, the age of the youngest peak.

Sample CT07RIM02-1 is a strongly tectonized, chloritic metasandstone from the Formation de Sainte Barbe (fig. 41A). The sample was collected a few meters away from a distinctive, maroon-weathering iron carbonate pod (fig. 41B) that resembles rocks at the nearby Guelb Moghrein copper deposit. The sample location is about 11 km to the NNW of Akjoujt (Akjoujt 1:200,000-scale sheet, number 1914). Of 120 zircons dated, 60 pass the LAICPMS filters. The probability curve shows major overlapping peaks at 591 and 614 Ma and a smattering of older zircons, mostly between about 1 and 2 Ga (fig. 41*E*). The youngest minor peak at 538 Ma sets the maximum depositional age as Early Cambrian.

DB07RIM01a, Groupe de Oumachoueima, Formation de St. Barbe, continued

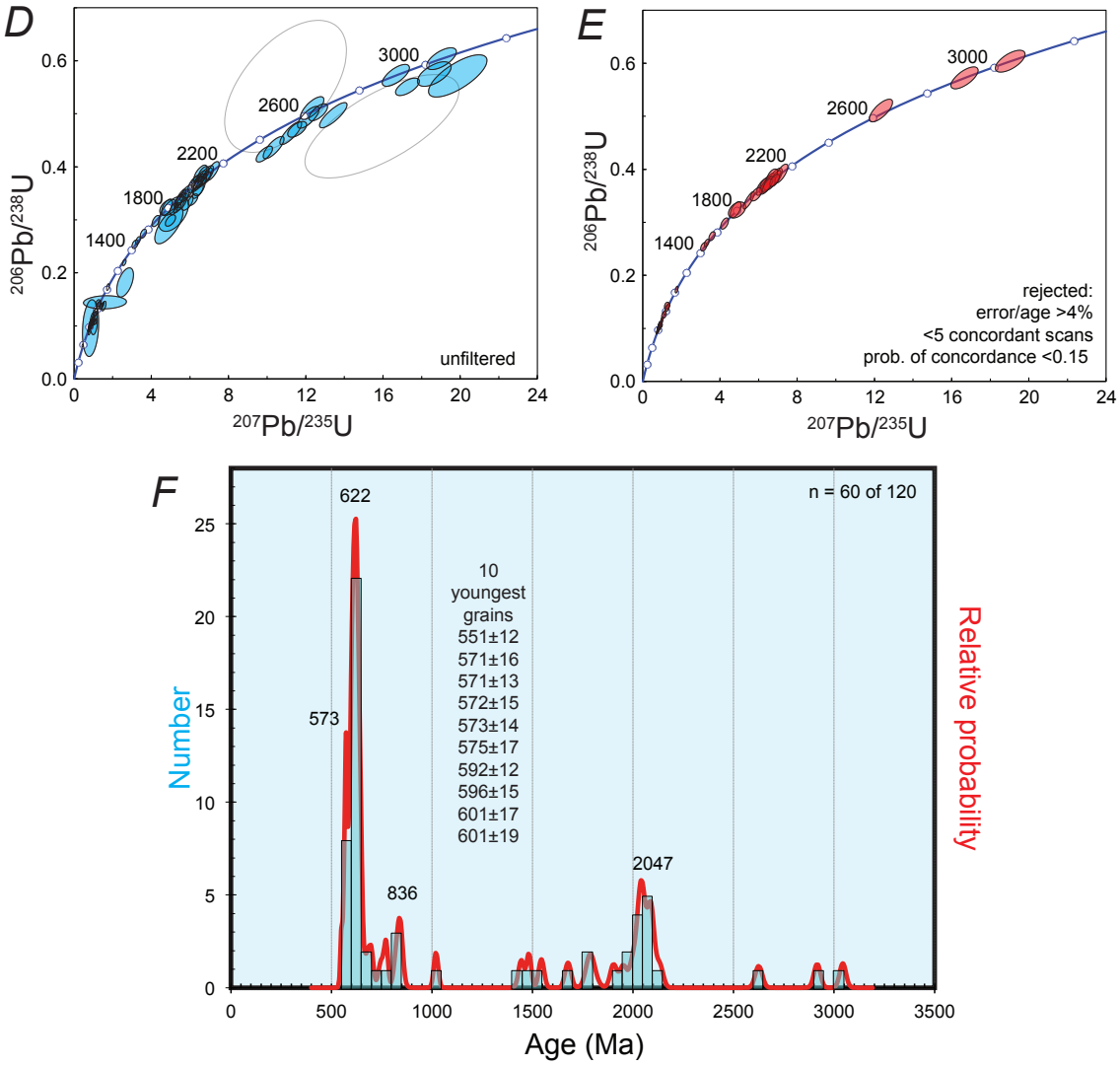


Figure 40. Detrital zircon data and photographs for sample DB07RIM01a from the Formation de Sainte Barbe. (*A*) Outcrop photograph of metasandstone from the sample location. (*B* and *C*) Photomicrographs of protomylonitic metasandstone under plane light and crossed polars, respectively. (*D* and *E*) Concordia diagrams. (*F*) Age distribution.

5.2. Groupe de Oumachoueima, undivided

Sample CT21 is a chlorite schist (fig. 42*A*) from an undivided part of the Groupe d'Oumachoueima near the Bou Serouai - Guelb Hammar (Km 14) copper occurrence (Akjoujt 1:200,000-scale sheet, number 1914). Detrital zircons were dated using the SHRIMP-RG in 2007; additional analyses were done in 2012. Representative cathodoluminescence images are shown in figure 42*B*. A total of 106 zircons were analyzed and 67 of these passed the filter of <10 percent discordance. The age distribution shows major peaks at 603 and 656 Ma, and minor ones at 2,059, 991, and 558 Ma (fig. 42*D*). The youngest peak sets the maximum depositional age in the late Neoproterozoic.

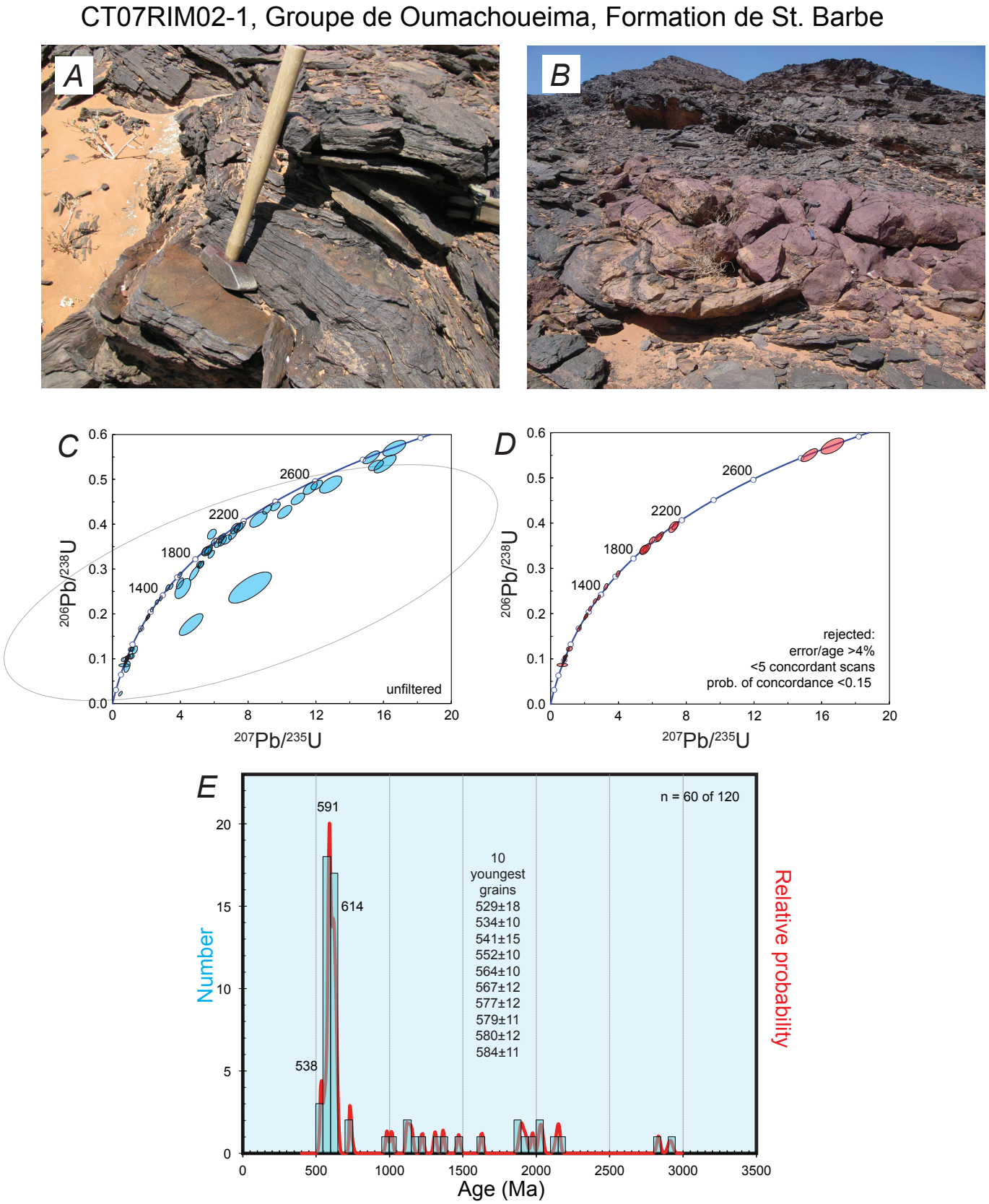


Figure 41. Detrital zircon data and photographs for sample CT07RIM02-1, from the Formation de St. Barbe. (*A* and *B*) Outcrop photographs of the sample location. The iron carbonate pod in (*B*) is a few meters structurally below the sampled horizon of chloritic metasandstone in (A). (*C* and *D*) Concordia diagrams. (*E*) Age distribution.

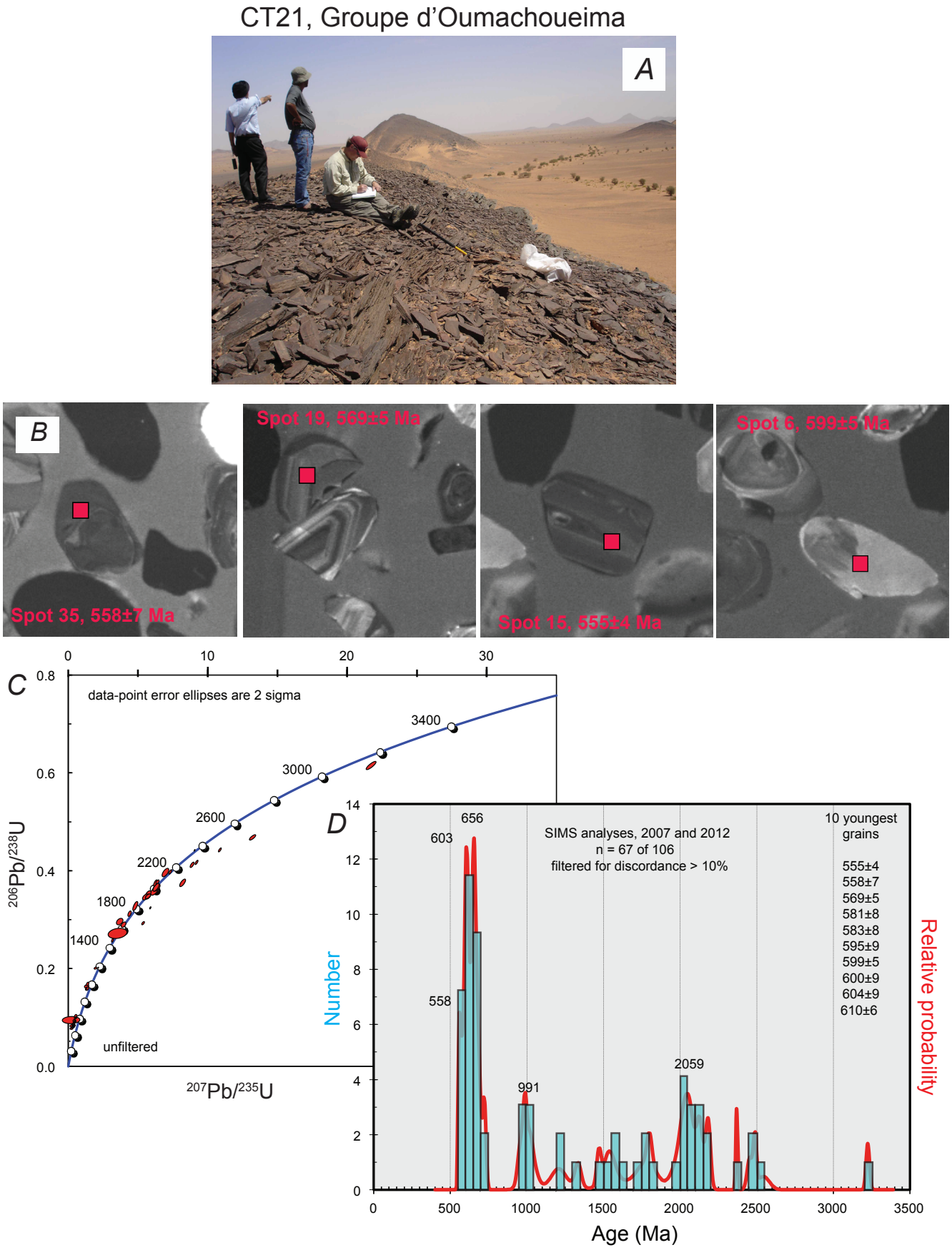


Figure 42. Detrital zircon data and photographs for sample CT21, from an undivided part of the Groupe d'Oumachoueima. (*A*) Outcrop photograph of metasandstone at the sample location. Photograph by Cliff Taylor. (*B*) CL (cathodoluminescent) SEM images of selected

zircons showing that late (continued)Neoproterozoic ages were obtained from a range of zircon types, and not from rims. Individual images are 200 microns on a side. (*C*) Concordia diagram showing unfiltered data. (*D*) Age distribution. This is one of the two samples that we collected on a brief reconnaissance trip early in 2007; hence the different sample numbering scheme.

5.3. Groupe de Oumachoueima, Atilis quartzite member

Sample DB07RIM02a is from a quartzite within the Groupe de Oumachoueima (fig. 43*A*). The GPS location plots within the outcrop belt of the Formation d'Irarchene El Hamra, which consists of a basal quartzite member (the Atilis Quartzite) overlain by quartz-chlorite ± muscovite schists plus subordinate quartzites and metagraywackes (Pitfield and others, 2004, Section 3.4.7.5). The sample is from a conspicuous band of quartzite subcrop in a region of poor exposure, and the GPS location is only 70 meters from the previously mapped boundary between the Atilis Quartzite Member and the rest of the Formation d'Irarchene El Hamra (Akjoujt 1:200,000-scale sheet, number 1914). We therefore assign the sample to the Atilis Quartzite Member. Of 120 zircons dated, 75 pass the LAICPMS filters. The age distribution shows a broad Paleoproterozoic to Mesoproterozoic high with closely spaced major peaks at 1,205 and 1,164 Ma, and lesser peaks at 1,509, 1,411, 1,320, and 974 Ma (fig. 43*F*). The single analysis at 370 Ma is discarded and the youngest peak, at 974 Ma, sets the maximum depositional age.

5.4. Groupe d'Eizzene, Formation de Raoui

Formation de Raoui of the Groupe d'Eizzene consists largely of metabasalt, with rare thin siliciclastic intercalations (Pitfield and others, 2004, Section 3.5.3). Sample DB07RIM03a is from subcrop of buff to white quartzite in a desolate area of poor exposure about 5 km west of the Atoma Nord copper occurrence (Akjoujt 1:200,000-scale sheet, number 1914). Of 120 zircons dated, only 34 pass the LAICPMS filters (figs. 44*C* and *D*). The age distribution shows a broad high between about 1 and 1.5 Ga with closely spaced peaks at 1,487, 1,381, 1,311, 1,212, 1,162, 1,099, 1,064, 1,021, and 986 Ma (fig. 44*E*). The single analysis at ca. 593 Ma is discarded. The youngest peak, at 986 Ma, which is based on two grains, sets the maximum depositional age.

5.5. Complexe d'Inchiri, Groupe de Hajar Dekhen – Kleouat

The Groupe de Hajar Dekhen – Kleouat is part of the Complexe d'Inchiri, a mapping catchall that includes both supracrustal and plutonic rocks. Sample DB07RIM17a, a quartzite (fig. 45*A*), is from along Khatt ech Cha'ba in the western part of the Akjoujt 1:200,000-scale sheet (number 1914). The results are problematic for two reasons. The first and easiest problem involves mapping. Based on its GPS coordinates, the sample was collected from what has been mapped as a granitic orthogneiss, unit HDgn of Pitfield and others (2004; unit HDg on the 1:1,000,000-scale geologic map). More properly, the sample belongs to unit HDs of Pitfield and others (2004; unit HDg on the 1:1,000,000-scale geologic map), which consists of metacarbonates and metasandstones. For the 1:1,000,000-scale geologic map, we resolved this minor problem by simply moving the mapped intrusive contact between the two units 100 m to the west; this is permitted by the patchy outcrop in the area. The second problem involves what may or may not be "too young" zircons. Of 120 zircons dated from sample DB07RIM17a, 88 pass the LAICPMS filters. The probability curve shows a single maximum at 564 Ma (fig. 45*F*). U/Th ratios near 1 suggest that these are not metamorphic ages. A straightforward interpretation, then, is that the zircons are detrital and that the maximum depositional age is 564 Ma. This conclusion does not violate any geologic constraints but it does complicate regional geologic relations. Except for these new zircon results, unit HDs has no direct age control, but it must be older than unit HCgn—which also has no direct age control. Another plutonic rock unit in the Complexe d'Inchiri about 20 km to the east, the "Métagranite de Hajar Dekhen" of Pitfield and others (2004), yielded a U-Pb zircon age of 599±8 Ma. Assuming that the 564-Ma zircon ages are detrital, unit HDgn must be younger than 564 Ma; hence the Complexe d'Inchiri must include at least two different-aged Neoproterozoic plutonic suites.

6.0. Rgueïbat Shield

The Rgueïbat Shield (also spelled Reguïbat) is a ca. 500 by 2,000 km belt of Archean and Paleoproterozoic rocks that trends southwest to northeast across Western Sahara, Mauritania, and Algeria. It comprises the northern basement exposure of the West African Craton.

6.1. Group de Lebzenia, Formation d'Aouéoua

The Chami Greenstone Belt is a supposedly Mesoarchean supracrustal province in the Tasiast mining district of the westernmost Rgueïbat Shield (Chami 1:200,000-scale sheet, number 2015). The rocks of the greenstone belt are assigned to the Groupe de Lebzenia, which includes the mainly metasedimentary Formation d'Aouéoua. Sample GB07RIM80a is a quartzite (fig. 46*A*). Out of 120 zircon ages, 44 passed the LAICPMS filters. The probability curve (fig. 46*D*) shows closely spaced maxima at 619 and 576 Ma and a smattering of older grains, especially around 2 Ga. These results are at odds with a U-Pb

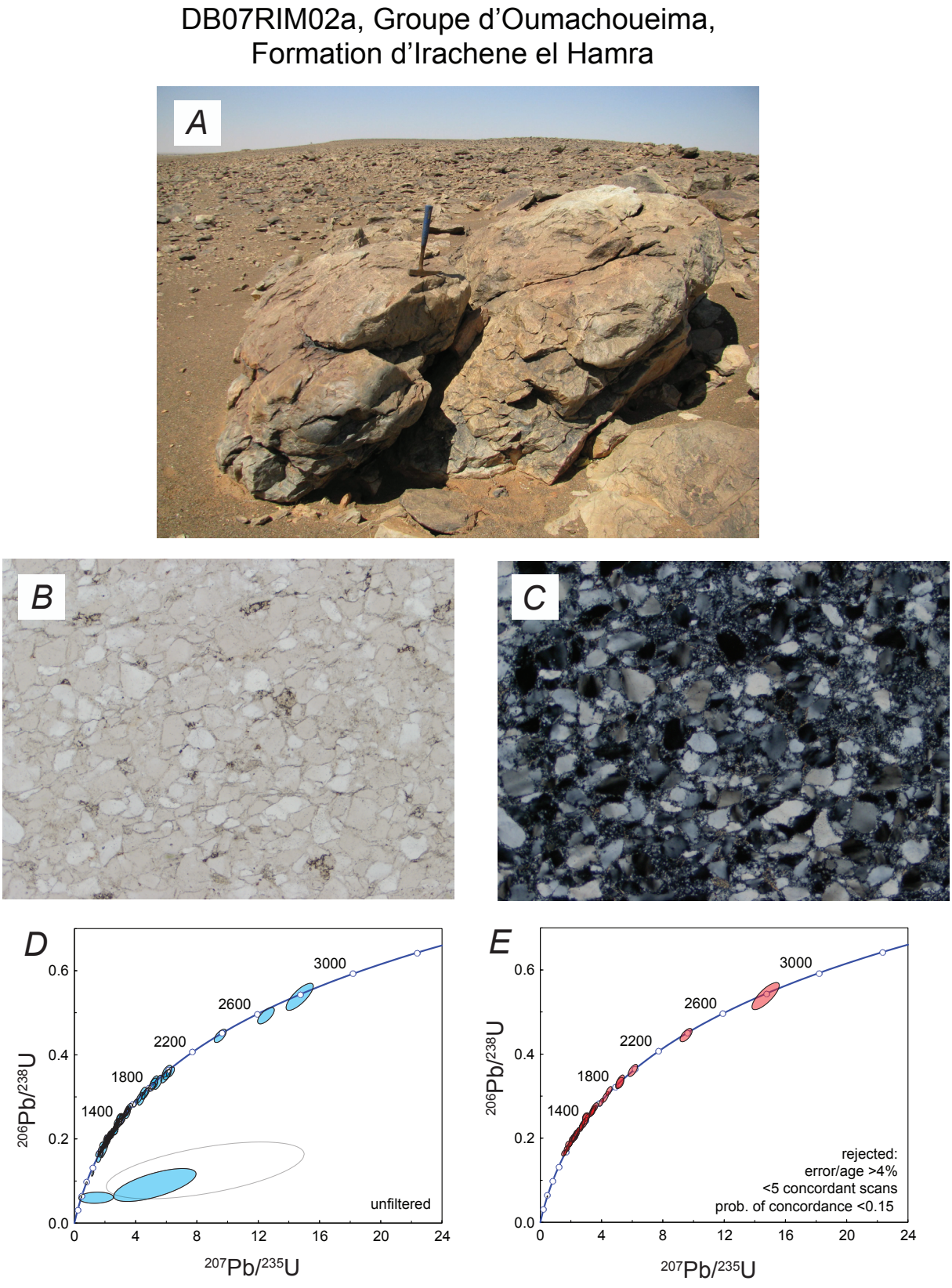


Figure 43. Detrital zircon data and photographs for sample DB07RIM02a, from the Atilis quartzite member of the Formation d'Irarchene El Hamra, Groupe d'Oumachoueima. (*A*) Outcrop photograph of quartzite from the sample location. (*B* and *C*) Photomicrographs of quartzite under plane light and crossed polars, respectively. (*D* and *E*) Concordia diagrams showing unfiltered and filtered data. (*F*) Age distribution.—Continued

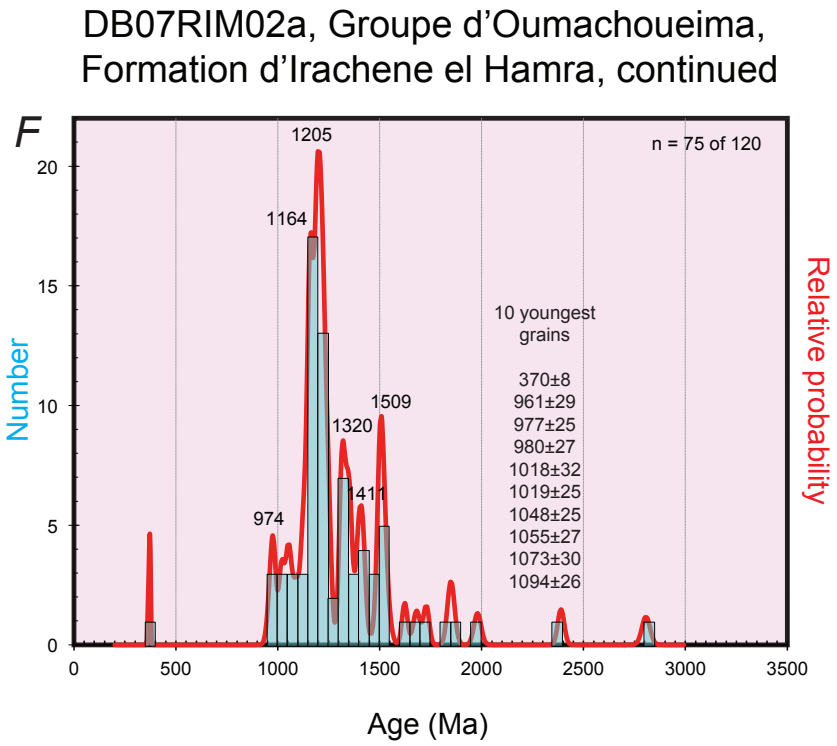


Figure 43. Detrital zircon data and photographs for sample DB07RIM02a, from the Atilis quartzite member of the Formation d'Irarchene El Hamra, Groupe d'Oumachoueima. (*A*) Outcrop photograph of quartzite from the sample location. (*B* and *C*) Photomicrographs of quartzite under plane light and crossed polars, respectively. (*D* and *E*) Concordia diagrams showing unfiltered and filtered data. (*F*) Age distribution.

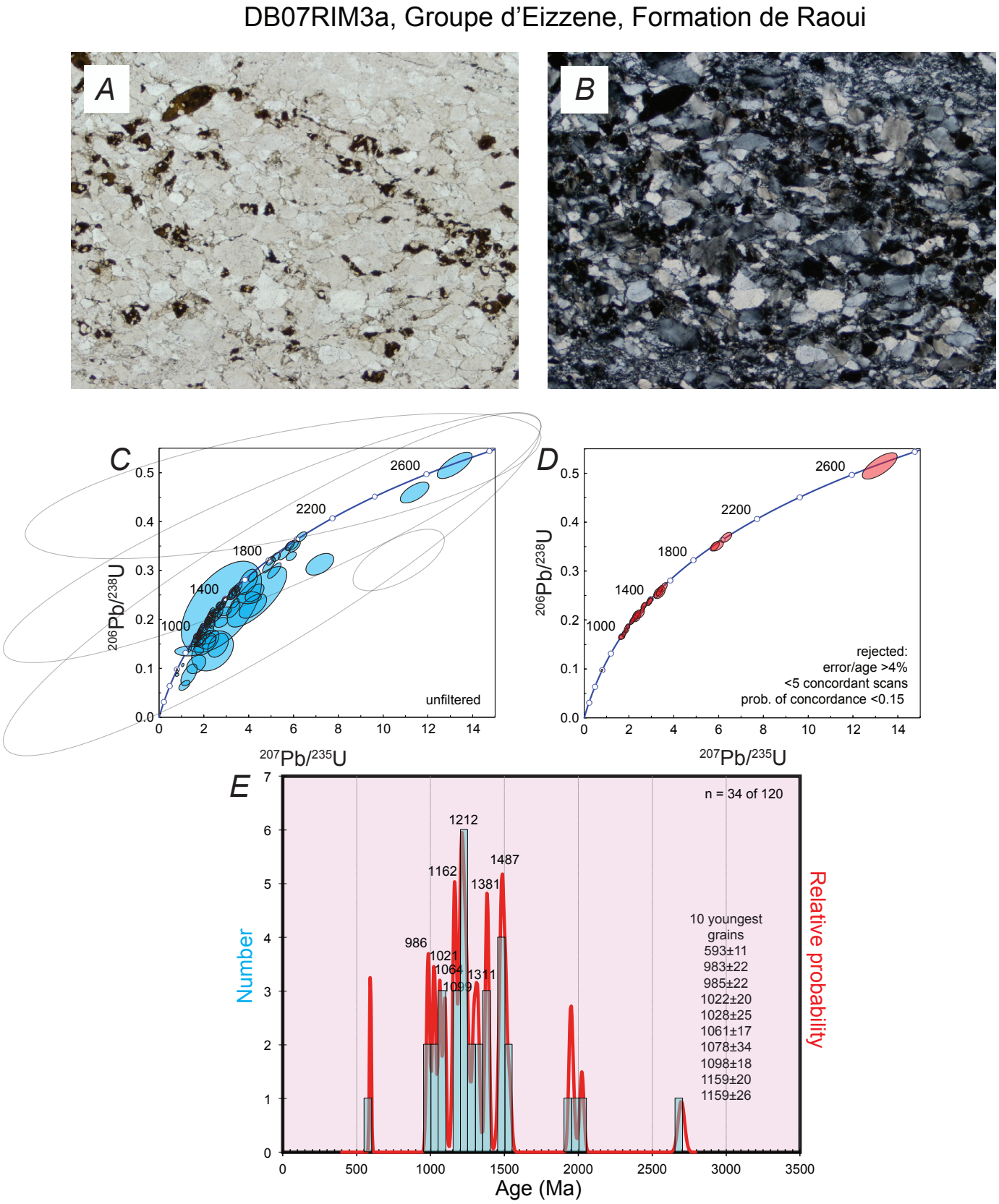


Figure 44. Detrital zircon data and photographs for sample DB07RIM03a, from the Formation de Raoui of the Groupe de Eizzene. (*A* and *B*) Photomicrographs of quartzite under plane light and crossed polars, respectively. (*C* and *D*) Concordia diagrams showing unfiltered and filtered data. (*E*) Age distribution.

DB07RIM17a, Complexe d'Inchiri, Groupe de Hajar Dekhen – Kleouat

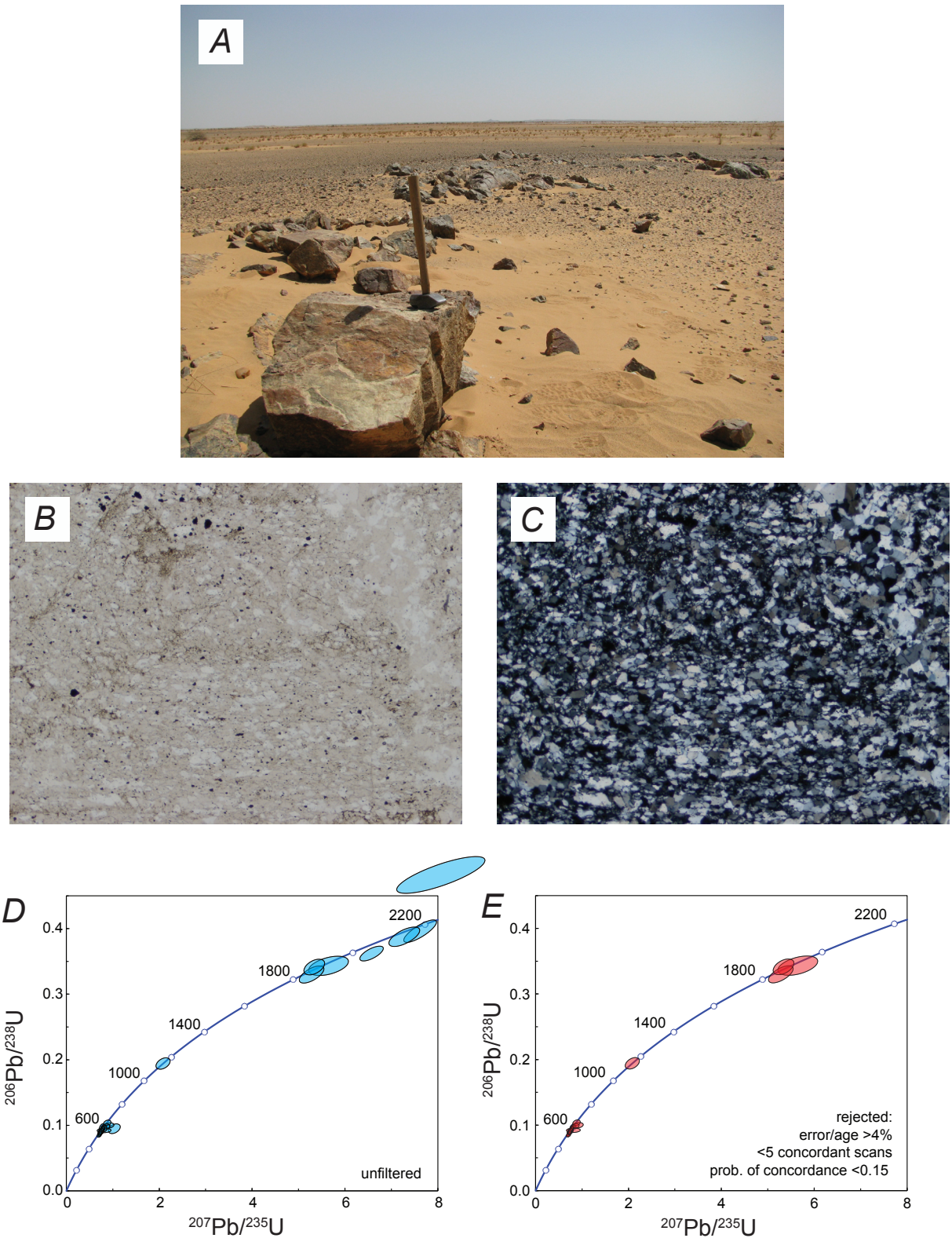


Figure 45. Detrital zircon data and photographs for sample DB07RIM17a, from the Groupe de Hajar Dekhen – Kleouat of the Complexe d'Inchiri. (*A*) Outcrop photograph of quartzite from the sample location—an area of sparse exposure. (*B* and *C*) Photomicrographs of quartzite under plane light and crossed polars, respectively. (*D* and *E*) Concordia diagrams showing unfiltered and filtered data. (*F*) Age distribution.—Continued

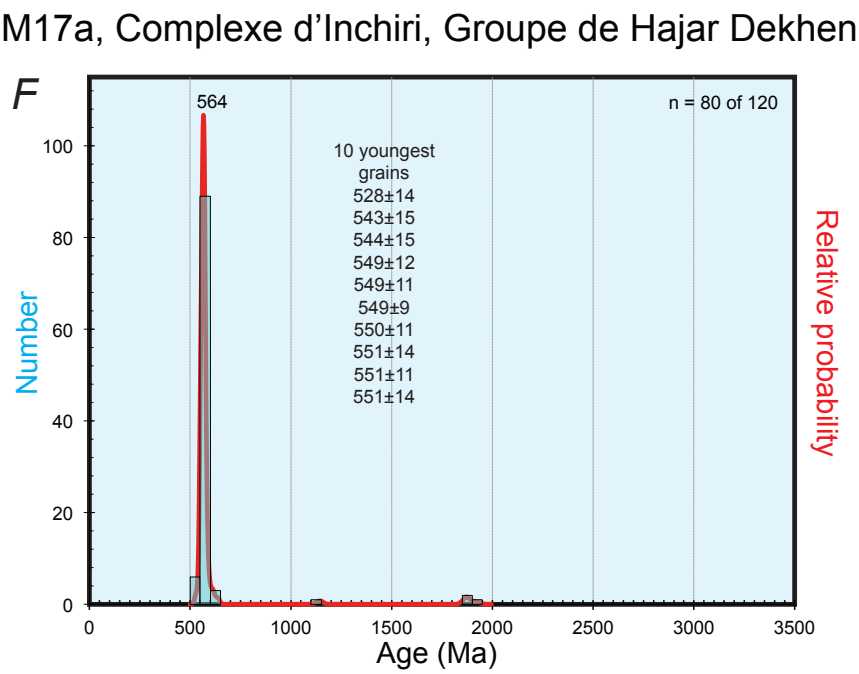


Figure 45. Detrital zircon data and photographs for sample DB07RIM17a, from the Groupe de Hajar Dekhen–Kleouat of the Complexe d'Inchiri. (*A*) Outcrop photograph of quartzite from the sample location—an area of sparse exposure. (*B* and *C*) Photomicrographs of quartzite under plane light and crossed polars, respectively. (*D* and *E*) Concordia diagrams showing unfiltered and filtered data. (*F*) Age distribution.

zircon age of 2,968±2 Ma from a metadacite that has been mapped as part of the Formation d'Aouéoua (Pitfield and others, 2004, Section 2.3.5). One possibility is that the sampled strata were mismapped as Archean and are, in fact, Neoproterozoic. In this case, the Chami Greenstone Belt would include both Archean and Neoproterozoic strata, a previously unsuspected possibility. Alternatively, the ca 600-Ma ages might represent a Pan-African overprint, as discussed in Section 7.6. The sample location is only about 20 km inboard of the inferred position of the Mauritanide deformation front, and the area has poor exposure, so either of these explanations is geologically plausible.

Sample GB07RIM82D is from a quartz-sericite vein (fig. 47*A*) about 6 km to the northeast in different strike belt of the Formation d'Aouéoua, from the Tasiast gold deposit at the Nord pit. This quartz-sericite vein cuts gray quartz that is related to gold mineralization. White mica was dated using the $^{40}Ar/^{39}Ar$ method. The age spectrum from this sample is internally complex and does not form an $^{40}Ar/^{39}Ar$ age plateau (fig. 47*B*). The $^{40}Ar/^{39}Ar$ data are consistent with either (1) multiple generations of white mica, or (2) a sample that initially recorded mica cooling or growth at ca. 2.6 Ga followed by a heating event sometime after ca. 2 Ga. In any case, there is no evidence of a Neoproterozoic event. Gold mineralization at Tasiast is likely older than 2,533 Ma.

6.2. Complexe d'Amsaga near Mennerat Iguilid tungsten occurrence

The Complexe d'Amsaga is the metaigneous and metasedimentary basement below the Taoudeni Basin at the Adrar escarpment. Samples were collected from near the Mennerat Iguilid tungsten occurrence near Oued Toueirga in the eastern Atar 1:200,000-scale sheet (number 2013).

Sample DB07RIM25a is an altered granitoid (figs. 48*A* and *B*). Zircons from this rock proved undatable owing to a combination of high common lead, Phanerozoic lead loss, and severe metamictization (fig. 48*E*). Secondary white mica from the same sample yielded a fairly robust integrated age of about 1,753 Ma that is interpreted as the time of cooling below ca. 350° C (fig. 48*F*).

Sample DB07RIM25C is from quartzite (fig. 49*A*) in a metasedimentary enclave within the altered granitoid, which we presumed to be a screen of country rock. Of 120 zircons analyzed, only 43 pass the LAICPMS filters. The probability curve shows major peaks at 1,221, 613, and 582 Ma and minor peaks at 2,044 and 1,807 Ma; no Archean ages were obtained (fig. 48*D*). This zircon age distribution is at odds with the mapped geology. One possibility is that the quartzite is Neoproterozoic and is in structural contact with an older granitoid. The sample location, however, is about 120 km inboard of the Mauritanide deformation front so this possibility seems unlikely. Another possibility is that the sample suffered nearly complete resetting associated with Pan-African orogenesis. Cross-contamination seems unlikely because the Neoproterozoic population is so large; a sample mix-up cannot be ruled out.

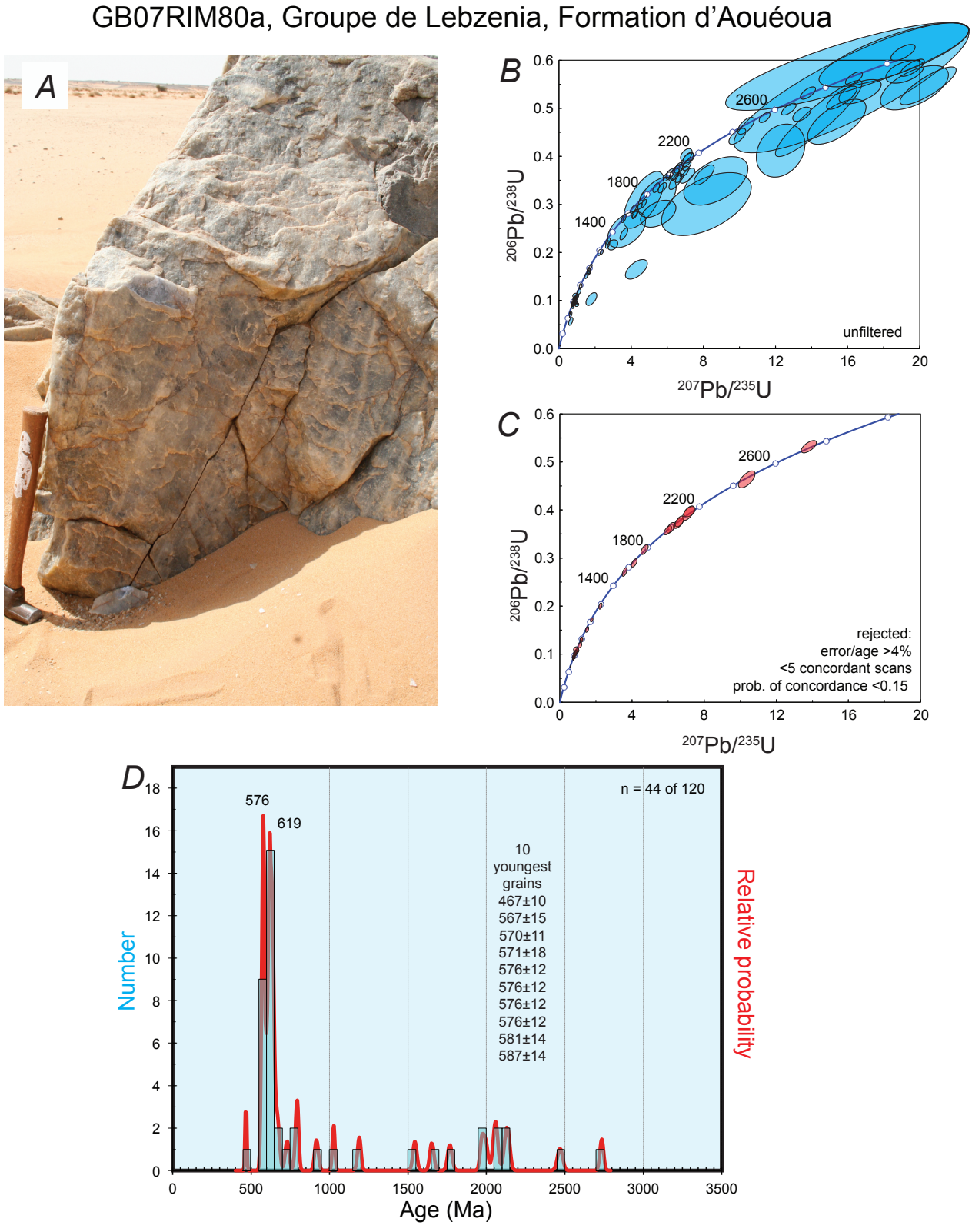


Figure 46. Detrital zircon data and photographs for sample GB07RIM80a, from the Formation d'Aouéoua of the Groupe de Lebzenia. (*A*) Outcrop photograph of quartzite from the sample location. Photography by Georges Beaudoin. (*B* and *C*) Concordia diagrams showing unfiltered and filtered data. (*D*) Age distribution.

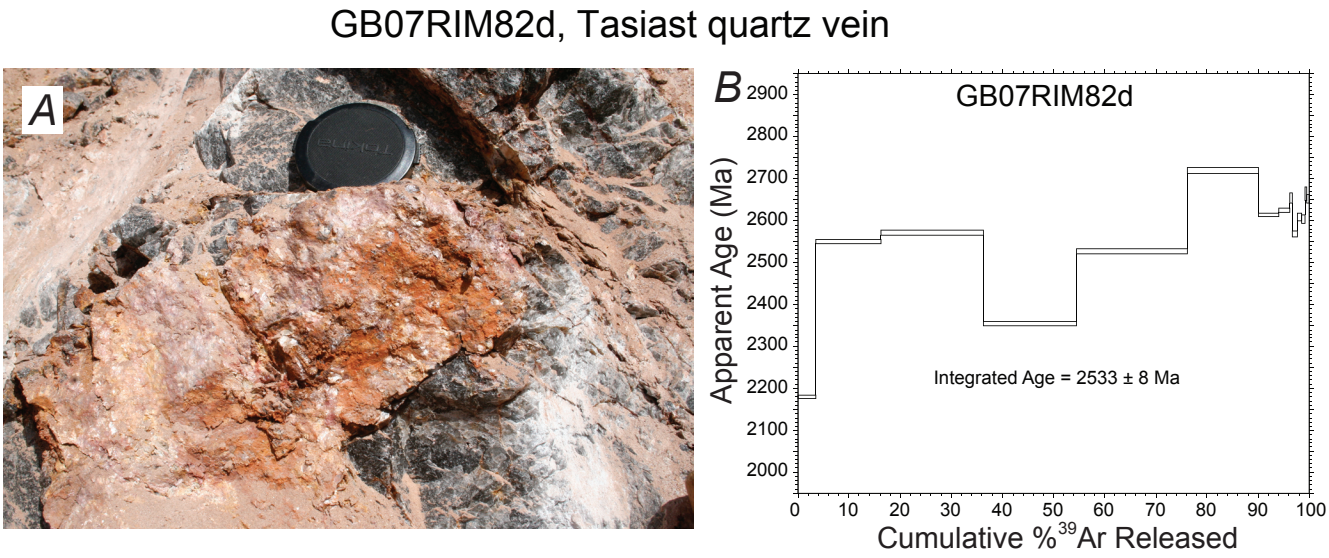


Figure 47. (*A*) Outcrop photograph of the sample location of sample GB07RIM82D, a quartz vein that cuts the Formation d'Aouéoua in the Tasiast region. Photograph by Georges Beaudoin. (*B*) Argon age-release spectrum for white mica.

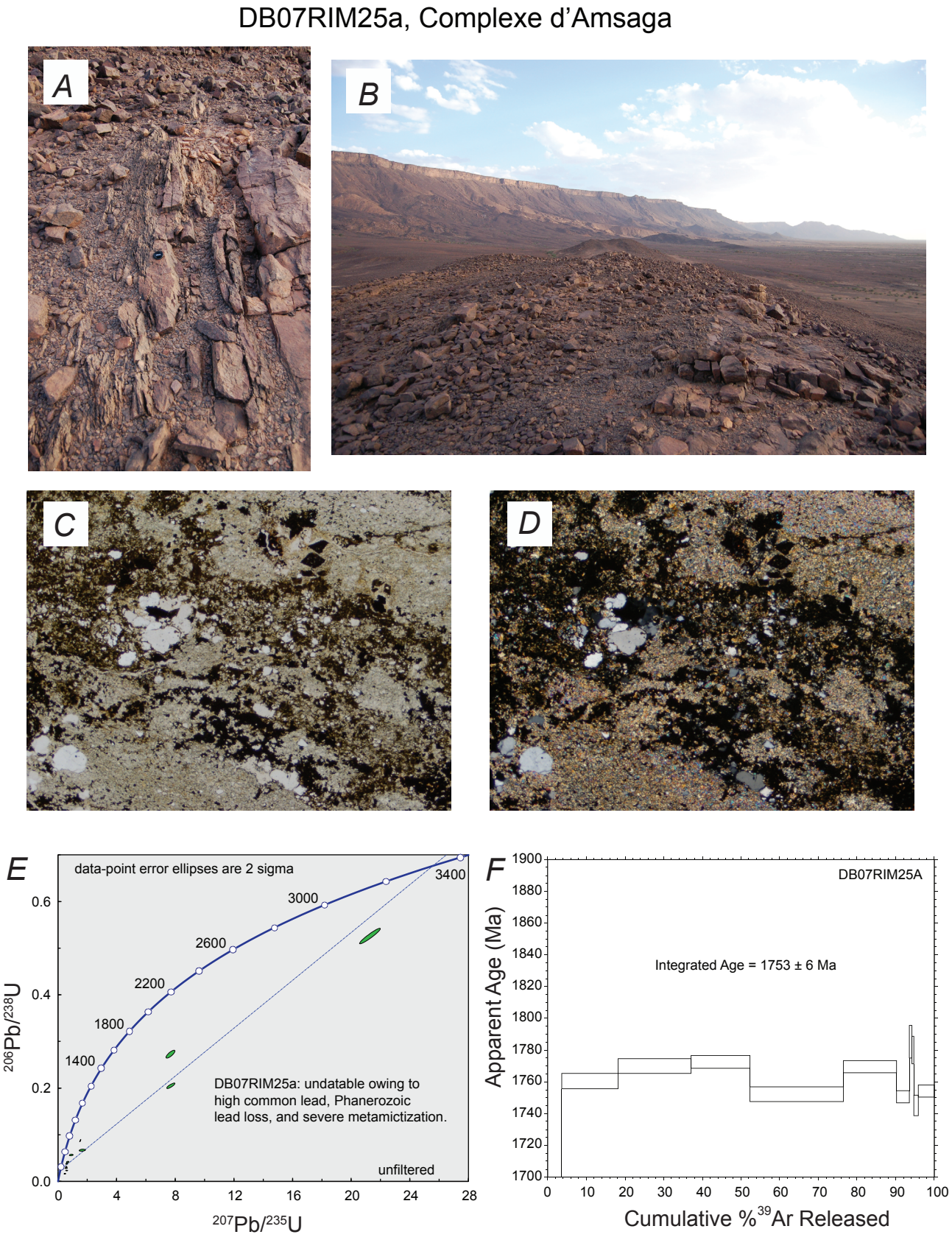
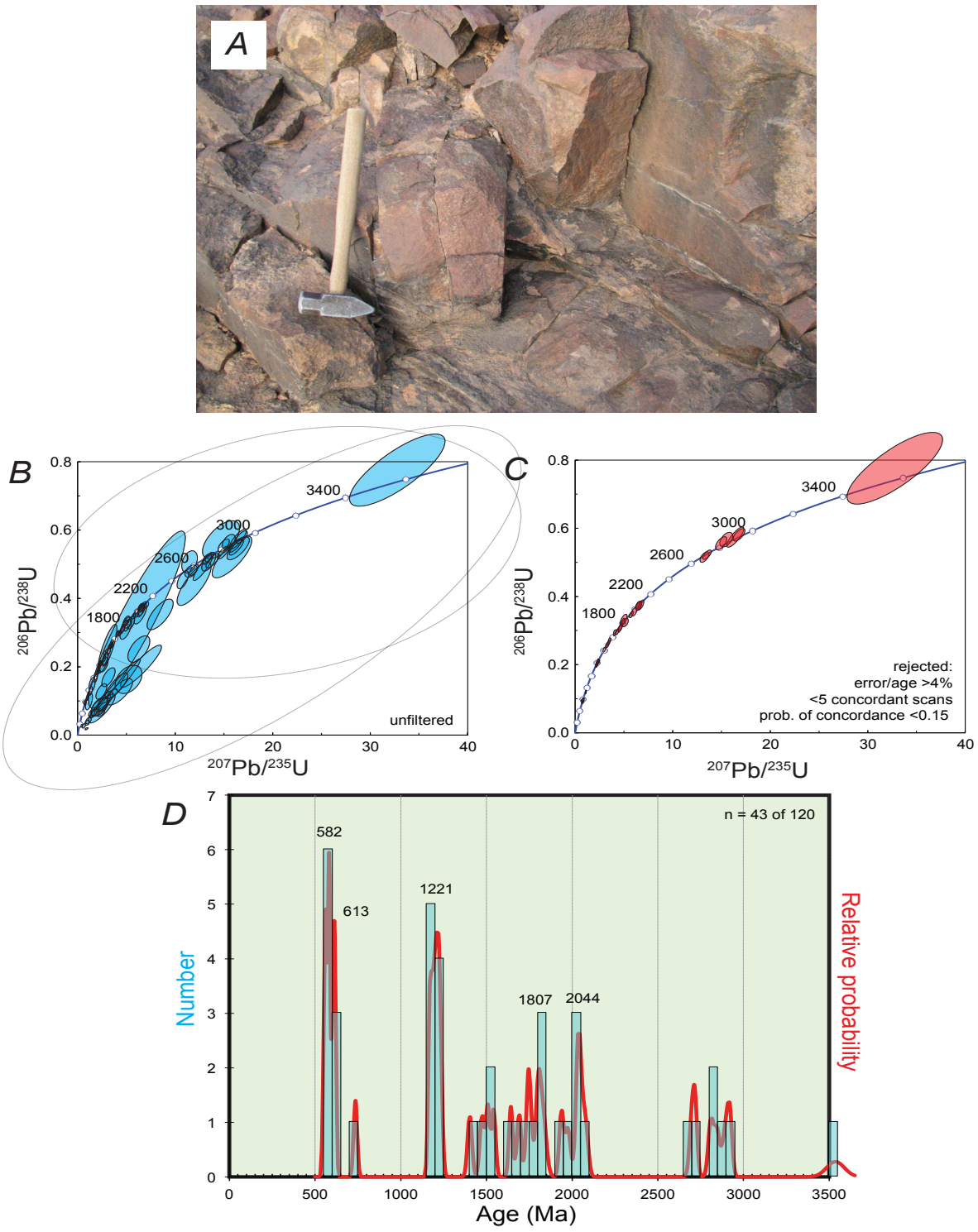


Figure 48. Geochronological data and photographs of granitoid sample DB07RIM25a from the Complexe d'Amsaga. (*A* and *B*) Outcrop photographs of granitoid from the sample location. (*C* and *D*) Photomicrographs of altered granitoid under plane light and crossed polars, respectively. (*E*) Concordia diagram showing complex, intractable zircon systematics. (*F*) Argon age-release spectrum for white mica.



9, Deliverable 53

Figure 49. Detrital zircon data and photographs for sample DB07RIM25C, from quartzite in the Complexe d'Amsaga. (*A*) Outcrop photograph of the sample location. (*B* and *C*) Concordia diagrams showing unfiltered and filtered data. (*D*) Age distribution.

6.3. Anorthosite in Complexe d'Amsaga Amsaga

Sample CT07RIM25-1 is from an unmapped anorthosite body within charnockitic gneiss in the Complexe d'Amsaga on the Atar 1:200,000-scale sheet (number 2013). Several large blocks of anorthosite dimension-stone have been quarried and shipped from this location; nearby at Guellâbet el Agueila is another anorthosite quarry (Indice 040IND0015). Zircons from sample CT07RIM25-1 were analyzed by the SIMS method and yielded a poorly resolved U-Pb concordia age of 2,930±33 Ma (fig. 50). Most of the zircons are discordant and those near concordia do not form a coherent grouping. Phanerozoic lead-loss is evident. Nonetheless, the sample is interesting as it appears to be the oldest "massif-type" anorthosite yet discovered (Ashwal, 2011).

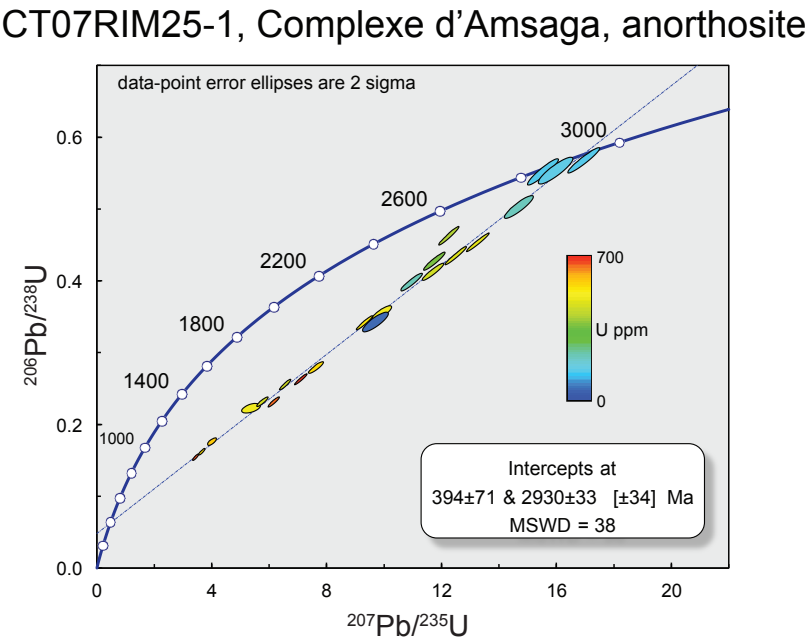


Figure 50. Concordia diagram *for sample* CT07RIM25-1, anorthosite from the Complexe d'Amsaga.

Samples DB07RIM32-1a and CT07RIM22-1 are from another previously unmapped anorthosite body or bodies on the Atar 1:200,000-scale sheet (number 2013) within an area mapped as unit Amlb, quartzofeldspathic gneiss. We sampled these rocks while trying, unsuccessfully, to find a mislocated strontium mineral occurrence. Coarse-grained and fine-grained phases were dated separately using the LAICPMS method. Zircons from a coarse-grained anorthosite (fig. 51*A*), sample DB07RIM32-1a, yielded a U-Pb concordia age of 2,718±7 Ma (figs. 51*B* and *C*). Zircons from a fine-grained anorthosite, sample CT07RIM22-1, yielded a U-Pb concordia age of 2,743±4 Ma (fig. 51*D*).

6.4. Complexe de Tiris

The Complexe de Tiris is the Archean basement in the Zouerate iron-mining district (Fderik 1:200,000-scale sheet, number 2012). At Kediat Idjil, the greenschist-facies Complexe d'Idjil and granulite-facies Complexe de Tiris are juxtaposed along a thrust contact. Sample DB07RIM45b is a deformed pegmatite pod from within the thrust zone (fig. 52*A*). A white mica separate yielded an integrated $^{40}Ar/^{39}Ar$ age of 2496±8 Ma (fig. 52*B*) but the age spectrum is difficult to interpret. The internal complexity of the age spectrum may indicate the presence of non-atmospheric trapped argon. One possible interpretation of this $^{40}Ar/^{39}Ar$ age spectrum is that initial cooling occurred at ca. 2.8 Ga with partial age resetting due to thermal overprinting at ca 1.6 Ga. These interpretations are preliminary and need to be supported by additional work.

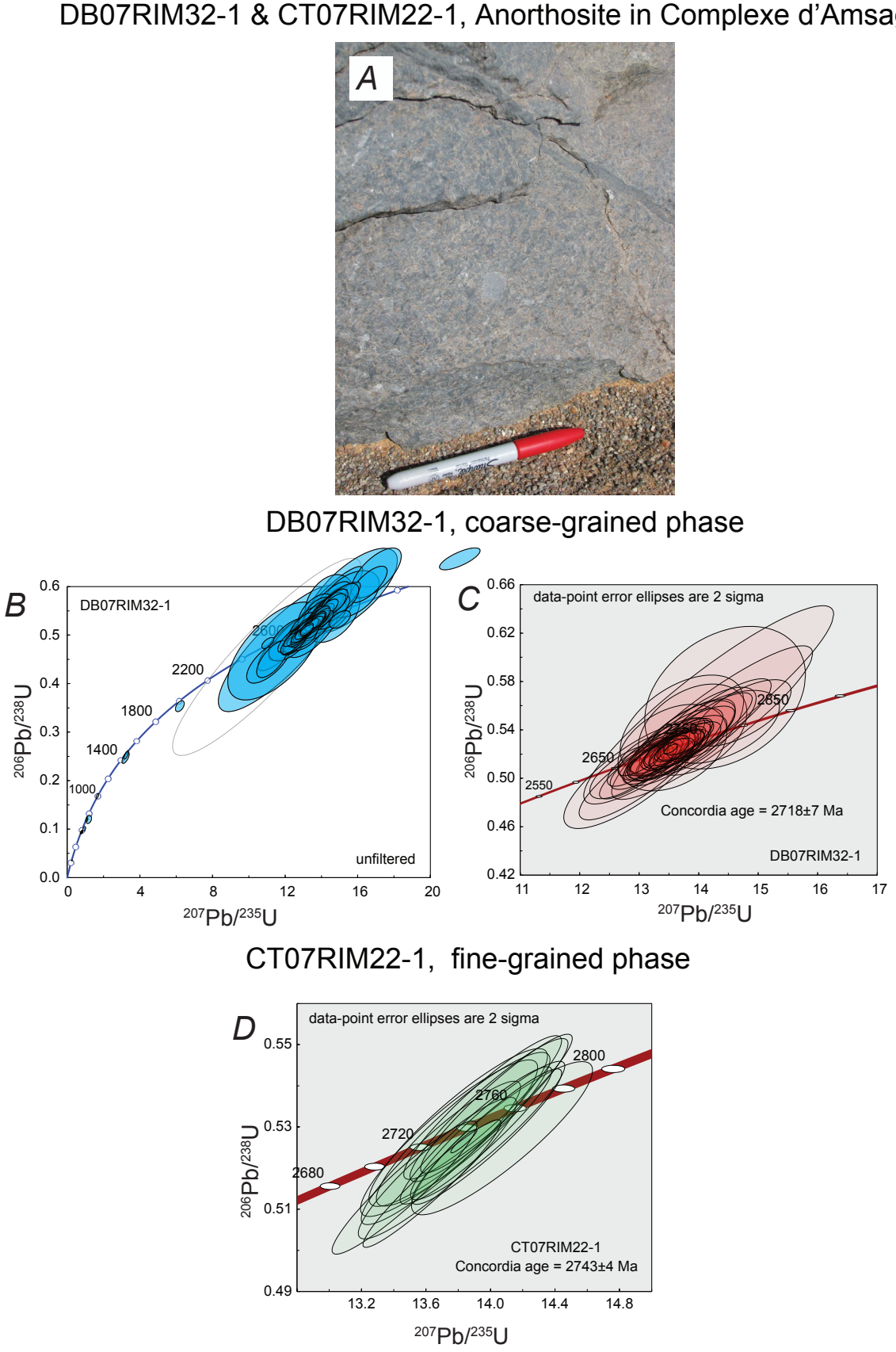


Figure 51. Zircon data and photographs for samples DB07RIM32-1a and CT07RIM22-1, different phases of an anorthosite body in the Complexe d'Amsaga. (*A*) Outcrop photograph of anorthosite sample DB07RIM32-1. (*B* and *C*) Concordia diagrams for coarse-grained anorthosite, sample DB07RIM32-1. (*B*) SIMS data, unfiltered. (*C*) LAICPMS data, filtered. (*D*) Concordia diagram for fine-grained anorthosite, sample CT07RIM22-1.

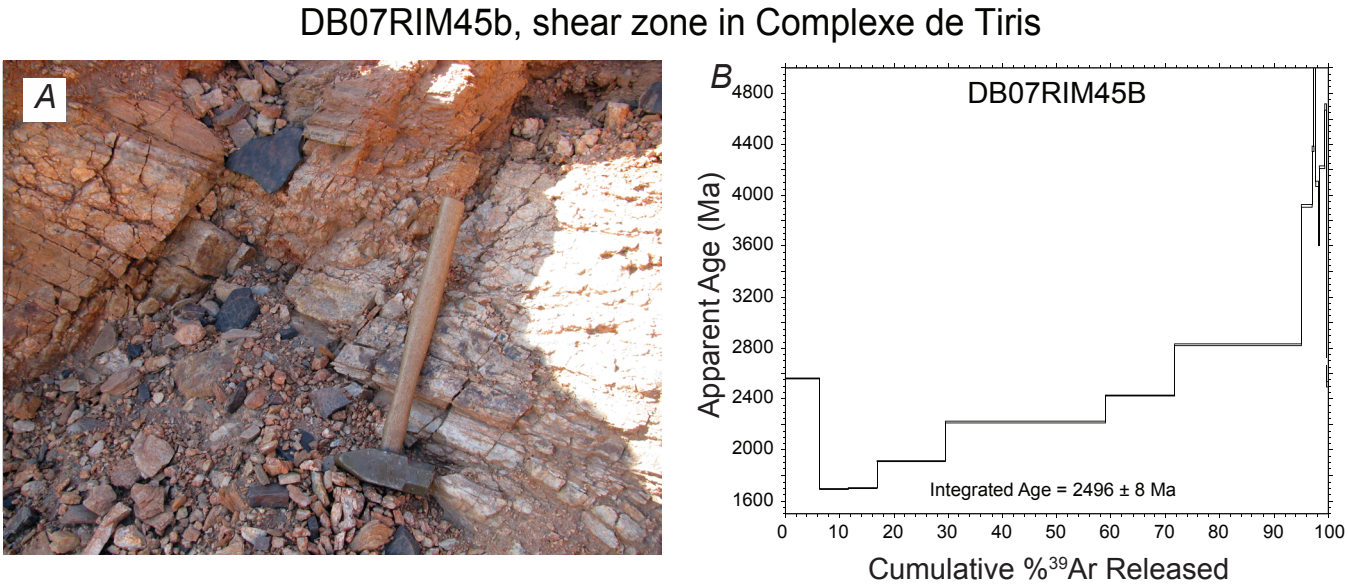


Figure 52. (*A*) Outcrop photograph of the sample location of sample DB07RIM45b, Complexe de Tiris. (*B*) Argon age-release spectrum for white mica.

Sample CT07RIM27 is a calcrete breccia (fig. 53A) from the weathered carapace of the Mhaoudât #4 iron mine (22.92158°N, 12.01114°W). Banded iron formation (BIF) from this pit is enriched in P_2O_5 (up to 14 percent). Results of apatite fission-track and apatite U-Pb double-dating by Paul O'Sullivan revealed a fission-track age of about 160 Ma (fig. 53*B*). These same apatite grains yielded poorly resolved U-Pb ages that cluster around 2,000–2,100 and 600 Ma. Accordingly, we interpret the apatites as detrital and their individual fission-track ages as recording their various times of exhumation below ca. 100° C. At about 160 Ma, this part of Mauritania would have been on or near a rift shoulder related to opening of the Central Atlantic Ocean, where seafloor spreading had begun about 20 m.y. before. (Steiner and others, 1998).

6.5. Complexe d'Idjil, Formation de Tazadit

The Complexe d'Idjil is a supracrustal succession of presumed Paleoproterozoic age in the Zouerate iron district (Fderik 1:200,000-scale sheet, number 2012). It includes quartzite, ferruginous quartzite, micaceous quartzite, and mica–quartz schist that locally reaches the staurolite grade of regional metamorphism (Schofield and others, 2006; Schofield and Gillespie, 2007). Mauritania's biggest iron mines are in this package. The Complexe d'Idjil overlies the Neoarchean Complexe de Tiris along a low angle thrust. Basement rocks of the Complexe de Tiris are metamorphosed to granulite facies and have U-Pb ages ranging from 2.83 Ga to 2.45 Ga (O'Connor and others, 2005). Our detrital zircon sample (DB07RIM46a) is from quartzite of the Formation de Tazadit (figs. 54*A* and *B*). Of 120 zircons analyzed, 31 pass the LAICPMS filters; the unfiltered concordia diagram shows clear evidence of young (Cenozoic or modern) lead loss (fig. 54*C*). The age distribution has maxima at 3,294 and 2,988 Ma (fig. 54*E*). The maximum depositional age based on detrital zircon alone can be set at the age of the youngest peak–2,988 Ma–but the actual depositional age is likely about a billion years younger.

Sample RIM07DB46b is a muscovite schist from the same outcrop. The $^{40}Ar/^{39}Ar$ data from this sample of white mica are broadly consistent with cooling of this rock below ca. 350°C at about 1970 Ma (fig. 54*F*). The younger ages in the first few laboratory degassing steps may be consistent with minor argon loss due to reheating.

6.6. Formation de Seyala

The Formation de Seyala (of Schofield and Gillespie, 2007) is a weakly metamorphosed belt of problematic origin in the Zouerate iron district (Fderik 1:200,000-scale sheet, number 2012). The rock consists of clasts of white quartzite (generally rounded) and tectonized iron formation (generally angular) in an argillaceous matrix (figs. 55*A*, *B*, and *C*). We did not observe bedding, but the thickness is substantial, and the overall impression is of a chaotic jumble. Schofield and Gillespie (2007) considered the unit to represent a thrust-related molasse sequence that was deposited during emplacement of a Paleoproterozoic supracrustal succession (iron formation and related strata) over Neoarchean basement gneisses of the Complexe de Tiris.

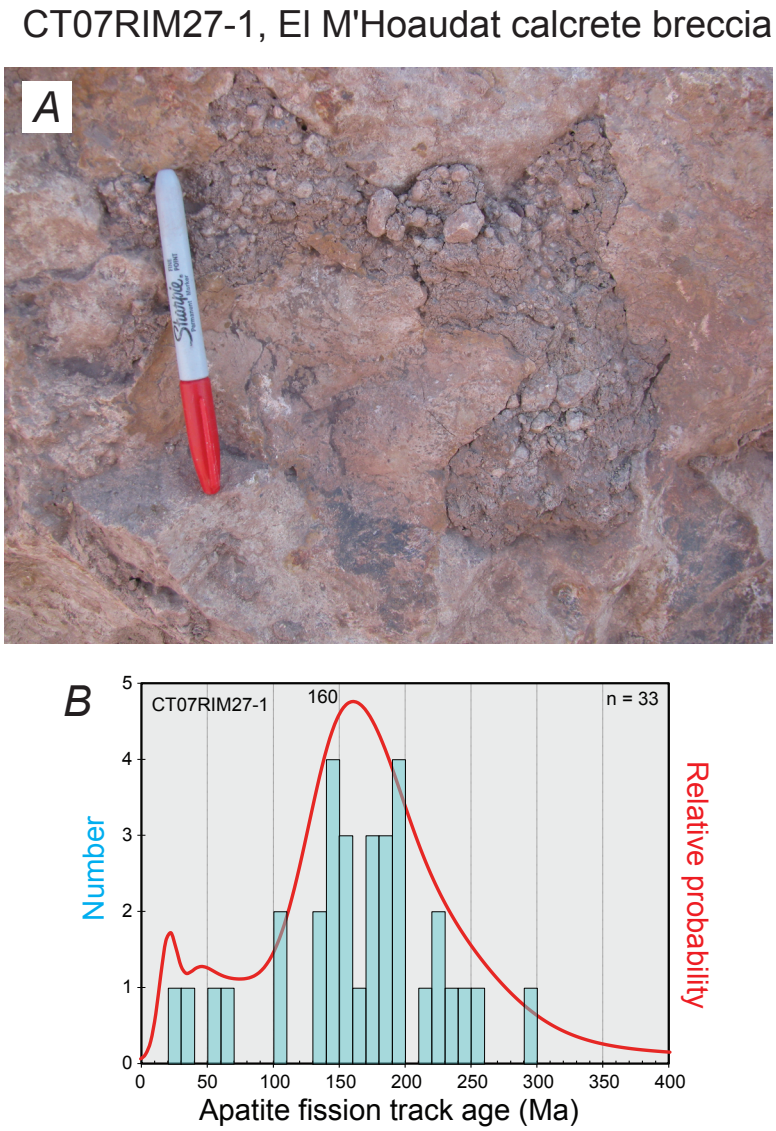


Figure 53. (*A*) Outcrop photograph of calcrete breccia, sample CT07RIM27-1, from the carapace of the Mhaoudât #4 iron mine. (*B*) Histogram of apatite fission-track ages. We interpret the apatite population as detrital and eroded from rocks that mostly cooled through 100° C during the Jurassic.

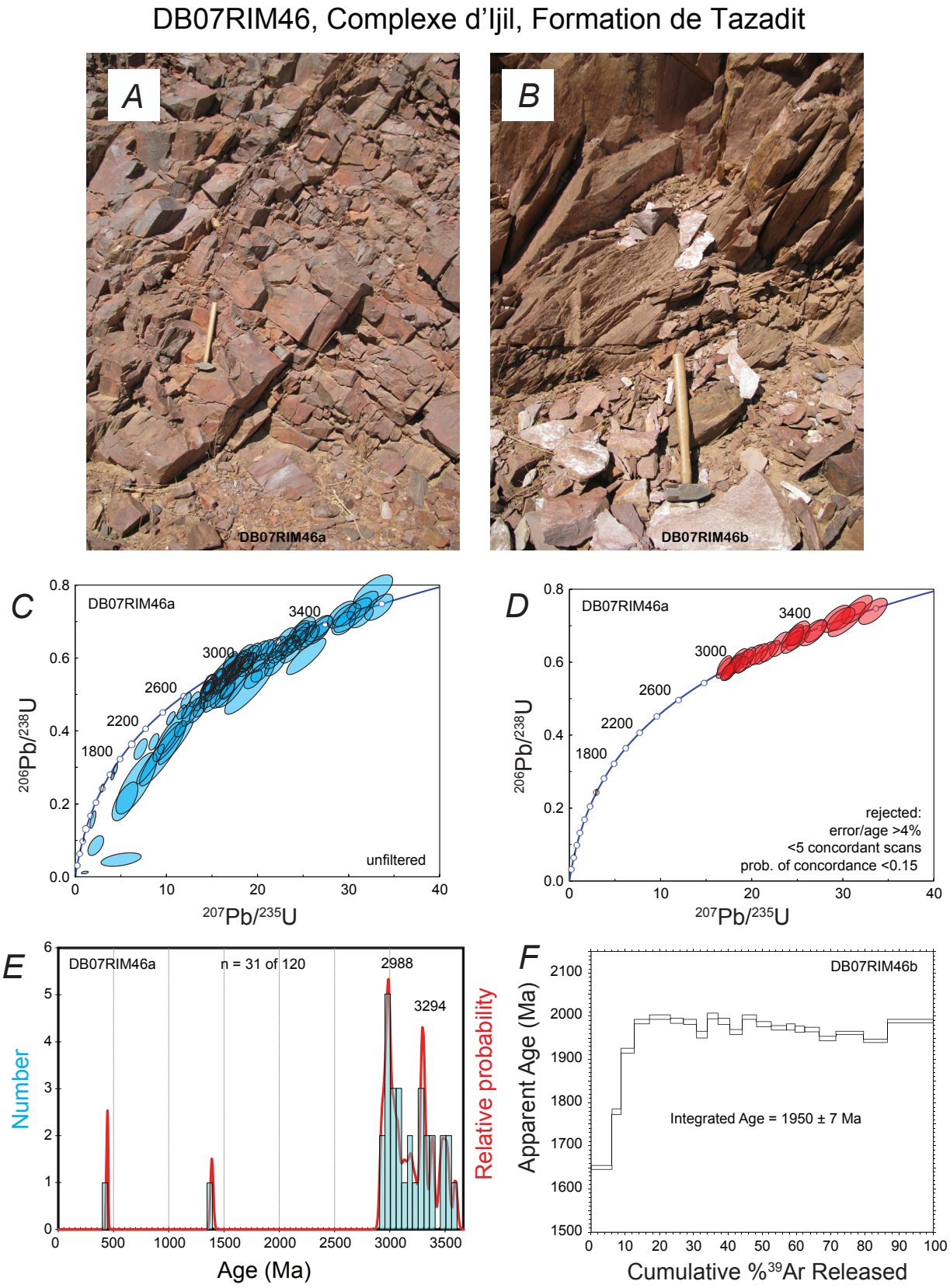


Figure 54. Geochronological data and photographs for sample DB07RIM46a and b, from quartzite in the Formation de Tazadit in the Complexe d'Idjil. (*A* and *B*) Outcrop photographs of the horizon sampled for DB07RIM46a and DB07RIM46b, respectively. (*C* and *D*) Corresponding concordia diagrams showing unfiltered and filtered data. (*E*) Detrital zircon age distribution for sample DB07RIM46a. (*F*) Argon age-release spectrum for white mica from sample DB07RIM46b.

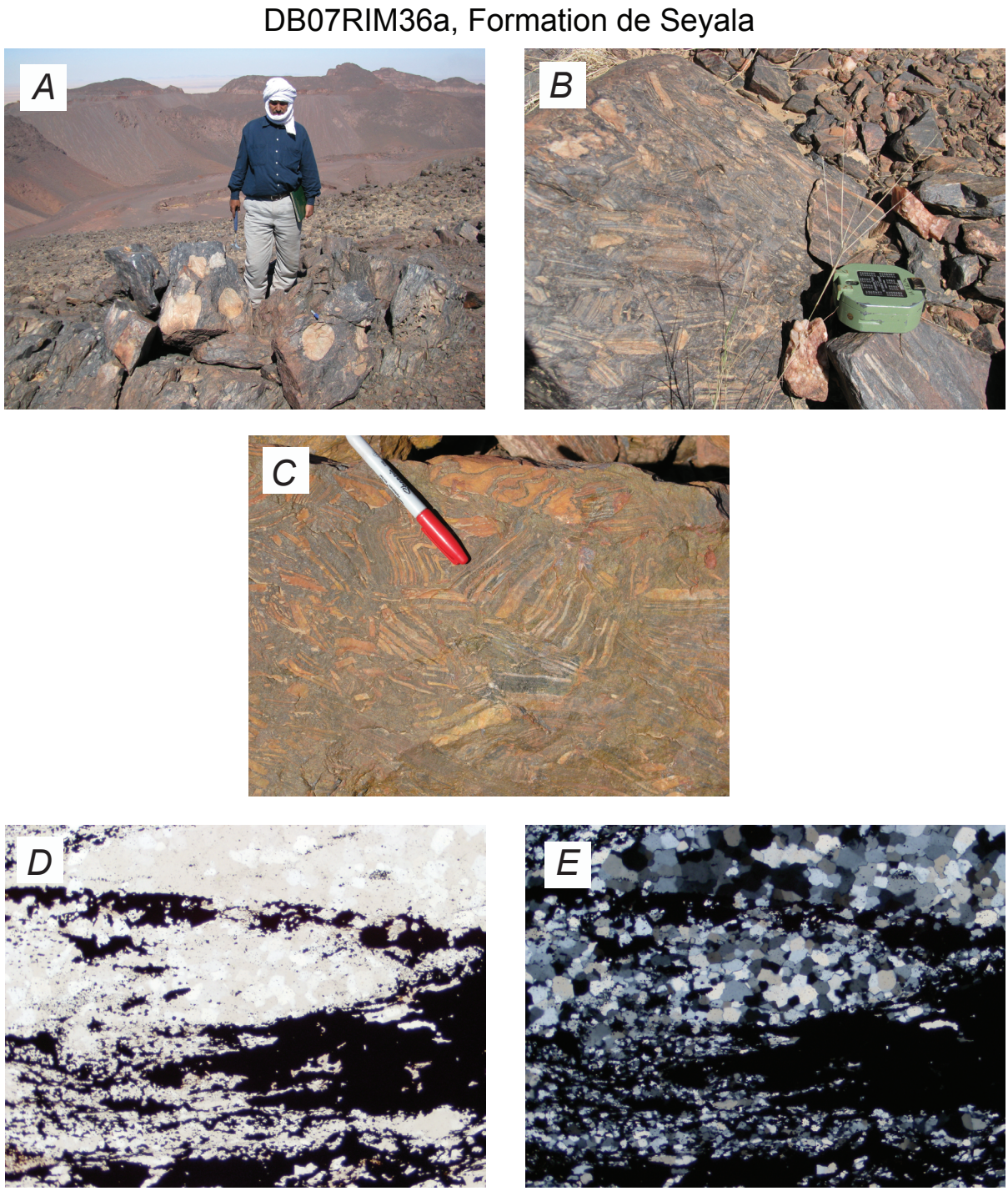


Figure 55. Detrital zircon data and photographs for sample DB07RIM36a, from the Formation de Seyala. (*A, B,* and *C*) Outcrop photographs of breccia from the sample location. (*D* and *E*) Photomicrographs of a clast of previously metamorphosed and deformed ferruginous quartzite under plane light and crossed polars, respectively. (*F* and *G*) Concordia diagrams of LAICPMS results showing unfiltered and filtered data. (*H*) Age distribution.—Continued

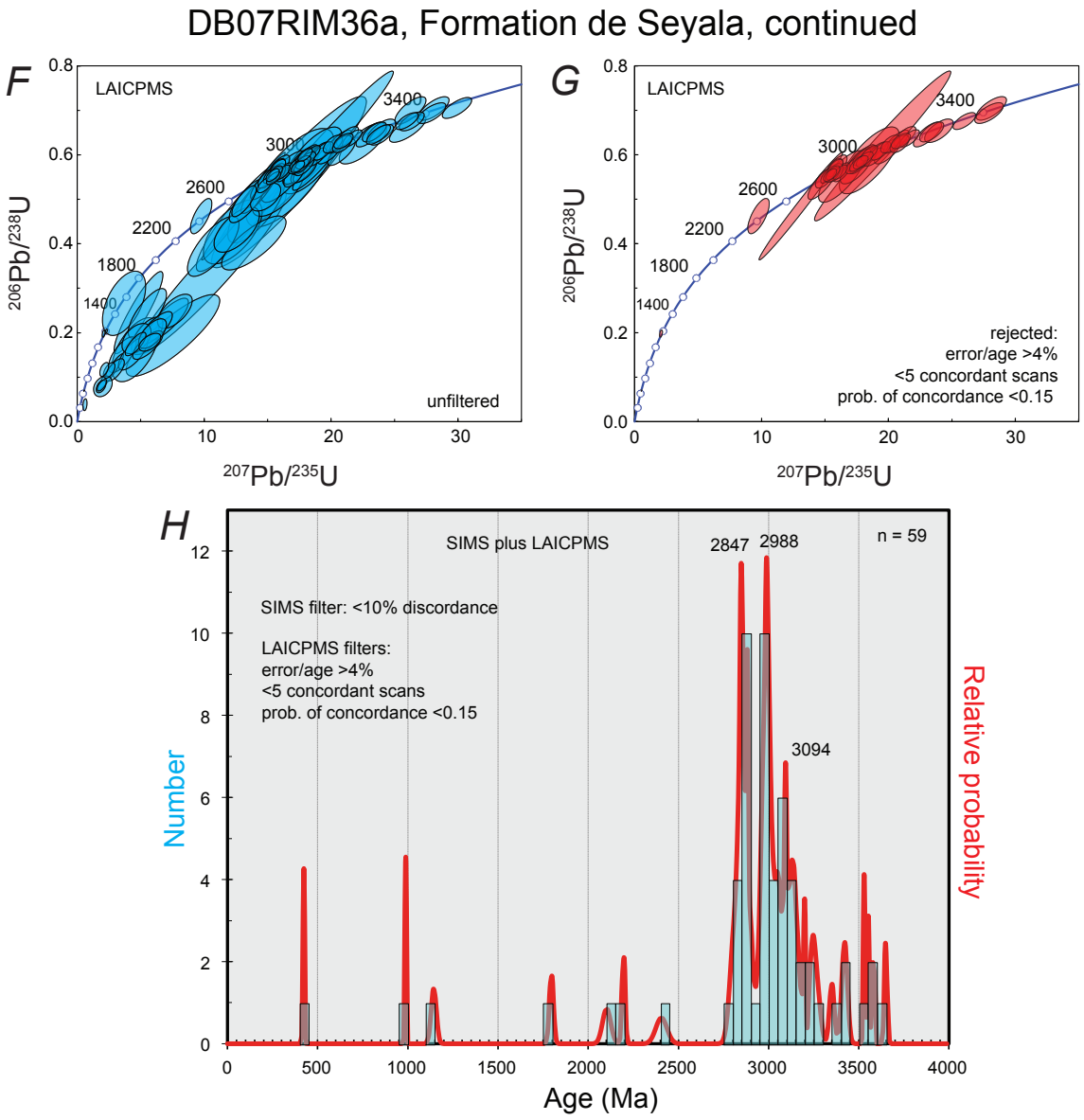


Figure 55. Detrital zircon data and photographs for sample DB07RIM36a, from the Formation de Seyala. (*A, B,* and *C*) Outcrop photographs of breccia from the sample location. (*D* and *E*) Photomicrographs of a clast of previously metamorphosed and deformed ferruginous quartzite under plane light and crossed polars, respectively. (*F* and *G*) Concordia diagrams of LAICPMS results showing unfiltered and filtered data. (*H*) Age distribution.

Detrital zircons from sample DB07RIM36a were analyzed by SIMS (in 2010, two mounts combined) and LAICPMS (in 2012). Both sets of analyses included abundant discordant grains such that only 30 grains passed the LAICPMS filters and only 29 grains passed the SIMS filters. The two datasets yielded similar age distributions, which are combined into a single probability plot (fig. 55*H*). This plot shows maxima at 3,094, 2,988, and 2,847 Ma. There is a smattering of younger zircons but none overlap in age. The youngest age peak, at 2,847 Ma, is probably close to a billion years older than the depositional age.

6.7. Groupe de Blekhzaymat

Several published lines of evidence indicate a Paleoproterozoic age for the Groupe de Blekhzaymat in northeastern Mauritania. Andesite in the Groupe de Blekhzaymat has a U-Pb zircon age of 2,069±10 (Lahondère and others, 2003, p. 163). In the southern part of its outcrop belt (Blekhzaymat 1:200,000-scale sheet, number 2407), the Blekhzaymat has been metamorphosed

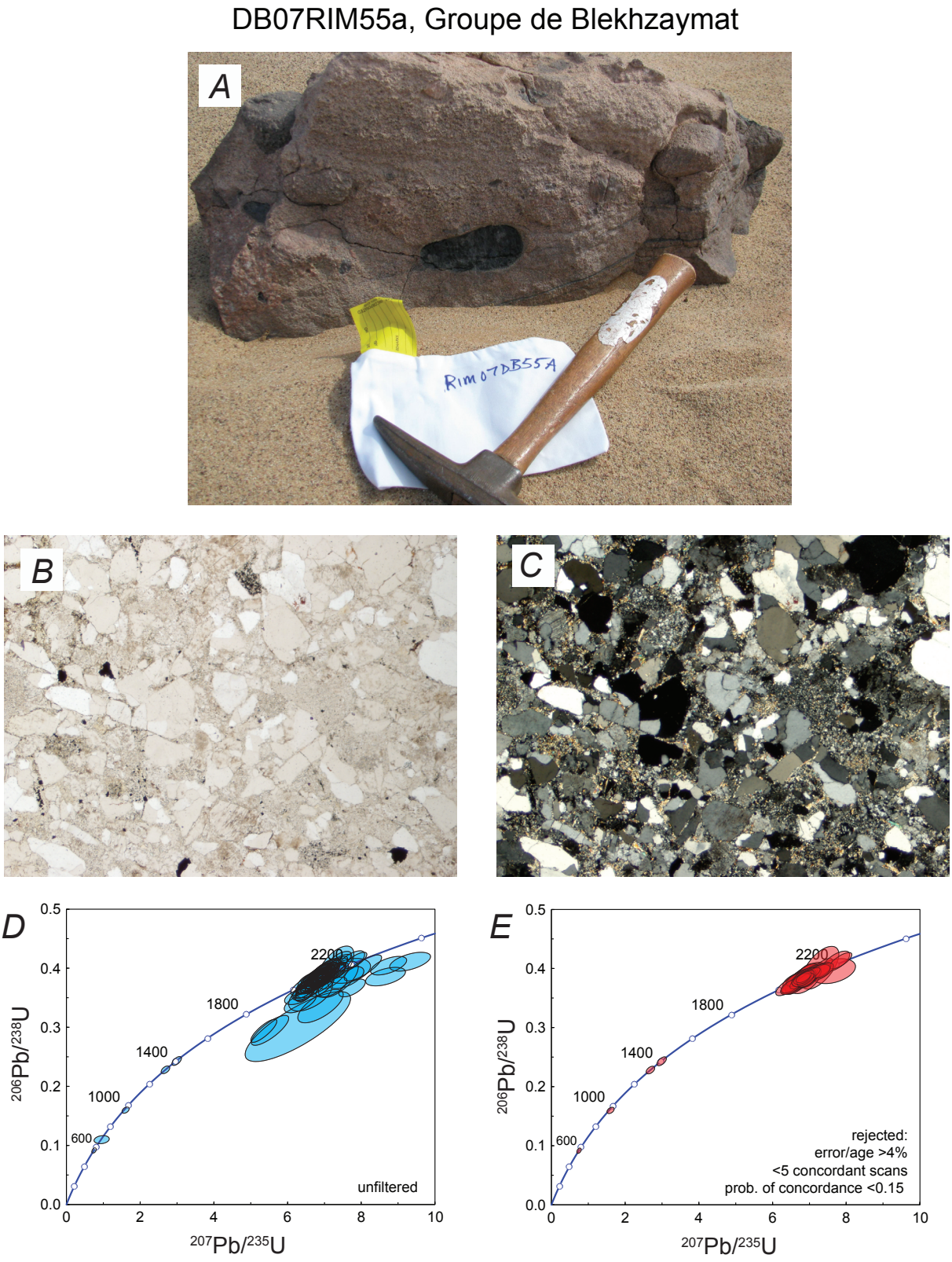


Figure 56. Detrital zircon data and photographs for sample DB07RIM55a, from the southern Groupe de Blekhzaymat. (*A*) Outcrop photograph of conglomeratic sandstone from the sample location. (*B* and *C*) Photomicrographs of sandstone under plane light and crossed polars, respectively. (*D* and *E*) Concordia diagrams showing unfiltered and filtered data. (*F*) Age distribution.—Continued

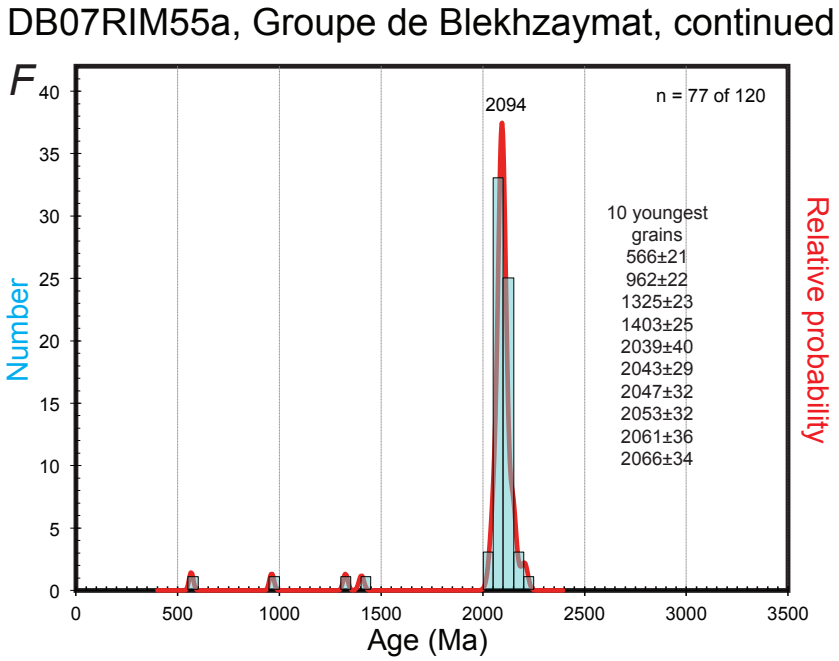


Figure 56. Detrital zircon data and photographs for sample DB07RIM55a, from the southern Groupe de Blekhzaymat. (*A*) Outcrop photograph of conglomeratic sandstone from the sample location. (*B* and *C*) Photomicrographs of sandstone under plane light and crossed polars, respectively. (*D* and *E*) Concordia diagrams showing unfiltered and filtered data. (*F*) Age distribution.

to hornfels adjacent to porphyritic granite of the Cortège de Yetti (1,995±20 Ma, U-Pb zircon) (Lahondère and others, 2003, p. 229). In addition, the Groupe de Blekhzaymat outcrop belt is overlapped by the Groupe de Douik at the base of the Taoudeni Basin section, which correlates with the >1,107-Ma Groupe de Char (see Section 3.1). Finally, as detailed in Section 6.8, two orogenic gold vein systems that cut the Groupe de Blekhzaymat in the north have yielded $^{40}Ar/^{39}Ar$ ages of 2,179±11 Ma and 2,063±7 Ma.

Sample DB07RIM55a is a red sandstone from the southern part of the Blekhzaymat outcrop belt (Blekhzaymat 1:200,000-scale sheet, 2407) from exposures of cobble-bearing coarse sandstone (fig. 56*A*). Of 120 analyses, 77 are concordant. The probability curve shows a major peak at 2,094 Ma where we set the maximum depositional age (fig. 56*F*).

Results from the northern part of the Groupe de Blekhzaymat outcrop belt are problematic. The Tindouf Basin lies just to the north. Here, the oldest strata are Ordovician and the map units strike roughly east-west and dip gently to the north, in contrast with the Groupe de Blekhzaymat whose beds strike roughly north-south and dip steeply. Sample DB07RIM54a is a purplish, foliated, medium-grained sandstone bed (fig. 57*A*) in an outcrop mostly of phyllite from a few kilometers south of the sub-Ordovician unconformity, in the Hassi Djebilet 1:500,000-scale sheet. Two splits of the same sample were run at different times. When the first analysis was done (lab number 952-15), the main goal was to constrain the maximum depositional age; euhedral zircons were therefore dated in preference to rounded ones on the assumption that the latter were more likely to have been through multiple sedimentary cycles. Out of 120 grains, 64 passed the LAICPMS filters (fig. 57*D* and *E*). The probability curve shows major peaks at 614 and 549 Ma and minor ones at 2,161, 2,057, 1,837, and 912 Ma (fig. 57*F*). This result concerned us because of the geologically constrained Paleoproterozoic depositional age. We therefore ran a second analysis (lab number 1284-8) on sample DB07RIM54a. This time, zircons were selected at random. Of 120 zircons analyzed, 52 are concordant (figs. 57*G* and *H*). The probability curve shows a major peak at 2,141 and only a minor one at 620 Ma (fig. 57I). The two probability curves are qualitatively similar, ruling out the possibility that the anomalous results of the first analysis were due to a sample mix-up. Both runs yielded problematically young, Neoproterozoic zircons, although there were fewer of these (8) in the second analysis. At face value, these young zircons would suggest a maximum depositional age of 549 Ma, seemingly impossible in light of the geologic constraints. We therefore suggest that the Neoproterozoic U-Pb ages record a Pan-African disturbance that reset some zircons. As discussed further in Section 7.6, Lahondère and others (2003, p. 164) reported something similar from an andesite in the Groupe de Blekhzaymat.

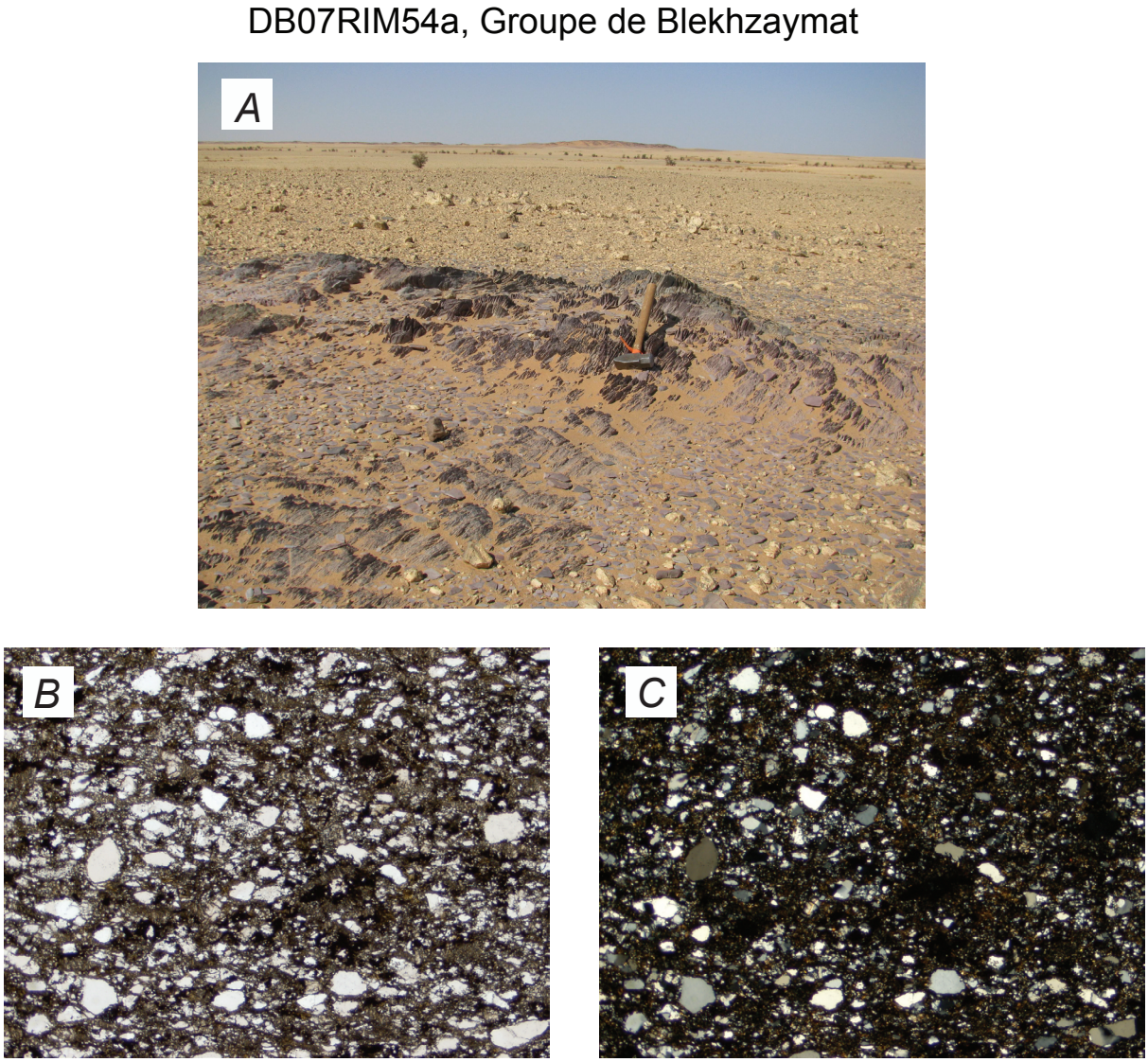


Figure 57. Detrital zircon data and photographs for sample DB07RIM54a from the northern Groupe de Blekhzaymat. (*A*) Outcrop photograph of sandstone from the sample location. (*B* and *C*) Photomicrographs of sandstone under plane light and crossed polars, respectively. (*D, E,* and *F*) Concordia diagrams and age distribution from the first analysis (lab number 952-12). (*G, H,* and *I*) Concordia diagrams and age distribution from the reanalysis (lab number 1284-04).—Continued

Another sample (CT07RIM37-1) from the northern part of the Blekhzaymat outcrop belt (Hassi Djebilet 1:500,000-scale sheet) is a foliated, friable, purplish tuffaceous rock (figs. 58*A* and *B*). We dated this sample using two methods: SIMS (9 zircons; fig. 58*C*) and then LAICPMS (120 zircons; figs. 58*D*, *E*, and *F*). The LAICPMS analyses resolved two populations, a major one at ca. 2,100 Ma and a minor one at 562 Ma. The SHRIMP and LAICPMS results were combined (fig. 58*G*) to determine the weighted mean $^{207}Pb/^{206}Pb$ age of 2,104±13 Ma, which we interpret as the igneous age of the tuff. We suggest that the Neoproterozoic ages record a Pan-African disturbance.

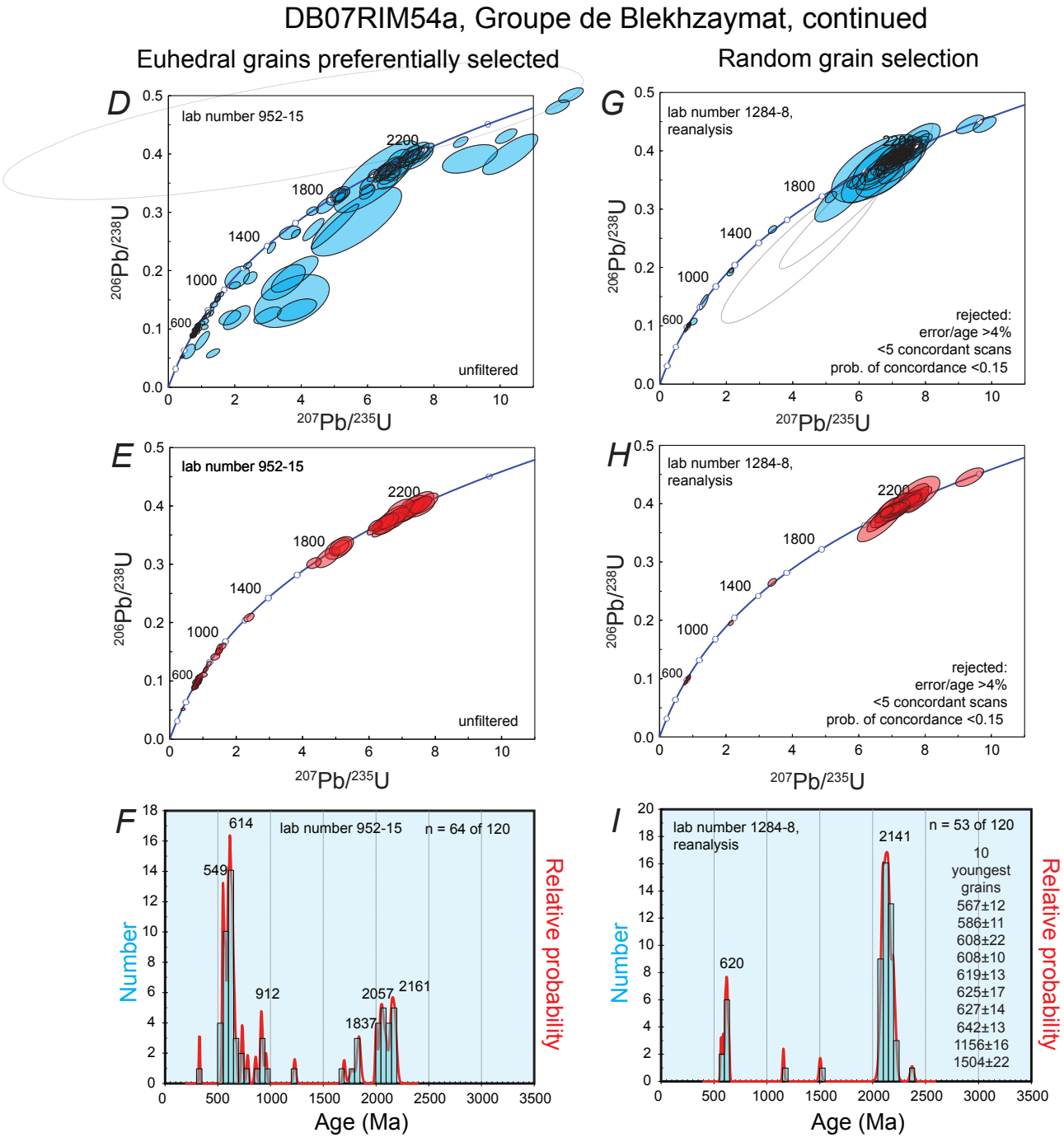


Figure 57. Detrital zircon data and photographs for sample DB07RIM54a from the northern Groupe de Blekhzaymat. (*A*) Outcrop photograph of sandstone from the sample location. (*B* and *C*) Photomicrographs of sandstone under plane light and crossed polars, respectively. (*D, E,* and *F*) Concordia diagrams and age distribution from the first analysis (lab number 952-12). (*G, H,* and *I*) Concordia diagrams and age distribution from the reanalysis (lab number 1284-04).

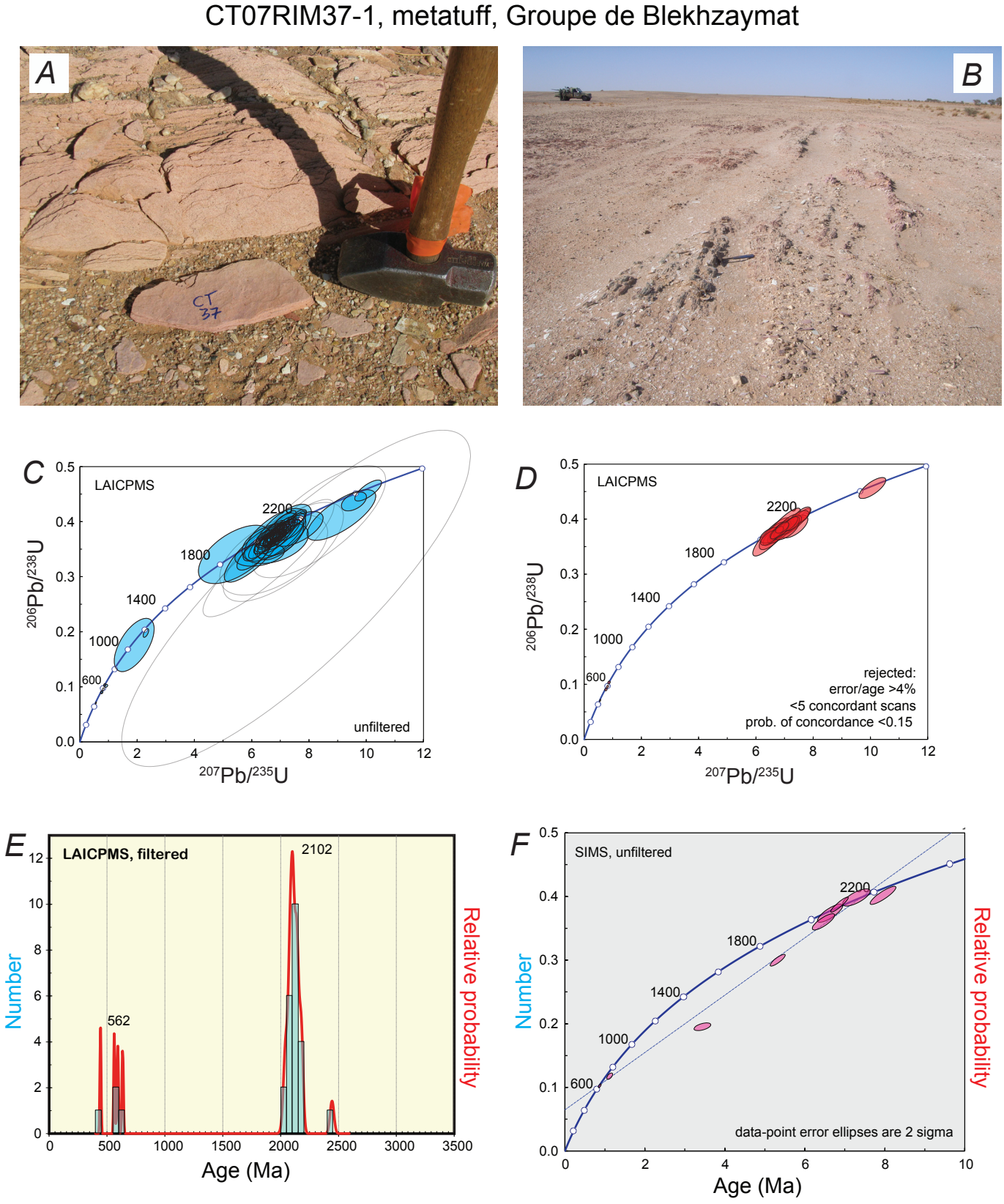


Figure 58. Zircon geochronological data and photographs for sample CT07RIM37-1 from the northern Groupe de Blekhzaymat. (*A* and *B*) Outcrop photographs of metatuff from the sample location. (*C*) Concordia diagram showing SIMS results. (*D, E,* and *F*) LAICPMS results: concordia diagrams for unfiltered and filtered data, and corresponding age distribution. (*G*) Weighted average age based on combined SIMS and LAICPMS data. —Continued

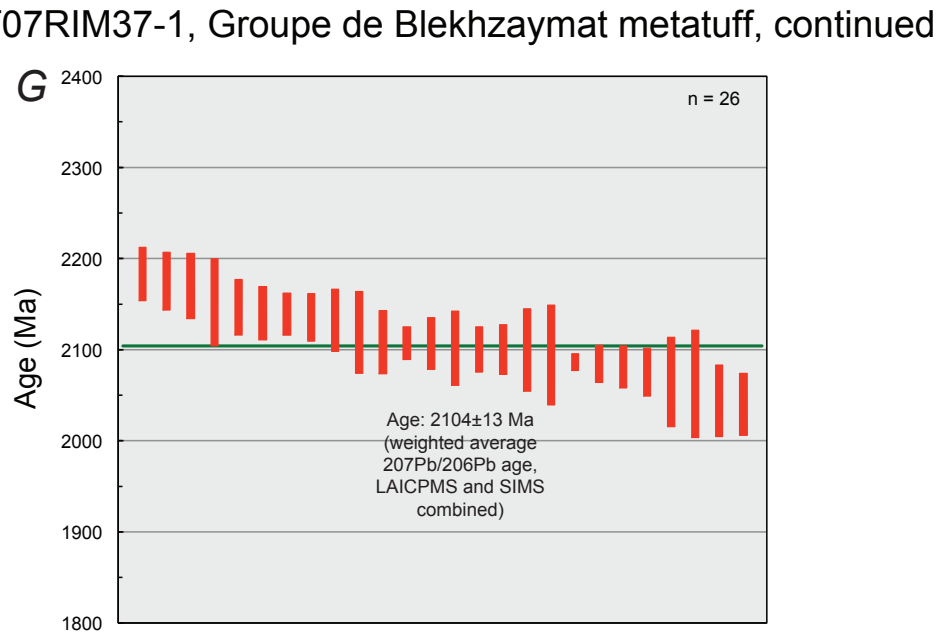


Figure 58. Zircon geochronological data and photographs for sample CT07RIM37-1 from the northern Groupe de Blekhzaymat. (*A* and *B*) Outcrop photographs of metatuff from the sample location. (*C*) Concordia diagram showing SIMS results. (*D, E,* and *F*) LAICPMS results: concordia diagrams for unfiltered and filtered data, and corresponding age distribution. (*G*) Weighted average age based on combined SIMS and LAICPMS data.

6.8. Quartz veins cutting the Groupe de Blekhzaymat

Hydrothermal veins that crosscut the Groupe de Blekhzaymat at two locations in the Hassi Djebilet 1:500,000-scale sheet were dated by the $^{40}Ar/^{39}Ar$ method. Sample GB07RIM40B is from the Bia-600 zinc occurrence[14], Indice 001IND0005 (fig. 59*A*). A white-mica separate yielded an irregular age spectrum corresponding to an integrated age of 2,179±11 Ma (fig. 59*B*). The $^{40}Ar/^{39}Ar$ data are interpreted to record regional cooling below ca. 350°C. The irregular pattern of the $^{40}Ar/^{39}Ar$ age spectrum could be due to multiple generations of mica, extraneous argon, or partial reheating after initial cooling (fig. 59*A*).

Sample GB07RIM42B is from the Bia-610 zinc occurrence, Indice 001IND0008 (fig. 59*C*). A white-mica separate yielded a $^{40}Ar/^{39}Ar$ plateau age of 2,061±7 Ma (fig. 59*D*). This age is interpreted to record cooling of this rock below about 350°C.

6.9. Complexe de Ghallamane

The Complexe de Ghallamane forms a number of separate outcrop belts of metasedimentary rocks surrounded by plutons of the Complexe de Tmeïmichatt Ghallamane. A granite-granodiorite unit of this intrusive suite yielded a U-Pb zircon age of 2,103±13 Ma (Lahondère and others, 2003, p. 96). Sample DB07RIM53a is from a coarse metasandstone (fig. 60*A*) interbedded with cordierite hornfels (Ain Ben Tïli 1:200,000-scale sheet, number 2509); the metamorphism is presumably due to one of the nearby plutons. Two splits of the same sample were run at different times. For the first analysis (lab number 952-14), the main goal was to constrain the maximum depositional age; euhedral zircons were therefore selected in preference to rounded ones on the assumption that the latter were more likely to have been through multiple sedimentary cycles. Out of 120 grains, 57 passed the LAICPMS filters (figs. 60*D* and *E*). The probability curve shows a major peak at 2,118 Ma and a minor peak at 582 Ma (fig. 60*F*). This result was a cause for concern because of the geologically constrained Paleoproterozoic depositional age. We therefore ran a second analysis (lab number 1284-7) on an archived split of sample DB07RIM53a. This time, zircons were selected at random. Of 120 zircons analyzed, 64 are concordant (figs. 60*G* and *H*). The probability curve shows a single peak at 2,142 Ma (fig. 60*I*). The two probability curves are qualitatively similar, although the second run yielded none of the problematically

[14] No zinc mineralization was found, only malachite staining.

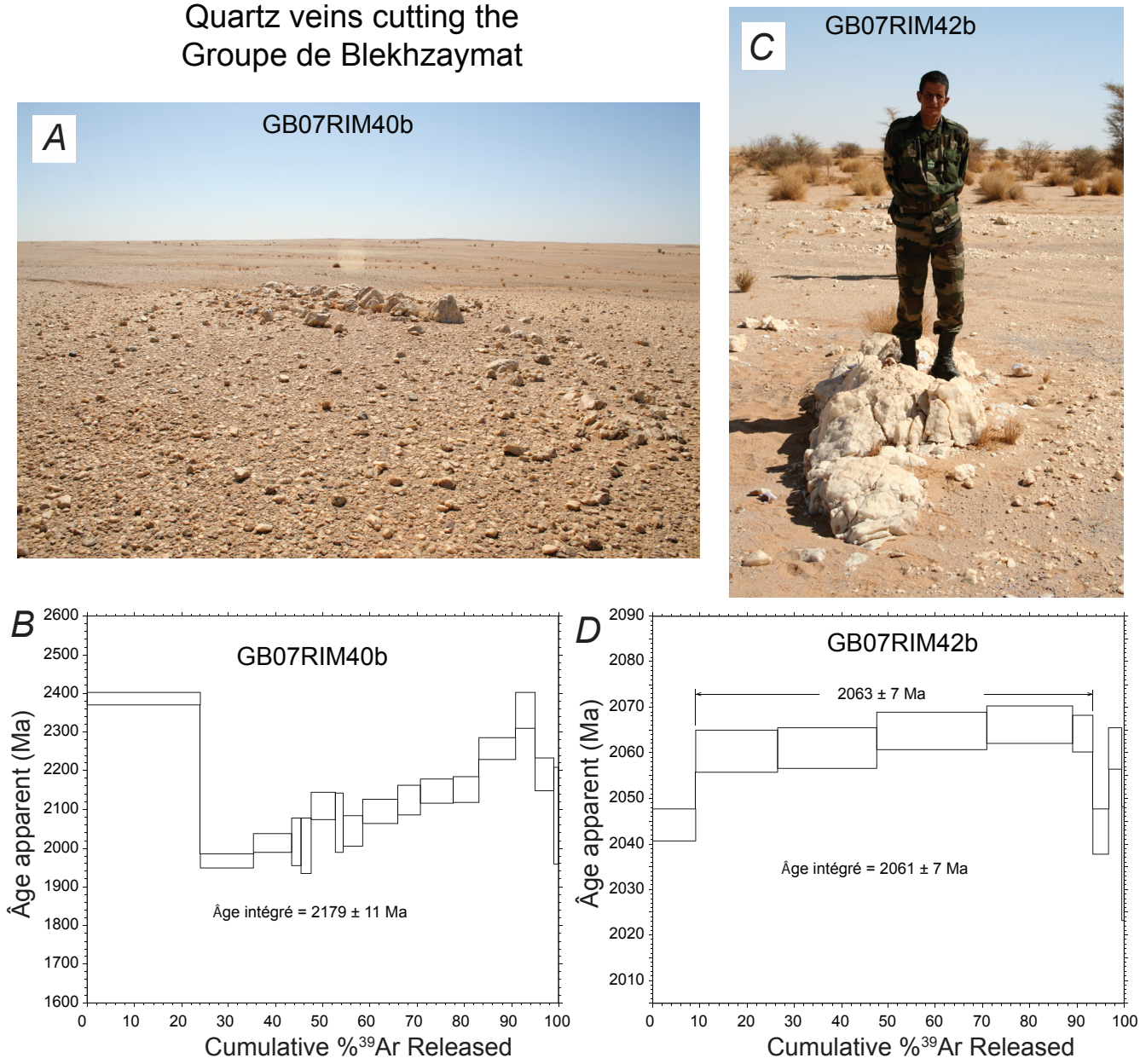


Figure 59. Outcrop photographs (by Georges Beaudoin) and corresponding argon age-release spectra for white mica fractions from quartz veins cutting the Groupe de Blekhzaymat. (A and B) Sample GB07RIM40b. (*C* and *D*) Sample GB07RIM42b.

young, Neoproterozoic zircons. In light of the geologic constraints, we suggest that the Neoproterozoic U-Pb ages record a Pan-African disturbance that reset a few zircons, and that the maximum depositional age is given by the single Paleoproterozoic maximum, which in the combined dataset is 2,135 Ma. In light of the $^{40}Ar/^{39}Ar$ results discussed below, deposition and tectonism must have both taken place during the Paleoproterozoic.

A sample of mica schist (DB07RIM53c) from the same outcrop was analyzed by the $^{40}Ar/^{39}Ar$ method (fig. 60*J*). Data from this sample support initial cooling below ca. 350° C at 2,014±12 Ma followed by partial radiogenic argon loss sometime later, likely after 1,750 Ma. The timing of initial cooling is robust, but determining the timing of the later reheating event is not as well constrained.

DB07RIM53a, Complexe du Ghallamane, Unit GLsc

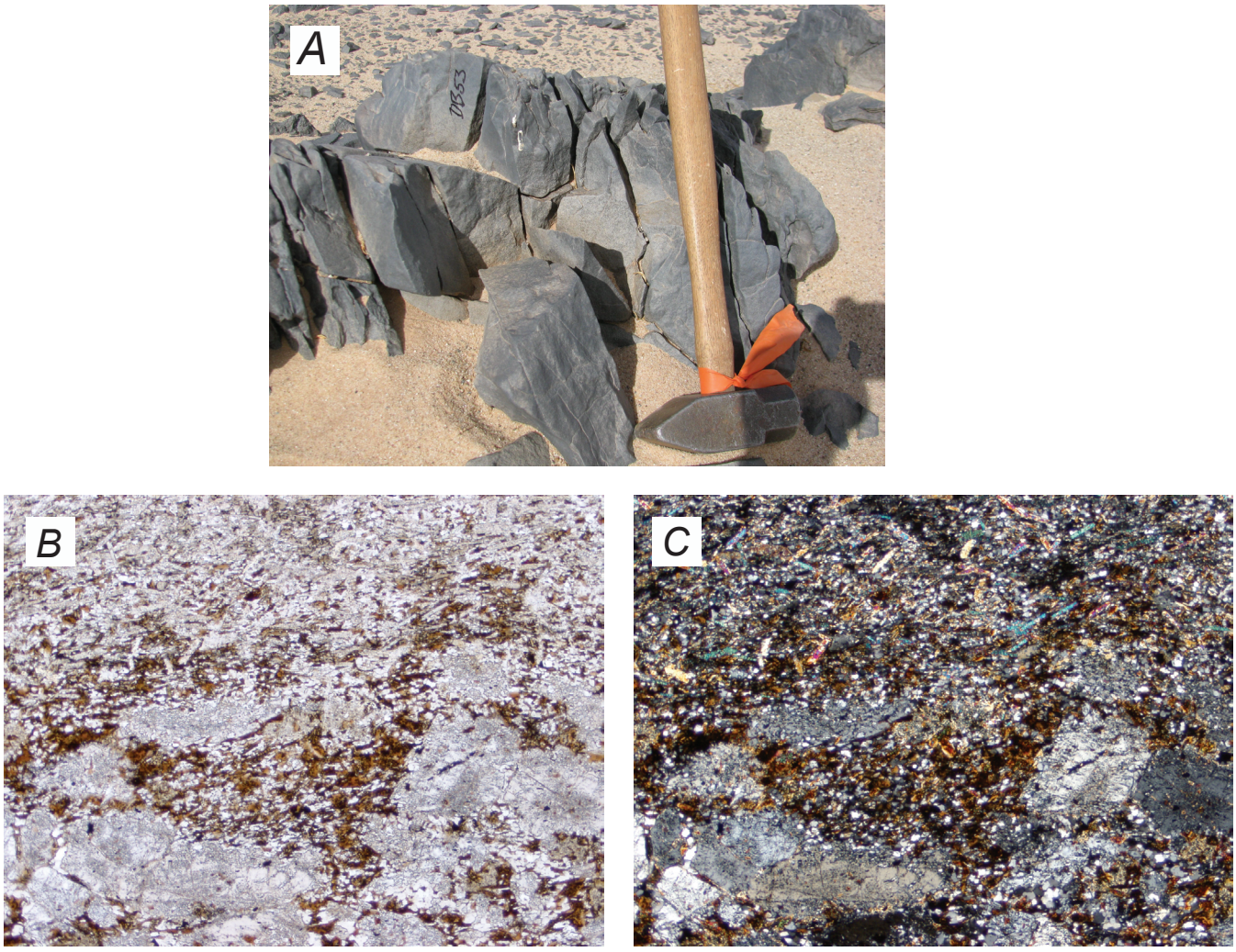
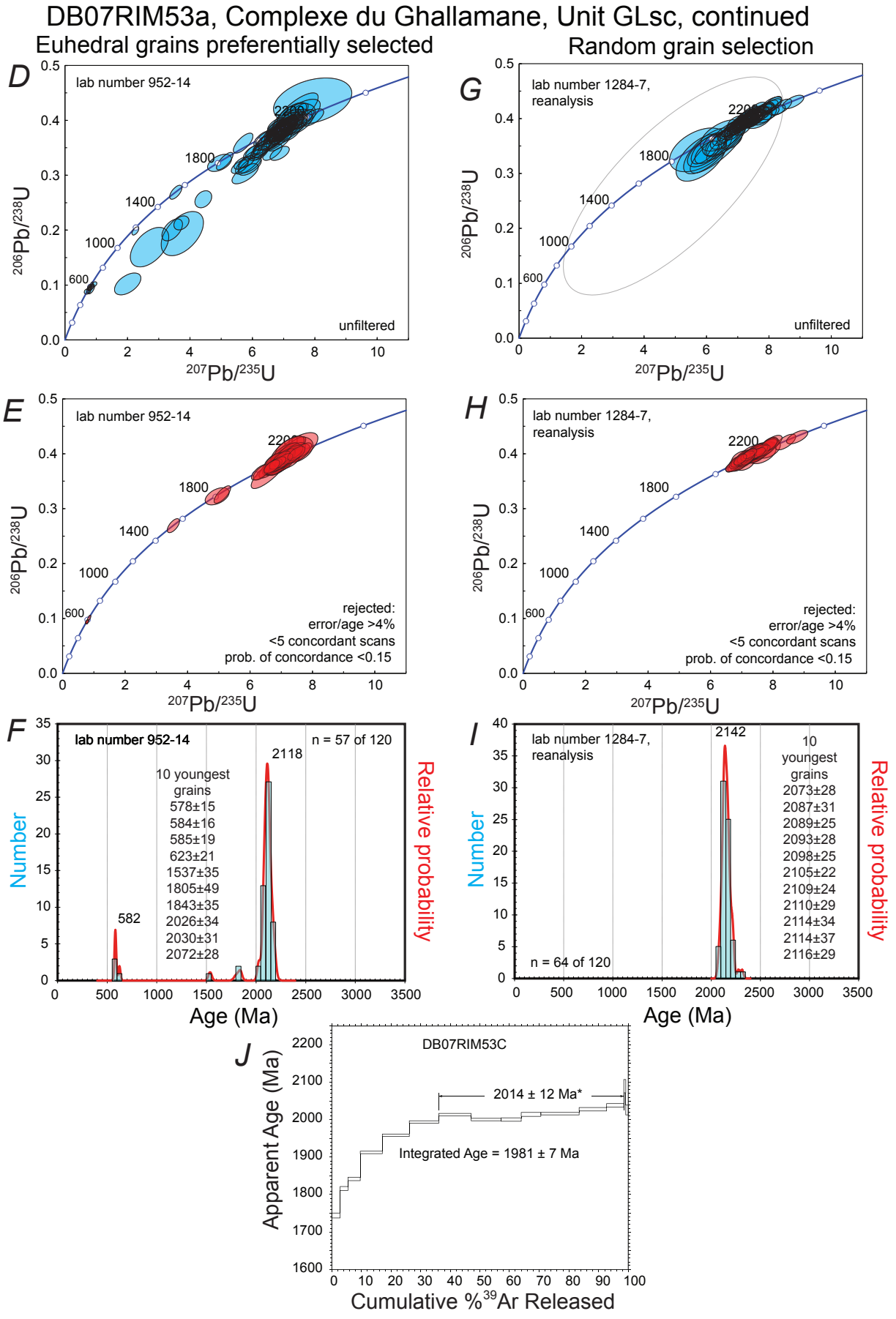


Figure 60. Geochronological data and photographs for sample DB07RIM53a from the Complexe de Ghallamane. (*A*) Outcrop photograph of metasandstone from the horizon sampled for DB07RIM53a. (*B* and *C*) Photomicrographs of DB07RIM53a under plane light and crossed polars, respectively. (*D, E,* and *F*) Concordia diagrams and corresponding age distribution plot from the first analysis of sample DB07RIM53a (lab number 952-14). (*G, H,* and *I*) Concordia diagrams and corresponding age distribution plot from the reanalysis (lab number 1284-7). (*J*) Argon age-release spectrum for metamorphic white mica from sample DB07RIM53c.—Continued on following page


DB07RIM53a, Complexe du Ghallamane, Unit GLsc, continued
Euhedral grains preferentially selected
Random grain selection
D
lab number 952-14
unfiltered
G
lab number 1284-7, reanalysis
unfiltered
E
lab number 952-14
rejected:
error/age >4%
<5 concordant scans
prob. of concordance <0.15
H
lab number 1284-7, reanalysis
rejected:
error/age >4%
<5 concordant scans
prob. of concordance <0.15
206Pb/238U
207Pb/235U
600
1000
1400
1800
2200
F
lab number 952-14
n = 57 of 120
10 youngest grains
578±15
584±16
585±19
623±21
1537±35
1805±49
1843±35
2026±34
2030±31
2072±28
582
2118
I
lab number 1284-7, reanalysis
n = 64 of 120
10 youngest grains
2073±28
2087±31
2089±25
2093±28
2098±25
2105±22
2109±24
2110±29
2114±34
2114±37
2116±29
2142
Number
Relative probability
Age (Ma)
J
DB07RIM53C
2014 ± 12 Ma*
Integrated Age = 1981 ± 7 Ma
Apparent Age (Ma)
Cumulative %39Ar Released

6.10. Complexe de Tsalabia el Khadra

The Complexe de Tsalabia el Khadra is a catch-all, dominantly supracrustal mapping unit that includes metaconglomerate, meta-arkose, epiclastite, tuffaceous schist, quartzite, rhyolite, amphibolite, metapyroxenite, and metagabbro (Lahondère and others, 2003, p. 70). Rocks assigned to the Complexe de Tsalabia el Khadra are intruded locally by the granite du Karêt, dated at 2,141±4 Ma (Lahondère and others, 2003, p. 82).

Sample DB07RIM52a is a grab sample from an unnamed map unit of epiclastite, tuffaceous schist, and quartzite (KHep of Lahondère and others, 2003) (Bel Guerdan 1:200,000-scale sheet, number 2510). The rock is a white, carbonate-cemented quartz arenite (fig. 61*A*). Two splits of the same sample were run at different times. When the original analysis (lab number 952-13) was done, the main goal was to constrain the maximum depositional age; euhedral zircons were therefore dated in preference to rounded ones on the assumption that the latter were more likely to have been through multiple sedimentary cycles. Of 120 zircons analyzed, 62 pass the LAICPMS filters (figs. 61*B* and *C*). The probability curve shows two closely spaced main peaks at 612 and 562 Ma and lesser peaks at 2,036, 1,196, and 1,024 Ma (fig. 61*D*). This result was incompatible with the geologically constrained Paleoproterozoic depositional age. We therefore ran a second analysis (lab number 1284-6) on sample DB07RIM52a. This time, zircons were selected at random. Of 120 zircons analyzed, 66 are concordant (figs. 61*E* and *F*). The probability curve shows two overlapping main peaks at 612 and 581 Ma and lesser peaks at 1,774 and 1,025 Ma (fig. 61*G*). The two probability curves are qualitatively similar, ruling out the possibility that the anomalous results of the first analysis were due to a sample mix-up. Considered together, the two runs of sample DB07RIM52a indicate a maximum depositional age 582 Ma, which is the youngest probability peak based on the combined datasets. This is about 1.5 billion years younger than the supposed depositional age of the Complexe de Tsalabia el Khadra. One viable interpretation is that within the mapped extent of the Complexe de Tsalabia el Khadra is a belt of Neoproterozoic or younger quartzite. In light of the limited, reconnaissance nature of geologic mapping in this remote part of the Rgueïbat Shield, we have adopted this interpretation for the 1:1,000,000-scale geologic map. Another possibility is that the Neoproterozoic U-Pb ages record a Pan-African disturbance that reset most of the zircon population, and that the maximum depositional age is given by the youngest Paleoproterozoic zircons.

DB07RIM52a, Complexe de Tsalabia el Khadra, Unit KHep



Figure 61. Geochronological data and photographs for sample DB07RIM52a from the Complexe de Tsalabia el Khadra. (*A*) Outcrop photograph of quartz arenite from the sample location. (*B, C,* and *D*) show the age distribution and concordia diagrams for the first analysis of sample DB07RIM52a (lab number 952-13). (*E, F,* and *G*) are for the reanalysis (lab number 1284-6).—Continued

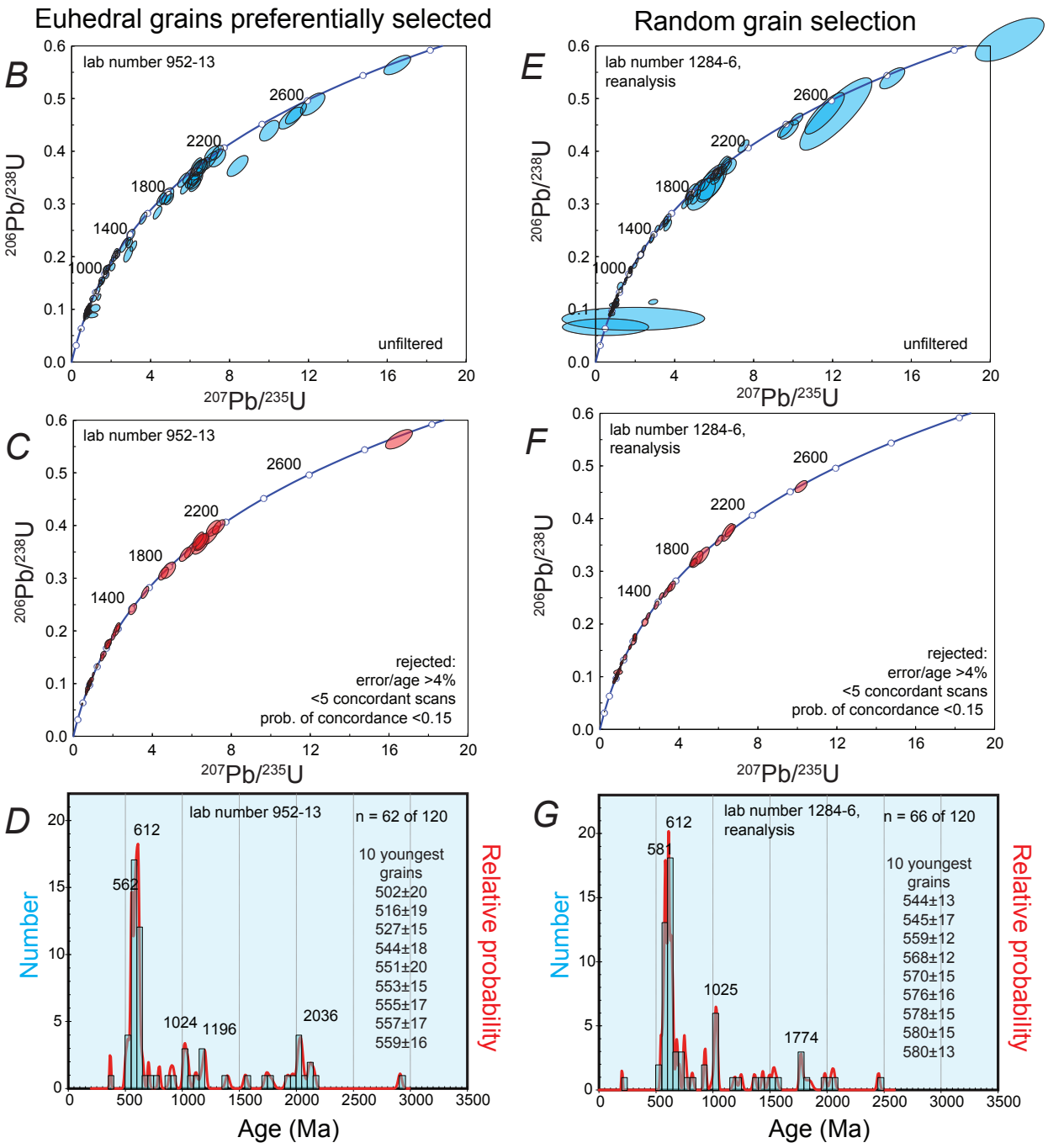


Figure 61. Geochronological data and photographs for sample DB07RIM52a from the Complexe de Tsalabia el Khadra. (*A*) Outcrop photograph of quartz arenite from the sample location. (*B, C,* and *D*) show the age distribution and concordia diagrams for the first analysis of sample DB07RIM52a (lab number 952-13). (*E, F,* and *G*) are for the reanalysis (lab number 1284-6).

6.11. Cortège de Gleibat Tenebdar

The Cortège de Gleibat Tenebdar is a Paleoproterozoic granitic complex in the Rgueïbat Shield. U-Pb ages of 2,073±3 and 2,068±6 Ma, both from biotite-amphibole granodiorites, were reported by Lahondère and others, 2003, p. 165). Sample DB07RIM51a is from Gleibat Tenebdar in the northern part of the 1:200,000-scale sheet of the same name (number 2410). Zircons from this fault-bounded slice of red, alkali-granite (fig. 62*A*) were dated with marginal success using the SIMS method. The zircons suffer from severe lead loss but the analyses are roughly collinear on a concordia diagram. The upper intercept age, which is helped by a single analysis that is nearly concordant, is 2,068±21 Ma (fig. 62*B*), in agreement with other dated phases of this igneous complex.

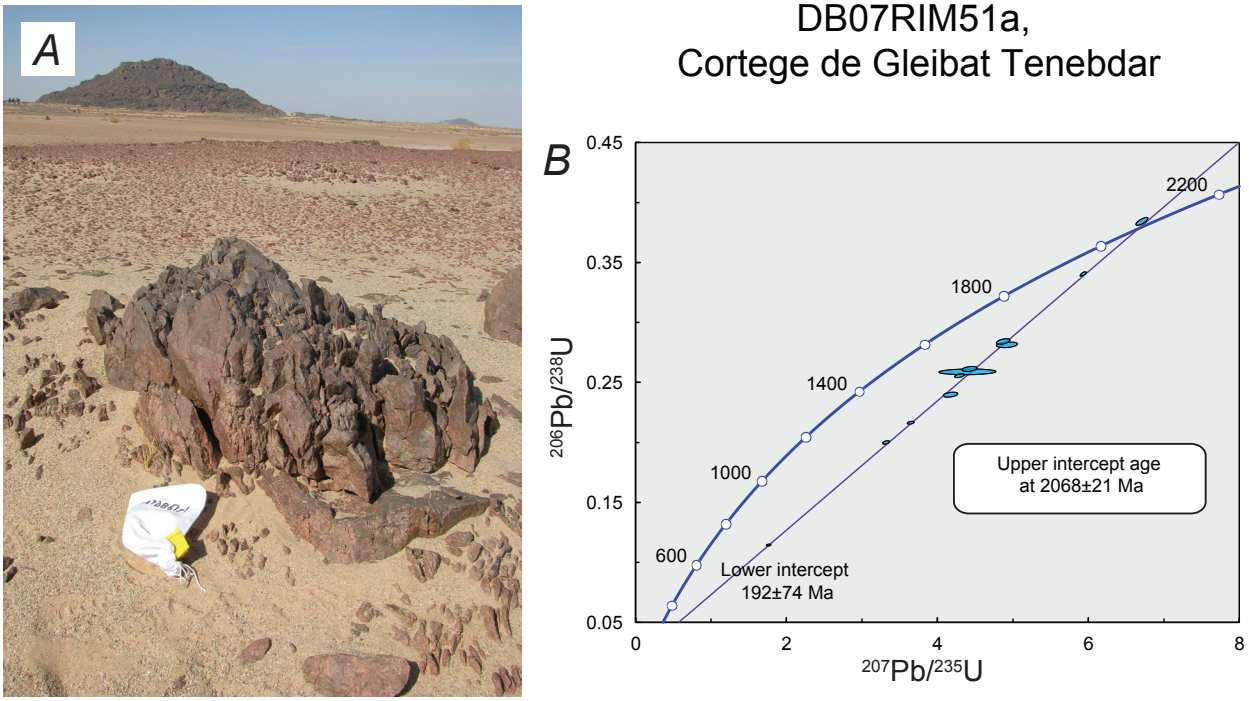
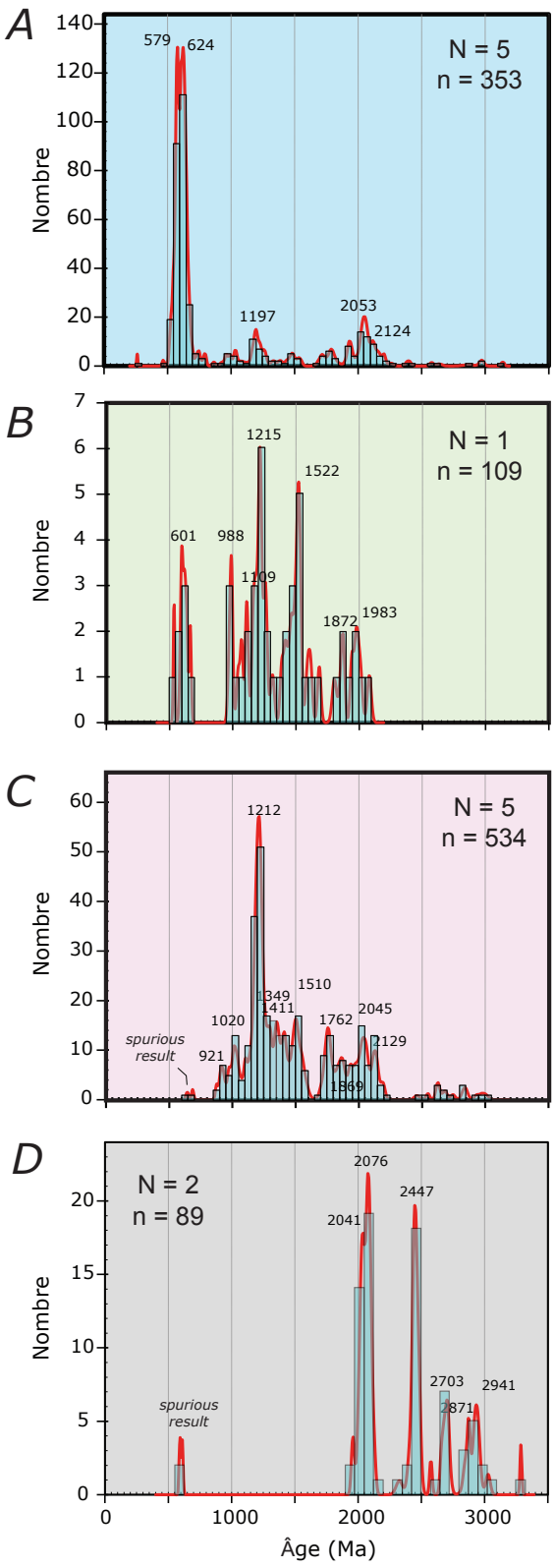


Figure 62. (A) Outcrop photograph of granite from the sample location for sample DB07RIM51a, Cortège de Gleibat Tenebdar. (B) Concordia diagram showing SIMS data.

7. Discussion

7.1. Detrital Zircon Barcodes

Detrital zircon age distributions from the Mesoproterozoic to Ordovician samples show recurring themes, which we here refer to as "barcodes" (composite relative probability plots with histograms). We identify four of these (fig. 63), which we name the Char, Assabet, Téniagouri, and Oujeft detrital zircon barcodes. The barcodes in figure 63 are based only on those samples whose geologic context is well understood, that is, samples from flat-lying or mildly deformed formations of the autochthon or parautochthon. Three of the four barcodes are composites from two or more samples that (1) are from the same portion of the stratigraphic succession, and (2) have similar zircon age distributions. Samples from tectonized rocks in the Mauritanide orogen with detrital zircon populations similar to three of the barcodes are also discussed in this light.



Oujeft barcode (younger Pan-African foreland basin)

Téniagouri barcode (older Pan-African foreland basin)

Assabet barcode (Early Neoproterozoic foreland basin)

Char barcode (West African Craton cover)

Figure 63. Composite age-distribution plots of the four detrital zircon barcodes arranged from young to old down the page. (*A*) The Oujeft barcode, which combines data from samples DB07RIM26a, (continued)DB07RIM28a, DB07RIM61a, DB07RIM75a, CT07RIM60-1. (*B*) The Téniagouri barcode, which is based on sample DB07RIM77a. (*C*) The Assabet barcode, which combines data from samples DB07RIM31a, DB07RIM59a, CT07RIM70-1, CT07RIM71-1, and CT07RIM72-1. (*D*) The Char barcode, which is based on combined data from samples DB07RIM23a (reanalysis) and CT22.

7.2. Char Barcode and the Mesoproterozoic Detrital Zircon Signature of the West African Craton

The Char detrital zircon barcode is a composite made from our two oldest samples from the Taoudeni Basin (fig. 8). The Groupe de Char directly overlies Complexe d'Amsaga basement rocks of the Taoudeni Basin along a profound unconformity. The Groupe d'Atar, in turn, overlies the Groupe de Char, and has a similar zircon age distribution. As described in Sections 3.1, many zircons in the Groupe de Char sample (CT22) showed evidence for significant lead loss, with only 17 ages surviving a fairly lenient filter. As described in Section 3.2, the Groupe d'Atar sample (DB07RIM23a) was analyzed twice and the results of the second run are adopted for the Char barcode. The Char barcode features major peaks at 2,447, 2,076, and 2,041 Ma and minor peaks at 2,941, 2,871, and 2,703 Ma (fig. 63*D*). The barcode is important for four reasons: (1) the strata on which it is based are adequately dated (the Groupe d'Atar is ca. 1,107 Ma as discussed in Section 3.2); (2) these strata rest on West African Craton basement; (3) the age maxima have plausible Rgueïbat Shield sources; and (4) the Char and subsequent Assabet barcodes are completely different and thus record a radical change in provenance.

7.3. The Assabet Barcode and Implications for Rodinia Supercontinent Reconstructions

The Assabet detrital zircon barcode is a composite of five samples having similar zircon age distributions (fig. 63*C*)—all of them flat-lying strata that were deposited on the West African Craton. It is named for the Groupe d'Assabet El Hassiane, which together with the Groupe d'Aioun, Groupe de Khang Naam, and Groupe de Cheikhia comprise a major clastic succession that covered large parts of the craton. The probability plot shows a major peak at 1,212 Ma and minor peaks at 2,129, 2,045, 1,869, 1,762, 1,510, 1,411, 1,349, 1,020, and 921 Ma; a conspicuous minimum is centered around 1,650 Ma. As noted previously, the Groupe d'Assabet El Hassiane was previously assigned a mid-Neoproterozoic age of ca. 695 Ma based on Rb-Sr geochronology of clays (Clauer, 1976; Clauer and others, 1982), a long-abandoned dating technique. The composite barcode includes two "young" grains (685±17 and 643±23 Ma) that are fairly close to the clay age, but these detrital zircon ages do not overlap within error and thus do not constitute a statistically significant population. The youngest detrital zircon age cluster from an individual sample is 878 Ma, from the Formation de Freidi of the Groupe d'Aioun.

Two samples of glaciogenic facies from the Groupe de Jbéliat (DB07RIM29c and CT07RIM73-1) have detrital zircon age distributions that resemble the Assabet barcode. The samples are from flat-lying strata whose position in the Taoudeni Basin succession is well constrained. In the composite age distribution that defined the Assabet barcode (fig. 63*C*), we left out the two Jbéliat samples because they represent a singular sedimentation event related to glacial scouring of the craton.

Four samples from the Mauritanide orogen carry the Assabet barcode. In the central Mauritanides, these are from the Groupe de Djonaba and the Groupe de Gadel. Both of these rock units have been interpreted as parautochthonous (Pitfield and others, 2004), as they crop out on the inboard (east) side of the belt of dismembered ultramafic rocks that mark the suture between rocks belonging to West Africa and rocks belonging to an allochthonous Neoproterozoic arc. In the northern Mauritanides, samples from both the Groupe de Eizzene and the Groupe de Oumachoueima carry the Assabet barcode. The most plausible interpretation is that all the strata in the Mauritanides that carry the Assabet barcode are parautochthonous and belong to the same early Neoproterozoic stratigraphic package as the flat-lying strata, the westernmost part of which was involved in Mauritanide shortening.

Another important occurrence of Neoproterozoic rocks that carry the Assabet barcode is in Ghana on the other side of the West African Craton. Kalsbeek and others (2008) reported detrital zircon data that are remarkably similar to the Assabet. Specifically, their sample GH2, from the Bombouaka Group at the base of the flat-lying Volta Basin succession, has age maxima at about 1,188, 1,964, 2,022, and 2,081 Ma. Kalsbeek and others (2008) alluded to older evidence (original source: Junner, 1940) that the Bombouaka was deposited by north-directed paleocurrents. Another of their samples (Gh12, Togo Unit) is from the Dahomeyide orogen; its detrital zircon population shows age maxima at 1,202, 1,534, and 1,799 Ma. Thus, the Assabet barcode is seen on the West African Craton as well as in the orogens that border it on both the east and west.

The prevailing tectonic interpretation of the Groupe d'Assabet El Hassiane dates from before any of these detrital zircon data were available. According to this interpretation, the Groupe d'Assabet El Hassiane and its correlatives were deposited in a Mauritanide foreland basin related to the Pan-African I orogeny at ca. 650 Ma (Pitfield and others, 2004, Section 7.2.1; and Lahondère and others, 2003, Section 7.2.3). The thickness, distribution, and fluvial facies are consistent with the proposed foreland-basin setting, as is the dramatic provenance shift from the Char to the Assabet barcodes. However, various lines of evidence are not so easily reconciled with deposition in a Mauritanide foreland basin. First, deposition of the Assabet and correlatives at ca. 650 Ma would imply a ca. 200 m.y. gap between the youngest zircon ages and the time of foreland-basin deposition. We are

unaware of another foreland basin in the world where something like this has been reported. Second, paleocurrent patterns in the Assabet El Hassiane and its correlatives are dominantly northward in three widespread locations across the Taoudeni Basin (fig. 64); this pattern is not easily reconciled with derivation from the Mauritanide orogen. Third, no *primary* zircon sources are known in the Mauritanides that could have shed the mainly Mesoproterozoic zircons that dominate the Assabet barcode. The only rocks in the Mauritanides that could have shed Mesoproterozoic zircons are metasedimentary rocks, as discussed previously. These tectonized strata are a plausible source of recycled Mesoproterozoic zircons, but this merely shifts the problem; what then was the source of the detrital Mesoproterozoic zircons in the parautochthonous West African rocks?

An alternative interpretation, proposed here, is that the Groupe de Assabet El Hassiane was deposited at ca. 850–975 Ma in an Early (as opposed to Late) Neoproterozoic foreland basin; we indicate this age assignment in the legend to the 1:1,000,000-scale geologic map (deliverable 51). As noted above, the thickness, distribution, and fluvial facies of strata that carry the Assabet barcode are consistent with a foreland-basin setting; the paleocurrent pattern (fig. 64) suggest that the sediment source was to the south (present direction). Such an orogen would have formed the southern margin of the West African Craton, roughly aligned with, and south of, the present-day coast of Ghana and Cote d'Ivoire.

Regardless of when in the Neoproterozoic the Assabet and equivalents were deposited (ca. 880 or ca. 650 Ma), the presence of a large volume of Mesoproterozoic-age detritus in Neoproterozoic strata in West Africa has important implications for hypothesized reconstructions of the Proterozoic supercontinent, Rodinia. The new detrital zircon results strongly suggest that at some point during the Neoproterozoic (ca. 875 Ma), the West African Craton must have been relatively close to a late Mesoproterozoic to earliest Neoproterozoic ("Grenville-age") orogen. Existing reconstructions of Rodinia do not satisfy this requirement (figs. 65 and 66). Reconstructions by Dalziel (1997), Pisarevsky and others (2003), and Li and others (2008) show West Africa restored to various positions against the Amazonian Craton and surrounded on three sides by the world ocean (fig. 65). In a very different reconstruction by Evans (2009), West Africa's Dahomeyide margin is restored to a position against the Canadian Cordilleran margin of Laurentia (fig. 65). In all of the reconstructions, a place was found for West Africa, but seemingly as an afterthought. One recent Rodinia reconstruction that specifically addresses the position of West Africa is by Johansson (2009) (fig. 66). This reconstruction, which deals with only part of Rodinia, puts the Mauritanide margin of West Africa against the southeastern margin of Baltica. Johansson's (2009) reconstruction shares the same shortcoming as the others: West Africa would have been far from any known 1.3 to 1.0 Ga orogenic belt that could have been a source for Mesoproterozoic detrital zircons. In summary, our new Mauritanian detrital zircon results reveal the need for a new Rodinia reconstruction.

7.4. The Oujeft Barcode and Relationship to Pan-African Orogeny

The Oujeft detrital zircon barcode is a composite of the five Groupe d'Oujeft samples having similar zircon age distributions (fig. 63*A*). Major peaks are at 624 and 579 Ma; lesser peaks are at 2,124, 2,053, and 1,197 Ma. The majority of zircons were directly or indirectly derived from late Neoproterozoic and Cambrian igneous sources (peaks at 624 and 579 Ma). The Paleoproterozoic (peaks at 2,124 and 2,053 Ma) and Mesoproterozoic zircons (peak at 1,197 Ma) are probably recycled detrital zircons from older strata in the Mauritanide orogen, as described in Section 7.2. These flat-lying Cambrian to Ordovician sandstones flank the Mauritanides, and can be interpreted as foreland-basin deposits based on their lithology, position, and age.

Strata carrying the Oujeft theme in the orogen can be interpreted as deposits of a deformed part of the same Pan-African foreland basin. In the central Mauritanides, samples from the Formation d'Oued Kav of the Groupe d'El Fadra displays the Oujeft barcode. Detrital zircon results from the Groupe des Oua-Oua, which were obtained during PRISM Phase 1a by BRGM (Lahondère and others, 2005, p. 473), also belong to Oujeft barcode as defined herein. In the northern Mauritanides, two samples from the Formation de Sainte Barbe and one from the undivided Groupe d'Oumachoueima display the Oujeft barcode.

Detrital zircon samples that have the Oujeft barcode are shown in a generalized time-distance plot that relates the undeformed and deformed rocks (fig. 67). This can be thought of as a *hypothetical* correlation chart, illustrating stratigraphic age assignments that could be inferred *if* the detrital zircon ages in the Mauritanide foreland basin adhere to the pattern seen in many other foreland basins. Three disclaimers must be mentioned. First, stratigraphic ages are very poorly constrained in the orogen—so poorly, in fact, that the new detrital zircon data provide the main age control. Second, as detailed in table 2, the "maximum depositional ages" quoted for each sample are somewhat subjective, especially for the small zircon populations in question. Third, the "maximum depositional age" of a sample need not be anywhere near the real depositional age, although in foreland-basin settings, the two are generally close. Bearing those qualifiers in mind, the most significant features of figure 67 are as follows. (1) Of the strata that carry the Oujeft barcode, the youngest are located in the flat-lying foreland (Groupe d'Oujeft) and the oldest are in the orogen (for example, Groupe d'El Fadra, Formation d'Oued Kav); this is the normal pattern worldwide, which is the simple consequence of the migration of a foreland basin in concert with the plate convergence responsible for its existence (Bradley and Kusky, 1986). (2) Detrital-zircon-based maximum depositional ages of rocks carrying the Oujeft barcode have a nearly continuous range from 574 to 524 Ma—a substantially greater range than the 575–550 Ma quoted for the Pan-African II orogeny by Lécorché and others (1989). Accordingly, we suggest that those strata in the orogen that carry the Oujeft barcode are part of the same depositional succession as the flat-lying rocks. All of these strata were deposited in a cratonward-migrating foreland-basin system that was being overridden or deformed on its western edge while the basin advanced eastward.

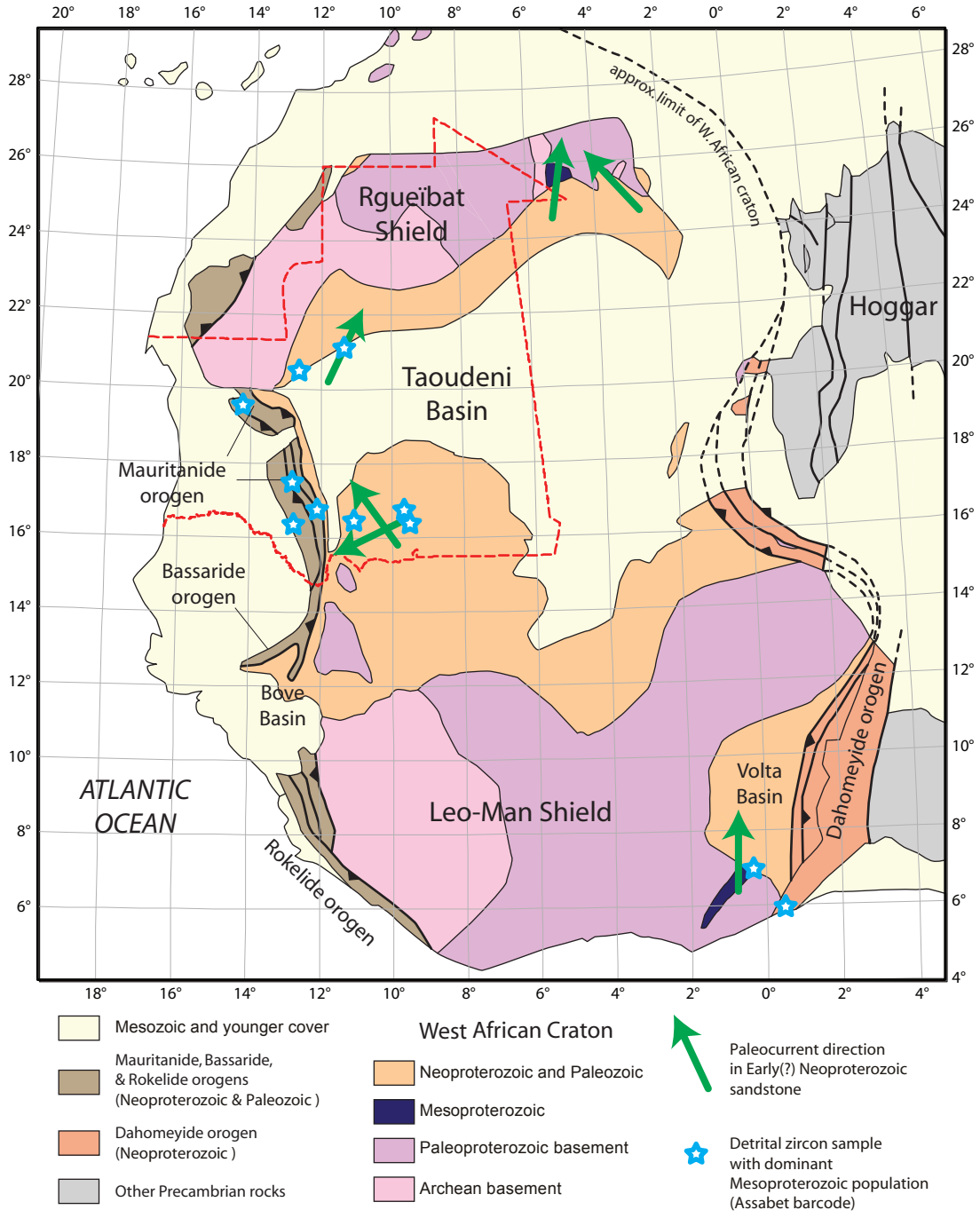


Figure 64. Map of the West African Craton and flanking orogens showing generalized paleocurrent directions (green arrows) and locations of detrital zircon samples that carry the Assabet barcode (blue stars). Paleocurrent directions are from fluvial facies of the Groupe d'Assabet El Hassiane at Guelb El Richat (Moussine-Pouchkine and Bertrand-Sarfati, 1997), the Groupe de Cheikhia in the Hank region (Moussine-Pouchkine and Bertrand-Sarfati, 1997), the Groupe d'Aioun in the extreme south of Mauritania (Lahondère and others, 2005, their figs. 13 and 14), and the Bombouaka Group in Ghana (Junner, 1940). Detrital zircon locations are from the present study except the Volta Basin and Dahomeyide samples, which are from Kalsbeek and others (2008).

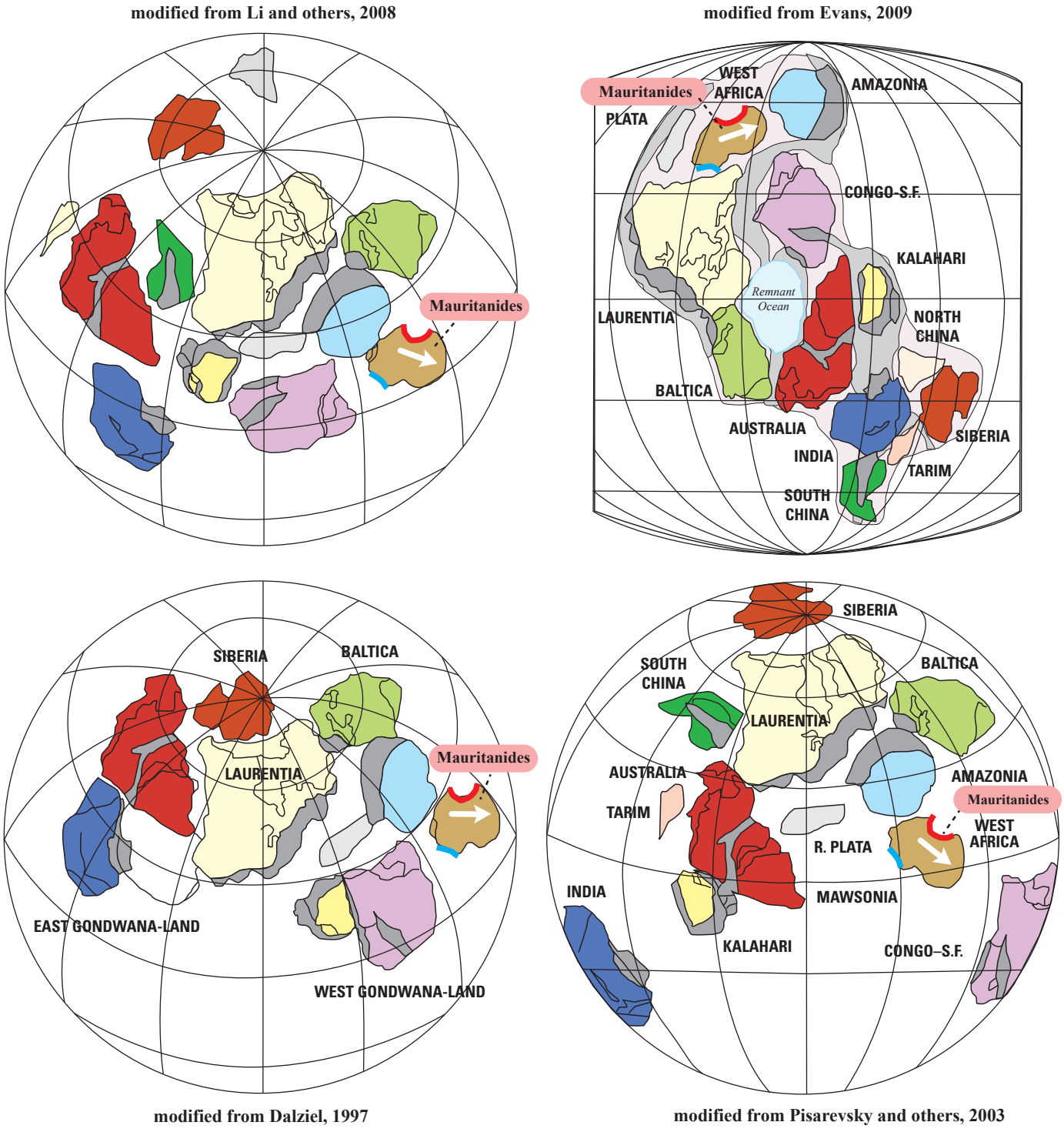


Figure 65. Four alternative reconstructions of the hypothetical supercontinent Rodinia, as modified from Evans (2009) from the original sources indicated. The continents are shown in the same colors on each Neoproterozoic world map. West Africa is colored brown; its Mauritanide margin is highlighted in red and its Dahomeyide margin in blue. The white arrows in each reconstruction are positioned over the Taoudeni Basin and represent the generalized paleocurrent direction for strata carrying the Assabet barcode, in restored coordinates. The gray belts show Mesoproterozoic ("Grenville-age") orogenic belts that broadly correspond to the age of detrital zircons. None of these reconstructions provides an obvious explanation for Mesoproterozoic detritus on the West African craton.

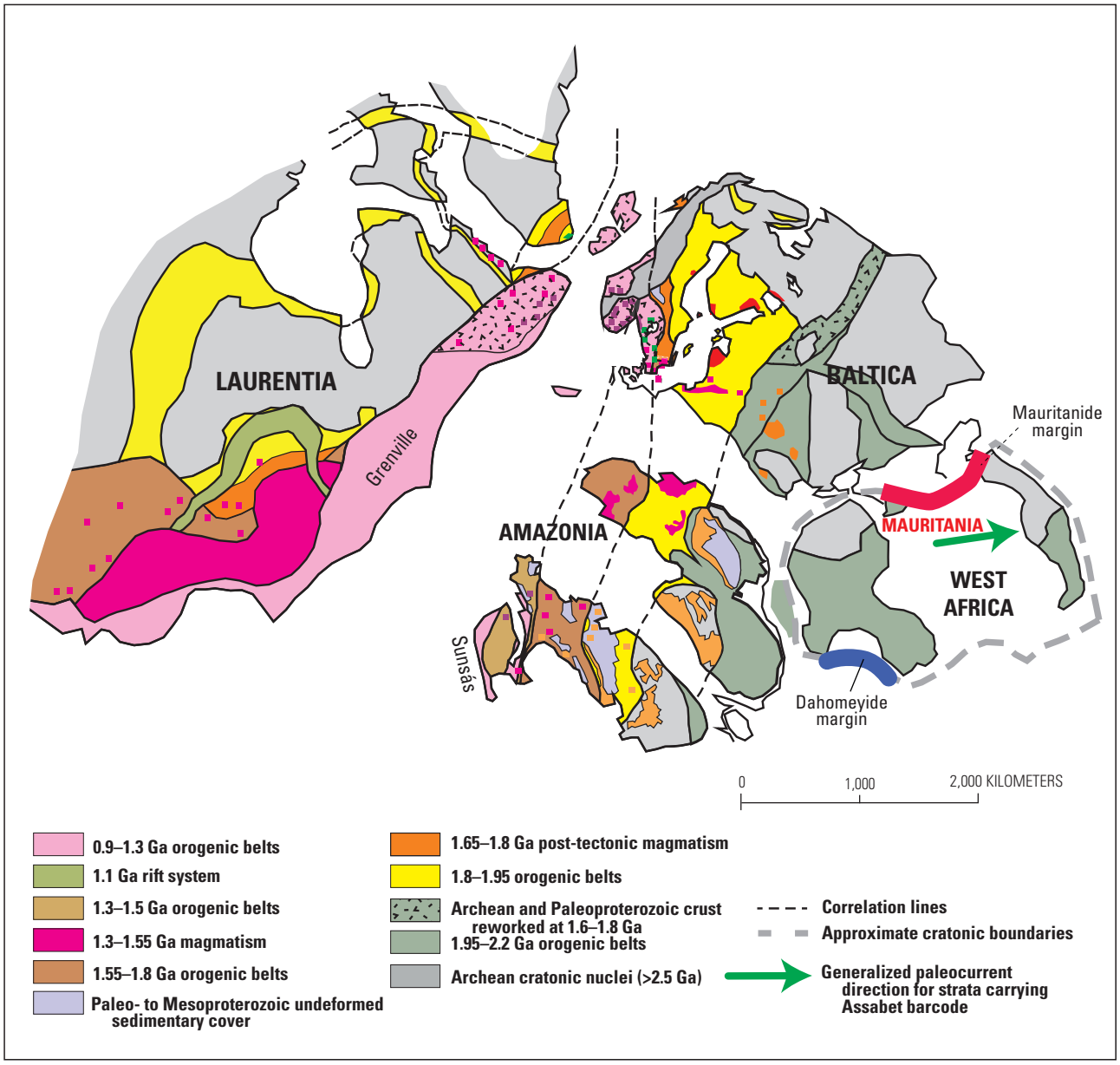


Figure 66. Proposed reconstruction of a portion of the hypothetical supercontinent Rodinia, modified from Johannson (2009). West Africa's Mauritanide margin is highlighted in red and its Dahomeyide margin in blue. The green arrow is positioned over the Taoudeni Basin; it represents the generalized paleocurrent direction, in restored coordinates, for strata carrying the Assabet detrital zircon barcode. Orogenic belts between 1,300 and 900 Ma are shown in pink. West Africa in this reconstruction is far from any potential zircon sources of this age.

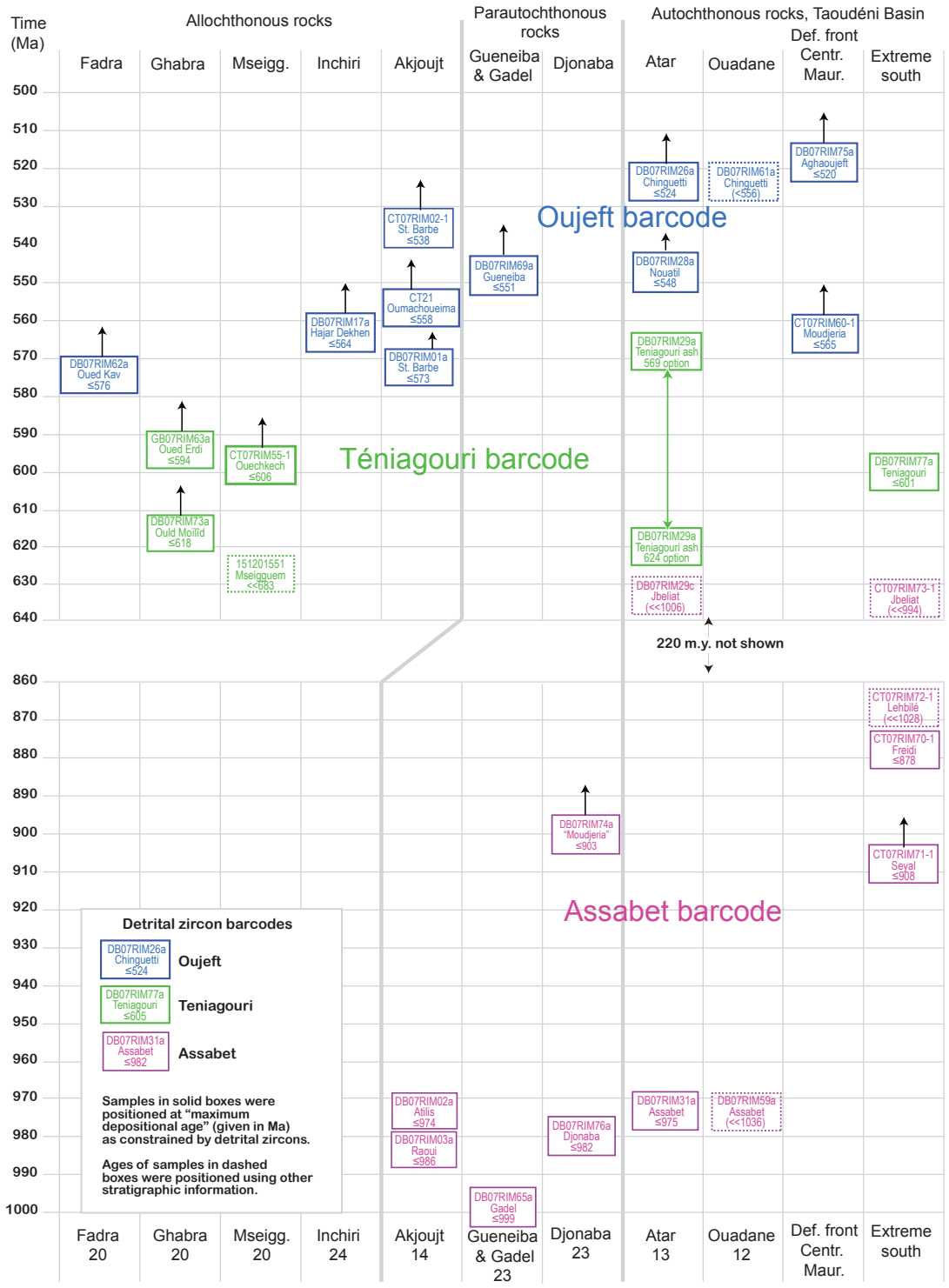


Figure 67. Provisional correlation chart based on detrital zircon results relating unfossiliferous, tectonized strata within the Mauritanide orogen to the essentially flat-lying Taoudeni Basin succession. Boxes correspond to individual samples; colors indicate the detrital zircon barcode assignment. Boxes with black, upward-pointing arrows are positioned at the "maximum depositional age;" actual depositional ages could be younger. Two options are shown for the age of sample DB07RIM29a of the Groupe de Téniagouri, depending on the interpretation of a complex zircon population. Numbers at the bottoms of the vertical columns are keyed to figure 7.

7.5. The Téniagouri barcode and relationship to Pan-African orogeny

The Téniagouri detrital zircon barcode (fig. 63*B*) combines the main elements of the Assabet and Oujeft barcodes. It is based on one detrital zircon sample from the gently dipping Groupe de Téniagouri. The rationale for basing a barcode on this single sample is that several other samples from within the orogen have similar detrital zircon populations, but the Téniagouri sample is the only one in a structurally simple setting, whose stratigraphic context is well constrained. Major population maxima in the Téniagouri barcode are at 1,522 and 1,215 Ma; lesser maxima are at 1,983, 1,872, 1,109, 988, and 601 Ma. The sample is from the Mauritanide foreland. Here, the Groupe de Téniagouri is an upward-prograding sequence from chert and siliceous siltstone at the base to flysch-like, tuffaceous turbidites at the top (Pitfield and others, 2004, Section 4.3.5). The succession of facies is similar to that seen worldwide in better-documented collisional foredeeps (Bradley, 2008).

Within the orogen, strata having the Téniagouri theme can be interpreted as an outboard part of a Pan-African foreland basin that was subsequently deformed. In the central Mauritanides, west of the suture zone, two samples from the Groupe d'El Ghabra and two samples from the Groupe d'El Mseigguem display the Téniagouri barcode (one of these was reported by Lahondère and others, 2005, their figure 78). In the northern Mauritanides, one sample from the Groupe de Eizzene is reminiscent of the Téniagouri barcode.

The Téniagouri barcode is similar to the Assabet barcode but with the addition of abundant ca. 600-Ma zircons. We suggest that it represents detritus from an early incarnation of the Mauritanide orogenic belt. Specifically, we suggest that the detrital zircons between about 2 and 1 Ga were recycled from tectonized strata having the Assabet barcode, and that the ca. 600-Ma zircons were derived from an orogenic source that included igneous rocks of that age. A significant conclusion is that the Téniagouri turbidites are far too young to have been derived syntectonically from the putative ca. 650-Ma orogen that Lécorché and others (1989) called Pan-African I. The maximum depositional ages of rocks having the Téniagouri theme continue the progression of ages so that together, samples carrying the Oujeft and Téniagouri barcodes have maximum depositional ages ranging nearly continuously from 622 to 520 Ma.

7.6. Late Paleozoic orogenesis in the Mauritanides

Perhaps owing to the phenomenon of "last-in, first-out", the youngest, ca. 300 Ma Hercynian event did not leave a vast foreland basin proximal to the Mauritanide orogen. The only late Paleozoic foreland-basin unit so far recognized is the Kandou Formation (Lahondère and others, 2005, p. 357–358), a localized, undeformed conglomerate that lies in thrust contact with tectonites of the Groupe de Gueneiba. The map extent of this unit is quite small and there is no direct age control so the interpreted Hercynian foreland-basin depositional setting is speculative.

Although we were unable to sample the Kandou Formation, we can make one new inference about the Hercynian event in the Mauritanides from the detrital zircon age distribution of the much younger (Jurassic or Cretaceous) Groupe de Néma. The detrital zircon age distribution of the Groupe de Néma sample (fig. 28) is reminiscent of the Oujeft barcode. We infer that the Groupe de Néma detritus was either derived from the Mauritanides directly or was recycled from strata like the Groupe de Oujeft. The Néma detrital zircon age distribution is notable for the lack of detrital zircons younger than Cambrian. This suggests that the Hercynian orogenic episode in Mauritania did not involve magmatism, an interpretation that was already hinted at by the lack of young plutons in the exposed part the Mauritanides. The Groupe de Néma's source region would not have been limited to just the fraction of the orogen that presently pokes through desert sands or Cenozoic coastal-plain deposits—well under one fourth on the African side of the Hercynian–Alleghanian orogen. Lack of late Paleozoic magmatism on the African side contrasts markedly with what is seen on the Appalachian side of the collisional orogen, where plutons date from all periods from Neoproterozoic to Permian (Hibbard and others, 2006).

7.7. Discussion of problematic detrital zircon results

Among the detrital zircon results presented and discussed in Sections 3 to 6, several samples yielded problematic results. Each of these samples has a variation of the same problem: ages near 600 Ma that at face value are too young for the putative depositional age.

We will consider several possible explanations for these unexpected results but first revisit three age determinations from the PRISM-I years. Both the BGS and the BRGM encountered the problem of "too-young" zircons in the Precambrian rocks of Mauritania. (1) In the Guelb Moghrein area, Pitfield and others (2004, Section 3.5.3.4; also Annexe 5, p. 8) recovered four morphologically distinct zircon populations from what was mapped as a leucotonalite that crops out as an inlier within the Groupe d'Eizzene outcrop belt. Nine euhedral zircons yielded a cluster of Mesoarchean $^{207}Pb/^{206}Pb$ ages with a mean of 2,909±18 Ma, consistent with a highly negative **ε**Nd whole rock value. This much information would suggest that the leucotonalite was correctly identified and is a Mesoarchean rock. However, sixteen zircons from the other populations, some of them

rounded, yielded a spread of concordant to nearly concordant results with $^{206}Pb/^{238}U$ ages between 882 and 540 Ma. In Annexe 5 of the Pitfield and others (2004) report, geochronologist M. Horstwood raised the possibility that the rock is a Neoproterozoic or younger (≥550 Ma) (meta)sedimentary rock formed from detritus derived in part from a Mesoarchean granitoid and in part from Neoproterozoic sources. The issue was left unresolved. (2) Lahondère and others (2003, p. 164) reported a similar problem with an andesite sample from the Groupe de Blekhzaymat. Based on analyses of 16 zircons, they reported four concordant ages: 3,049±5, 2,069±10, 1,782±38 Ma, and 594±12. The largest cluster of analyses suggests the geologically reasonable age of 2,069 Ma for the andesite. The other ages represent single zircons. The 3,049 Ma can be interpreted as a detrital or xenocrystic zircon that was incorporated into the andesite when it erupted, but this interpretation cannot also work for the concordant 1,782 and 594 Ma zircons, which are younger than the interpreted eruptive age. One or the other of these younger ages could record a resetting event—but not both, because both are concordant. Lahondère and others (2003) did not offer an interpretation. (3) The mafic to intermediate Ahmeyim Great Dyke cuts Mesoarchean rocks of the Tasiast region. Pitfield and others (2004, Section 5.1.2.6; also Annexe 5, p. 10–11, sample 201401401) reported four concordant U-Pb TIMS ages on single zircon crystals with ages of about 750, 600, and 550 Ma; they quoted an age of about 550 Ma. A latest Neoproterozoic age is problematic, however, because the sample is a foliated gabbro from a cratonic region where the last penetrative deformation took place in the Archean. More recently, Tait and others (2013) reported U-Pb TIMS ages on four badelleyite fractions, which give a tight upper intercept age of 2,733±2 Ma. The badelleyite age is geologically reasonable whereas the young zircon ages are not.

Turning to our problematic results, one scenario is that certain samples and sample numbers were inadvertently switched. This possibility seems remote, considering the careful sample-handling protocols that we have routinely used for decades. Although it cannot be specifically assessed for all samples, a sample mix-up can be absolutely ruled out for samples DB07RIM23a (Groupe d'Atar), DB07RIM52a (Complexe de Tsalabia el Khadra), DB07RIM53a (Complexe de Ghallamane), or DB07RIM54a (Groupe de Blekhzaymat). After the first round of analyses, when these particular samples yielded many "too young" ages, we submitted another split of each one to Apatite to Zircon, Inc., where they were treated as blind samples. The results are sufficiently similar (the differences being attributable to different picking strategies) to rule out a sample mix-up for any of these rocks. In addition, as described above, the BGS and BRGM also encountered "too young" zircons in the Rgueïbat Shield, so the problem is not traceable to a single lab or a single research team.

What if small amounts of contaminating zircon crept in during sample handling? Indeed, it is this concern that has led the global community of detrital zircon geochronologists to minimize the importance of age "populations" defined by a single zircon, as we have done in this study. A careful review revealed no obvious steps in the mineral separation process at Apatite to Zircon, Inc. where cross-contamination could have taken place. At times during field work, our sample bags took on the reddish tint of Sahara sand, but the amount of loose sand that might have entered the crusher along with a particular rock sample would have been miniscule, the proportion of zircon in Saharan sand is likewise tiny, and not all of these zircons would pass concordance filters—making it highly unlikely that contaminating zircons could significantly modify any of the age distribution plots.

Next we consider the possibility that a "Pan-African" overprint were responsible for the ca. 600 Ma ages. A new compilation of the most reliable isotopic ages from Mauritania (fig. 68) shows $^{40}Ar/^{39}Ar$ age maxima at 624 and 595 Ma, which are about the same age as the anomalously young zircons. If a 2,000-Ma zircon suffered partial lead loss at 600 Ma, it would plot off concordia on a cord between 2,000 and 600 Ma, but if the same zircon suffered complete lead loss at ca. 600 Ma, it would plot as a 600 Ma zircon on concordia.

Growth of new zircon, or zircon rims, during a ca. 600-Ma Pan-African event is a variant on this possibility. Unfortunately, the bulk of our analyses were by LAICPMS without CL imaging, so this possibility cannot be evaluated by inspection for most samples. However, our SIMS analyses were done using CL images, largely as an aid in positioning the ion beam. One sample, CT21 (Groupe d'Oumachoueima) yielded an unexpected population of ca. 600 Ma zircons (fig. 42); CL images of these zircons show that the young ages are not from rims (fig. 42*B*). It should be possible to work around the lack of CL images for most samples because Th and U abundances are routinely obtained during SIMS and LAICPMS analyses. This works because metamorphic zircons or overgrowths ("rims") on preexisting zircons commonly have low thorium contents (Rubatto, 2002) and low Th/U ratios (typically <0.07). Our data show, however, that Th/U for the "too young" zircons is in the normal range for igneous zircons, typically on the order of 1 (tables 7 and 8). Another consideration is that although a Pan-African event might explain some anomalous ca. 600 Ma ages, this explanation cannot apply to samples that have more than one population of too-young zircons, such as concordant age clusters at ca. 1,000 and 600 Ma in a supposedly 2,000 Ma rock (for example, fig. 61).

Therefore, for all of the samples in question, we must seriously entertain the possibility that the problematic ages represent real detrital ages. Certain samples may be from rocks that were incorrectly mapped or from map units that were assigned an erroneous age. Given the dearth of detailed modern studies in Mauritania, the reconnaissance level of most geologic mapping, the remoteness and difficult access, the generally low percentage of outcrop, and the complexity of the geologic history, it is likely that mapping misassignments and incorrect age assignments exist.

7.8. Implications for Correlation and Mapping

In this final section we highlight results that suggest modifications to the geology of Mauritania. As described in Sections 7.2 to 7.5, our detrital zircon results from the Taoudeni Basin reveal a sequence of four barcodes from samples having

approximate depositional ages of 1100, 900, 600, and 550 Ma. These themes not only elucidate the history of the Taoudeni Basin, but also improve our understanding of the metasedimentary rocks of the Mauritanide orogen through the possible correlations and maximum depositional ages shown in figure 67. Taken together, the detrital zircon results from the Taoudeni Basin and Mauritanide comprise a coherent and informative dataset.

Some of our samples suggest minor changes to positions of boundaries on the geologic map. Although these changes are too small to show at the 1:1,000,000 scale, we modified geologic contacts in the GIS anyway. The details are described in the write-ups of the individual samples as follows:

- Formation de Freidi, sample CT07RIM70-1 (Section 3.4).
- Sample DB07RIM74a was from rocks mapped as the Formation de Moudjeria in the Groupe de Oujeft, but the detrital zircons suggest that the rocks belong to the Groupe de Djonaba (Section 3.9).
- Groupe de Gadel, sample DB07RIM65a (Section 4.2).
- Groupe de Gueneiba, sample DB07RIM69a (Section 4.3).
- Groupe de Gàoua, samples GB07RIM61A and GB07RIM62C (Section 4.8).
- Groupe de Oumachoueima, Atilis Quartzite member, sample DB07RIM02a (Section 5.3).
- Groupe de Hajar Dekhen–Kleouat, sample DB07RIM17a (Section 5.5).

Other definite or possible revisions to the geology that are more complicated than simply moving a map boundary are as follows:

- Sample DB07RIM29C and DB07RIM80a, both diamictites assigned to the Groupe de Jbéliat, appear unlikely to be the same till sheet. We suspect that the tillite at DB07RIM80a is the product of a younger, Ediacaran glaciation (Section 3.5), but do not have enough information to warrant a change to the 1:1,000,000-scale geologic map (Deliverable 51).
- Sample DB07RIM76a, from the Groupe de Djonaba, reveals that this unit includes deformed strata that correlate with the Groupe d'Assabet El Hassiane (Section 4.1).
- Sample CT07RIM55-1, from the Groupe d'El Mseigguem, reveals that this map unit is an artificial construct that includes strata both predating and postdating ca. 637-Ma plutonism (Section 4.4).
- Samples GB07RIM63a and DB07RIM73a from the Groupe d'El Ghabra reveals that this map unit is another artificial construct that includes strata both predating and postdating ca. 680-Ma plutonism (Section 4.6).
- In the Guelb Moghrein area, our six samples reveal three distinct age groups: Mesoarchean, early Neoproterozoic, and late Neoproterozoic to Cambrian. Sample CT07RIM10-1 of St. Barbe volcanics is Mesoarchean in age. These rocks must be part of a thrust slice of ancient basement that is tectonically interleaved with much younger rocks. In contrast, siliciclastic rocks from the Formation de St. Barbe clearly match the Oujeft barcode and are late Neoproterozoic to possibly even Cambrian in age. Moreover, samples of the Formation de Raoui and the Atilis quartzite member of the Groupe d' Oumachoueima yielded detrital zircon barcodes that closely resemble the Assabet barcode. Thus the Formation de St. Barbe as currently mapped is an artificial construct of three unrelated components (Sections 5.1 to 5.4).
- Previously unmapped Archean anorthosites were found and dated at two locations in the Complexe d'Amsaga: CT07RIM25-1 and CT07RIM22-1 (Section 6.3).
- The Paleoproterozoic supracrustal Complexe de Tsalabia El Khadra is interpreted to include at least one small outcrop area of Neoproterozoic quartzite. On the 1:1,000,000 scale geologic map, we have excised one polygon from the Paleoproterozoic part of the unit and assigned it a Neoproterozoic age (Section 6.10).

8. Geologic and Tectonic Framework of Mauritania

Mauritania is divisible into five main geologic provinces (fig. 7): the Rgueïbat Shield—a Mesoarchean to Paleoproterozoic basement complex; the Taoudeni Basin—a Mesoproterozoic to Cretaceous intracratonic basin; the Mauritanide orogen—a Neoproterozoic to Permian mountain belt; the Tindouf Basin—a Paleozoic to Cretaceous basin; and the Atlantic coastal basin—a Jurassic to Recent passive margin succession. In the following, the chain of plate-tectonic events is reconstructed from the rocks

of these four belts, drawing on information and ideas from elsewhere in the world as the mobility of the plates and the scale of plate tectonics demand. The events are discussed in the order in which they occurred, past to present. They have been reconstructed in reverse order, however, starting with what is seen today and working backward into deep time where the rock record is meager and hard to read. Much of the older history relies on isotopic ages, both new and previously published. These are summarized in tables 2, 3, 4, and 9 and figures 2 through 6.

8.1. Archean Geology and Tectonics

The Archean part of the Rgueïbat Shield in Mauritania has been subdivided in various ways (Key and others, 2008; Schofield and others, 2012) (fig. 7). In the extreme west is the Tasiast-Tijirit terrane of Key and others (2008). It is a classic greenstone, granite, and gray gneiss assemblage. The oldest rocks are migmatitic orthogneisses of the Complexe de Çtel Ogmâne (Pitfield and others, 2004, Section 2.3.3.1). These rocks are undated but probably older than 2,970 Ma, as they are overlain by the greenstone belts. Seven greenstone belts are included within the Tasiast-Tijirit terrane, which from east to west are the Hadeibt Lebtheinîyé, Hudeibt Agheyâne, Chami, Kreidat, Sebkhet Nich, Ahmeyim, and Tijirit Greenstone Belts. These supracrustal belts are all mapped as parts of the same rock unit, the Groupe de Lebzenia; rock types include quartzite, phyllite, banded iron formation, volcaniclastic metasediments, felsic to mafic metavolcanics, and mafic and ultramafic intrusive rocks. A felsite yielded a concordant U-Pb zircon age of 2,968±2 Ma (Pitfield and others, 2004, Section 2.3.5). The mafic metavolcanics have a MORB signature but the intermediate rocks have an arc signature (Pitfield and others, 2004, Section 2.3.6). Pitfield and others (2004, their Fig. 2.10) depicted the greenstone belts as synclinal structures. Pitfield and others (2004, Section 2.3.6) indicated that volcanism immediately preceded collision with the neighboring Choum-Rag El Abiod terrane. Tonalites and granites, now gneissic, were emplaced after collision, at ca. 2,920 Ma. An undated intrusive phase of fertile granites and associated LCT pegmatites came sometime later.

The boundary between the Tasiast-Tijirit and Choum-Rag el Abiod terranes is a transpressional flower structure—the Tacarat-Inemmaudene Shear Zone (Schofield and others, 2006) (fig. 7). Deformation is dated at 2,954±11 based on the U-Pb zircon age of granitic augen gneiss of the Cortège d'Aoutitilt, which was emplaced syntectonically within the shear zone (Pitfield and others, 2004, Section 2.2.5).

The Ahmeyim Great Dyke, now tightly dated at 2,733±2 Ma (Tait and others, 2013) intruded the Tasiast-Tijirit terrane after penetrative deformation. It is interpreted to be a vestige of a Large Igneous Province, or LIP, and will likely serve as a key to Archean continental reconstructions (Tait and others, 2013).

The Mauritanian part of the Tasiast-Tijirit terrane is bounded to the east by the Complexe d'Amsaga, a tract of deeply eroded Archean continental crust that Pitfield and others (2004) assigned to the Choum-Rag el Abiod terrane (fig. 7). The oldest known rock is an orthogneiss that yielded a U-Pb zircon age range between 3,515 and 3,422 Ma (Potrel and others, 1996). A younger, charnockitic orthogneiss yielded a U-Pb zircon age of 2,986±8 Ma (Potrel and others, 1998). Strongly deformed and metamorphosed supracrustal rocks in the Complexe d'Amsaga include amphibolite, banded iron formation, sillimanite-garnet-cordierite-gneiss, quartz-muscovite schist, and metacarbonate rocks (Pitfield and others, 2004, Section 2.2.3.10). Concordant sheets of anorthosite are found throughout the Complexe d'Amsaga; two phases of one body yielded U-Pb zircon ages of 2,743±4 and 2,718±7 Ma, whereas another yielded a poorly resolved age of 2,930±33 Ma (Section 6.3). A crosscutting granite phase of the Cortège de Touijenjert Modreïgue yielded a U-Pb zircon age of 2,726±7 (Potrel and others, 1998).

Adjoining the Complexe d'Amsaga to the north is another belt of deeply eroded continental crust, the Complexe de Tiris (fig. 7). O'Connor and others (2005) included the Complexe de Tiris in the Choum-Rag el Abiod terrane, whereas Schofield and others (2012) were noncommittal on its terrane affinity. One of its main components, the Formation d'El Gheicha, is a paragneiss of mostly aluminous protoliths with minor mafic and Fe-rich marker units, metamorphosed to granulite facies conditions (O'Connor and others, 2005, Section 2.6.4). Another of its main components, the Formation de Mirikli, consists quartzofeldspathic gneisses and minor mafic, calc-silicate, and Fe-rich marker units, which have been migmatized and intruded by anatectic granites (O'Connor and others, 2005, Section 2.6.4). Schofield and others (2012) reported a U-Pb zircon age between 2,948±11 and 2,875±18 Ma from a Formation de Mirikli granitoid. A foliated, anatectic granite yielded a zircon (crystallization) age of 2,654±8 Ma and a monazite (metamorphic) age of 2,482±7 Ma (Schofield and others, 2012)[15]. Younger granites of the Cortège de F,derik have yielded U-Pb zircon ages of 2,520±29 Ma and 2,472±6 Ma (O'Connor and others, 2005, Section 2.7.6).

To the east of the Complexe de Tiris is an extensive plutonic complex, the Cortège de Zednes (fig. 7). Tonalite yielded a U-Pb zircon age of 3,044±5 Ma; foliated charnockite yielded a zircon age of 2,856±6 Ma; and a mylonitized monzodiorite yielded a U-Pb zircon age of 2,832 ± 4 Ma (Lahondère and others, 2003, Section 2.2.4)[16].

[15] Note that O'Connor and others (2005, Section 2.6.9) reported slightly different ages from this sample (22120276).

[16] These three ages are concordant SIMS results; microprobe monazite ages also reported by Lahondère and others (2003) are in the same Mesoarchean range

The extreme north and east of the Archean craton is underlain by the Complexe de Temmimichate Tsabya (fig. 7), another granulite-facies tract containing Mesoarchean rocks. Rocks include metadunite, metagabbro, amphibolite, anorthosite, and granitic orthogneiss (Lahondère and others, 2003, Section 7.1.1.1). U-Pb zircon ages from intrusive rocks of the Cortège de Zednes (see above) constrain the Mesoproterozoic age.

The Archean core of the West African craton in Mauritania thus had a long and complex history of polyphase orogenesis and magmatism, with the first recognized pulse at either 3,515 or 3,422 Ma and the youngest around 2,472 Ma. Collision at ca. 2,954 Ma between the Tasiast-Tijirit and Choum-Rag el Abiod terranes marks an important orogenic pulse.

8.2. Paleoproterozoic Geology and Tectonics

The eastern half of the Rgueïbat Shield consists almost entirely of Paleoproterozoic rocks (fig. 7) between 2,200 and 2,000 Ma in age. Extrapolating names from the Man-Leo Shield, orogenic events during this interval have been variously referred to as Eburnean (Schofield and others, 2006; Peucat and others, 2005) or Birimian (Lahondère and others, 2003). In Mauritania, the Paleoproterozoic part of the Rgueïbat Shield consists of a continental-margin orogen (Groupe de Rich Anajim) that lies between the Archean cratonic core and a vast magmatic-arc province that stretches eastward some 500 km to the Algerian border. A second Paleoproterozoic arc complex (the Eglab) has been identified in Algeria (Peucat and others, 2005).

The Archean basement rocks are flanked to the north and northeast by strongly tectonized supracrustal rocks of the Groupe de Rich Anajim (fig. 7), which include metamorphosed quartzites, limestones, pelites, and BIF. Schofield and others (2006) interpreted these rocks as a continental margin succession, deposited at what was then the edge of the craton. This continental margin can be inferred to have been a passive margin as opposed to a convergent one because of the nature of the protolith assemblage (Schofield and others, 2006) and because of a notable lack of Paleoproterozoic magmatism in the Archean domain. The postulated passive-margin setting also provides a good explanation for the existence, location, and structure of problematic, low-grade supracrustal rocks at Kediat Idjil and El Mhaoudât in the Zouerate iron district. Schofield and Gillespie (2007) suggested that these successions, which include the Superior-type iron ores that are so critical to Mauritania's economy, are klippe with stratigraphic ties to the Groupe de Rich Anajim. The orogeny that deformed these supracrustal rocks is inferred to have been an arc-passive margin collision, adding to the list of more than 80 such orogenies that have been documented in the global rock record (Bradley, 2008). The age range of passive margin deposition is conjectural but likely began after the development at ca. 2,482 Ma of metamorphic monazite in the Neoarchean anatectic granite in the Complexe de Tiris that was mentioned above. The collisional demise of the passive margin must predate intrusion at 2064±12 Ma of a pluton in the Sfariat belt; this pluton was synchronous with late-collisional sinistral transpression (Schofield and others, 2006), indicating that initial collision happened some time earlier.

The Paleoproterozoic arc complex that is inferred to have collided with the Archean craton consists mostly of plutons belonging to ten intrusive suites, interrupted by belts of deformed supracrustal rocks that have a northwesterly structural grain (fig. 7). Lahondère and others (2003) assigned the Paleoproterozoic rocks to the (informally defined) eobirimien, mésobirimien, tardibirimien, néobirimien, and post-néobirimien tectono-magmatic phases[17].

Eobirimien rocks in the Rgueïbat Shield are largely supracrustal (fig. 7) and are older than 2150 Ma. From west to east the supracrustal belts include (1) the Complexe d'Aguelt abd el Maï—a mixed supracrustal and intrusive assemblage that includes metamorphosed mafic rocks, quartzite, and marble (Lahondère and others, 2003, Section 2.3.1.1.1); (2) the Complexe de Tsalabia El Khadra—mafic, intermediate, and felsic metavolcanic rocks, marble, quartzite, and meta-arkose (Lahondère and others, 2003, Section 2.3.1.1.3); (3) the Complexe du Ghallamane—aluminous and calcareous schist and gneiss, quartzite, meta-arkose, and amphibolite (Lahondère and others, 2003, Section 2.3.1.1.2). New detrital zircon data indicate a depositional age of 2,135 Ma or younger for a metasandstone in the Complexe du Ghallamane (Bradley and others, 2015b); at least part of this belt thus appears to be mésobirimien.

The mésobirimien extended from ca. 2,150 to 2,078 Ma (Lahondère and others, 2003, Section 7.1.1.2). An extensive calc-alkaline suite of mainly diorite, tonalite, and granodiorite was emplaced in the central part of the Paleoproterozoic domain (fig. 7). These rocks comprise the Complexe de Tin Bessais; they have yielded U-Pb zircon ages of 2,146±5, 2,141±4, and 2,122±5 Ma (Lahondère and others, 2003, Section 2.3.2.4.1). Later in the mésobirimien, a vast intrusive complex of evolved, peraluminous granites was emplaced farther west (fig. 7). These rocks comprise the Complexe de Tmeïmichatt Ghallamane; they have yielded U-Pb zircon ages from 2,118±14, 2,103±13, and 2,078±5 Ma (Lahondère and others, 2003, Section 2.3.2.1.2).

Supracrustal and intrusive rocks in the narrow age range 2,073 to 2,067 Ma are assigned to the tardibirimien (fig. 7). The Groupe de Legleya, in the west, consists of felsic volcanic rocks, tuff, granophyre (2,072±6 Ma, U-Pb zircon), microgranite,

---

but are less reliable.

[17] These are names for orogenic phases that have an implicit time significance even, as in the present case, when they are applied to orogenic events far from the type area. English equivalents would be early Birimian, middle Birimian, late Birimian, very late Birimian, and post-Birimian, respectively.

microgabbro, and basalt (Lahondère and others, 2003, Section 2.3.3.4). The Groupe d'Imourène, in the central part of the Paleoproterozoic domain, includes intermediate and felsic volcanics (2,067±9 Ma, U-Pb zircon; Lahondère and others, 2003, Section 2.3.3.4) and shallow intrusives plus sandstone and conglomerate. The most easterly Paleoproterozoic supracrustal belt in Mauritania is the Groupe de Blekhzaymat, which consists mostly of sandstone and conglomerate, plus lesser felsic to intermediate volcanic rocks. Age control is provided by U-Pb zircon ages of 2,069±10 Ma from andesite (Lahondère and others, 2003, Section 2.3.3.4.2) and 2,104±13 Ma from a rhyolitic tuff (Bradley and others, 2015a). Detrital zircons indicate minimum depositional ages of 2,141 and 2,094 Ma for two Groupe de Blekhzaymat samples (Bradley and others, 2014a). The Cortège de Gleïbat Tenebdar records coeval granodiorite plutonism in the west, with U-Pb zircon ages of 2,068±6 Ma, 2,073±3 and 2,059±4 Ma. (Lahondère and others, 2003, Section 2.3.3.4).

The **néobirimien** is represented by three late granitic complexes that together span most of the Paleoproterozoic outcrop belt (fig. 7). In the eastern third of the Paleoproterozoic domain is the extensive Cortège du Yetti; across the western two-thirds is the even more extensive Complexe d'Adam Esseder; and in the extreme west, along the boundary between Paleoproterozoic and Archean domains, is the Cortège des Sfariat. Age control on the néobirimien granitoids is based on microprobe monazite ages and thus is only approximate, in the range 2,040 to 1,995 Ma (Lahondère and others, 2003, Section 2.3.4.2).

The **post-néobirimien** rocks belong to two alkaline to peralkaline intrusive suites: the Cortège Alkalin de Tigsmat El Akhdar in the west and the Cortège de Bir Moghreïn in the east (fig. 7). These are undated.

The Paleoproterozoic part of the Rgueïbat Shield continued eastward into Algeria. In the Eglab massif, Peucat and others (2005) described a mature magmatic arc with relics of ca. 2.7-Ga basement and arc activity from ca. 2,210 to 2,180 Ma. They regarded this as a separate arc from the Paleoproterozoic magmatic arc complex of Mauritania, and invoked a collision between the two arcs at ca. 2,070 Ma.

Late, cross-cutting mafic dikes are a conspicuous feature of the Rgueïbat Shield. They are generally regarded as late Paleoproterozoic to Mesoproterozoic in age but, as critiqued by O'Connor and others (2005, Section 2.9.5), the age control is based on obsolete methods. Dosso and others (1979) reported an Rb-Sr "isochron" age of 1,609±45 Ma, but this was obtained from ten widely scattered dolerite dike samples from Rgueïbat Shield, of varying orientations, and the resulting "age" is of questionable significance. Modern geochronological studies on these dikes are needed for Proterozoic global plate reconstructions; cratonic-scale dike swarms are regarded as vestiges of Large Igneous Provinces, or LIPS (Ernst and Buchan, 2001), and the ages and paleolatitudes of these dikes swarms can be used to piece together past continental configurations.

8.3. Mesoproterozoic to Paleozoic Tectonic Record in the Taoudeni Basin

The Taoudeni Basin is a vast depocenter covering much of the West African Craton. Its Mesoproterozoic to Cretaceous sedimentary fill (fig. 8) is essentially undeformed except along the orogenic front of the Mauritanides, and where locally faulted along its northern margin. Our new detrital zircon data have so far revealed succession of four detrital zircon themes (fig. 63), reflecting changing tectonics and provenance. The following discussion focuses on the classic section in the Adrar region.

The oldest stratigraphic unit is the Groupe de Char, which consists of sandstone and conglomerate derived from the Rgueïbat Shield. Deposition was controlled at least in part by normal faulting, suggesting an extensional setting (Pitfield and others, 2004, Section 7.2.1). The Groupe de Char was long assigned to the Neoproterozoic but is now squarely in the Mesoproterozoic based on the age cited below from the overlying Atar Group; this makes the Groupe de Char too old to be in any way related to the breakup of Rodinia, which had not yet even come together (cf. Pitfield and others, 2004, Section 7.2.1). The Atar Group, which has yielded a weighted average Re-Os age of 1,106±10 Ma (Rooney and others, 2010), is mainly stromatolitic limestone and dolostone. Pitfield and others (2004, Section 7.2.1) noted that there are no obvious controls of sedimentation during Atar deposition. Detrital zircons from the Groupes de Char and d'Atar together defined the Atar barcode (fig. 63D) with major peaks at 2,447, 2,076, and 2,041 Ma. All zircons in these rocks can be traced to West African craton sources (Bradley and others, 2015a).

Next in the succession is a thick package of sandstone: the Groupe d'Assabet El Hassiane. The most important finding from our detrital zircon studies is that these sandstones have yielded mainly Mesoproterozoic detrital zircons that must have been derived from a "Grenville-age" orogenic belt (Bradley and others, 2015a). Specifically, the Assabet barcode features a broad maximum spanning ca. 2,150 to ca. 875 Ma, with a prominent peak at 1,012 Ma and an equally prominent gap at ca. 1,700-1,600 Ma (fig. 63C). Two alternative interpretations are offered here. Model 1: One possibility is that the detrital zircons came from a source in the Mauritanide orogen. This scenario is broadly consistent with earlier interpretations (for example, Lahondère and others, 2003, Section 7.2.3) that the Groupe d'Assabet El Hassiane and its correlatives were deposited in a Pan-African foreland basin. Moreover, two unexpectedly old belts of rocks have recently been documented. An exotic terrane in the Souttoufide segment of the orogen in Western Sahara (fig. 64) has yielded isotopic ages of ca. 1,200–950 Ma (Villeneuve and others, 2006, 2010). An exotic metasedimentary and metaigneous basement complex has also been found in the Central Mauritanides where $^{40}Ar/^{39}Ar$ ages as old as 847±7 Ma have been obtained (Caby and Kienast, 2009). Model 2 takes into account the generally northerly paleocurrent directions seen in the Groupe d'Assabet El Hassiane and its correlatives (fig. 64). This pattern could be

explained if these strata were deposited in a continental-scale foreland basin shed from a ca. 900-Ma orogen to the south, along or near the present (unexposed) southern margin of the West African Craton. More data are needed to evaluate these models.

The Groupe d'Assabet El Hassiane is overlain along a gentle angular unconformity by Mauritania's best known rocks, the glaciogenic Groupe de Jbéliat. The unconformity attests to an episode of broad warping after deposition of the Groupe d'Assabet El Hassiane. Pitfield and others (2004, Section 7.2.1) suggested that both the deformation and the Assabet El Hassiane clastics record Pan-African I orogenesis, but for this to be the case, deformation would have to have preceded foreland-basin deposition—the opposite of the normal and readily explained order. Direct age constraints on the Jbéliat are poor, but it has been correlated with the global Marinoan glaciation (Shields and others, 2007), the younger of two Neoproterozoic Snowball Earth episodes, at 635 Ma (Macdonald and others, 2010). Our new U-Pb zircon date of 622±1 Ma from the overlying Groupe de Téniagouri (Bradley and others, 2013) provides a bracketing age. According to Deynoux (1985), the Jbéliat ice sheet flowed north to south (present directions) from the area of the Rgueïbat Shield. Our new detrital zircon results from the Jbéliat tillite along the Adrar Escarpment show that it was largely derived from material recycled from the next-older rock unit, the Groupe d'Assabet El Hassiane (Bradley and others, 2013).

In the cratonic succession, the unequivocal record of Mauritanide tectonism begins only above the Jbéliat glacial deposits. The Groupe de Téniagouri includes a lower, distal, siliceous mudstone facies with interbedded tuffs, and an upper, orogenically derived turbidite facies. The tightest U-Pb zircon ages from the tuffs are 622±1 Ma (Bradley and others, 2013) and 610±6 Ma (Lahondère and others, 2005, Section 2.3.8.4). The turbidites yielded a detrital zircon signature (fig. 63*B*) that is reminiscent of the Groupe d'Assabet El Hassiane but with the addition of a new source with an age ca. 605 Ma, which is inferred to have been a magmatic arc that was colliding with West Africa at this time. A significant conclusion is that the Téniagouri turbidites are too young to have been derived syntectonically from the putative ca. 650-Ma orogen that Lécorché and others (1989) called Pan-African I, but too old for the putative ca. 575-550-Ma Pan-African II. Regardless of semantics, the Téniagouri is a classic underfilled foredeep succession, of the kind seen worldwide during the onset of arc-passive margin collision (Bradley, 2008).

The Groupe de Téniagouri is overlain by the Groupe de Nouatil and Groupe d'Oujeft of latest Neoproterozoic to Cambrian. These strata are mostly sandstone although the Nouatil also includes dolostones. The Oujeft barcode (fig. 63*A*), defined on the basis of these two units, is broadly similar to the Téniagouri barcode with the addition of younger zircons that are responsible for an age peak at 579 Ma and attenuate the older signal. We interpret these strata as synorogenic to immediately post-orogenic foreland-basin deposits.

8.4. Mesoproterozoic to Paleozoic Tectonic Record in the Mauritanide Orogen

Having examined the orogen from the vantage point of its foreland basin, we now consider the complementary record from the Mauritanides. The Mauritanide orogen is a polydeformed, east-directed thrust belt that is broadly divisible into eastern (parautochthonous) and western (allochthonous) parts. Unraveling the orogenic evolution is hampered by the fact that most of the rocks were formed and first experienced deformation and metamorphism in the Neoproterozoic—but were re-imbricated some 300 million years later.

The eastern part of the orogen (fig. 7) consists of parautochthonous Neoproterozoic and lower Paleozoic siliciclastic rocks of inferred West African origin. Pitfield and others (2004, Section 7.3.2.1) identified deformed equivalents of the Groupes de Nouatil, de Téniagouri, and de Jbéliat—all of which are depositionally tied to West African cratonic basement. Metamorphism is at sub-greenschist facies.

The Mauritanide continental margin of West Africa is inferred to have been formed as a result of rifting and then seafloor spreading (Villeneuve and Cornée, 1994), when an unknown continent, microcontinent, or arc drifted away at some time during the Neoproterozoic. In our view, unequivocal passive-margin or rift deposits remain to be documented in the orogen and the age of breakup is not well constrained. Pitfield and others (2004, Section 3.8.3.6) suggested that breakup is recorded by peralkaline magmatism as young as 676±8 Ma in a tectonic window through the Mauritanide thrust stack at Bou Naga (Blanc and others, 1992). Dallmeyer and Lécorché (1989) documented $^{40}Ar/^{39}Ar$ cooling ages on metamorphic hornblende of 720-700 Ma in rocks that they interpreted as rift-related metavolcanics (Fârkâka Association, now Groupe de Gadel); rifting, in that scenario, would have been older.

The Complexe de Gorgol Noir (of Pitfield and others, 2004, Section 3.1.2.1) lies outboard of the parautochthon (fig. 7). It includes ultramafic massifs and a mélange-like tectonic assemblage of mica schist, quartzite, amphibolite, and serpentinite, and is interpreted to mark a Pan-African suture zone (Pitfield and others, 2004). Metasandstone from the Groupe de Gadel in this belt has yielded detrital zircons that match the Assabet barcode, suggesting a link to the craton for certain of the rocks in this complex zone (Bradley and others, 2015c). The ultramafic rocks have been interpreted as dismembered ophiolites (Dia, 1984; Remy, 1985) and as remnants of a Neoproterozoic oceanic basin. However, Pitfield and others (2004, Section 3.3.5) reported that the highest thrust slice in the Complexe de Gorgol Noir is a gabbro-granodiorite suite of arc affinity, with a U-Pb zircon age of 665±3 Ma; Lahondère and others (2005, Section 3.5.3.4) reported similar ages of 671±8 Ma and 670±6 Ma from diorite and

granodiorite in this belt. A tonalite in the Gadel outcrop belt yielded a U-Pb zircon age of 637.2±4.4 Ma (Lahondère and others, 2005, Section 3.4.2.4). Accordingly, the dismembered ophiolite is probably a forearc ophiolite. Metamorphic conditions reached amphibolite facies in some fault slices within Complexe de Gorgol Noir. Metamorphic white micas from the Groupe de Gadel have yielded a number of very similar $^{40}Ar/^{39}Ar$ plateau ages between 597 and 582 Ma (Dallmeyer and Lécorché, 1989).

The remainder of the exposed Mauritanide orogen, outboard of the Complexe de Gorgol Noir, is a polyphase thrust belt containing allochthonous rocks, which Pitfield and others (2004) assigned to the Super-groupe de Mbout (fig. 7). Metavolcanic rocks, both felsic and mafic, are important components. Detrital zircons from the allochthonous domain are reminiscent of the Téniagouri and Oujeft barcodes (Bradley and others, 2015a). We therefore infer that some of the allochthonous strata, although currently in the Mauritanide hinterland, were deposited in the Pan-African foreland basin in the late Neoproterozoic. Cross-cutting granitoids have yielded concordant U-Pb zircon ages of 685±18 (late to post-kinematic) and 637±5 (post-kinematic) (Pitfield and others, 2004, Section 3.4.7.5).

After the PRISM-I mapping was completed, Caby and Kienast (2009) documented an allochthonous belt of high-grade, metaigneous and metasedimentary basement in the Gàoua window (fig. 7)[18]. Metamorphic hornblende from these rocks yielded $^{40}Ar/^{39}Ar$ cooling ages of 847±7 and 734±8 Ma (Dallmeyer and Lécorché, 1989); the age spectra are disturbed but the metamorphism must be older than the putative Pan-African I age of ca. 650 Ma. A plausible interpretation is that this was basement to an arc that collided with West Africa during a Neoproterozoic orogeny that is older than Pan-African I as traditionally dated.

The youngest deformation in the Mauritanides took place in the Pennsylvanian to Permian and is commonly referred to as Hercynian. Thrust faults shortened Pan-African tectonites, dramatically altering the original orogenic architecture, but produced almost no new rocks in Mauritania. The main evidence for late Paleozoic tectonism comes from numerous $^{40}Ar/^{39}Ar$ ages from metamorphic white mica that are near 300 Ma (Dallmeyer and Lécorché, 1989; Bradley and others, 2015a). The only Hercynian foreland-basin unit so far recognized is the Kandou Formation (Lahondère and others, 2005, p. 357–358), a localized, undeformed conglomerate that lies in thrust contact with tectonites of the Groupe de Gueneiba (fig. 7). The map extent of this unit is quite small and there is no direct age control so the interpreted Hercynian foreland-basin depositional setting is speculative. There are no known late Paleozoic plutons in Mauritania. All this contrasts markedly with what is seen on the Appalachian side of the collisional orogen: a well developed foreland basin preserves a thick Pennsylvanian to Early Permian molasse succession, and the orogen is riddled with granitic plutons having a bimodal age distribution of 326–305 and 300–282 Ma (Speer and others, 1994).

In summary, the site of the future Mauritanide orogen is interpreted to have formed during the early or mid-Neoproterozoic with breakup of West Africa and the departure of an unknown block. Subsequently, a magmatic arc, perhaps built on Early Neoproterozoic continental basement, approached and then collided with the Mauritanian margin during an event that could be called Pan-African I. Initial collision would likely have been followed immediately by a subduction flip, with the new subduction zone dipping beneath the collided arc toward Africa. Latest Neoproterozoic to Cambrian magmatism, shortening, and foreland-basin sedimentation ("Pan-African II") would have been in convergent-margin regime. Magmatism during this interval is well represented in the detrital zircon record (Oujeft barcode) and suggests that many plutons of this age range likely lie buried beneath the coastal plain.

8.5. Tindouf Basin

The Tindouf Basin is the northern counterpart of the Taoudeni Basin, the two being separated by the broad structural arch of Archean and Paleoproterozoic basement of the Rgueïbat Shield. Two outcrop belts of Tindouf Basin strata crop out in Mauritania, the Zemmour noir area in the west and the Nord-Yetti area in the east. The portion of the Zemmour within Mauritania is the frontal 40 km of a much wider fold-and-thrust belt (Michard and others, 2010). The fold-and-thrust belt itself is a Hercynian feature but farther outboard, in Western Sahara, is a Neoproterozoic orogen with a complex history (Michard and others, 2010). This northern sector of the West African craton's western margin thus shares a broadly similar history to the Mauritanide sector, with Pan-African and Hercynian orogenic events. In the Zemmour noir region, Paleoproterozoic basement rocks of the Rgueïbat Shield are unconformably overlain by an Ordovician to Devonian continental-margin succession of the Groupes d'Oumat el Ham, de Garat el Hamoueïd, de Gara Bouya Ali, and du Zemmour. Anticlines in Mauritania's farthest outboard part of the fold-and-thrust belt exposed considerable older strata: stromatolitic dolostones of the Groupe d'El Thlethyate, which has been correlated with the Groupe d'Atar and thus is likely Mesoproterozoic in age.

The Nord-Yetti area exposes a broadly similar stratigraphic section but the strata are essentially undeformed, being far beyond the Hercynian deformation front. The oldest strata here belong to the glaciogenic Groupe de Garat El Hamoueïd of Ordovician age. This is overlain by Silurian to Carboniferous mainly marine strata assigned to the Groupes de Gara Bouya Ali, du Zemmour, and de Ouarkziz (Lahondère and others, 2003, Section 4).

[18] This detailed mapping was not integrated into Deliverable 51 or 52.

8.6. Mesozoic to Cenozoic Geology and Tectonics

Central Atlantic Magmatic Province. The next milestone in Mauritania's geologic record came after a long period of quiescence and signaled the end of Pangea: a huge pulse of basaltic magmatism in the form of dikes, sills, and flows. It is known as the Central Atlantic Magmatic Province, or CAMP, and it is dated at ca. 200 Ma (Olsen and others, 2003). CAMP was one of the most extensive Large Igneous Provinces, or LIPs, in the Phanerozoic. Remnants of CAMP are spread across West Africa, Iberia, North America, and South America; on a pre-drift restoration, CAMP appears to have had an area of about 7 million km^2 (Verati and others, 2005). In Mauritania, igneous rocks known or inferred to be part of CAMP are widespread as mafic dikes, sills, flows, and pipes in the Taoudeni Basin and as dikes in the Rgueïbat Shield.

Opening of the Atlantic. Seafloor spreading was preceded by a lengthy period of rifting, and in particular, asymmetric rifting, whereby the rocks on one side were pulled out (or educted) from the beneath the rocks of the other side; the conjugate margins thus formed are referred to as lower-plate and upper-plate margins, respectively. The Mauritanian margin is interpreted to be an upper plate margin and the corresponding North American sector, from Virginia to North Carolina, is a lower-plate margin (Etheridge and others, 1990). There are no known rift deposits preserved onshore in Mauritania. In a schematic cross section of the margin that extends offshore nearly to the 2000-m isobath, Davison (2005) depicted rift basins at depth; these basins include Jurassic salt.

Mauritania's passive margin. The coast of Mauritania is part of Africa's Atlantic passive margin. Seafloor spreading along this sector of continental margin started about 187 to 184 million years ago as deduced from the age of oceanic basalts that have been fortuitously uplifted in the Canary Islands as a result of younger volcanism (Steiner and others, 1998). Since the Early Jurassic, this portion of the Atlantic has opened more or less symmetrically at an average rate of 1.6 cm/yr. During this time, Mauritania's passive margin has thermally subsided and a thick prism of deeper-water sediments has accumulated offshore and a thinner prism of shallower-water, marginal marine, and nonmarine sediments has accumulated onshore. The Jurassic strata are largely carbonates and the Cretaceous and younger strata are largely siliciclastic (Davison, 2005).

Present-day tectonics. Mauritania is on the African Plate, which is cored by the African continent but also includes attached oceanic lithosphere in the Central Atlantic, South Atlantic, Southern, and Indian Oceans as well as the Gulf of Aden, Red Sea, and Mediterranean Sea. Although Africa is in relative motion with respect to all its bounding plates, it is unique among the plates in that it is virtually immobile in an absolute (mantle) reference frame, and has been since 30 Ma (Burke and Gunnell, 2008). A consequence is that Africa has a globally unique basin-and-swell topography, the highs and lows being interpreted as surface manifestations of mantle convection cells (Burke and Gunnell, 2008). Mauritania itself sits on one of the few parts of Africa that does not show an obvious surface expression of this continent-scale topographic pattern.

8.7. Mauritanian Tectonic Evolution in the Context of the Supercontinents Nuna, Rodinia, Gondwana, and Pangea

Nuna. The Paleoproterozoic orogen of northern Mauritania is one of dozens of orogens worldwide having the general age range 2,150 to 1,750 Ma (Bradley, 2011). In Laurentia, for example, the Archean Superior and Slave cratons are joined across Paleoproterozoic the Trans-Hudson orogen (Hoffman, 1989). Laurentia can be seen as the remnant of a formerly much larger supercontinent, called Nuna (Hoffman, 1997)[19], that formed during a series of collisions until about 1,750 Ma (Bradley, 2011). The Eburnean of northern Mauritania might very well have been one of the orogens involved in the assembly of Nuna, but if so, whatever craton once lay to the north or east would have drifted away during the Neoproterozoic and West Africa's place in Nuna is essentially unconstrained.

Rodinia. Rodinia is the name applied to a hypothesized supercontinent that came together around the end of the Mesoproterozoic as a result of collisions such as the Grenville orogen of eastern Laurentia (Hoffman, 1997). The configuration of Rodinia itself is controversial, as shown in four alternative reconstructions in figure 65; an even deeper issue is the untested assumption that all the continents came together as one. In the various Rodinia reconstructions, the placement of West Africa is not well constrained, and none of the existing Rodinia reconstructions adequately account for the new information about the Groupe d'Assabet El Hassiane, so a new Rodinia model is needed. The continental margin that eventually would become the Mauritanide orogen is interpreted to have formed during the early or mid-Neoproterozoic with breakup of the part of Rodinia and the departure of an unknown block from West Africa. Other unknown blocks departed from West Africa's eastern and northern margins. The global search for these continents should prove tractable because the Rgueïbat Shield has distinctive age provinces at ca. 2.9, 2.7. 2.4, and 2.1 Ga (fig. 68).

Gondwana. The term Gondwana is applied to a clustering of the southern half of the world's continents, which came together during a series of collisions in the Late Neoproterozoic and Cambrian. Whether or not it should qualify as a

[19] Whatever the specifics of the plate reconstruction, the term *Nuna* is preferred over *Columbia* (Rogers and Santosh, 2002) because of priority.

supercontinent is a semantic distinction, (Bradley, 2011), the issue being that it only contained about half of the world's continental area. Certain details of Gondwana reconstruction are open to debate but West Africa's neighbors are well known, because the African part of Gondwana remains intact today. Pan-African orogenies in Mauritania happened during the assembly of Gondwana, but these only had the minor effect of adding a narrow arc terrane along the outer margin of the growing supercontinent.

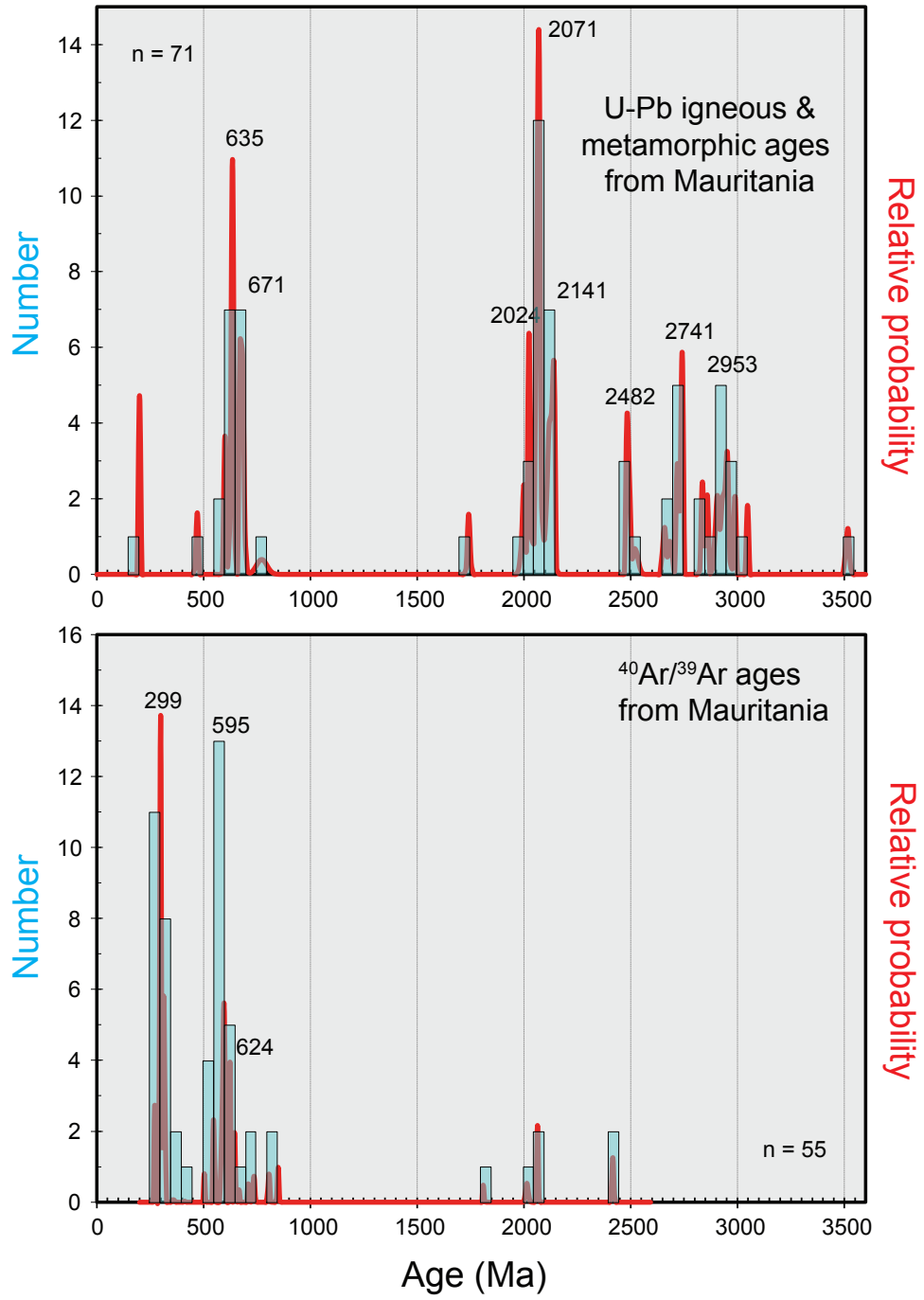


Figure 68. (*A*) Histogram of U-Pb ages from Mauritania, from data in tables 1 and 9. (*B*) Histogram of $^{40}Ar/^{39}Ar$ ages from Mauritania, from data in tables 3 and 9.

Pangea. The Hercynian-Alleghanian orogeny involved final convergence between Africa and Laurentia, completing the assembly of the most recent supercontinent, Pangea, during the Carboniferous and Permian. In the aftermath of these collisions, Mauritania lay astride a huge mountain range—the Trans-Pangea Mountains. With the circum-Atlantic continents in their pre-drift configuration, Mauritania restores next to eastern seaboard of the United States, against the States of Virginia and North Carolina, (Etheridge and others, 1990). Several hundred kilometers of continental crust—all of it involved in the Hercynian-Alleghanian Orogeny—lies hidden beneath the two continental shelves. If this orogeny involved closure of an ocean, and not merely convergence between already juxtaposed continents, the suture must lie beneath one or the other of the continental shelves. These shelves are the product of the breakup of Pangea and the start of the next, half-finished supercontinent cycle.

9. References Cited

Ashwal, L.D., 2011, The temporality of anorthosites: The Canadian Mineralogist, v. 48, p. 711–728.

Benan, C.A.A, and Deynoux, Max, 1998, Facies analysis and sequence stratigraphy of Neoproterozoic Platform deposits in Adrar of Mauritania, Taoudeni basin, West Africa: Geologische Rundschau, v. 87, p. 283–302.

Bickford, M.E., Cullers, R.L., Shuster, R.D., Premo, W.R., and Van Schmus, W.R., 1989, U-Pb zircon geochronology of Proterozoic and Cambrian plutons in the Wet Mountains and southern Front Range, Colorado: Geological Society of America Special Paper 235, p. 49–64.

Black, L.P., Kamo, S.L., Allen, C.M., Davis, D.W., Aleinikoff, J.N., Valley, J.W., Mundil, R., Campbell, I.H., Korsch, R.J., Williams, I.S., and Foudoulis, C. 2004. Improved $^{206}Pb/^{238}U$ microprobe geochronology by the monitoring of trace-element related matrix effect; SHRIMP, ID-TIMS, ELA-ICP-MS and oxygen isotope documentation for a series of zircon standards: Chemical Geology, 205, p.15–140.

Blanc, A., Bernard Griffiths, J., Caby, R., Caruba, C., Caruba, R., Dars, R., Fourcade, S. and Peujat, J.J., 1992, U-Pb dating and isotopic signature of the alkaline ring complexes of Bou Naga (Mauritania): its bearing on late Proterozoic plate tectonics around the West African Craton: Journal of African Earth Sciences, v. 14, p. 301–311.

Bowring, J.F., McLean, N.M., and Bowring, S.A., 2011, Engineering Cyber Infrastructure for U-Pb Geochronology, Tripoli and U-Pb_Redux: Geochemistry, Geophysics, Geosystems, v. 12, Q0AA19, DOI:10.1029/2010GC003479.

Bradley, D.C., 2008, Passive margins through Earth history: Earth-Science Reviews, v. 91, p. 1–26 and supplementary data, 33 p., http://www.sciencedirect.com/science/article/pii/S0012825208000871.

Bradley, D.C., 2011, Secular trends in the geologic record and the supercontinent cycle: Earth-Science Reviews, v. 108, p. 16–33, and supplementary data, 17 p. doi: 10.1016/j.earscirev.2011.05.003.

Bradley, D.C., Motts, H.A., Horton, J.D., Giles, Stuart, and Taylor, C.D., 2015a, Geologic map of Mauritania (phase V, deliverables 51a, 51b, and 51c), chap. A1 *of* Taylor, C.D., ed., Second projet de renforcement institutionnel du secteur minier de la République Islamique de Mauritanie (PRISM-II): U.S. Geological Survey Open-File Report 2013–1280-A1, 3 pl., scale 1:1,000,000, http://dx.doi.org/10.3133/ofr20131280/. [In English and French.]

Bradley, D.C., Horton, J.D., Motts, H.A., and Taylor, C.D., 2015b, Structure map of Mauritania (phase V, deliverables 52a and 52b), chap. A2 *of* Taylor, C.D., ed., Second projet de renforcement institutionnel du secteur minier de la République Islamique de Mauritanie (PRISM-II): U.S. Geological Survey Open-File Report 2013–1280-A2, 2 pl., scale 1:1,000,000, http://dx.doi.org/10.3133/ofr20131280/. [In English and French.]

Bradley, D.C., and Kusky, T.M, 1986, Geologic evidence for the rate of plate convergence during the Taconic arc-continent collision: Journal of Geology, v. 94, p. 667–681.

Burke, Kevin, and Gunnell, Yanni, 2008, The African Erosion Surface—A continental-scale synthesis of geomorphology, tectonics, and environmental change over the past 180 million years: Geological Society of America Memoir 201, 66 p., doi: 10.1130/2008.1201., http://memoirs.gsapubs.org/content/201/1.full.

Caby, Renaud, and Kienast, J,R., 2009, Neoproterozoic and Hercynian metamorphic events in the Central Mauritanides—Implications for the geodynamic evolution of West Africa: Journal of African Earth Sciences, v. 53. issue 3, p 122–136.

Chang, Zhaoshan, Vervoort, J.D., McClelland, W.C., and Knaack, Charles, 2006. U-Pb dating of zircon by LA-ICP-MS: Geochemistry, Geophysics, Geosystems, American Geophysical Union, v. 7, no. 5, 14 p.

Clauer, Norbert 1976, Geochimie isotopique du strontium des milieux sedimentaires: Application a la geochronologie de la couverture du craton ouest-africain: Sci. Geol., Strasbourg, Fr. Memoir 45, 256 p.

Clauer, Norbert, Caby, Renaud, Jeannette, Daniel and Trompette, Roland, 1982, Geochronology of sedimentary and metasedimentary Precambrian rocks of the West African Craton: Precambrian Research, v. 18, p. 53–71.

Clement, S.W.J., and Compston, W., 1994, Ion probe parameters for very high resolution without loss of sensitivity. U.S. Geological Survey Circular 1107, p. 62.

Dallmeyer, R.D., and Lécorché, J.P., 1990, $^{40}Ar/^{39}Ar$ polyorogenic mineral age record within the central Mauritanide orogen, West Africa: Tectonophysics, v. 177 p. 81–107.

Dalziel, I.W.D., 1997, Neoproterozoic-Paleozoic geography and tectonics: review, hypothesis, environmental speculation: Geological Society of America Bulletin, v. 109, p. 16–42.

Davison, Ian, 2005, Central Atlantic margin basins of North West Africa: Geology and hydrocarbon potential (Morocco to Guinea): Journal of African Earth Sciences, v. 43, p. 254–274.

Dia, O., 1984, La chaîne panafricane et hercynienne des mauritanides face au bassin proterozoique supérieur à dévonien de Taoudeni dans le secteur clé de Mejéria (Taganet, Sud R.I.M.): Lithostratigraphie et tectonique. Un example de tectonique tangentielle superposé:Thèse Doct. Sci., Univ. Aix-Marseille III, 516 p.

Deynoux, Max, 1985, Terrestrial or waterlain glacial diamictites? Three case studies from the Late Precambrian and Late Ordovician glacial drift in West Africa: Palaeogeography Palaeoclimatology Palaeoecology, v. 51, p. 97–141.

Deynoux, Max, Affaton, Pascal, Trompette, Roland, and Villeneuve, Michel, 2006, Pan-African tectonic evolution and glacial events registered in Neoproterozoic to Cambrian cratonic and foreland basins of West Africa: Journal of African Earth Sciences 46, 397–426.

Dickinson, W.R., and Gehrels, G.E., 2009, Use of U–Pb ages of detrital zircons to infer maximum depositional ages of strata: A test against a Colorado Plateau Mesozoic database: Earth and Planetary Science Letters, v. 288, p. 115–125.

Donelick, R.A., O'Sullivan, P.B., and Ketcham, R.A., 2005, Apatite fission track analysis: Reviews in Mineralogy and Geochemistry, v. 58, p. 49–93.

Dosso, L., Vidal, P., Sichler, B. and Bonifay, A., 1979, Age Précambrien de dolerites de la Dorsale Reguibat (Mauritanie): Comptes Rendus de l'Académie des Sciences de Paris, v. 288, p. 739–742.

Ernst, R.E., and Buchan, K.L. 2001, Large mafic magmetic events through time and links to mantle-plume heads, *in* R.E. Ernst & K.L. Buchan, eds., Mantle plumes—Their identification through time: Geological Society of America Special Paper 352, p. 483–575.

Etheridge, M.A., Symonds, P.A., and Lister, G.S., 1990, Application of the detachment model to reconstruction of conjugate passive margins: American Association of Petroleum Geologists Memoir 46, p. 23–40.

Evans, D.A.D., 2009, The palaeomagnetically viable, long-lived and all-inclusive Rodinia supercontinent reconstruction, *in* Murphy, J.B., Keppie, J.D., and Hynes, A.J., eds., Ancient Orogens and Modern Analogues: London, Geological Society, Special Publication 327, p. 371–404.

Gehrels, G.E., Valencia, V.A., and Ruiz, Joaquin, 2008. Enhanced precision, accuracy, efficiency, and spatial resolution of U-Pb ages by laser ablation-multicollector-inductively coupled plasma-mass spectrometry: Geochemistry Geophysics Geosystems, American Geophysical Union, v. 9, 13 p.

Gerstenberger, H., and Haase, G., 1997, A highly effective emitter substance for mass spectrometric Pb isotope ratio determinations: Chemical Geology, v. 136, no. 3–4, p. 309–312.

Ghienne, J.-F., 2002, Late Ordovician sedimentary environments, glacial cycles, and post-glacial transgression in the Taoudeni Basin, West Africa: Palaeogeography, Palaeoclimatology, Palaeoecology, v. 189 (2003), p. 117–145.

Gradstein, F.M., and Ogg, J.G., 2004, A geologic time scale 2004: Cambridge, Cambridge University Press, 598 p., 1 plate.

Gunn, A.G., Pitfield, P.E.J., McKervey, J.A., Key, R.M., Waters, C.N., and Barnes, R.P., 2004, Notice explicative des cartes géologiques et gîtologiques à 1/200 000 et 1/500,000 du Sud de la Mauritanie. Volume 2—Potentiel Minier: DMG, Ministère des Mines et de l'Industrie, Nouakchott.

Hebert, C.L., Kaufman, A.J., Penniston-Dorland, S.C., and Martin, A.J., 2010, Radiometric and stratigraphic constraints on terminal Ediacaran (post-Gaskiers) glaciation and metazoan evolution: Precambrian Research, v. 182, p. 402–412.

Hibbard, J.P., van Stall, C.R., Rankin, D.W., and Williams, H., 2006, Lithotectonic map of the Appalachian Orogen, Canada and United States of America: Geological Survey of Canada, Map 2096A, scale 1:1,500,000, 2 sheets.

Hoffman, P.F., 1989, Precambrian geology and tectonic history of North America, *in*: Bally, A.W., and Palmer, A.R eds., The Geology of North America—An overview: Boulder, Colo., Geological Society of America, v. A, p. 447–512.

Hoffman, P.F., 1997. Tectonic genealogy of North America, *in* van der Pluijm, B.A., and Marshak, S., eds., Earth Structure—An introduction to structural geology and tectonics: McGraw-Hill, New York, p. 459–464.

Hoffman, P.F., and Li, Z.X., 2009, A palaeogeographic context for Neoproterozoic glaciation: Palaeogeography, Palaeoclimatology, Palaeoecology, v. 277, p. 158–172.

Hurford, A.J., and Green, P.F., 1982, A users' guide to fission track dating calibration: Earth and Planetary Science Letters, v. 59, p. 343–354.

Ireland, T.R, and Williams, I.S., 2003, Considerations in zircon geochronology by SIMS: Reviews in Mineralogy and Geochemistry, v. 53, p. 215–241.

Jaffey, A.H., Flynn, K,F., Glendenin, L.E., Bentley, W.C., and Essling, A.M., 1971, Precision measurement of half-lives and specific activities of ^{235}U and ^{238}U: Physical Review C, v. 4, no. 5, p. 1889–1906.

Johansson, Åke, 2009, Baltica, Amazonia and the SAMBA connection—1000 million years of neighbourhood during the Proterozoic?: Precambrian Research, v. 175, p. 221–234.

Junner, N.R., 1940, Geology of the Gold Coast and western Togoland with revised geological map (1:1,000,000): Gold Coast Geological Survey Bulletin 11, 40 p.

Kalsbeek, Feiko, Frei, D., and Affaton, Pascal, 2008, Constraints on provenance, stratigraphic correlation and structural context of the Volta basin, Ghana, from detrital zircon geochronology: An Amazonian connection?: Sedimentary Geology, v. 212, p. 86–95.

Ketcham, R.A., Donelick, R.A., and Carlson, W.D., 1999, Variability of apatite fission-track annealing kinetics, III, Extrapolation to geological time scales: American Mineralogist, v. 84, p. 1235–1255.

Ketcham, R.A., Donelick, R.A., and Donelick, M.B., 2000, AFTSolve—A program for multi-kinetic modeling of apatite fission-track data: Geological Materials Research, v. 2, no. 1, p. 1.

Key, R.M., Loughlin, S.C., Gillespie, M., Del Rio, M., Horstwood, M.S.A., Crowley, Q.G., Darbyshire, D.P.F., Pitfield, P.E.J., and Henney, P.J., 2008, Two Mesoarchaean terranes in the Rgueïbat shield of NW Mauritania: Geological Society, London, Special Publication 297, p. 33–52.

Krogh, T.E., 1973, A low-contamination method for hydrothermal decomposition of zircon and extraction of U and Pb for isotopic age determinations: Geochimica et Cosmochimica Acta, v. 37, no. 3, p. 485–494.

Kuiper, K.F., Deino, A.L, Hilgen, F.J., Krijgsman, W., Renne, P.R., and Wijbrans, J.R., 2008, Synchronizing rock clocks of earth history: Science, v. 320, p. 500–504.

Lahondère, D., Roger, J., Le Métour, and Callec, Y., 2010, Carte géologique à 1/1,000,000 de la Mauritanie: République Islamique de Mauritanie, Ministère des Mines et de l'Industrie, Nouakchott, 1 sheet.

Lahondère, D., Roger, J., Le Métour, J., Donzeau, M., Guillocheau, F., Helm, C., Thiéblemont, D., Cocherie, A., and Guerrot, C., 2005, Notice explicative des cartes géologiques à 1/200 000 et 1/500 000 de l'extrême sud de la Mauritanie: DMG, Ministère des Mines et de l'Industrie, Nouakchott, Rapport BRGM/RC-54273-FR, 610 p.

Lahondère, D., Thieblemont D., Goujou J.-C., Roger J., Moussine-Pouchkine A., Le Metour J., Cocherie A., and Guerrot C., 2003. Notice explicative des cartes géologiques et gîtologiques à 1/200 000 et 1/500 000 du Nord de la Mauritanie. volume 1. DMG, Ministère des Mines et de l'Industrie, Nouakchott.

Lécorché, J.P., Dallmeyer, R.D., and Villeneuve, M., 1989, Definition of tectonostratigraphic terranes in the Mauritanide, Bassaride and Rokelide orogens, West Africa, *in* Dallmeyer, R.D., ed., Terranes in the circum-Atlantic Paleozoic orogens: Geological Society of America Special Paper 230, p. 131–144.

Li, Z.-X., Bogdanova, S. V., Collins, A.S., Davidson, A., De Waele, B., Ernst, R.E., Fitzsimons, I.C.W., Fuck, R.A., Gladkochub, D.P., Jacobs, J., Karlstrom, K.E., Lu, S., Natapov, L.M., Pease, V., Pisarevsky, S.A., Thrane, K. , and Vernikovsky, V., 2008, Assembly, configuration, and break-up history of Rodinia—A synthesis: Precambrian Research, v. 160, p. 179–210.

Ludwig, K.R., 1998, On the treatment of concordant uranium-lead ages: Geochimica et Cosmochimica Acta, v. 62, p. 665–676.

Ludwig, K.R., 2001, Squid 1.00. A users manual: Berkeley Geochronology Center Special Publication No. 2, 17 pp.

Ludwig, K.R., 2003, Isoplot 3.00, A Geochronological Toolkit for Microsoft Excel: Berkeley Geochronology Center, Special Pblication No. 4a, Berkeley, California.

Macdonald, F.A., Schmitz, M.D., Crowley, J.L., Roots, C.F., Jones, D.S., Maloof, A.C., Strauss, J.V., Cohen, P.A., Johnston, D.T., and Schrag, D.P., 2010, Calibrating the Cryogenian: Science, v. 347, p. 1241–1243.

Marot, A., Stein, G., Artignan, D., and Milesi, J.-P., 2003. Notice explicative des cartes géologiques et gîtologiques à 1/200 000 et 1/500 000 du Nord de la Mauritanie. Volume 2 – Potentiel Minier: DMG, Ministère des Mines et de l'Industrie, Nouakchott.

Martyn, J.E., and Strickland, C.D., 2004, Stratigraphy, structure and mineralisation of the Akjoujt area, Mauritania: Journal of African Earth Sciences, 38, 489–503.

Mattinson, J.M., 2010, Analysis of the relative decay constants of ^{235}U and ^{238}U by multi-step CA-TIMS measurements of closed-system natural zircon samples: Chemical Geology, v. 275, p. 186–198.

McLean, N.M., Bowring, J.F. and Bowring, S.A., 2011, An Algorithm for U-Pb isotope dilution data reduction and uncertainty propagation: Geochemistry, Geophysics, Geosystems, v. 12, Q0AA18, DOI:10.1029/2010GC003478.

Meyer, F.M., Kolb, J., Sakellaris, G.A., and Gerdes, A., 2006, New ages from the Mauritanides Belt—Recognition of Archean IOCG mineralization at Guelb Moghrein, Mauritania: Terra Nova, v. 18, p. 345–352.

Michard, A.G., Soulaimani, Abderrahmane, Hoepffner, Christian, Ouanaimi, Hassan, Baidder, Lahssen, Rjimati, E.C., and Saddiqi, Omar, 2010, The south-western branch of the Variscan belt—Evidence from Morocco: Tectonophysics, v. 492, p. 1–24.

Moussine-Pouchkine, Alexis, and Bertrand-Sarfati, Janine, 1997, Tectonosedimentary subdivisions in the Neoproterozoic to Early Cambrian cover of the Taoudeni Basin (Algeria-Mauritania-Mali): Journal of African Earth Sciences, v. 24, p. 425–443.

North American Commission on Stratigraphic Nomenclature, 1983, North American stratigraphic code (no. 5): American Association of Petroleum Geologists Bulletin, v. 67, p. 841–875.

O'Connor, E.A., Pitfield, P.E.J., Schofield, D.I., Coats, S., Waters, C., Powell, J., Ford, J., Clarke, S., and Gillespie, M., 2005, Notice explicative des cartes géologiques et gîtologiques à 1/200000 et 1/500000 du Nord-Ouest de la Mauritanie: DMG, Ministère des Mines et de l'Industrie, Nouakchott.

Olsen, P.E., Kent, D.V., Et-Touhami, Mohammed, and Puffer, John, 2003, Cyclo-, magneto-, and bio-stratigraphic constraints on the duration of the CAMP event and its relationship to the Triassic-Jurassic boundary: Geophysical Monograph Series, v. 136, p. 7–32.

Paces, J.B., and Miller, J.D., 1993, U-Pb ages of the Duluth Complex and related mafic intrusions, northeastern Minnesota—Geochronologic insights into physical, paleomagnetic and tectonomagmatic processes associated with the 1.1 Ga mid-continent rift system: Journal of Geophysical Research, v. 98, p. 13,997–14,013.

Paton, Chad, Woodhead, J.D., Hellstrom, J.C., Hergt, J.M., Greig, Alan, and Maas, Roland, 2010, Improved laser ablation U-Pb zircon geochronology through robust downhole fractionation correction: Geochemistry, Geophysics, Geosystems, v. 11, Q0AA06, doi:10.1029/2009GC002618.

Peucat, J.-J., Capdevila, Ramon, Drareni, Amar, Mahdjoub, Yamina, and Kahoui, Mohamed, 2005, The Eglab massif in the West African Craton (Algeria), an original segment of the Eburnean orogenic belt—Petrology, geochemistry and geochronology: Precambrian Research, v. 36, p. 309–352.

Pisarevsky, S.A., Wingate, M.T. D., Powell, C.M., Johnson, S., and Evans, D.A.D, 2003, Models of Rodinia assembly and fragmentation, *in* Yoshida, M., Windley, B.F., and Dasgupta, S., eds., Proterozoic East Gondwana—Supercontinent assembly and breakup: Geological Society of London, Special Publication 206, p. 35–55.

Pitfield, P.E.J., Key, R.M., Waters, C.N., Hawkins, M.P.H., Schofield, D.I., Loughlin, S., and Barnes, R.P., 2004, Notice explicative des cartes géologiques et gîtologiques à 1/200 000 et 1/500 000 du Sud de la Mauritanie. Volume 1—géologie: DMG, Ministère des Mines et de l'Industrie, Nouakchott.

Potrel, Alain, Peucat, J.-J., and Fanning, C.M., 1998, Archean crustal evolution of the West African Craton: example of the Amsaga Area (Rgueïbat Rise). U-Pb and Sm-Nd evidence for crustal growth and recycling: Precambrian Research, v. 90, p. 107–117.

Potrel, Alain, Peucat, J.-J., Fanning, C.M., Auvray, Bernard, Burg, J.P., and Caruba, Christiane, 1996, 3.5 Ga old terranes in the West African craton, Mauritania: Journal of the Geological Society, v. 153, p. 507–510.

Rémy, P., 1985, Caracteres tholeiitiques et alcalines dans le material ophiolitique du groupe d'El Aouidja (Mauritanides centrales): Ophiolitic, v. 10, p. 391–410.

Rogers, J.J.W., and Santosh, M., 2002, Configuration of Columbia, a Mesoproterozoic supercontinent: Gondwana Research, v. 5, p. 5-22.

Rooney, A.D., Selby, D., Houzay, J.-P., Renne, P.R., 2010, Re–Os geochronology of a Mesoproterozoic sedimentary succession, Taoudeni basin Mauritania—Implications for basin-wide correlations and Re–Os organic-rich sediments systematics: Earth and Planetary Science Letters, v. 289, p. 486–496.

Rubatto, Daniela, 2002, Zircon trace element geochemistry: partitioning with garnet and the link between U–Pb ages and metamorphism: Chemical Geology, v. 184, p. 123–138.

Salpeteur, Ignace, 2005, Mining prospects in the South for Mauritania: Geological survey of the extreme south of Mauritania (PRISM project), DMG, Ministry for the Mines and Industry, Nouakchott, and report BRGM/RC-54132-FR, Orleans, 100 p.

Schofield, D.I., Horstwood, M.S.A., Pitfield, P.E.J., Crowley, Q.G., Wilkinson, A.F., and Sidaty, H.C.O., 2006, Timing and kinematics of Eburnean tectonics in the central Rgueïbat Shield, Mauritania: Journal of the Geological Society of London, v. 163, p. 549–560.

Schofield, D.I., and Gillespie, M.R., 2007, A tectonic interpretation of "Eburnean terrane" outliers in the Rgueïbat Shield, Mauritania: Journal of African Earth Sciences, v. 49, p. 179–186.

Schofield, D.I., Horstwood, M.S.A., Pitfield, P.E.J., Gillespie, M., Darbyshire, F., O'Connor, E.A., and Abdouloye, T.B., 2012, U-Pb dating and Sm-Nd isotopic analysis of granitic rocks from the Tiris Complex—New constaints on key events in the evolution of the Rgueïbat Shield, Mauritania: Precambrian Research, v. 204–205, p. 1–11.

Speer, J.A., McSween, H.Y., Jr., and Gates, A.E., 1994, Generation, Segregation, Ascent, and Emplacement of Alleghanian Plutons in the Southern Appalachians: The Journal of Geology, v. 102, p. 249–267.

Shields, G.A.,Deynoux, Max, Strauss, Harald, Paquet, Hélène, and Nahon, Daniel, 2007, Barite-bearing cap dolostones of the Taoudéni Basin, northwest Africa—Sedimentary and isotopic evidence for methane seepage after a Neoproterozoic glaciation: Precambrian Research, v. 153, p. 209–235.

Stacey J.S. and Kramer J.D., 1975, Approximation of terrestrial lead isotope evolution by a two-stage model: Earth and Planetary Science Letters, v. 26, pp. 207–221.

Steiger, R.H. and Jäger, E., 1977, Subcommission on geochronology: Convention on the use of decay constants in geo- and cosmochronology: Earth and Planetary Science Letters, v. 36, p. 369–371.

Steiner, Christian, Hobson, Alice, Favre, Philippe, Stampfli, G.M., and Hernandez, Jean, 1998, Mesozoic sequence of Fuerteventura (Canary Islands)—Witness of early Jurassic sea-floor spreading in the Central Atlantic: Geological Society of America Bulletin, v. 110, p. 1304–1317.

Tait, J., Straathof, G., Söderlund, U., Ernst, R.E., Key, R., Jowitt, S.M., Lo, K., Dahmada, M.E.M., and N'Diaye, O., 2013, The Ahmeyim great dyke of Mauritania—A newly dated Archaean intrusion: Lithos, v. 174, p. 323–332, http://dx.doi.org/10.1016/j.lithos.2012.09.014.

Thiéblemont, Denis, Goujou, J.C., Egal, Emmanuel, Cocherie, Alain, Delor, Claude, Lafon, J.M., and Fanning, C.M., 2004, Archean evolution of the Leo Rise and its Eburnean reworking: Journal of African Earth Sciences, v. 39, p. 97–104.

Thompson, M.D., and Bowring, S.A., 2000, Age of the Squantum "tillite", Boston Basin, Massachusetts; U–Pb zircon constraints on terminal Neoproterozoic glaciation: American Journal of Science, v. 300, p. 630–655.

Verati, C., Bertrand, H., and Féraud, G., 2005, The farthest record of the Central Atlantic Magmatic Province into West Africa craton—Precise $^{40}Ar/^{39}Ar$ dating and geochemistry of Taoudeni basin intrusives (northern Mali): Earth and Planetary Science Letters, v. 235, p. 391– 407.

Villeneuve, Michel, and Cornée, J.J., 1994, Structure, evolution, and paleogeography of the West African craton and bordering belts during the Neoproterozoic: Precambrian Research, v. 69, p. 307–326.

Villeneuve, Michel, Bellon, Hervé, El Archi, Abdelkrim, Sahabi, Mohamed, Rehault, J.P., Olivet, J.L., Aghzer, A.M., 2006, Evénements panafricains dans l'Adrar Souttouf (Sahara marocain): Comptes Rendus Géoscience, v. 338, p. 359–367.

Villeneuve, Michel, El Archi, Abdelkrim, and Nzamba, J., 2010, Les chaînes de la marge occidentale du Craton Ouest-Africain, modèles géodynamiques, mobiles belts on the western part of the West African Craton and geodynamic interpretations : Comptes Rendus Geoscience, v. 342, p. 1–10.

Williams, I.S., 1997, U-Th-Pb geochronology by ion microprobe: Reviews in Economic Geology, v. 7, p. 1–35.

Zhang, Ming, Ewing, R.C., Boatner, L.A., Salje, E.K.H., Weber, W.J., Daniel, Philippe, Zhang, Yanwen, and Farnan, Ian, 2009, Pb^{+} irradiation of synthetic zircon ($ZrSiO_4$)—Infrared spectroscopic study—Reply: American Mineralogist, v. 94, p. 856–858.

Appendix A1. Analytical Methods for $^{40}Ar/^{39}Ar$ Geochronology

The $^{40}Ar/^{39}Ar$ analyses were performed at the USGS in Denver, Colorado. High purity mineral separates together with standards were irradiated for 50 megawatt hours in the central thimble position of the USGS TRIGA reactor using cadmium lining to prevent nucleogenic production of ^{40}Ar. The neutron flux was monitored using Fish Canyon Tuff sanidine, using an age of 28.20 Ma ± 0.08 Ma (Kuiper and others 2008); isotopic production ratios were determined from irradiated CaF_2 and KCl salts. For this irradiation, the following argon production values from calcium and potassium were measured: ^{36}Ar derived from $^{37}Ca = 2.447 \times 10^{-4} \pm 0.47 \times 10^{-4}$; ^{39}Ar derived from $^{37}Ca = 6.5 \times 10^{-4} \pm 0.53 \times 10^{-4}$; and ^{38}Ar derived from $^{39}K = 1.29 \times 10^{-2} \pm 0.01 \times 10^{-2}$. The irradiated samples and standards were loaded into 3 mm wells within a stainless steel planchette attached to a fully automated ultra high vacuum extraction line constructed of stainless steel. Samples were incrementally degassed and/or fused using a 20W CO_2 laser equipped with a beam homogenizing lens. The gas was expanded and purified by exposure to a stainless steel cold finger maintained at −140°C and two hot SAES GP50 getters. Following purification the gas was expanded into a Mass Analyser Products 215-50 mass spectrometer and argon isotopes were measured by peak jumping using an electron multiplier operated in analog mode. Data were acquired during 10 cycles and time zero intercepts were determined by best-fit regressions to the data. Ages were calculated from data that were corrected for mass discrimination, blanks, radioactive decay subsequent to irradiation, and interfering nucleogenic reactions.

Table 1. Summary of USGS igneous zircon geochronology results.

Figure number	Sample number	Lab number	Latitude	Longitude	Map unit	Crystallization age (igneous zircons-Ma)	Description	Notes	Year and method
19	DB07RIM29a	952-46	20.4971	-12.87567	Gr. de Teniagouri, Fm. de Bouly	623.5 or 569.4±0.4	Tuff interbedded with siltstone, near Atar	SIMS analyses indicate ca. 630 Ma age but with poor resolution. CA-TIMS analyses yielded 7 overlapping concordant results with a weighted average age of 623.5±5.5 Ma. A younger zircon age at 569.4±0.4 Ma may correspond to the eruptive age and the 623.5-Ma cluster may represent xenocrysts.	2009, SIMS; 2012, CA-TIMS
37	DB07RIM64a	952-54 & 1284-10	17.47236	-12.96754	Cortege de Kelbe	Undatable	Foliated granitoid	Other phases of this igneous complex have Neoproterozoic isotopic ages. Paleoproterozoic zircons in this sample are interpreted as xenocrystics in a melt that did not crystallize new zircons.	2012, SIMS; 2012, LAICPMS
39	CT07RIM10-01	952-45 & 1284-2	19.64872	-14.13991	Gr. d'Oumachouema, Fm. de St. Barbe	2839±14	Banded quartz-kspar-amphibole (meta-rhyolite?) host to quartz-wolframite-malachite veins.	Igneous age based on youngest probability peak; older zircons are interpreted as detrital.	2012, SIMS ; 2012, LAICPMS
48	DB07RIM25a	952-56	20.68434	-13.19708	Complexe d'Amsaga	Undatable	Deformed granitoid	All zircon recovered was badly metamict.	2012, SIMS
50	CT07RIM25-1	952-49	21.25933	-13.15357	Complexe d'Amsaga Complex, unit Amlb	2930±33	Anorthosite: homogenous, equigranular, coarse crystalline "black granite" from quarry.	Complex zircon systematics; poor upper intercept age. This appears to be the oldest massif-type anorthosite yet known.	2012, SIMS; 2012, LAICPMS
51	DB07RIM32-1a	952-52	21.08348	-13.16768	Complexe d'Amaga, anorthosite	2718±7	Anorthosite, coarse-grained phase	Concordia age	2010, SIMS
51	CT07RIM22-1	952-48	21.083334	-13.166667	Complexe d'Amsaga Complex, unit Amlb	2743±4	Dark, fine grained anorthosite.	Concordia age	2012, SIMS

Table 1. Summary of USGS igneous zircon geochronology results.—Continued

Figure number	Sample number	Lab number	Latitude	Longitude	Map unit	Crystallization age (igneous zircons-Ma)	Description	Notes	Year and method
62	DB07RIM51a	952-53	24.7835	-10.45706	Cortège de Gleibat Tenabdar	2068±21	Red, alkali granite	Upper intercept age	2011, SIMS
58	CT07RIM37-1	1284-3	26.33772	-8.53738	Gr. de Blekhzamat, Fm. d'Aguelt Nebkha	2113±17	Quartz-veined pyritic metatuff	Igneous age based on youngest probability peak. Older zircons are interpreted as detrital; younger zircons are interpreted as being partly reset.	2012, SIMS; 2012, LAICPMS
not shown	DB07RIM47a	952-47	22.7055	-12.51691	Complexe d'Ijil Complex	Undatable	Contorted clay zone in BIF. Collected as a possible tephra.	No igneous zircon recovered	2009, SIMS
not shown	DB07RIM22b	952-25	20.259537	-13.216916	Complexe d'Amsaga	Undatable	Paleosol weathered on granitoid	No igneous zircon recovered	2012, SIMS
not shown	CT07RIM54-5	952-51	16.84516	-12.75505	Gr. d'El Mseigguem, Fm. d'Ouechkech	Undatable	Felsic metatuff	No igneous zircon recovered	2012, SIMS; 2012, LAICPMS

Table 2. Summary of USGS detrital zircon geochronology results.

Figure number	Sample number	Lab number	Latitude	Longitude	Map unit	Description	Max. depos. age (MDA) in Ma judging only from detrital zircons	Depositional age assignment (in Ma) for this study	Notes on detrital zircons	Year and method
9	CT22		20.259361	-13.215861	Gr. de Char	Tan, fine-grained, well-sorted sandstone from outcrop in roadcut. Collected 10 m above unconformity with Amsaga basement.	2054	~1125	MDA based on youngest probability peak. Detrital zircons provide no useful age constraints. Must be older than Re-Os age of ca. 1107 Ma from overlying Atar Group.	2007, SIMS
10	DB07RIM23a	952-12 & 1284-04	20.29909	-13.17002	Gr. d'Atar Gp, Fm. de Foum Chor	Sandstone	2031	~1107	Detrital zircons provide no useful age constraints. Age assignment based on Re-Os. Some zircons partly reset and a few grains totally reset at ca. 606 Ma	2012, LAICPMS
11	DB07RIM31a	952-43	20.717	-12.73111	Gr. d'Assabet el Hassiane, Sous-groupe de Tin Bessais	Sandstone	975	975	MDA based on youngest probability peak of 3 ages. Could be even younger if Aioun Gr. results are brought in, say ca. 878 Ma.	2012, LAICPMS
12	DB07RIM59a	952-11	21.16323	-11.3894	Gr. d'Assabet el Hassiane, unit AhTb	Sandstone, near Guelb er Richat	1036	975	Detrital zircons provide only general age constraints, with MDA based on the youngest peak, of 4 ages. This is from stratigraphically higher than sample DB07RIM31a and has to be younger.	2012, LAICPMS

Table 2. Summary of USGS detrital zircon geochronology results.—Continued

Figure number	Sample number	Lab number	Latitude	Longitude	Map unit	Description	Max. depos. age (MDA) in Ma judging only from detrital zircons	Depositional age assignment (in Ma) for this study	Notes on detrital zircons	Year and method
13	CT07RIM70-1	952-38	16.44493	-9.237	Gr. d'Aioun, Fm. de Freidi	Coarse grained sandstone.	878	878	MDA based on youngest probability peak of 2 grains. The 200K geologic map shows this lat-long as Bouly Fm, Teniagouri Gr. Based on the rock type and DZ barcode we think that the 200K map is slightly off and this sample belongs to Freidi Fm.	2012, LAICPMS
14	CT07RIM71-1	952-39	16.6429	-9.63002	Gr. d'Aioun, Fm. de Seyal	Coarse grained, dune cross-bedded sandstone.	909	909	MDA based on youngest probability peak. Depositional age assumed to be about the same as MDA in keeping with the inferred foreland-basin setting.	2012, LAICPMS
15	CT07RIM72-1	952-40	16.55001	-11.17997	Gr. de Khaang Naam, Fm. de Lehbilé	Fine grained sandstone.	1128	870	Detrital zircons provide no useful age constraints. Age assignment based on stratigraphic position above Freidi Fm of Gr. d'Ajoun.	2012, LAICPMS
16	DB07RIM29c	952-08	20.4971	-12.87567	Gr. de Jbéliat	Tillite near Atar	1006	635	Detrital zircons provide no useful age constraints. Age assignment based on correlation of Gr. de Jbéliat with global Marinoan glaciation.	2012, LAICPMS

Table 2. Summary of USGS detrital zircon geochronology results.—Continued

Figure number	Sample number	Lab number	Latitude	Longitude	Map unit	Description	Max. depos. age (MDA) in Ma judging only from detrital zircons	Depositional age assignment (in Ma) for this study	Notes on detrital zircons	Year and method
17	CT07RIM73-1	952-34	16.58967	-11.29394	Gr. de Jbéliat	Coarse grained, arkosic red sandstone. Soft-sediment defortmation.	994*	635	Detrital zircons provide no useful age constraints. Age assignment based on correlation of Gr. de Jbéliat with global Marinoan glaciation.	2012, LAICPMS
18	DB07RIM80a	952-27	14.835259	-11.925647	Gr. de Jbéliat	Tillite with tuffaceous matrix, near Senegal River.	648	635 or maybe younger	MDA based on mean of 3 youngest overlapping ages. Different barcode from the other two Jbéliat samples, with youngest zircons close to the inferred depositional age, which itself rests on correlation with Marinoan glaciation.	2012, LAICPMS
20	DB07RIM77a	952-10	15.13696	-12.17747	Gr. de Teniagouri, Sous-groupe de Koumba Ndao	Tuffaceous sandstone turbidites near Selibabi.	601	601	MDA based on the youngest peak, of 5 ages. Depositional age assumed to be about the same as MDA because of foreland-basin setting.	2012, LAICPMS
21	DB07RIM28a	952-42	20.502785	-12.854843	Gr. de Nouatil	Sandstone	540	~535	MDA based on 2 youngest overlapping ages. Must be older than 524 and younger than 548.	2012, LAICPMS

Table 2. Summary of USGS detrital zircon geochronology results.—Continued

Figure number	Sample number	Lab number	Latitude	Longitude	Map unit	Description	Max. depos. age (MDA) in Ma judging only from detrital zircons	Depositional age assignment (in Ma) for this study	Notes on detrital zircons	Year and method
22	DB07RIM26a	952-29	20.505436	-12.842389	Gr. d'Oujeft, Fm. de Chinguetti	Sandstone	524	524	MDA based on youngest probability peak of 2 grains. Depositional age assumed to be about the same as MDA because of foreland-basin setting. Consistent with age near C-O boundary of younger Terguent Fm.	2012, LAICPMS
23	DB07RIM61a	952-35	20.92858	-11.5921	Gr. d'Oujeft, Fm. de Chinguetti	Ouadane	552	525	Detrital zircons provide only general age constraints. Extrapolate age from same unit near Atar, sample DB07RIM26a.	2012, LAICPMS
24	DB07RIM75a	952-09	16.34693	-11.97703	Gr. d'Oujefte, Sous-groupe d'Aghaoujeft	Sandstone in Mauritanide foreland basin.	524	510	MDA based on mean of 3 youngest overlapping ages. Depositional age assumed to be a little younger than MDA, because this unit is a little younger than Fm. de Chinguetti as per position on the Pitfield and others (2004) Sud1 correlation chart.	2012, LAICPMS
25	CT07RIM60-1	952-36	15.91161	-11.86834	Gr. d'Oujeft, Fm. de Moudjeria	Quartzofeldspathic sandstone.	543	~525	MDA is the mean of the 3 overlapping youngest DZ ages. About the same age as the Fm. de Chinguetti as per position on the Pitfield and others (2004) Sud1 correlation chart.	2012, LAICPMS

Table 2. Summary of USGS detrital zircon geochronology results.—Continued

Figure number	Sample number	Lab number	Latitude	Longitude	Map unit	Description	Max. depos. age (MDA) in Ma judging only from detrital zircons	Depositional age assignment (in Ma) for this study	Notes on detrital zircons	Year and method
26	DB07RIM74a	952-18	16.29167	-12.08789	Gr. d'Oujeft, supposedly Fm. de Moudjeria	Sandstone in Mauritanide foreland basin, near Mauritanide deformation front	903	903	MDA based on the youngest peak, of 2 ages. We think that this sandstone was mismapped as Moudjeria and really ought to be Assabet or equivalent.	2012, LAICPMS
27	CT07RIM59-1	952-30	15.93484	-12.00753	Gr. de Tichit, Fm. de Tabarit El Kbir	Mature, well-sorted, cross-bedded quartz sandstone.	548*	444	This is from the Late Ordovician glacial interval. Detrital zircons provide no useful age constraints.	2012, LAICPMS
28	CT07RIM62-1	952-37	16.66927	-7.24465	Gr. de Nema Gp, Fm. d'Adeile Fm	Brown, blocky, thick-bedded, fine to medium grained quartzofeldspathic sandstone.	525	~150	Detrital zircons provide no useful age constraints. Mesozoic, younger than 200 Ma based on field relations.	2012, LAICPMS
29	DB07RIM76a	952-28	16.27028	-12.16705	Gr. de Djonaba	Djonaba Gp, graywacke, near Mauritanide thrust front	982	~980	MDA based on the youngest peak, of 3 ages. We match the protolith to the Assabet barcode.	2012, LAICPMS
30	DB07RIM65a	952-34	16.88596	-12.72495	Gr. de Gadel	Metaconglomerate	999	~995	MDA based on youngest probability peak of 7 ages. We match the protolith to the Assabet barcode.	2012, LAICPMS
32	DB07RIM69a	952-22	16.98177	-12.63972	Gr. de Gueneba	Quartzite interbedded with dolostone	551	~550	MDA based on mean of 2 youngest overlapping ages. We match the protolith to the Oujeft barcode.	2012, LAICPMS

Table 2. Summary of USGS detrital zircon geochronology results.—Continued

Figure number	Sample number	Lab number	Latitude	Longitude	Map unit	Description	Max. depos. age (MDA) in Ma judging only from detrital zircons	Depositional age assignment (in Ma) for this study	Notes on detrital zircons	Year and method
33	CT07RIM55-1	952-19	16.84567	-12.75303	Gr. d'El Mseigguem, Fm. d'Ouechkech	Metasandstone	567	~560	MDA is the mean of the 3 overlapping youngest DZ ages. We match the protolith to the Oujeft barcode.	2012, LAICPMS
34	GB07RIM63A	1284-9	17.08795	-12.9394	Gr. d'El Ghabra , Fm. d'Oued Erdi.	Tuffaceous sandstone	594	594	MDA based on the youngest peak, of 9 ages. We match the protolith to the Teniagouri barcode.	2012, SIMS & LAICPMS
35	DB07RIM73a	952-24	16.33721	-12.62448	Gr. d'El Ghabra, Fm. d'Ould Moilid	Metagraywacke	606	606	MDA based on mean of 3 youngest overlapping ages. We match the protolith to the Teniagouri barcode.	2012, LAICPMS
36	DB07RIM62a	952-20	17.41983	-13.1377	Groupe d'El Fadra, Unit FrKc	Metasandstone	553	~550	MDA based on mean of 3 youngest overlapping 3 ages. We match the protolith to the Oujeft barcode.	2012, LAICPMS
40	DB07RIM01a	952-04	19.8079	-14.38875	Gr. de Oumachouema, Fm. de St. Barbe	Chloritic metasandstone	573	~570	MDA based on the youngest probability peak, an 8 grain shoulder. We match the protolith to the Oujeft barcode.	2012, LAICPMS
41	CT07RIM02-01	952-26	19.83974	-14.41061	G. d'Oumachouema, Fm. de St. Barbe	Chloritic semischist above pod of iron-carbonate	538	~535	MDA based on youngest 3 grain shoulder. We match the protolith to the Oujeft barcode.	2012, LAICPMS

Table 2. Summary of USGS detrital zircon geochronology results.—Continued

Figure number	Sample number	Lab number	Latitude	Longitude	Map unit	Description	Max. depos. age (MDA) in Ma judging only from detrital zircons	Depositional age assignment (in Ma) for this study	Notes on detrital zircons	Year and method
42	CT21		19.819333	-14.298833	Gr. d'Oumachoueima, undivided	Platy, thin-bedded sandtone/tuff near top of unit	558	~555	MDA based on youngest probability peak. We match the protolith to the Oujeft barcode.	2007 & 2012, SIMS
43	DB07RIM02a	952-03	19.84547	-14.4313	Gr. de Oumachoue-ma, Formation d'Irarchene El Hamra	Quartzite	974	~970	MDA based on young-est probability peak of 3 grains. We match the protolith to the Assabet barcode.	2012, LAICPMS
44	DB07RIM03a	952-31	19.8935	-14.43958	Gr. de Eizzene, Fm. de Raoui	Quartzite	986	~980	MDA based on young-est probability peak of 2 grains. We match the protolith to the Assabet barcode.	2012, LAICPMS
45	DB07RIM17a	952-41	19.68005	-14.77687	Complexe d'Inchiri, Gr. de Hajar dekhen – Kleouat	Quartzite	538	~535	MDA based on young-est probability peak of 3 grains. We match the protolith to the Oujeft barcode. Possible incon-sistency: this part of the Complexe d'Inchiri has been contact metamor-phosed; one phase of the responsible granite complex was dated at 599±8 Ma.	2012, LAICPMS

Table 2. Summary of USGS detrital zircon geochronology results.—Continued

Figure number	Sample number	Lab number	Latitude	Longitude	Map unit	Description	Max. depos. age (MDA) in Ma judging only from detrital zircons	Depositional age assignment (in Ma) for this study	Notes on detrital zircons	Year and method
46	GB07RIM80A	952-16	20.535261	-15.554685	Gr. de Lebzenia, Fm. d'Aouéoua	Hematized and sericitized quartzite from the Vararate West occurrence	576		Problem: Supposedly an Archean supracrustal sequence. Possible explanations include Neoproterozoic resetting, structural complexities responsible for a Pan-African inlier in the Tasiast region, or a sample mixup.	2012, LAICPMS
49	DB07RIM25c	952-17	20.68434	-13.19708	Complexe d'Amsaga	Quartzite	582		Problem: supposedly an Archean supracrustal sequence. Possible explanations include Neoproterozoic resetting or a sample mixup.	2012, LAICPMS
54	DB07RIM46a	952-06	22.67848	-12.46013	Complexe d'Ijil, Fm. de Tazadit, lower member	Quartzite	2988	~2100	Detrital zircons provide no useful age constraints. Age assignment based on the tectonic model of Schofield and Gillespie (2007)	2012, LAICPMS
55	DB07RIM36a	952-05	22.68599	-12.54027	Complexe d'Ijil, Fm. de Seyala	Conglomerate	2851	~2060	Detrital zircons provide no useful age constraints. Age assignment based on the tectonic model of Schofield and Gillespie (2007)	2012, SIMS; 2012, LAICPMS
56	DB07RIM55a	952-44	24.49981	-7.42639	Gr. de Blekhzaymat, Unit BZam2, southern outcrop belt.	Sandstone / conglomerate	2043	~2040	MDA based on mean of 3 youngest overlapping ages.	2012, LAICPMS

Table 2. Summary of USGS detrital zircon geochronology results.—Continued

Figure number	Sample number	Lab number	Latitude	Longitude	Map unit	Description	Max. depos. age (MDA) in Ma judging only from detrital zircons	Depositional age assignment (in Ma) for this study	Notes on detrital zircons	Year and method
57	DB07RIM54a	952-15 & 1284-8	26.51881	-8.46481	Gr. de Blekhzaymat, northern outcrop belt.	Metasandstone	2141	~2000	Using data from the re-analysis: The 620 peak may be a Pan-African overprint. MDA is based on the youngest Paleoproterozoic peak of 6 ages.	2012, LAICPMS
60	DB07RIM53a	952-14 & 1284-7	25.363297	-9.91157	Complexe du Ghallamane, unit GLsc	Metasandstone	2083	~2080	MDA based on mean of 3 youngest overlapping ages.	2012, LAICPMS
61	DB07RIM52a	952-13 & 1284-6	25.15799	-10.12549	Complexe de Tsalabia el Khadra, unit Khep	Quartz arenite	581	~545	Two almost identical results from the two splits of this sample. Depositional age is very likely Neoproterozoic, with an MDA of 545 based on the 2 youngest overlapping ages. If so, the sample would be from an inlier or fault basin on top of Reguibat Shield basement.	2012, LAICPMS

Table 3. Summary of USGS $^{40}Ar/^{39}Ar$ geochronology results.

Figure number	Sample number	Latitude	Longitude	Map unit	Lithology	Description	Integrated Age (Ma)	Plateau Age (Ma)	Comments
31	DB07RIM66a (1)	16.87144	-12.70554	Gr. de Gadel	schistose meta-conglomerate	So-called "melange" unit, qtz-mica schist matrix to metaconglomerate, fine white-mica fraction.	572 ± 3	X	Poor-looking age spectra. This sample is a fine-grained separate.
31	DB07RIM66a (2)	16.87144	-12.70554	Gr. de Gadel	schistose meta-conglomerate	So-called "melange" unit, qtz-mica schist matrix to metaconglomerate, coarse white-mica fraction.	593 ± 3	594 ± 7	Age spectra looks good. Plateau contains ~90% of argon released. This is a laser analysis of a single grain.
38	GB07RIM52A	17.49381	-12.91467		quartz sericite vein	Quartz fragments rich in sericite collected from mineral occurrence Iguerj	356.8 ± 1.8	X	Age spectra looks OK
38	GB07RIM61A	17.28512	-12.91928		quartz sericite vein	Quartz fragments rich in sericite collected from mineral occurrence Chlakh Lhemir	298.6 ± 1.5	298.6 ± 1.7	Age spectra looks good. Plateau contains ~65% of argon released.
38	GB07RIM62C	17.26708	-12.9162		quartz sericite vein	Quartz fragments rich in sericite collected from mineral occurrence Chlakh Lhemir	294.8 ± 1.5	X	Age spectra looks OK.
38	GB07RIM69A	16.71545	-12.77247		quartz sericite vein	Quartz fragments rich in sericite collected from mineral occurrence Vararate Nord	648 ± 4	X	Poor-looking age spectra.
47	GB07RIM82D	20.568767	-15.505248		quartz-sericite vein	Quartz fragments rich in sericite collected from mineral occurrence Tasiast	2533 ± 8	X	Poor-looking age spectra.
48	DB07RIM25a	20.68434	-13.19708	Complexe d'Amaga	granite	Tungsten occurrence, Amsaga complex, granite with white mica	1753 ± 6	X	Age spectra looks OK.
52	DB07RIM45b	22.69307	-12.4593	Complexe de Tiris	micaceous mylonite	Mylonite from thrust contact between Kediat Idjil over Tiris near Zouerate	2496 ± 8	X	Poor-looking age spectra.
54	DB07RIM46b	22.67848	-12.46013	Complexe d'Ijil, Fm. de Tazadit, lower member	muscovite schist	Mica schist, lower "member" Kediat Idjil in roadcuts on field trip	1950 ± 7	X	Age spectra looks OK.
59	GB07RIM40B	26.51736	-8.46409	Vein cuts Gr. de Blekhzaymat	quartz sericite vein	Quartz fragments rich in sericite; mineral occurrence BIA601	2179 ± 11	X	Age spectra looks OK.

Table 3. Summary of USGS $^{40}Ar/^{39}Ar$ geochronology results.—Continued

Figure number	Sample number	Latitude	Longitude	Map unit	Lithology	Description	Integrated Age (Ma)	Plateau Age (Ma)	Comments
59	GB07RIM42B	26.46834	-8.46793	Vein cuts Gr. de Blekhzaymat	quartz sericite vein	Quartz fragments rich in sericite; mineral occurrence BIA611	2061 ± 7	2063 ± 7	Age spectra looks good. Plateau contains ~85% of argon released.
60	DB07RIM53c	25.36297	-9.91157	Complexe de Ghallamane, unit GLsc	hornfels metatur-bidites	Unit GLsc, Complexe du Ghallamane, metasandstone.	1981 ± 7	2014 ± 12	Age spectra looks OK. First 40% of argon released step up to plateau.
The following samples yielded no useful results									
not shown	CT07RIM47-1	17.42013	-13.13654	El Fadra Gp-Oued Kav Fm.	quartz-ankerite vein	2” thick quartz-ankerite vein cutting greenschist and muscovite schist. Abundant thin quart-ankerite and quartz-calcite-epidote veins in outcrop.	Undatable	Undatable	No separable mica.
not shown	CT07RIM49-2	17.36106	-12.81517	Gueneiba Gp-Oued Amour Fm	sericite-quartz veined goethite	Small E-W ridge of massive goethite cut by quartz-malachite veins at mineral occurrence El Aouidja	Undatable	Undatable	Sample analyzed; not mica. Possibly pyrophyllite.
not shown	DB07RIM25b	20.68434	-13.19708	Complexe d’Amaga	quartzite	Tungsten occurrence, Amsaga complex, quartzite with metamorphic white mica	Undatable	Undatable	No separable mica.
not shown	DB07RIM63b	17.49605	-12.97836	Gr d’El Fadra, Fm d’El Hneikat	quartz muscovite schist	Magkta Lahjar area, Fm. d’El Hneikat, quartz-mica schist to date metamor-phism in vicinity of mineral occurrence Magkta Lahjar	Undatable	Undatable	Sample not analyzed.
not shown	DB07RIM71a	16.67589	-12.70435	Gr. d’El Ghabra	muscovite schist	Gr. d’El Ghabra, Au occurrence, mica schist in shear zone	Undatable	Undatable	Sample analyzed; not mica. Possibly pyrophyllite.
not shown	GB07RIM41A	26.47964	-8.45411		quartz sericite vein	Quartz fragments with possible oxidized sulfide grains, rich in sericite; mineral occurrence BIA621	Undatable	Undatable	No separable mica.

Table 4. Apatite fission track (AFT analytical data, sample CT07RIM27-1, lab number 952-02.

Nom de l'analyse	TF age (Ma)	95%-CI (Ma)	95%+CI (Ma)	Age U-Pb (Ma)	2 sigma (Ma)	Ns
9522a1_1	62.22	42.83	136	1487.03	329.32	3
9522a1_2	20.02	13.04	37.28	0	0	4
9522a1_3	38.29	26.39	84.39	2522.13	791.07	3
9522a1_4	182.26	50	68.54	1912.39	167.77	54
9522a1_5	0	0	0	0	0	7
9522a1_6	135.65	49.12	76.56	2316.61	240.43	23
9522a1_7	163.18	47.73	67.11	2227.66	359.59	44
9522a1_8	159.87	44.54	61.45	2094.62	243.26	52
9522a1_9	0	0	0	0	0	10
9522a1_10	0	0	15.85	2024.94	271.05	0
9522a1_11	57.95	50.16	362.5	336.8	349.8	1
9522a1_12	185.97	58.44	84.66	2011.81	274.87	35
9522a1_13	248.98	92.49	145.5	600.16	187.15	21
9522a1_14	181.92	115.58	309.4	2098.15	502.91	4
9522a1_15	217.67	85.42	139.09	2050.16	425.69	18
9522a1_16	0	0	0	0	0	76
9522a1_17	196.88	94.31	178.53	2140.65	508.65	10
9522a1_18	196.7	88.66	159.44	2314.07	369.32	12
9522a1_19	410.38	152.74	238.85	2091.15	539.38	21
9522a1_20	255.65	132.26	268.37	2183.05	781.96	8
9522a1_21	144.25	60.61	103.7	0	0	15
9522a1_22	8257.27	6368.56	11324.68	0	0	39
9522a1_23	153.48	65.66	113.75	2183.25	343.49	14
9522a1_24	100.65	76.34	308.63	1877.44	701.91	2
9522a1_25	755.02	289.8	454.16	2145.44	1175.89	19
9522a1_26	151.77	70.51	130.36	2170.36	363.49	11
9522a1_27	132.13	54.1	90.95	1909	286.05	16
9522a1_28	175.5	94.48	201.49	2093.11	680.05	7
9522a1_29	199.27	57.41	80.15	1978.96	189.09	46
9522a1_30	297.68	116.3	188.1	1851.76	272.6	18
9522a1_31	223.14	103.35	189.71	2177.63	563.98	11
9522a1_32	145.32	39.81	54.6	613.76	115.94	55
9522a1_33	234.6	87.75	138.69	2092.11	451.29	21
9522a1_34	191.17	99.03	202.27	2124.47	694.22	8
9522a1_35	107.9	93.39	659.36	0	0	1
9522a1_36	175.69	87.09	170.44	2080.5	386.29	9
9522a1_37	149.83	72.06	137.37	2127.56	475.41	10
9522a1_38	225.99	92.64	155.14	2177.95	801.33	16
9522a1_39	179.86	39.98	51.2	2093.86	234.95	124
9522a1_40	146	39.9	54.67	2006.93	269.21	56

Table 4. Apatite fission track (AFT analytical data, sample CT07RIM27-1, lab number 952-02.—Continued

Nom de l'analyse	TF age (Ma)	95%-CI (Ma)	95%+CI (Ma)	Age U-Pb (Ma)	2 sigma (Ma)	Ns
"Pooled age" (Ma)	170.18			Nombre des points		37
95%-CI (Ma)	14.44			Nombre des traces		811
95%+CI (Ma)	15.76			Rho		0.000039169
wmean pz:sz UCa	1.1398			+/- 1 sigma		8.6892E-07
wmean pz:unk Ca	1.0079			Cation isotopique		43Ca
relerr pz:sz	0.0859			chi-carré		116.7689
relerr analyste	0			Q(chi-carré)		0
relerr déficit	0.426			Moyenne Dpar (um)		2.25
relerr Ca apfu	0			Moyenne Dper (um)		0.49
Zeta primaire	8.329			Moyenne [U] (ppm)		14.01
+/- 1 sigma	0.1418			Moyenne [Th] (ppm)		19.6
				Moyenne [Sm] (ppm)		146.23
				Initiales de l'analyste		pos

Link to table 5. $^{40}Ar/^{39}Ar$ analytical data.

Table 6. U-Pb CA-TIMS analytical data.

						Ratios								Age (Ma)				
Sample	**Pb(c)**	**Pb***	**Th**	**206 Pb**	**208 Pb**	**206 Pb**		**207 Pb**		**207 Pb**		**206 Pb**		**207 Pb**		**207 Pb**		**corr.**
Fractions	**(pg)**	**Pb(c)**	**U**	**204 Pb**	**206 Pb**	**238 U**	**err**	**235 U**	**err**	**206 Pb**	**err**	**238 U**	**err**	**235 U**	**err**	**206 Pb**	**err**	**coef.**
(a)	**(b)**			**(c)**	**(d)**	**(e)**	**(2s%)**	**(e)**	**(2s%)**	**(e)**	**(2s%)**		**(2s)**		**(2s)**		**(2s)**	
DB07RIM29a A to Z mineral separate																		
z1	0.6	12.0	1.31	612.5	0.405	0.10099	(0.48)	0.84635	(1.63)	0.06081	(1.54)	620.19	2.83	622.64	7.61	631.6	33.1	0.342
z2	0.5	10.9	1.59	525.8	0.493	0.10111	(0.36)	0.84320	(1.75)	0.06051	(1.66)	620.94	2.15	620.91	8.11	620.8	35.9	0.327
z3	0.3	11.5	1.46	566.7	0.454	0.10236	(0.33)	0.85511	(1.69)	0.06061	(1.60)	628.25	1.98	627.45	7.89	624.6	34.6	0.338
z4	0.3	14.6	0.59	872.2	0.182	0.10817	(0.30)	0.92327	(1.15)	0.06193	(1.07)	662.08	1.89	664.09	5.62	670.9	22.8	0.408
z5	0.4	13.3	1.22	690.0	0.378	0.10126	(0.27)	0.84150	(1.44)	0.06030	(1.41)	621.76	1.62	619.98	6.67	613.5	30.5	0.185
DB07RIM29a Youngest grains on grain mount prepared by USGS																		
z19	0.3	41.1	0.46	2503.0	0.142	0.09232	(0.07)	0.75417	(0.37)	0.05928	(0.36)	569.23	0.36	570.64	1.63	576.3	7.9	0.264
z21	0.4	6.3	0.35	410.1	0.109	0.09588	(0.29)	0.78767	(2.23)	0.05961	(2.16)	590.20	1.66	589.85	9.97	588.5	46.8	0.296
DB07RIM29a MIT processed																		
z1Cr	0.4	1.2	0.77	86.6	0.238	0.10253	(2.71)	0.87197	(11.86)	0.06171	(11.32)	629.23	16.26	636.64	56.10	663.0	242.6	0.308
z2Cr	0.4	2.8	0.99	165.9	0.307	0.10051	(0.59)	0.83065	(5.52)	0.05997	(5.38)	617.37	3.47	613.97	25.42	601.4	116.5	0.279
z3Cr	0.3	4.6	1.21	252.5	0.375	0.10080	(0.96)	0.82750	(3.95)	0.05956	(3.73)	619.11	5.65	612.22	18.17	586.8	80.9	0.348
z4Cr	0.3	5.0	1.51	256.1	0.469	0.10348	(4.42)	0.86704	(6.72)	0.06079	(4.76)	634.79	26.72	633.96	31.68	631.0	102.6	0.707
z5Cr	0.3	10.3	1.29	527.8	0.400	0.10146	(0.80)	0.84682	(2.04)	0.06056	(1.83)	622.96	4.76	622.90	9.50	622.7	39.5	0.442
z6Cr	0.3	1.2	1.05	78.7	0.327	0.09377	(3.73)	0.77127	(14.38)	0.05968	(13.56)	577.78	20.64	580.49	63.56	591.1	294.1	0.341

[a]Thermally annealed and pre-treated single zircon.

[b]Total common-Pb in analyses.

[c]Measured ratio corrected for spike and fractionation only.

[d]Radiogenic Pb.

[e]Corrected for fractionation, spike, blank, and initial common Pb. Also corrected for initial Th/U disequilibrium using radiogenic 208Pb and Th/U[magma] = 2.8
Mass fractionation correction of 0.25%/amu ± 0.04%/amu (atomic mass unit) was applied to single-collector Daly analyses.
Total procedural blank less than 0.5 pg for Pb and less than 0.1 pg for U.
Blank isotopic composition: 206Pb/204Pb = 18.31 ± 0.53, 207Pb/204Pb =15.38 ± 0.35, 208Pb/204Pb = 37.45 ± 1.1.
Corr. coef. = correlation coefficient.
% discordance = 100 - (100 * (206Pb/238U date) / (207Pb/206Pb date))
Ages calculated using the decay constants λ238 = 1.55125E-10 and λ235 = 9.8485E-10 (Jaffey et al. 1971).

Link to table 7. LAICPMS analytical data.

Link to table 8. SIMS analytical data.

Link to table 9. Compilation of published isotopic ages from Mauritania.

Appendix A2. Analytical Methods forU-Pb CA-TIMS Geochronology at Massachusetts Institute of Technology

To minimize the effects of Pb-loss in zircon, grains were pre-treated using the chemical abrasion or CA-TIMS technique of Mattinson (2005, 2010). This technique allows preferential dissolution of high-U domains in zircon crystals that are most susceptible to radiation damage and lead loss. Annealing occurred at 900°C for 60 hours. The annealed grains were subsequently loaded into 200µl FEP Teflon® microcapsules and leached in 29M HF within high pressure Parr® vessels at 210°C for 12-14 hours. The partially dissolved sample was then transferred into 3ml Savillex® FEP beakers, fluxed successively with 4N HNO_3 and 6N HCl over a hot plate and inside an ultrasonic bath, and rinsed with several milliliters of ultra-pure water in between. Zircon grains were loaded back into their microcapsules, spiked with a mixed ^{205}Pb-^{233}U-^{235}U tracer solution and dissolved completely in 29M HF at 210°C for 48 hours.

Dissolved Pb and U were chemically separated using a miniaturized HCl-based ion-exchange chemistry procedure modified after Krogh (1973), using 50 µl columns of AG1x8 anion-exchange resin. Both Pb and U were loaded with a silica gel - H_3PO_4 emitter solution (Gerstenberger and Haase, 1997) on single degassed Re filaments and their isotopic compositions were measured on the VG Sector 54 multi-collector thermal ionization mass spectrometer at MIT. Lead isotopic measurements were made in a peakhopping mode by ion counting using a Daly photomultiplier detector with a ^{206}Pb ion beam intensity of 1.0 to 2.5 x 10-14 Amps usually maintained in the course of data acquisition. Uranium isotopes were measured as oxide ions on three Faraday detectors in a static mode with an average $^{235}U^{16}O_2$+ ion-beam intensity of 8.0 x 10-13 Amps.

Measured isotopic ratios were corrected for mass-dependent isotope fractionation, as well as for U and Pb contributions from the spike and laboratory blanks. Pb/U ratios were also corrected for initial Th/U disequilibrium in magma. Data reduction and error propagation was carried out using applications Tripoli and U-Pb_Redux developed as part of the EARTHTIME initiative (Bowring and others, 2011; McLean and others, 2011). In general, $^{206}Pb/^{238}U$ dates are considered the most precise and accurate. Our calculated weighted mean $^{206}Pb/^{238}U$ dates are derived from coherent clusters of the youngest zircon analyses in each sample. Calculated U-Pb dates are reported at 95% confidence level (Table 1 and Figure 5). Uncertainties in U-Pb dates are reported as ±X/Y/Z, where X is the internal (analytical) uncertainty in the absence of all external errors, Y incorporates the U-Pb tracer calibration error and Z includes the latter as well as the decay constant errors of Jaffey and others (1971). The external uncertainties must be taken into account if the results are to be compared with U-Pb dates obtained in other laboratories with different tracers (Y) or ones derived from other isotopic chronometers (for example, Re-Os) (Z). However, for establishing a high-resolution chronology based on the results of this study alone, only the analytical uncertainties (X) should be considered.

Appendix A3. U-Pb Zircon SHRIMP-RG Techniques (U.S. Geological Survey-Stanford University)

Zircon separations were done on at the U.S. Geological Survey in Anchorage using standard density and magnetic separation techniques. Zircons were hand picked for final purity, mounted on double stick tape on glass slides in 1 x 6 mm rows, cast in epoxy, ground and polished to a 1 micron finish on a 25 mm diameter by 4 mm thick disc. All grains were imaged with transmitted light and reflected light (and incident light if needed) on a petrographic microscope, and with cathodoluminescence and back scattered electrons as needed on a JEOL 5600 SEM to identify internal structure, inclusions and physical defects. The mounted grains were washed with 1N HCl or EDTA solution (if acid soluble) and distilled water, dried in a vacuum oven, and coated with Au. Mounts typically sat in a loading chamber at high pressure (10-7 torr) for several hours before being moved into the source chamber of the SHRIMP-RG. Secondary ions were generated from the target spot with an O_2^- primary ion beam varying from 4-6 nA. The primary ion beam typically produces a spot with a diameter of 20-40 microns and a depth of 1-2 microns for an analysis time of 9-12 minutes. Nine peaks are measured sequentially for zircons (the SHRIMP-RG is limited to a single collector, usually an EDP electron multiplier): $^{90}Zr_2{}^{16}O$, ^{204}Pb, Bgd (0.050 mass units above ^{204}Pb), ^{206}Pb, ^{207}Pb, ^{208}Pb, ^{238}U, $^{248}Th^{16}O$, $^{254}U^{16}O$. Autocentering on selected peaks and guide peaks for low or variable abundance peaks (i.e. $^{96}Zr^{216}O$ 0.165 mass unit below ^{204}Pb) are used to improve the reliability of locating peak centers. The number of scans through the mass sequence and counting times on each peak are varied according to sample age and U and Th concentrations to improve counting statistics and age precision. Measurements are made at mass resolutions of 6000-8000 (10% peak height), which eliminates all interfering atomic species. The SHRIMP-RG was designed to provide higher mass resolution than the standard forward geometry of the SHRIMP I and II (Clement and Compston, 1994). This design also provides very clean backgrounds and combined with the high mass resolution, the acid washing of the mount, and rastering the primary beam for 90-120 seconds over the area to be analyzed before data are collected, assures that any counts found at mass of ^{204}Pb are actually Pb from the zircon and not surface contamination. In practice greater than 95% of the spots analyzed have no common Pb. Concentration data for zircons are standardized

against zircon standard SL-13 (238 ppm U) or CZ3 (550 ppm U) and age data against AS3 and AS57 zircons (1098 Ma) from the Duluth Gabbro (Paces and Miller, 1993), RG-6 (1440 Ma, granite of Oak Creek stock, Bickford and others, 1989), or R33 (419 Ma, quartz diorite of Braintree complex, Vermont, John Aleinikoff, personal communication) which are analyzed repeatedly throughout the duration of the analytical session. Data reduction follows the methods described by Williams (1997) and Ireland and Williams (2003) and use the Squid and Isoplot programs of Ludwig (2001, 2003).

Appendix A4. Analytical Methods for U-Pb LAICPMS Geochronology by Apatite to Zircon, Inc. at Washington State University

***LA-ICP-MS Session Details*—**Data were collected for the following isotopic masses: ^{202}Hg, ^{204}Hg+^{204}Pb, ^{206}Pb, ^{207}Pb, ^{208}Pb, ^{232}Th, ^{235}U, and ^{238}U (250 data scans over 30 s) followed by ^{28}Si and ^{91}Zr (5 data scans over 4 s). The instruments used were a New Wave YAG 213 nm laser ablation (LA) system in line with a Finnigan Element2 magnetic sector, inductively coupled plasma, mass spectrometer (ICP-MS) at the Washington State University Geoanalytical Laboratory in Pullman, Washington, U.S.A. All analyses were performed using a 20 μm spot. Following approximately 6 s of background data collection, laser ablation commenced and data were collected for the ablated material. Ablated material was transported to the plasma line using He; Ar was the plasma gas.

Zircon standards for which independently accepted ages are published were designated as primary, secondary, and tertiary for purposes of U-Pb age calibration (table A7). Two primary and two secondary standard spots were analyzed prior to and following each group of ~25-30 tertiary standards and/or unknown sample spots. Five spots of each tertiary standard were analyzed near the beginning and again near the end of the session.

***Data Modeling*—**Previous LA-ICP-MS studies of U-Pb zircon dating deployed the so-called intercept method which assumes that isotopic ratio varies linearly with scan number due solely to linearly varying isotopic fractionation (Chang and others, 2006; Gehrels and others, 2008). For the intercept method, a line is fitted to background-corrected isotopic ratio (for example, ^{206}Pb/^{238}U) versus data scan number and the intercept of the fitted line (corresponding to data scan number = 0) is used as the isotopic ratio for age calculation and the error on the intercept is used for age error calculation. In this study, individual isotopes were modeled by fitting a sum of 10 Gaussian equations to the raw signal data (not background corrected) using chi-squared minimization. Two fitting passes were performed: after the first pass, all raw signal values greater than two standard deviations away from the sum of fitted Gaussians were designated outliers; the second pass fit the sum of Gaussians to the data excluding the outliers. The advantage of the present approach is that it avoids the assumption of linearly varying isotopic ratio with scan number, an assumption easily violated for zircons that may contain useful information (for example, a zircon for which the ablation pit variably penetrates two zones having different U-Pb ages).

Measured background values for each isotope at each LA-ICP-MS spot were calculated as follows: (1) the final background scan was assigned as the scan closest to the global minima ^{232}Th and ^{238}U values; if no such global minima were found, the analysis was deemed a failure; (2) a line was fitted to the background values, outliers identified, and a line again fitted to the data excluding the outliers; (3) for a fitted line exhibiting a negative slope (indicative of a decaying background), the value of the line at the last background scan was assigned as the background value; for a fitted line exhibiting a zero or positive slope, the mean value of the data excluding the outliers was assigned as the background value; and (4) the error of the background value was set equal to the standard deviation of the all background values (excluding outliers) about their fitted line (negative slope) or mean (zero or positive slope).

Session-wide fitted background values for each isotope were determined using all zircon standards and applied to all spots in the session. These steps were taken for each isotope: a) measured background value versus spot number in the session was fitted to a 3rd-order polynomial, outliers identified, and the fitting repeated excluding the outliers, and b) fitted background at each session spot was calculated using the 3rd-order polynomial. Session-wide fitted background error was set equal to the standard deviation of the measured background values (excluding outliers) about their respective fitted 3rd-order polynomial. For any spot (standard or unknown) where the measured background value exceeded the session-wide fitted value by more than 2σ, the background error was set equal to 1σ plus one half of the amount by which the measured background value exceeded the session-wide fitted value by 2σ.

The sum of fitted Gaussians was used here primarily to identify outlier data and characterize signal noise. After the second fitting pass, the standard deviation of the non-outlier data about their respective sum of fitted Gaussians was taken as the absolute signal error for each data scan. When N data scans contribute to a single isotopic signal value used for age calculation (only concordant scans when the number of concordant data scans is greater than zero; all data scans for common Pb-correction based on isotopic sums), the error of the single isotopic signal value was set equal to the product of $N^{1/2}$ and the absolute signal error for a each data scan.

***Pb/U Fractionation Factor*—**Fractionation factors were determined for each data scan of each primary standard spot. For a particular isotopic ratio (for example, $^{206}Pb/^{238}U$), the fractionation factor as used here equals the accepted isotopic ratio divided by the measured ratio. A two dimensional grid (spot number, scan number) of fractionation factors for each isotopic ratio was constructed for the session as a whole by fitting a series of 4th-order polynomials (excluding outliers). Under the operating conditions of the LA-ICP-MS sessions in this study, fractionation factors were found to vary strongly with scan number, decreasing with increasing scan number (presumably due to increasing ablation pit depth and the effect this had on fractionation; for example, Paton and others [2010]).

Fractionation factors were calculated using isotopic values based on the sum of fitted Gaussians. Ages, including when the standards were treated as unknowns, were calculated using raw isotopic signal values (excluding outliers) to avoid any bias due to artifacts of the fitting of the sum of Gaussians.

***Fractionation Factor Adjustment for Integrated α-damage*—**Zircon is widely known to accumulate α-radiation damage (for example, Zhang and others, 2009 and references therein). It is assumed here that increased α-damage in a zircon leads to a decrease in the hardness of the zircon; this in turn leads to a faster rate of laser penetration into the zircon during ablation leading to a shift in isotopic fractionation. Ages calculated for the primary, secondary, and tertiary zircon standards, when those standards were treated as unknowns were used to construct a fractionation factor correction curve (exponential form). Much previous work has attempted to understand the chemical basis for why some standards work better with some zircons. The notion of matrix-matched standard and unknown zircons has been proposed largely on the basis of trace element chemistry (for example, Black and others, 2004). Here, time and crystallographic damage, parameters invisible to instruments used to characterize trace element chemistry, were introduced and applied in conjunction with U and Th chemistry.

***Common Pb Correction*—**Common Pb was subtracted out using the Stacey and Kramer (1975) common Pb model for Earth. Ages and common Pb ratio were determined iteratively using a pre-set, session-wide minimum common Pb age value (default for each session was the age of the oldest age standard, which for both Ap and Zrn was 1,099 Ma FC-1 and/or FC-5z).

***Preferred Age*—**Uranium decay constants and the $^{238}U/^{235}U$ isotopic ratio reported in Steiger and Jäger (1977) were used in this study. $^{207}Pb/^{235}U_c$ ($^{235}U_c = 137.88^{238}U$), $^{206}Pb/^{238}U$, and $^{207}Pb/^{206}Pb$ ages were calculated for each data scan and checked for concordance; concordance here was defined as overlap of all three ages at the 1σ level (the use of 2σ level was found to skew the results to include scans with significant common Pb). The background-corrected isotopic sums of each isotope were calculated for all concordant scans. The precision of each isotopic ratio was calculated by using the background and signal errors for both isotopes. The fractionation factor for each data scan, corrected for the effect of accumulated α-damage, was weighted according to the ^{238}U or ^{232}Th signal value for that data scan; an overall weighted mean fractionation factor for all concordant data scans was used for final age calculation.

If the number of concordant data scans for a spot was greater than zero, then either the $^{206}Pb/^{238}U$ or $^{207}Pb/^{206}Pb$ age was chosen as the preferred age, whichever exhibited the lower relative error. If zero concordant data scans were observed, then the common Pb-corrected age based on isotopic sums of all acceptable scans was chosen as the preferred age. Common Pb was subtracted out using the Stacey and Kramer (1975) common Pb model for Earth. Ages and common Pb ratio were determined iteratively using a pre-set, session-wide minimum common Pb age value; the default for each session was the age of the oldest age standard which for both Ap and Zrn was 1099 Ma FC-1 and (or) FC-5z.

Appendix A5. Analytical Methods for Apatite Fission Track Geochronology by Apatite to Zircon, Inc.

Apatite mineral concentrates were produced, mounted, etched, and analyzed (both AFT ages and confined track length determinations) following the procedures summarized in Donelick and others (2005). If possible, each analysis included at least 25 single-grain ages and 125 confined track length measurements. The apatite grain mounts were irradiated using fission fragments from a ^{252}Cf source in a vacuum chamber in order to enhance the number of confined tracks available for measurement (Donelick and others, 2005). The external detector method (EDM) and the zeta calibration method of Hurford and Green (1982) were used for all samples. The observed fission-track age spread was determined statistically using the c^2 test, which indicates the probability that all grains counted belong to a single population of ages. A probability of <5% is evidence of an asymmetric spread of single-grain ages, and that the weighted mean age should be used.

The variation in apatite composition within and between individual samples may provide an important tool in constraining a sample's thermal history because different compositional species have different total annealing temperatures, below which apatites begin to accumulate fission tracks. Therefore, different grains within a sample may record different parts of a sample's thermal history. In order to determine variations in composition between grains, we collected measurements of the Dpar parameter from every apatite grain analyzed for either AFT age or confined track-length determination. Dpar is the mean

fission-track etch pit diameter parallel to the crystallographic c-axis for each apatite grain. A complete description of the Dpar parameter and its usefulness and relationship to AFT annealing kinematics is presented in Donelick and others (2005).

The AFT data were modeled using the multi-kinetic fission track-annealing model of Ketcham and others (1999). A Dpar value was determined for every apatite grain during each AFT age or length analysis. For quantitative interpretation, the coupled Dpar+apatite fission-track data were imported into the multi-kinetic fission-track annealing simulation model (AFTSolve; Ketcham and others, 2000) where the track lengths and single-grain ages are plotted against Dpar. AFTSolve then allows the user to interactively sub-divide the fission track data into kinetic or chemical populations, after which the resulting pooled AFT ages and mean track lengths of each population are calculated and displayed. Every kinetic population within each individual sample was subsequently modeled simultaneously using the inversion procedure outlined in Ketcham and others (2000). For all samples, the inversion was run using 20,000 Monte Carlo models, with a starting constraint of a temperature of 250°C at 60 Ma (intrusion age of batholith) and a present-day mean annual surface temperature of 0°C.

ISSN 2331-1258 (online)
http://dx.doi.org/10.3133/ofr20131280